Updating of Finite Element Model of Cable-stayed Bridges for Improved Dynamic Characteristization and Active Seismic Response Control Implementation

Submitted in partial fulfillment of the requirements
For the degree of

DOCTOR OF PHILOSOPHY

By

Atanu Kumar Dutta

Civil Engineering Department
INDIAN INSTITUTE OF TECHNOLOGY, GUWAHATI

(2007)

CERTIFICATE

*This is to certify that the thesis entitled '**Updating of Finite Element Model of Cable-stayed Bridges for Improved Dynamic Characteristization and Active Seismic Response Control Implementation'** submitted by **Mr. Atanu Kumar Dutta** to the **Indian Institute of Technology, Guwahati** for the degree of Doctor of Philosophy in Civil Engineering is a record of bonafide research work carried out by him under our supervision and guidance. The thesis work, in our opinion, has reached the requisite standard fulfilling the requirement for the degree of Doctor of Philosophy.*

The results contained in this thesis have not been submitted in part or full to any other university or institute for award of any degree or diploma.

(Anjan Dutta)
Associate Professor
Dept of Civil Engineering
Indian Institute of Technology
Guwahati-781039

(S. K. Deb)
Associate Professor
Dept of Civil Engineering
Indian Institute of Technology
Guwahati-781039

ACKNOWLEDGEMENTS

The author is indebted to his guides Dr. Anjan Dutta and Dr. S K Deb for their immaculate guidance, meticulous supervision, kind help, moral support and constant encouragement throughout this work.

The author is grateful to the Govt. of Assam for sponsoring him for this work. He is thankful to the Jorhat Engineering College for sparing him for this period.

He thanks the members of his doctoral committee Dr. S Talukdar, Dr. D Maity, Prof. A D Shahasrabhudhe and Dr. U S Dixit for their encouragement and suggestions during various stages of the work. He is grateful to all the faculty members of the Dept of Civil Engineering, IITG for their kind encouragement and to the staff of the computational lab, specially Arun, for his help. He expresses his thanks to Indrani, Mrinal, Manas, PP, Lego da, Hopeful, Nagendra and co-researchers at IITG for their encouragement and support in many forms.

The author acknowledges with gratitude the financial support by NPEEE (National Programme on Earthquake Engineering Education, Ministry of Human Resources Development, Govt of India) for six months' visit to US to do a part of his research. He is grateful to the Dept of Civil and Environmental Engineering, University of South Carolina, USA for hosting him as a visiting scholar. He expresses his heartfelt gratitude to Dr. Juan M Caicedo, Assistant Professor, Dept of Civil and Environmental Engineering, USC for his kind guidance. The author is indebted to him for giving access to his FEM toolbox in Matlab®. He expresses his special thanks to Mr. Boris Zarate, his co-researcher at the USC, for his constant help and encouragement. He is thankful to Ron, Vinay, Abijit, Veeru, Siva, Ravi and all for making his stay in the university a memorable one.

The author expresses his deep sense of gratitude to Prof. Shirley J Dyke of Washington University, St. Louis, USA for giving him exposure to the world class laboratory facility at her department and for her invaluable suggestions for the present work.

He is grateful to the Principal, Jorhat Engineering College, Prof. Bibeka Nanda Choudhury, HOD Civil Engg Dept and colleagues Nayanmoni, Abhijit, Utpal, Mrinal and all for extending encouragement and help.

He is grateful to all his family members for sharing his agony and ecstasy during this period. He is thankful to his parents, parents-in-laws, uncles, cousins, sister Runjun, sisters-in-law Lizy, Purabi, Bhanti, brothers Shanatanu and Jan, brothers-in-law Bibeka, Baba and Kalyan and last but not the least, his wife Monisa, who shared all his troubles with a bold face, and son Abir who suffered his long absences with an endearing smile.

Finally, the author is indebted to the society for creating an ambience of academic pursuit, while going through a tumultuous time itself.

(Atanu Kumar Dutta)

Chapter 1

INTRODUCTION & LITERATURE SURVEY

1.1 Introduction

Cable-stayed bridges have gained popularity in the category of long span bridges over the last three decades due to improved structural performance and aesthetic appeal in comparison to suspension bridges. It is appreciated that development of a numerical model, which simulates natural frequencies and mode shapes of the structure, is an important step for computation of dynamic responses of a cable-stayed bridge. However, building a numerical model to represent dynamic characteristics of a cable stayed bridge is rather difficult as this flexible structure exhibits complex behavior with the flexural, lateral and torsional motions being very often coupled. As a consequence, structural characteristics and responses predicted by idealized finite element (FE) models have discrepancies and errors as compared to those obtained from the actual measurements. Lack of proper idealization of the complex structure is regarded as one of the main causes of such discrepancies in a numerical model for a cable-stayed bridge. Modal identification through full-scale testing is the most reliable method to determine the true dynamics properties (e.g. natural frequencies, damping ratios and mode shapes) of a structure. This serves as a basis for validating and/or updating an analytical model of a structure so that the model represents the actual structural properties and the boundary conditions. The grey areas of the modeling, such as the damping property of the structure, idealization of bearings, appropriate representation of mass and stiffness can be suitably incorporated in the FE model through model updating in conjunction with the system identification data.

The protection of cable stayed bridges against seismic excitation is an active area of research. Active control system can offer the advantage of being able to dynamically modify the response of a structure in order to increase its safety and reliability. An active control strategy serves as a benchmark for evolving other control strategies. It also serves as a guide and reduces the number of iterations in building a real system for control implementation. In an active control strategy the control effort is dictated by the states of the numerical model and hence accuracy in modeling of the structure is of paramount importance. Thus, model updating would play an important role in evolving a more realistic active control strategy. The present work primarily addresses the dual issues of model updating and designing of active controllers based on the updated model. Two real life cable stayed bridges have been considered for the study.

1.2 Literature Survey

The literature survey for the present work has been divided broadly into two parts. The background of finite element model updating for cable stayed bridge has been discussed and then, the backdrop of active control of cable stayed bridge against seismic excitations has been explored.

1.2.1 Model updating of cable stayed bridges

Various FE modeling techniques have evolved down the age [Nazmy *et. al.* (1990), Wilson *et. al.* (1991a), Boonyapinyo *et. al.* (1994), Dyke *et. al.* (2000)] to represent the static and dynamic behaviour of the cable-stayed bridges. A cable-stayed bridge comprises of different structural elements, such as the cables, deck, pylon and bearings, each warranting a unique modeling approach. Owing to the complexity in modeling, the FE models usually fail to represent the experimentally observed modal characteristics. The modal identification of Quincy Bayview Bridge, Illinois, USA by Wilson *et. al.* (1991b) and of Bill Emerson Memorial Bridge, Missouri, USA by Song *et. al.* (2006) have indicated certain inadequacies of corresponding FE models by Wilson *et. al.* (1991a) and Dyke *et. al.* (2000). The modeling aspects of these two cases have been presented in the following paragraphs.

(a) Case-1: The FE model proposed by Wilson *et. al.* (1991a) for Quincy Bayview Bridge in Illinois, USA was an innovative model and was referred by Dyke *et. al.* (2000) to develop the FE model of Bill Emerson Memorial Bridge, Missouri, USA for phase-I benchmark problem for control of seismic response. The model by Wilson *et. al.* (1991a) was the first model of its kind to have the most compact representation of deck in the form of a spine with translational and rotational lumped masses connected to the spine by rigid links. The cables were connected to the spine through rigid links.

Other components of this model were, (1) modeling of cable as truss element using Ernst's equivalent Young's modulus, (2) beam element for modeling pylon and the spine and, (3) bearing links to model the deck-pylon connections. The bearing elements were idealized as vertical and horizontal links with fictitious material and sectional properties. The stiffness of the bridge structure needed for eigen value analysis was evaluated based on the design configuration. The configuration due to dead load was not used for the eigen analysis. During the modal identification of the structure by Wilson *et. al.* (1991b) using ambient vibration data, it was found that the numerical model was fairly successful in representing the flexural modes, albeit with slightly lower frequencies. However, more importantly, the model was not successful in capturing first few transverse experimental modes of the structure. It is, therefore, an important case for a study on model updating of cable-stayed bridge.

(b) Case-2: The FE model of Bill Emerson Memorial Bridge, Missouri, USA was developed for benchmark control problem for seismic response of cable stayed bridge [Dyke *et. al.* (2000), Turan (2001)]. The model was subsequently modified and transferred to Matlab® environment and was used for structural health-monitoring study by Caicedo (2003). The FE modeling was done in the line with that of Wilson *et. al.* (1991a) barring one major change. Constraint equations were used for modeling the rigid and bearing links instead of using the fictitious material properties. The bridge was instrumented extensively for collection of ambient vibration data [Celebi (2006)] with a total of 66 accelerometers located suitably over the structure and the surrounding soil. Based on this data, system identification was conducted using Auto-Regressive and Moving Average Vector (ARMAV) method by Song *et. al.* (2006). The data is also used for identification of the modal parameters with Natural Excitation Technique and Eigenvalue Realization Algorithm (NExT-ERA) by Caicedo *et. al.* (2006). In this method, first NExT has been used to create signals with the same characteristics of free-response data from ambient vibration records. These records have been used by the ERA to arrive at a state-space representation of the structure. Modal parameters such as natural frequencies, mode shapes and damping ratios have been calculated from the identified state-space model. Both the studies [Song *et. al.* (2006), Caicedo *et. al.* (2006)] have established limitations of the numerical model by modified by Caicedo (2003) in simulating the experimentally observed modal data.

The performances of FE models from Case-1 and Case-2 against respective modal identification data strongly suggest for a case for model updating of the two models. Proper updating to represent experimentally observed modal parameters is necessary to have more realistic models to go for investigation of the dynamic behaviour and control study on both the bridges. However, the nature of deficiencies of each of the models suggest for separate updating treatment for these. Accordingly the two cases for updating have been taken up.

(a) Updating option (Case-1): The cables being the structural element responsible for the distinctive behaviour of the cable-stayed bridge, modeling of cables have attracted significant research attention. It has been a normal practice among the researchers to model the cables as truss elements using equivalent Young's modulus of Ernst [Nazmy *et. al.* (1990), Wilson *et. al.* (1991a), Boonyapinyo *et. al.* (1994), Dyke *et. al.* (2000)]. However, researchers [Jayaraman *et. al.* (1981), Karoumi (1999)] have pointed out the lacunae of using truss element for modeling the cable in a cable-stayed bridge and have preferred to adopt the exact elastic catenary element for modeling the same. Jayaraman *et. al.* (1981) presented the formulation for a small-strain elastic catenary element and demonstrated its utility through static and dynamic problems. Karoumi (1999) simplified the formulation and used the same for 2-D analysis of a long span cable. The results were compared with single truss element with equivalent Young's modulus and it was observed that catenary element resulted in less deflection than truss element for higher tension in the cable. It was pointed out that equivalent modulus approach accounted only for slackening effect of the cable due to sag and not for its stiffening effect due to large displacements. It has been appreciated that the cable stayed bridge is subjected to high geometric nonlinearity during the dead load; however, it behaves almost linearly during subsequent live loads [Nazmy *et. al.* (1990), Karoumi (1999), Dyke *et. al.* (2000)]. Wang *et. al.* (1996) made a parametric study on cable stayed bridges for individual effects of different sources of nonlinearity. It was concluded that for dead load deformation analysis, the large deflection is found to contribute the most to the nonlinearity, with cable sag contributing the least. It may be recalled from the observations of Koroumi (1999) that the formulation for equivalent modulus for cable modeled as truss element accounts only for sag, whereas the geometry of the cable is accounted for in the formulation for cable as elastic catenary. Thus, it can be concluded from the observations by Wang *et. al.* (1996), in conjunction with Karoumi (1999), that catenary formulation for cable is more appropriate when dead load deformed structure is used for modal analysis. Karoumi (1999) had validated the superiority of catenary element in modeling cable comparison to that of the conventional truss element using a 2-D case. For 3-D representation of a cable Karoumi (1999) suggested for a formulation by Jayaraman *et. al.* (1981), where the out of plane stiffness of the cable element was extrapolated from the in-plane stiffness by dividing the same by the horizontal projection of the cable. It may be concluded that using the catenary element to model the cable in the FE model by Wilson *et. al.* (1991a) should lead to the representation of transverse behaviour of the bridge observed in the experimental modal characteristics by Wilson *et. al.* (1991b). Further, it should lead to a better representation of the flexural and torsional modes if the modal characteristics are tested on the configuration corresponding to the dead load deformation of the structure. This is due to the fact that the cable element gets stiffer during nonlinear behviour of the structure [Karoumi (1999)].

(b) Updating option (Case-2): Significant uncertainties in modeling of cable-stayed bridge may also arise due to idealization related to dimension, supports, local geometry etc. Model updating is more effective if it is based on system identification data. Updating of finite element model using structural identification data has emerged in 1990's as a subject of great importance for mechanical and aerospace engineering. However, identification-based model updating has been found to be difficult to apply to civil engineering structures. This is because of the difficulties in prototype testing and experimental data analysis arising from the nature, size, location and usage of these structures. Aktan *et. al.* (1998) conducted a parameter grouping and sensitivity study on a bridge by considering material properties, boundary and continuity conditions and geometric properties as the model parameters. Very few works have been reported on model updating of cable-stayed bridges. Research on applications of model updating method to dynamic assessment of a cable-stayed bridge was investigated by Brownjohn *et. al.* (2000). Zhang *et. al.* (2000) used optimization approach to update the FE model of a suspension bridge. The main approaches of system identification are enumerated by Zhang *et. al.* (2000) as: (a) optimal matrix updating, (b) sensitivity-based parameter estimation, and (c) neural-networks updating. Zhang *et. al.* (2001) updated the model of a cable-stayed bridge using sensitivity based parameter-estimation approach.

The ambient vibration method has been widely used [Wilson *et. al.* (1991b), Chang *et. al.* (2001), Ren *et. al.* (2004a), Ren *et. al.* (2005b), Ren *et. al.* (2005c), Giraldo *et. al.* (2006), Caicedo *et. al.* (2006)] in modal identification and health monitoring of cable stayed bridges, due to its simplicity and cost effectiveness. Stochastic Subspace Identification (SSI) method has been advocated by Giraldo *et. al.* (2006) as a better option than other output only identification methodologies for modal identification. In the study Giraldo *et. al.* (2006) concluded that the SSI requires less parameter to setup and is faster and easier to implement.

Model-updating can be more effective if it is carried out through optimization of selected FE parameters to match the identified modal characteristics. *Model to Generate Alternatives* (MGA) is an optimization technique to arrive at multiple choices of optimized solutions that have similar value of cost function. MGA was developed with the goal of providing solutions to complex, incomplete problems by coupling the computational power of computers with human intelligence [Brill *et. al.* (1990)]. MGA has been previously applied to land use planning [Brill *et. al.* (1992)], structural optimization [Baugh *et. al.* (1997)] and seismic design and evaluation supports for pipes [Gupta *et. al.* (2005)].

1.2.2 Control of cable stayed bridge against seismic excitation

Modern control strategies for seismic response control of cable-stayed bridge have evolved in the last decade. Passive control of a cable stayed bridge against seismic excitations was discussed on a simplified 2-D model by Ali *et. al.* (1995). In contrast to passive control devices, active control system is more flexible and effective in dynamically reducing the response of a structure against excitations, thereby increasing the safety and reliability of the structure. However, active control of cable-stayed bridges represents a challenging problem and very little has been reported in the literature on this subject. The problem particularly arises due to large number of degrees of freedom associated with 3-D modeling of the structure of flexible nature.

Dyke *et. al.* (2000) introduced the phase-I benchmark control problem for seismic response control of cable stayed bridge, the Bill Emerson Memorial Bridge, Missouri, USA in which a Linear Quadratic Gaussian (LQG) controller was designed and its efficacy was checked against select earthquake excitations. The block diagram for the controller has been shown in Fig. 1.1. Here $\mathbf{y_e}$ is the evaluation output, $\mathbf{y_m}$ is the measurement output, $\mathbf{y^s}$ is the discretized sensor output, **u** is the control signal, $\mathbf{y_f}$ is the feedback vector **f** is the force vector from control device and is the earthquake excitation.

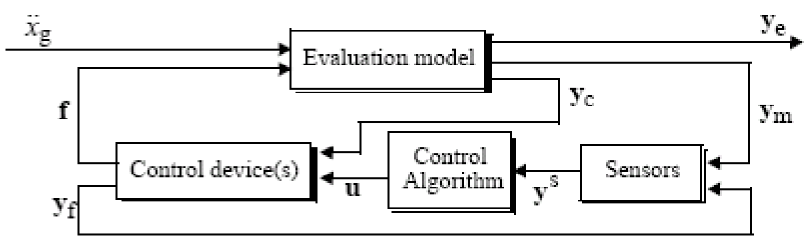

Fig. 1.1 Block diagram for representation of control system

The control devices comprised of hydraulic actuators that have been placed on the deck pylon interface and deck abutment/pier interface as shown in Fig. 1.2. The controller was evaluated based on its effectiveness in controlling the pylon forces at key locations. It was ensured that during this process the cable tensions were within permissible limits.

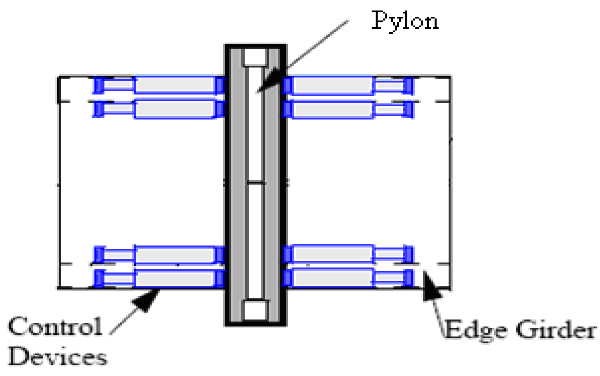

Fig. 1.2 Placement of actuators

He *et. al.* (2001) applied a resetting semiactive stiffness damper to control the peak dynamic response in the benchmark problem proposed by Dyke *et. al.* (2000) and validated its utility against the sample LQG controller. The schematic diagram of the system has been illustrated in Fig. 1.3. The utility of passive viscous and fluid dampers was also demonstrated in this study.

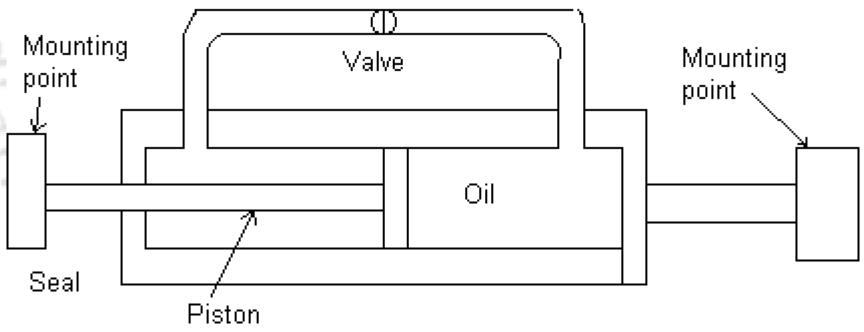

Fig. 1.3 Schematic diagram of stiffness damper

Park *et. al.* (2003a) presented a passive-active system for seismic response control of a cable-stayed bridge the arrangement of which has been shown in Fig. 1.4. Lead rubber bearings were used as passive devices, whereas hydraulic actuators were used as active controlling devices. A control algorithm based on LQG was used for the active controller. The arrangement for actuators and sensors has been illustrated in Fig. 1.4 (a) and configuration of the lead rubber bearings (LRB) and hydraulic actuators (HA) have been shown in Fig. 1.4 (b).

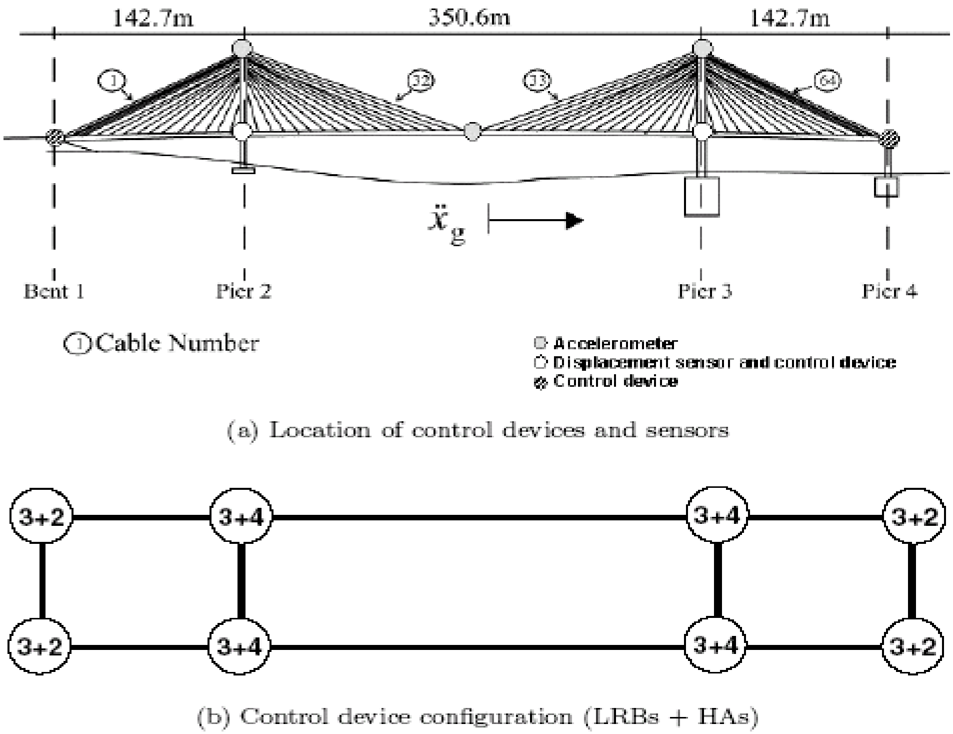

Fig. 1.4 Schematic diagram of Bill Emerson Memorial Bridge and location of control devices and sensors

Caicedo *et. al.* (2003) introduced the phase-II benchmark problem involving more complex structural behavior with the inclusion of multi-support and transverse excitations. In this study an active controller was designed and its efficacy was tested for control of key responses of the bridges. Yang *et. al.* (2003) applied two H_2 based control strategies for the phase-I benchmark bridge problem. The locations of the actuators have been illustrated in Fig. 1.5.

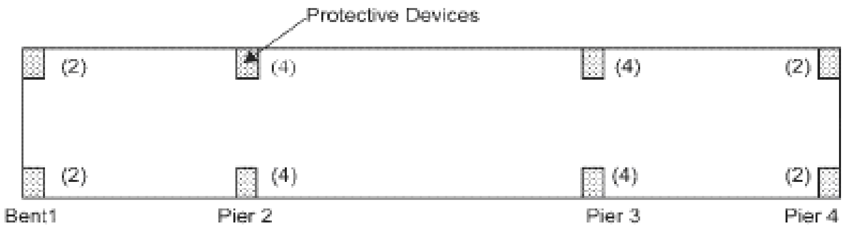

Fig. 1.5 Locations of control devices

Park *et. al.* (2003b) presented a hybrid control strategy for benchmark problem. The control devices were passive base isolation device with H_2/LQG based active control system of ideal hydraulic actuators. In a subsequent study, Park *et. al.* (2003c) included magnetorheological fluid damper (MRD) with Lead Rubber Bearing (LRD) for a hybrid control strategy for the phase-II benchmark problem proposed by Caicedo *et. al.* (2003). The block diagram for the control strategy has been illustrated in Fig. 1.6. Here $\mathbf{y_e}$, $\mathbf{y_m}$, $\mathbf{u}$, $\mathbf{y_f}$ and $\mathbf{f}$ have the same meaning as in Fig. 1.1. The vectors $\mathbf{x_f}$ and indicate the states signaling to LRD while $\mathbf{f}_{\text{passive}}$ and $\mathbf{f}_{\text{semi-active}}$ are the force vectors from the passive and semi-active devices respectively. and are the acceleration and displacement record from the earthquake input.

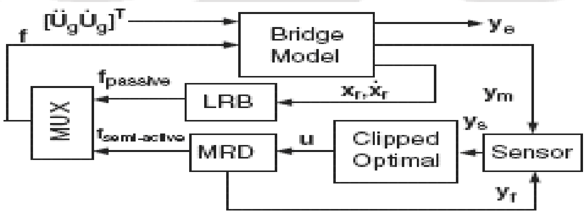

Fig. 1.6 Block diagram of hybrid control strategy combining LRDs and MRDs

Bontempi *et. al.* (2003) discussed three comparative schemes each of active and passive control on the phase-I benchmark problem. The block diagram for the active control strategy is the same as shown in Fig. 1.1, whereas the same for the passive control strategy has been illustrated in Fig. 1.7. The symbols in this figure have the same meaning as in Fig. 1.1

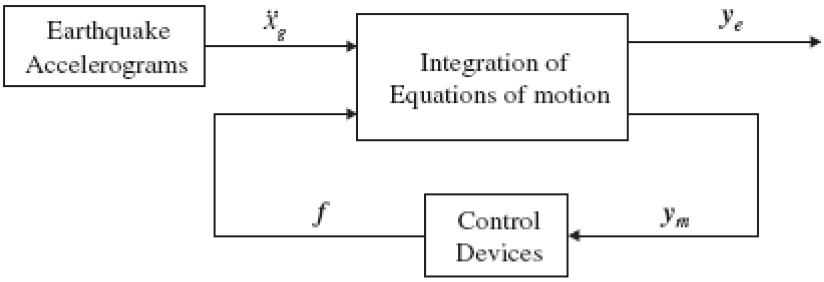

Fig. 1.7 Block diagram for passive control system

For the active control strategy the study proposed active hydraulic devices on deck-support connections and on longest cables. The scheme for placing sensors and actuators has been illustrated in Fig. 1.8. The passive devices included viscous, viscoelastic dampers and elastoplastic dampers.

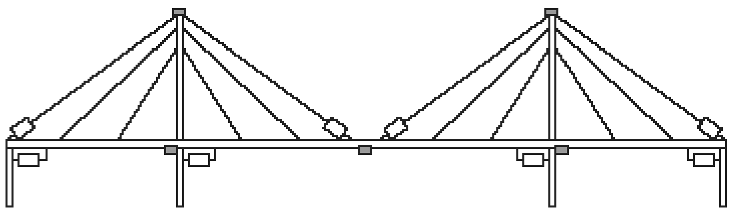

Fig. 1.8 Positions of actuators (   ) and sensors (   )

Iemura *et. al.* (2003) investigated the effectiveness of a variable damper employing pseudo-negative stiffness (PNS) control at deck pylon connections for the phase-I benchmark problem. The concept of interaction of PNS control device with member stiffness and the combined hysteretic loop has been illustrated in Fig. 1.9. The schematic diagram showing the placement of the different component of the control devices have been presented in Fig. 1.10.

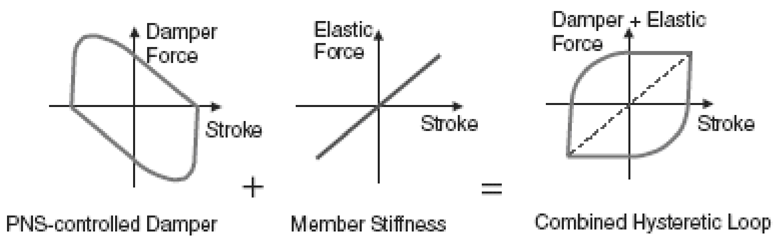

Fig. 1.9 Concept of PNS controlled damper and elastic member hysteretic loop

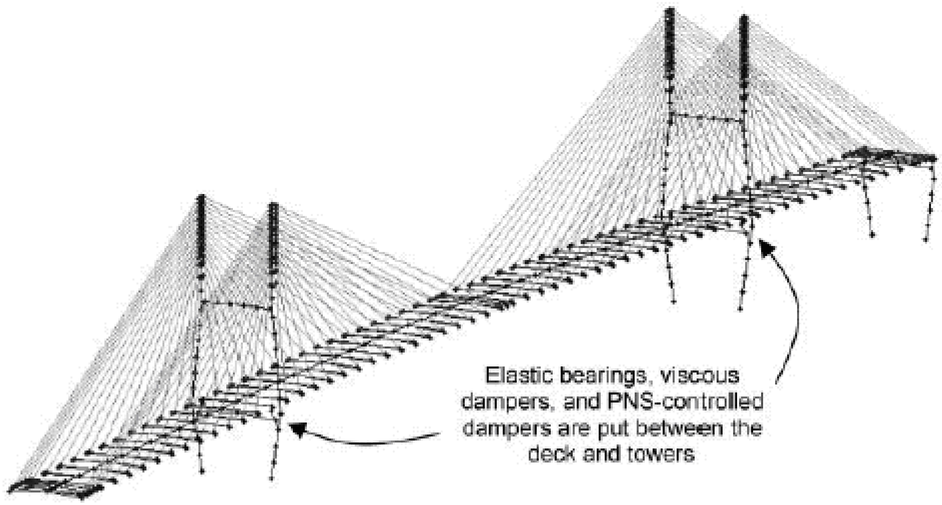

Fig. 1.10 The placement of control devices

Dai *et. al.* (2004) proposed a semiactive control strategy for the phase-II benchmark problem with magnetorheological damper and an LQG-clipped optimal control algorithm.

Kim *et. al.* (2005) proposed a wavelet-hybrid feedback least mean squared control algorithm on the phase-I benchmark model. Park *et. al.* (2005) introduced a hybrid method involving a hierarchical structure of a fuzzy supervisor with several sub-controllers for the phase-I benchmark problem. The schematic representation of this control strategy is as per Fig. 1.11.

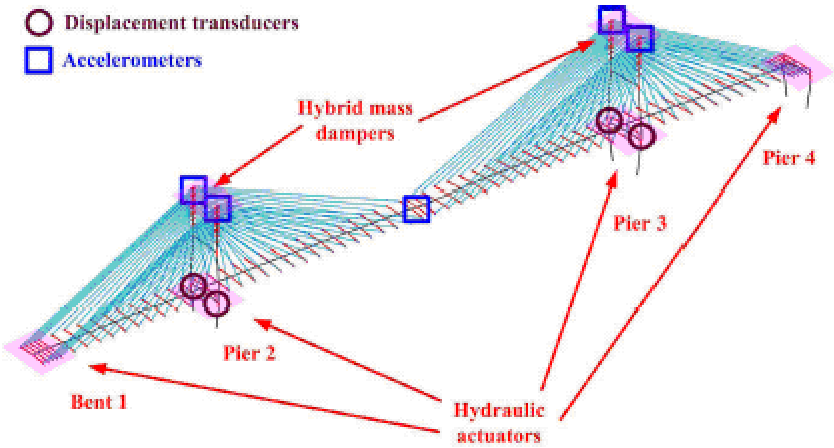

Fig. 1.11 Layout of control devices and sensors

It has been observed that among the available control strategies, active control strategy has been used as a benchmark to test and compare other control studies [Housner *et. al.* (1997)]. It is also adopted as the benchmark control strategy in problem formulated by Dyke *et. al* (2003). It has the potential to serve as a guide to building of real system while reducing the number of iterations in achieving this objective [Housner *et. al.* (1997)]. On the other hand, the semi-active control though excels over active control in its requirement of less power for implementation, the applicability is observed to be restricted. It is noted that "in most cases semi-active devices are designed to operate in the 'post yield' region, when the stress exceeds some controllable threshold; this makes them inappropriate for vibration of small amplitude where the stresses remains below the minimum controllable threshold in the device" [Preumont (2002)]. In case of cable-stayed bridges, the nonlinearity has been assumed to be predominantly geometric, which arises out of large dead load deformation of the structure. The structure is therefore expected to be in the 'pre-yield' stage and hence the active control strategy is preferred over the semi active control.

1.3 Objective and Scope of the Present Study

In this section the objective and scope of the present work has been enumerated based on the detailed literature survey.

1.3.1 Objective of the present investigation

In the present investigation, two bridges, namely, Quincy Bayview Bridge, Illinois, USA and Bill Emerson Memorial Bridge, Missouri, USA have been chosen as sample cable-stayed bridges for the studies on seismic response control. These two bridges have been selected due to the availability of structural details including sectional as well as material properties. Further, experimental responses of both the bridges are also available in the literature. However, the literature review has made it clear that the FE models of Quincy Bayview Bridge, Illinois, USA by Wilson *et. al.* (1991a) and Bill Emerson Memorial Bridge, Missouri, USA by Dyke *et. al.* (2000) and Caicedo *et. al.* (2003) are not fully adequate in representing the experimentally observed modal characteristics. These models are needed to be updated appropriately before these could be further used for dynamic response evaluation of the structure against seismic excitation. It has also been observed from the literature that certain cable tensions cross the permissible limits under certain seismic excitations and hence seismic response control has been felt necessary. An active control strategy has been adopted in the present study for the seismic response control of both the bridges. Accordingly, active controllers are needed to be designed against seismic excitations using these updated models to realize a more realistic control strategy. The controller is required to be tested in line with the benchmark problem of cable-stayed bridge for control of seismic response by Dyke *et. al.* (2000).

1.3.2 Scope of the present investigation

The scope of the present investigation has been explored in this section with an aim to realize the objectives cited in the previous subsection. It has been realized that the updating of the two FE models may be done with the help of respective experimental modal identification data. However, the same approach of updating may not work for both the models as the identified inadequacies of the respective models are different in nature. In the first model, the lacuna was primarily with respect to non representation of experimentally observed transverse behaviour, while in the second, it was the non representation of the identified flexural frequencies. Further, in the second case, the update could be carried out using the available ambient vibration data. Accordingly, the scope of updating the two models may be identified separately. Once the models are updated, active control strategy may be implemented using these models.

In case of updating the FE model of Quincy Bayview Bridge, Illinois, USA, the primary update may be contemplated in terms of modeling the cable element. The equivalent truss element may be replaced by the elastic catenary element. It is expected that the by virtue of the cable becoming stiffer in its plane during large displacement [Karoumi (1999)], the flexural frequencies would be better represented. However, the most significant scope for improving the dynamic characteristics of the model is corresponding to the representation of the lateral mode, which arises from the fact that in the catenary formulation, cable has less out-of-plane stiffness in comparison to planar stiffness [Jayaraman (1981)]. This apparently is more natural and is likely to provide closer representation of the actual structural behaviour of the cable. Further, the FE model of the bearing element may be done using constraint equation instead of using fictitious sectional and material properties. It is expected that updating the model with the use of constraint equation would make the model more numerically stable for further analysis as well as for employing the active control strategy. Moreover, the observed lower frequencies in flexural modes may also be due to the adoption of a linear model for eigen analysis. For a highly nonlinear structure such as such as the cable stayed bridge, it is always appropriate to use the dead load deformed configuration as the basis for the model to be used for eigen analysis. Hence, there exists a scope to improve the FE model for the bridge using the configuration arrived through nonlinear static analysis. There is further scope for using stability functions in the beam element formulation of the FE model to account for the P-Δ effect in deck and pylon while the structure deforms under dead load. The more conventional penalty approach in representing boundary conditions in the FE model may also be avoided as this could introduce numerical instability during nonlinear static analysis. Thus, it is very likely that these modifications would result in an updated finite element model that would represent the flexural and torsional modes of the experimental observations to a closer extent.

The FE model for Bill Emerson Memorial Bridge, Missouri, USA presents a case for an optimization-based update as ambient vibration data is available for this structure. Here, the experimentally observed mode shapes are the same as that from the FE model, but the corresponding frequencies are much higher. Hence the natures of updates are expected to be different to that of the model for Quincy Bayview Bridge. The modal parameters can be identified using SSI. Significant structural parameters such as deck-pylon interface, deck-mass and deck-stiffness may be optimized to match the available modal parameters. Optimization of the structural parameters may be carried out to form alternative updates using MGA. Finally the updated model could be selected by choosing the most realistic model among all the alternative solutions.

There is further scope for using both the updated FE models for evolving active control strategy against seismic excitations. The controllers based upon these models are likely to be more realistic in nature. The reason behind this is the fact that these FE models are based on the updated models that represent the dynamic characteristics of the actual structures to the closest extent. It has been observed that active control system can work as linear controller, which is simple to execute through a digital implementation. Amongst the other control alternatives, the hybrid system is relatively complicated to implement as it is a two system controller. Moreover, the passive part of the hybrid controller is basically a nonlinear controller. As the present controller has been assumed to be a linear one, the study has been limited to an active controller only. Looking at the background of active control strategy using modern algorithms such as the LQG it has been appreciated that the controller works on the states from a numerical model [Tewari (2002)]. However, to make the FE model manageable for implementation of active control strategy, proper reduction scheme may be adopted to arrive at more compact model to design the control strategy. These reduction schemes are to be validated so that the reduced models are able to represent the modal properties of the respective structures. The model may be represented in states space to devise the modern control strategy such as an LQG based controller. The controller must also be tested for stability. Then the controllers may be evaluated based on its controlling performance in the line with the benchmark criteria. The controller may also be checked against various types of earthquake excitations to validate its robustness. Moreover, both uniform support and multiple support cases may be investigated for the selected excitations. Finally the control may be simulated numerically using modern software such as the Simulink® from control system toolbox of Matlab®. The controllers for both the bridges may be tested against the same seismic excitations as the bridges fall into same geographical location.

1.4 Outline of the Thesis

The thesis has been organized into six chapters.

The second chapter deals with the updating of the FE model of Quincy Bayview Bridge, Illionois, USA. Updates have been proposed after comparison of modal characteristics of the FE model with those from experimentally observed modal parameters. Alternative updated models have been presented using a combination of modeling options. The configurations corresponding to the dead load deformed structure have been arrived at by carrying out nonlinear static analysis on the models. Modal characteristics for each alternative model corresponding to this configuration have been evaluated and compared with that from identified results. The model that represents the identified modal characteristics to the closest extent has been chosen as the updated model.

In the third chapter design of an active controller for the Quincy Bayview Bridge against seismic excitation of select earthquakes has been presented. Guyan Reduction scheme has been implemented for the updated model from Chapter 2. Transfer function has been used to validate reduction process. Sensors and actuators have been interfaced to the model and it has been represented in state space environment. The state space model has been further reduced with balance realization to remove the states that have less contribution towards controllability and observability of the system. N-S excitation components of three representative earthquakes, El Centro, Mexico City and Gebze have been selected for checking the efficacy of the controller in reducing key structural responses. An LQG controller has been designed and numerically simulated against the uniform support and multiple support excitations of selected earthquakes using Simulink® of Matlab®.

The fourth chapter takes up the updating of the FE model of Bill Emerson Memorial Bridge. Modal identification has been carried out using the SSI and the identified parameters compared with those from the FE model. The structural parameters for updating of the FE model have been chosen. MGA has been used to obtain alternative solutions using nonlinear minimization technique. The best update has been chosen from these alternatives.

Design of active controller for the updated model of the Bill Emerson Memorial Bridge against seismic excitation has been taken up in the fifth chapter. The updated model from Chapter 4 has been used for designing the controller. A procedure, similar to the one adopted for the design of the controller in case of Quincy Bayview Bridge as in Chapter 3, has been followed here.

Summary and conclusion have been presented in the sixth and the last chapter. Conclusions from model updating and design of controller from both the bridges have been presented. It has been concluded that model updating is unique for a particular bridge and distinctive strategy is needed for the same. Future scope of model identification of the Bill Emerson Bridge has been discussed in particular. In this context, the possibility of further update based on the results of more sensor data, has also been discussed. The scope for further control studies has also been included.

1.5 Conclusion

The broad frame-work for the current study of model-updating and design of active controllers against seismic excitations for two real-life bridges have been presented in this chapter. The background of the problem has been discussed in detail. The objectives for the present work have been defined and the scope of achieving the same has been presented. The detailed organization of the present work has also been presented at the end.

Chapter 2

MODEL UPDATING OF QUINCY BAYVIEW BRIDGE,

ILLINOIS, USA

2.1 Introduction

This chapter deals with the updating of a three dimensional (3-D) FE model of Quincy Bayview Bridge, Illinois, USA as introduced by Wilson *et. al.* (1991a). The objective of the updating is to arrive at a model, which simulates experimentally observed modal characteristics to the closest extent. The updating has been attempted primarily by using catenary element for modeling of cables in place of equivalent truss element, constraint equations in place of bearing elements in the deck-pylon interface as well as for rigid links connecting the spine with cables. Due to the existence of large axial force, the *P*- effect for deck and pylon members have been considered. The configuration of the updated model for linear dynamic analysis is adopted from the dead load deformed shape, which has been arrived at using nonlinear static analysis. The modal characteristics of the updated model have been validated with experimentally observed values. Further, the performance of the updated model has also been compared with alternative models formed by a combination of truss or catenary element in modeling of stay cables, and with or without *P*- effect on deck and pylon.

2.2 Structural Description

The Quincy Bayview Bridge, Illinois, USA was designed in 1983 and was completed in 1987. The view of the structure is shown in Fig. 2.1. The material and sectional properties of different components of the bridge are described in detail in Wilson *et. al.* (1991a) and are provided briefly in this section.

Fig. 2.1 Quincy Bayview Bridge, Illinois, USA

The bridge consists of two H-shaped concrete pylons, double-plane fan type cables, and a composite concrete-steel girder bridge deck. The main span is 274 m and there are two equal side-spans of 134 m for a total length of 542 m. There are a total of 56 high strength steel cables, 28 supporting the main span and 14 supporting each of the side spans. The sectional details of the deck slab have been illustrated in Fig. 2.2.

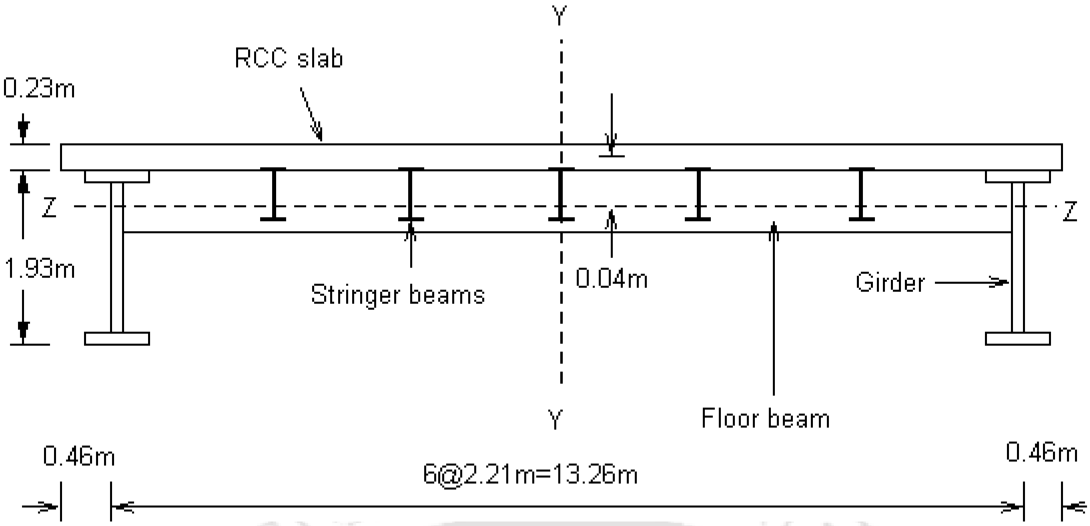

Fig. 2.2 Deck sectional properties [Wilson *et. al. (1991a)*]

The deck is 12 m wide measured centre to centre of cables. It is made of pre-cast post tensioned concrete slab with thickness and width as 0.23 m and 14.18 m respectively. The slab is supported by five longitudinal steel stringers equally spaced at 2.21 m c/c. Floor beams, oriented in the transverse direction to the main girder, are spaced at 9.14 m c/c. They transfer the loads of the slabs to the main girder oriented longitudinally along the edges of the deck. Supplementary longitudinal beams, cross bracings and bearing plates are used at these anchoring locations for strengthening purpose. The sectional details of each of the pylon have been presented in Fig. 2.3.

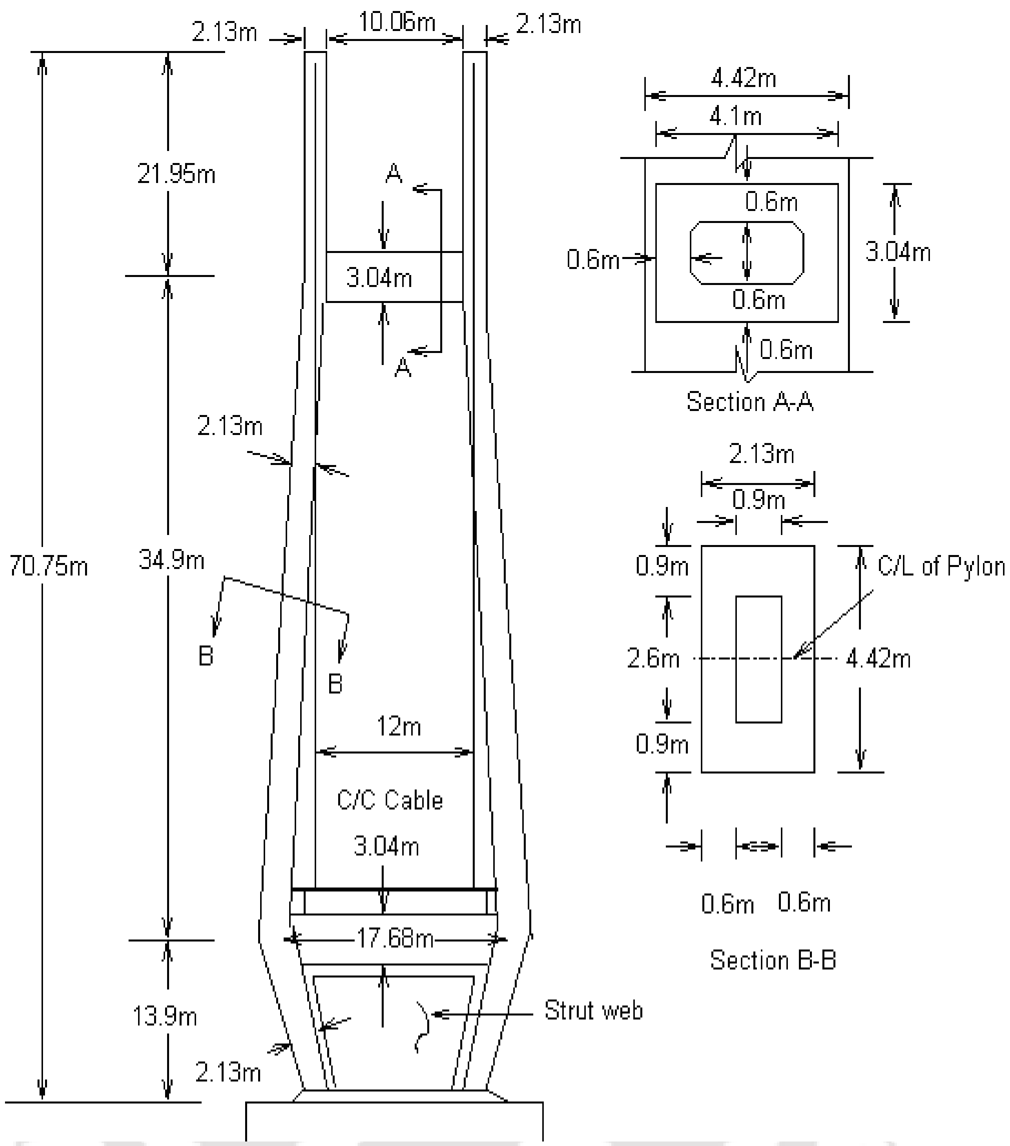

Fig. 2.3 Pylon sectional properties [Wilson *et. al. (1991a)*]

Each of the pylons consists of two concrete legs, an upper strut connecting the two legs and a lower strut supporting the deck. The cross-sections at different locations of the pylon have been illustrated in the Fig. 2.3. The pylon legs below the deck are of solid concrete connected by a 1.22 m thick stiffening wall acting as web.

The bearing system comprises of vertical link, steel and elastomeric bearing. The deck is tied down to the abutments by a tension link mechanism. This permits rotation of the deck about vertical and transverse axes. There are horizontal and vertical bearings at each of the deck-pylon interface. The vertical steel bearing allows the deck to slide in the longitudinal direction. It is restrained from excessive sliding by elastomeric bearings at these locations. Rotation of the deck about the transverse axis is permitted here.

The cables comprise of 6.4 mm diameter wires with an ultimate strength of 1600 MPa. They are of four different cross sectional areas: (1) 89.67 cm^2, (2) 67.74 cm^2, (3) 53.67 cm^2 and (4) 34.83 cm^2, as shown in Fig. 2.4. The cables are helically wrapped with a polyethylene covering and are grouted and sealed. They are anchored to the main girders and floor beams at 18.29 m interval, where the spacing for side span is 19.20 m. The cables are connected to the pylon top at an interval of 2.74 m.

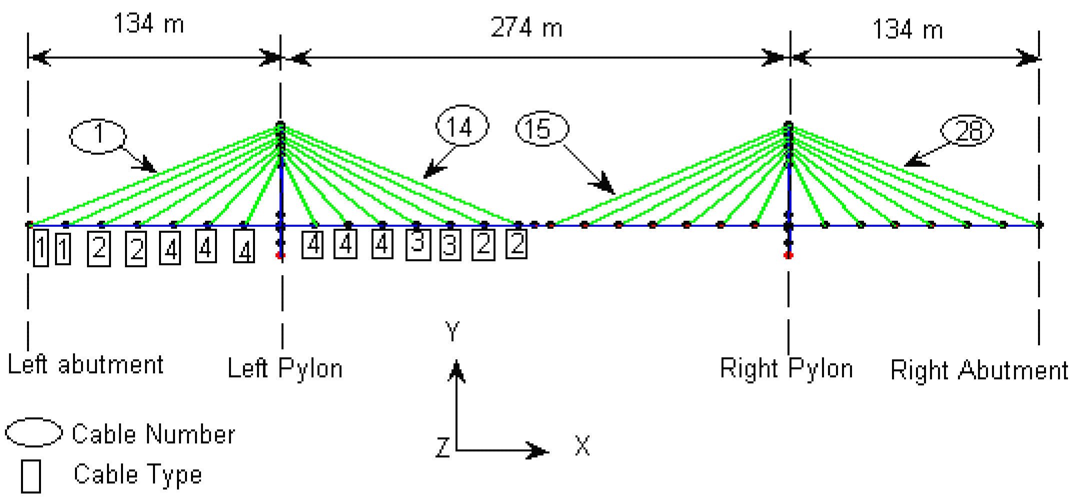

Fig. 2.4 Line diagram of the bridge with cable type

2.3 Finite Element Modeling

The detailed finite element modeling of the updated structure is presented in this section. The modeling of each of the different components of the structure, e.g. deck, cables, pylons and bearings has been dealt with separately.

2.3.1 Modeling of deck

The modeling of the deck is followed from the model adopted by Wilson *et. al.* (1991a). It is observed that the modeling the deck as single spine concept fails to simulate torsional behaviour of the deck. Hence the cross-section of the deck is considered as thin walled open section. This is converted as an equivalent steel C-section with dimensions as shown in Fig. 2.5. The sectional properties adopted for equivalent C-section are as follows: area: 0.8268 m^2, transverse moment of inertia: 19.75 m^4, vertical moment of inertia: 0.3409 m^4 and torsional moment of inertia: 0.0271 m^4.

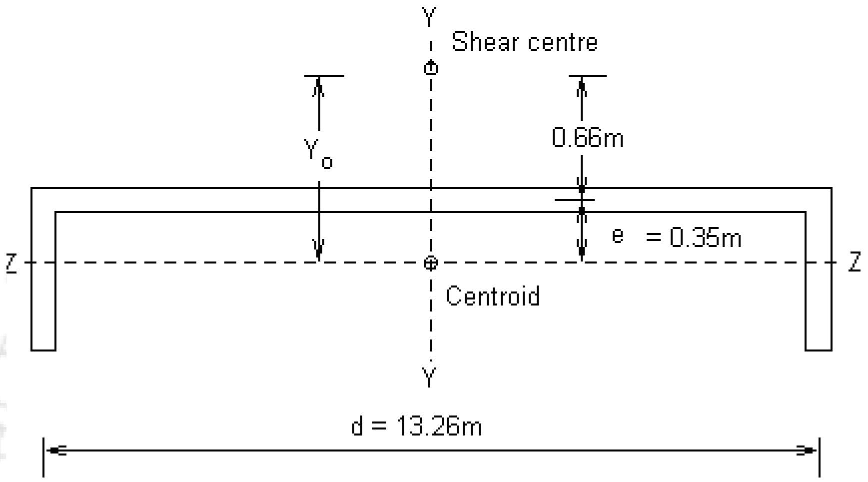

Fig. 2.5 Equivalent steel C- section for deck [Wilson *et. al. (1991a)*]

Referring to Fig. 2.5, shear centre is located through C-section analogy as,

(2.1)

where, Y_0 is the distance between shear centre and centre of mass, e is the distance between the neutral axis and the middle of the concrete slab, d is the distance between the webs of the two steel beams located along the edges of the deck, A is the transformed cross-sectional area of deck and I_z is the moment of inertias about Z axis.

Pure torsional constant for a thin walled C-section is given by,

(2.2)

where, b is the depth of element and t is the flange thickness. The warping constant is calculated as,

(2.3)

where, I_y is the moment of inertias about Y axis. Taking account of this effect of warping, the equivalent torsional stiffness of the deck is obtained as in Wilson *et. al.* (1991a),

(2.4)

where, G is the shear modulus of steel, J_{eq} is the equivalent torsional constant, J_{pure} is the pure torsional constant, E is the modulus of elasticity of steel, and L is the length of the main span. The equivalent sectional and material properties of the C-section have been ascribed to the spine. The spine is located along the shear centre of the C-section and is discretized using beam elements.

The connectivity of the cable ends to the spine is done through rigid link as per the model proposed by Wilson *et. al.* (1991a). The distribution of lumped masses from different components of the deck in the model considered by Wilson *et. al.* (1991a) is shown in Fig. 2.6.

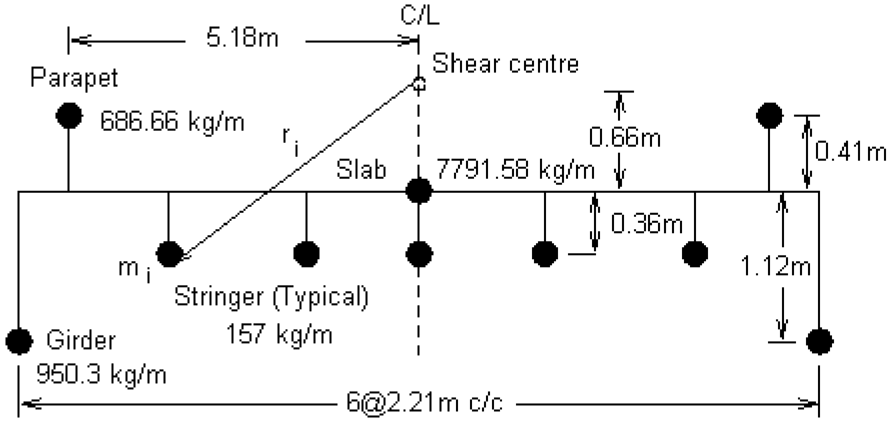

Fig. 2.6 Mass distribution of the deck [Wilson *et. al. (1991a)*]

The representation of lumped masses is further simplified in the model [Wilson *et. al.* (1991a)] with two lumped translational masses at the ends of rigid links. This mass distribution has been shown in Fig. 2.7. The calculated translational mass for each deck segment for main span is 113857.75 kg, whereas the same for the side span is 108401.58 kg.

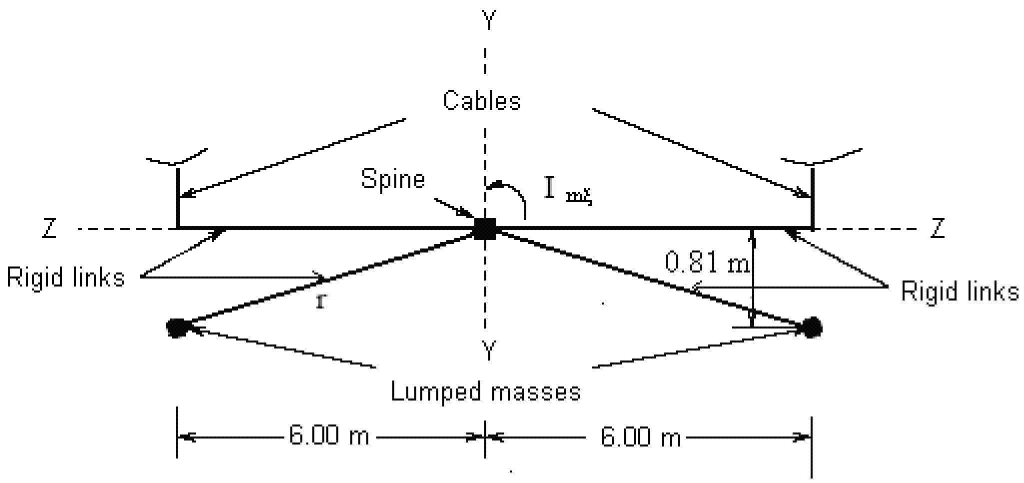

Fig. 2.7 Finite element model for deck

Mass moment of inertia for the deck is calculated using,

(2.5)

where, is the actual mass moment of inertia of deck segment between the cable anchor points about axis (where represents X, Y, Z). is mass moment of inertia of ith element about its own centroidal axis, m_i is elemental mass, r_i is radial distance of ith mass from the centre of rotation (Fig. 2.6). Certain corrections are to be made to the mass moment of inertia of the spine node as the distributed masses are lumped and placed at the end of the rigid links. These corrections are computed as follows:

$$\Delta\xi = \quad (2.6)$$

Here, $\Delta\xi$ is the corrective mass moment of inertia about ξ axis (ξ is for X, Y, Z), M is the lumped mass(kg) and r(m) is the radial distance of lumped mass from shear centre. The corrections for side span and main span are as shown in Table 2.1 [Wilson *et. al.* (1991a)].

Table 2.1 Mass moment of inertia (kgm^2) correction at spine node

Correction Component	Side Span	Main Span
ΔX	-3437505.38	- 3273011.26
ΔZ	3041032.37	2315571.11
ΔY	7971638.25	700154.47

2.3.2 Modeling of pylon

Pylons are discretized with beam elements with nodes introduced at locations of sectional changes. A comparatively coarser mesh has been considered adequate as the pylon is much stiffer than the deck. The beam formulations with or without stability factors accounting for *P-* effect has been adopted in order to evaluate the influence of beam column effect on the model as the structure deforms under dead load. This approach has also been adopted to model the deck.

2.3.3 Beam element formulations including P- effect

The finite element formulation for beam element to account for the *P-* effect in beam element through stability functions have been enumerated by Nazmy *et. al.* (1990).

The 12×12 element stiffness matrix has been presented in Eq. (2.7) with reference to notations in Fig. 2.8.

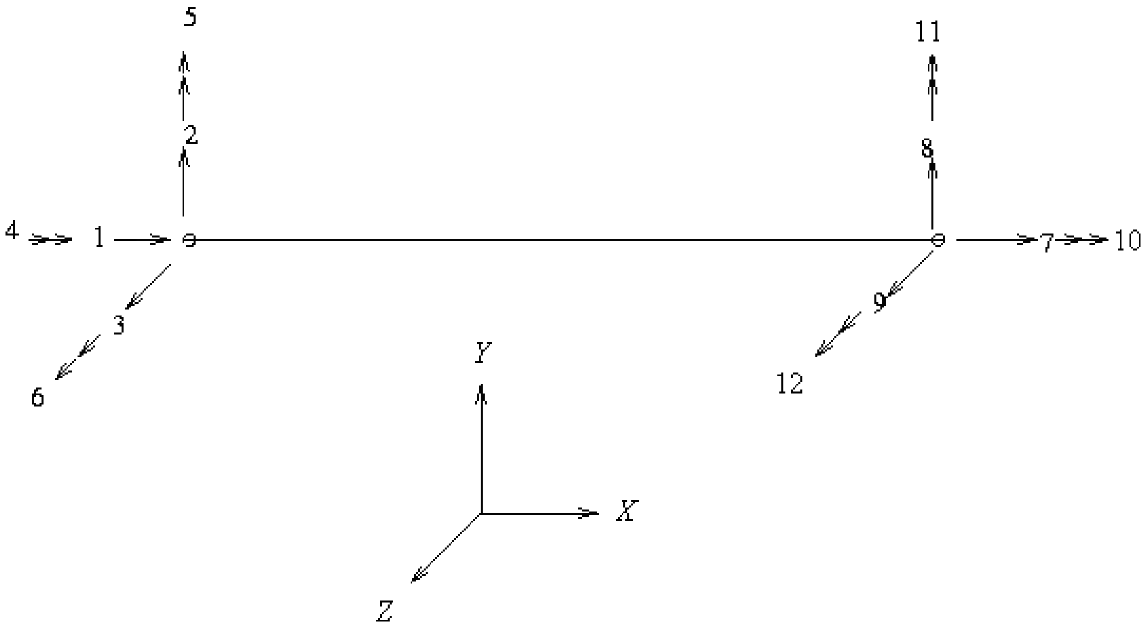

Fig. 2.8 Degrees of freedom of a beam-column element in local coordinates

(2.7)

where, L is the member length, and the S's are the stability functions.

through modify the bending stiffness of the member about the local Y *axis,* while through modify the bending stiffness of the member about the local Z axis; modifies the axial stiffness. If axial forces in the bending member are zero, all the S's take the value of unity. The stability functions can be expressed in terms of member axial force P, the member end moments M_1 and M_2 at both ends about the local Y and Z axes, as shown in Fig. 2.9.

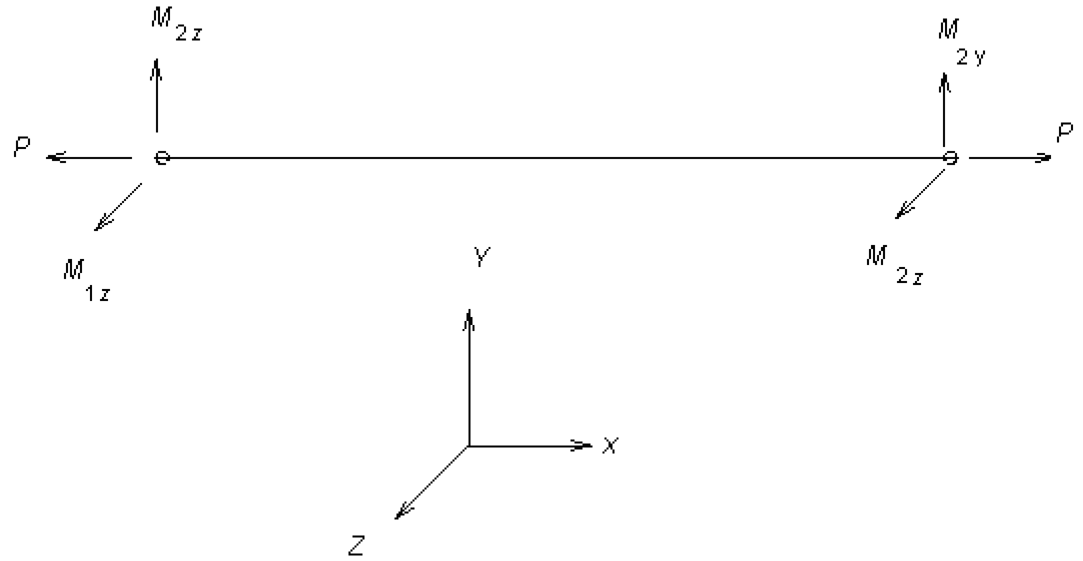

Fig. 2.9 Axial forces and end moments for a beam element

For a tension member (P is positive) the stability functions through are as shown in Eqs. (2.8) to (2.11),

(2.8)

(2.9)

(2.10)

(2.11)

where, , , and (2.12)

For a compression member (P is negative), the stability functions are defined as,

(2.13)

(2.14)

(2.15)

(2.16)

where, (2.17)

The stability functions S_{1y} through S_{4y} can be determined in the same way by replacing I_z by I_y in the above equations. The stability factor S_5, corresponding to axial dofs, can be determined following the procedure enumerated below:

For a tension member (P is positive),

(2.18)

where,

(2.19)

in which, and,

(2.20)

in which, .

For a compression member (*P* is negative),

(2.21)

where,

(2.22)

and,

(2.23)

The stiffness matrix for a beam-column element, as given by Eq. (2.7), is in fact the secant stiffness matrix. The tangent stiffness matrix of such an element has been obtained using the large deflection theory and nonlinear strain-displacement relationship [Nazmy *et. al.* (1990)] as,

(2.24)

where, is the beam element tangent stiffness matrix in the local coordinates, is the elastic stiffness matrix of the beam element given by Eq. (2.7), and is the geometric stiffness of the beam element.

The geometric stiffness matrix is given by,

(2.25)

in which, *P* is the axial force in the beam, and *L* is its length.

2.3.4 Modeling of cable

Two primary approaches for modeling of cables have been discussed in this section. The cable has been modeled as both truss element with equivalent modulus and as catenary element.

(a) Stiffness of cable as equivalent truss element: Modeling the cable as a truss element with Ernst's equivalent Young's modulus is written as,

(2.26)

where, *is equivalent modulus,* E *is Young's modulus of cable material,* w *is the* unit weight of cable per unit length, *is horizontal projected length of the cable,* A *is* the cross sectional area of the cable, *T* is the prevalent cable tension. As pointed out by Karoumi (1999), the formulation in Eq. (2.26) can account only for the slackening of the cable from sag due to self weight; the stiffening effect on the cable due to large displacement, which is generally the case with flexible structures like the cable stayed bridge, cannot be properly accounted for in this formulation.

(b) Stiffness of cable as elastic catenary element: The stiffness formulation of cable as catenary element has been developed following the procedure enumerated in Jayaraman *et. al.* (1981). The typical cable profile with associated forces is illustrated in Fig. 2.10, where H and V being the horizontal and vertical projection on local *X* and *Y* axes, F_1 through F_4 are the nodal forces at the nodes *i* and *j* in the direction of local *X* and *Y* axes.

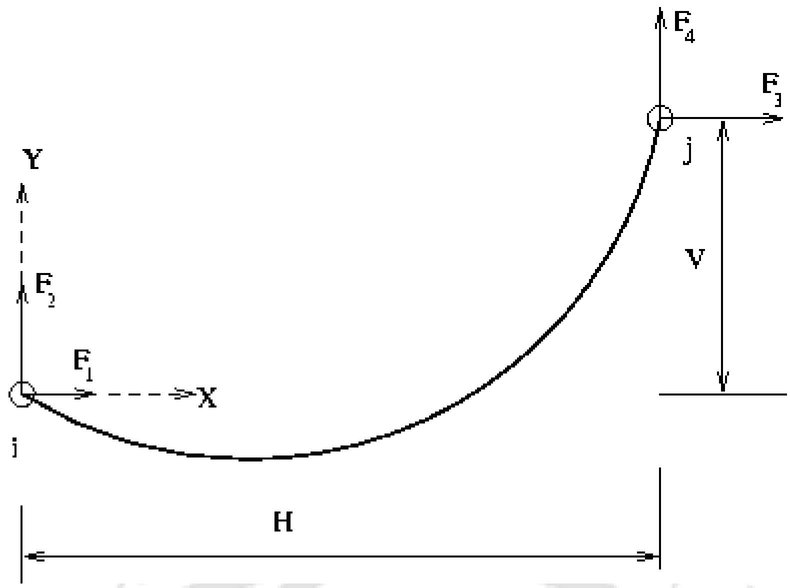

Fig. 2.10 Catenary element

The flowchart shown in Fig. 2.11 explains the iterative procedure for arriving at the nodal forces in the cable element.

Input: *w, E, A,* L_u *, tolerance, co-ordinates of nodes i and j*

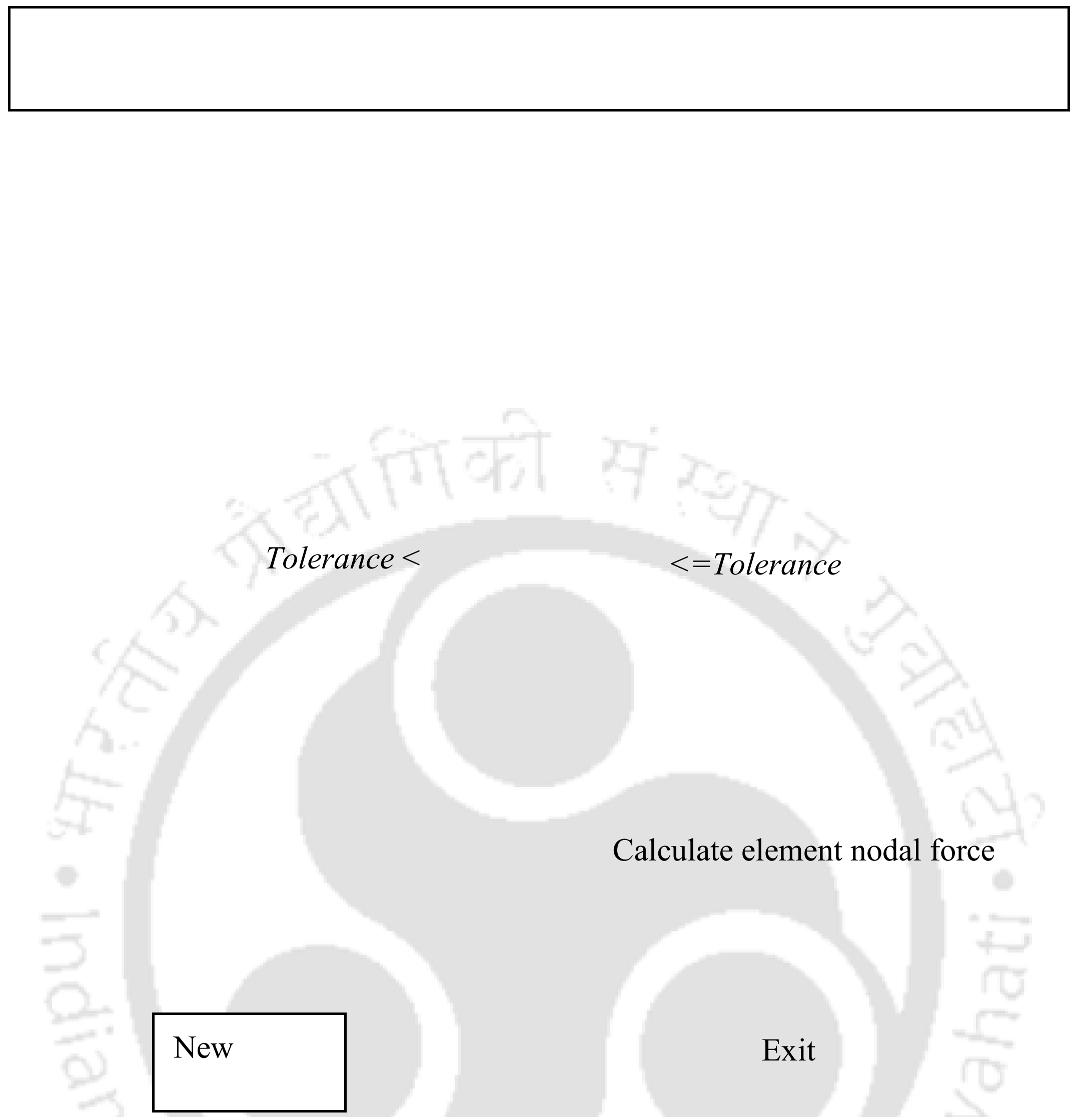

Fig. 2.11 Flowchart for catenary element analysis

After the evaluation of the nodal forces, the element stiffness matrix for elastic catenary is written as [Jayaraman *et. al.* (1981)],

(2.27)

where, the coefficients are in terms of the nodal forces. It may be noted that the stiffness in the out of plane (*YZ* plane) is extrapolated from the inplane stiffness (*XY)* by dividing the nodal force with the horizontal projection of the cable (*H)*. Since the value of *H* is quite large, it is clear that the out of plane stiffness of the cable will be quite low as compared to the inplane stiffness. When this catenary element is used to model the cables for the bridge, it is expected that the above mentioned low out of plane stiffness should help in representation of the transverse mode of the deck as observed in the experimental results.

The stiffness matrix is evaluated in the local *XY* plane (in the plane of the element) and is transformed to the global *XYZ* coordinate system for assemblage into the structure stiffness matrix by the usual coordinate transformation technique. The transformed stiffness matrix is as given in Eq. (2.28),

(2.28)

where,

(2.29)

Here, and are the cosine and sine of the angle between the local xy plane and global XY plane of the cable.

It has been observed that the formulation of elastic catenary element accounts for large displacement of the nodes in addition to sag effect of the cable due to self weight. Thus, catenary element represents the true nature of the cables as structural elements, which are flexible in nature and undergo large displacement in field condition. Most importantly, this formulation represents the low out of stiffness of the cable to a closer extent.

(c) Element mass matrix: Mass discretization is done by lumping of the element mass at both ends of the cable. Lumped masses at the nodes are given by where, is the unstressed length of the cable, A is the area of cross section of the cable and ρ is the mass density of the cable material.

2.3.5 Rigid links

The concept of kinematic constraint is used for modeling the rigid links, where constraint equations relate the displacements of two joints. The procedure is presented in detail in SAP manual (2000) and also enumerated by Franklin *et. al.* (2002). One of these two joints is termed as *master*, to which the displacements of the other joint, termed as *slave,* can be related. Eqs. (2.30) relate the translations (, ,), the rotations (, ,) and the coordinates (x, y, z) of the master *and the* slave*, all taken* in the constraint local coordinate system.

(2.30)

where, , *and* . Here, the suffix s *stands* for *slave* and *m* represents *master* node. The displacements of *slave* node can thus be transformed from the displacements of the *master* node through the transformation matrix as follows,

(2.31)

In the context of the present study, the spine nodes are considered as the *master* nodes and the nodes connecting the cables to the spine via rigid links are considered as the *slave* nodes for the evaluation of stiffness. For transformation of mass, the lumped mass nodes on the either side of the spine are considered as *salve* nodes. Thus, corresponding to each *master* node along the spine, there exist two *slave* nodes on either side of spine. With these transformation matrices, the mass and stiffnesses of the slave nodes are transformed to the spine master nodes. The representation of rigid links in terms of kinematic constraints can thus result in substantial reduction of the degrees of freedom.

2.3.6 Modeling of bearing

The deck-tower bearings have been modeled using the constraint equations Eqs. (2.30). In the finite element model, the spine node (*slave* node) is constrained with the pylon nodes at lower strut (*master* nodes) as illustrated in Fig. 2.12.

The constraint equations are applied with respect to translational dofs in the longitudinal direction and in the rotational dofs about the vertical axis. These equations represent the boundary conditions that permit the end of the deck to rotate freely about the vertical *(Y)* and transverse *(Z)* axis. Rotation about the longitudinal axis *(X)* and all three translational dofs are restrained in the two abutments.

The discretized model of the cable-stayed bridge as per the model proposed by Wilson *et. al.* (1991a) is shown in Fig. 2.13. The model has 82 beam elements, 56 cable elements. In the updated model 10 constraint equations have been used to represent the bearings between deck and pylon. The 128 rigid links of the model connecting the spine nodes with the cable ends and the translational masses are also represented by constraint equations. The updated model has a total dof of 458, whereas the original 3-D finite element model in Wilson *et. al.* (1991a) contains a total dof of 1248. The pylon bases have been considered as fixed with respect to all the displacement components.

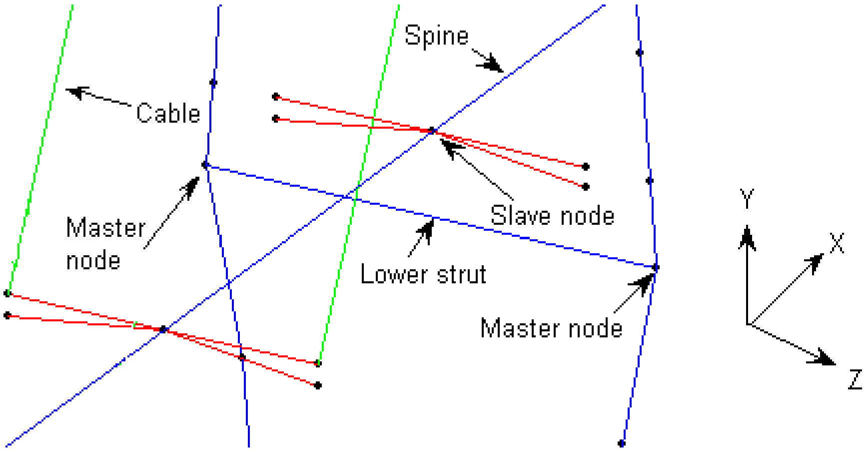

Fig. 2.12 Master and slave nodes in pylon-bearing connection

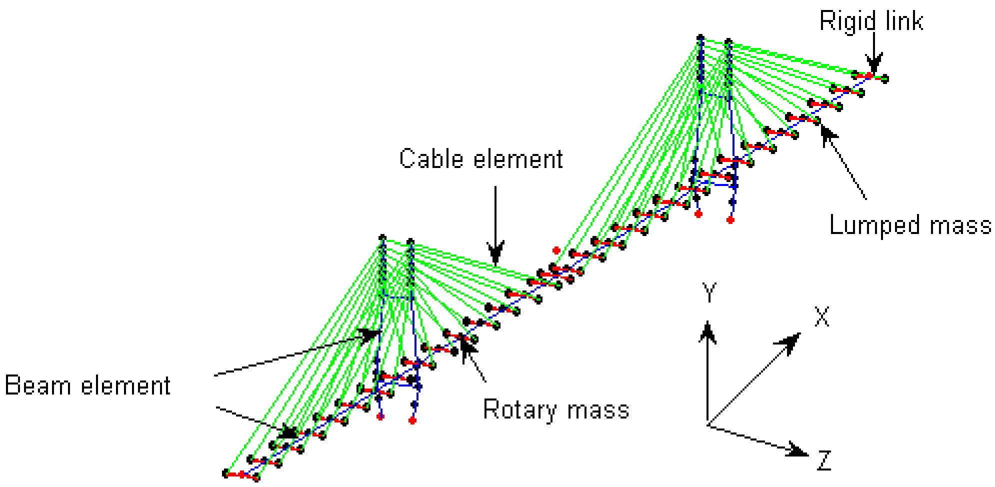

Fig. 2.13 Finite element model

2. 4 Nonlinear Static Analysis

The basic difference between non-linearity of a cable structure and a non-cable structure is illustrated in Fig. 2.14. It is apparent from the figure that the stiffness of the non-cable structure shows a progressively decreasing tendency while that of a cable structure shows a gradually increasing tendency. Nonlinearity of non-cable structure is primarily because of material nonlinearity, which results in decreasing stiffness because of onset of plastic deformation. On the other hand, nonlinearity of cable structure is geometric. It has a stiffening effect due to large displacement [Karoumi (1999)]. Hence its stiffness shows progressive increasing tendency, instead.

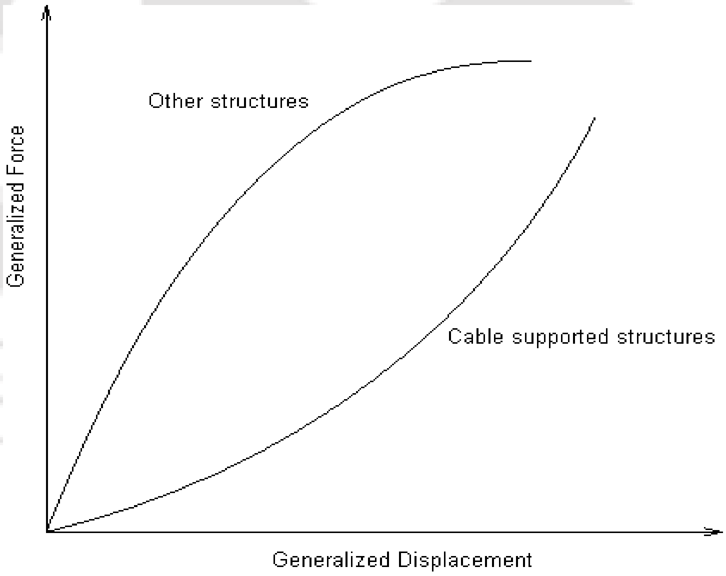

Fig. 2.14 Difference of nonlinearity of cable and non-cable supported structure

The nonlinearity in a cable-stayed bridge originates from following primary sources: (1) the nonlinear axial force-elongation relationship for the inclined cable-stays due to sag caused by their own weight, (2) non-linear axial force and bending moment-deformation relationship for the pylons and the longitudinal girder elements under combined bending and axial forces, (3) geometry change caused by large displacement in this type of structure under dead loads as well as environmental design loads.

The mixed incremental-iterative procedure has been adopted for nonlinear static analysis of the structure. As the nonlinearity in cable-stayed bridges is predominantly geometric in nature, the stiffness has been updated for the change in geometry alone, considering materials in the elastic range. The tangent stiffness at the beginning of each load step is considered for the step-by-step analysis. A large number of load steps are used in order to account for the huge dead load of the structure. The method has been illustrated in Fig. 2.15.

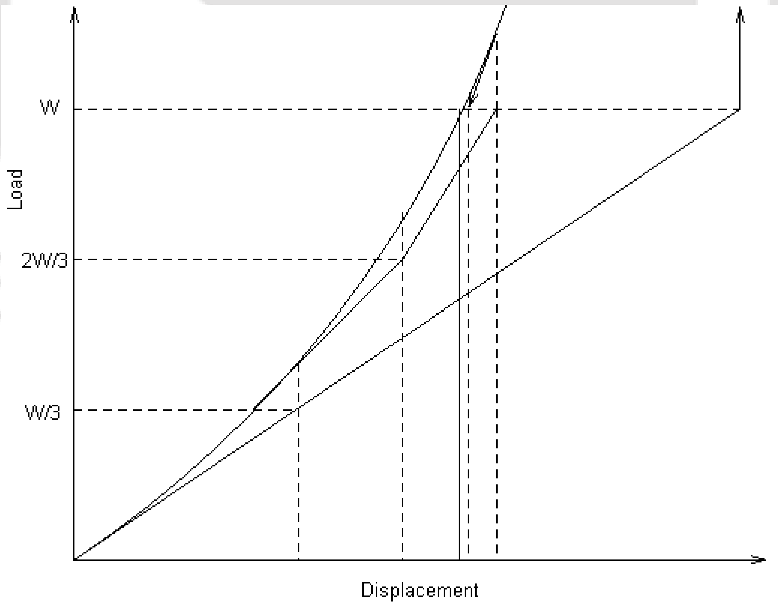

Fig. 2.15 Mixed incremental iterative method of analysis

Four numerical models have been considered for nonlinear static analysis for the bridge. The objective is to evaluate the influence of different modeling strategies on the final configuration of the bridge under the dead load. The descriptions of each of the models are:

Model I: Cable modeled as truss element with equivalent modulus; deck and pylon modeled with beam element without considering their *P-* effect.

Model II: Cable modeled as truss element with equivalent modulus; deck and pylon modeled with beam element considering *P-* effect.

Model III: Cable modeled with elastic catenary element; deck and pylon modeled with beam element without considering their *P-* effect.

Model IV: Cable modeled with elastic catenary element; deck and pylon modeled with beam element considering *P-* effect.

It may be mentioned that the proposed updated model for the numerical model considered by Wilson *et. al.* (1991a) corresponds to the *Model IV.* Other models (*Models I−III)* have been considered to compare their relative performance and to observe whether *Model IV* qualifies as the most suitable update. A computer program has been developed in Matlab® to perform the nonlinear static analysis. The initial deck profile has been assumed to be horizontal. In absence of data on pretension, an iterative way has been adopted to find out the final tension of the cable at dead load deformed configuration. For this a pretension of 30% of ultimate cable tensions of the respective cable types have been considered as initial tension. Member forces including the cable tensions have been updated after each load step. It may be mentioned that the stability factors in beam element formulation will remain as unity in case of *Models II* and *IV,* where *P-* effect for deck and pylon is not considered. The incremental-iterative procedure is continued till the unbalanced joint loads converge. The final tensions serve as the initial tension for the next iteration. An outer iterative loop, as illustrated in the flowchart (Fig. 2.16), has been adopted to arrive at the convergence of cable tensions. The outer convergence corresponds to the dead load deformed structure with final cable tensions and final member forces. It may be mentioned that irrespective of the initial pretension, the final tension configuration attained is the same if the iterations are carried out.

1.5 Modal Analysis

The stiffness matrices used in the modal analysis of the four numerical models correspond to the final geometry, member forces, as well as the cable tensions of the dead-load deformed structure. The frequencies and mode shapes obtained from modal analysis have been compared with those from experimental results reported by Wilson *et. al.* (1991b). As modal characteristics are the best indicator of the appropriateness of a model, this comparative study would indicate whether the proposed updated model is the best among the four alternatives. The effect of using *P*- effect of beam element on the modal characteristics is also explored in this section.

Input: co-ordinates, sectional data, material data, cable initial tensions

Initialize stability functions, cable equivalent modulus /cable stiffness

Initialize member geometry, D.L. member forces, and unbalanced joint load

Form tangent stiffness matrix, apply incremental load,

Update stability function/member stiffness, cable tension/cable stiffness

Calculate member forces and unbalance joint load for each load step

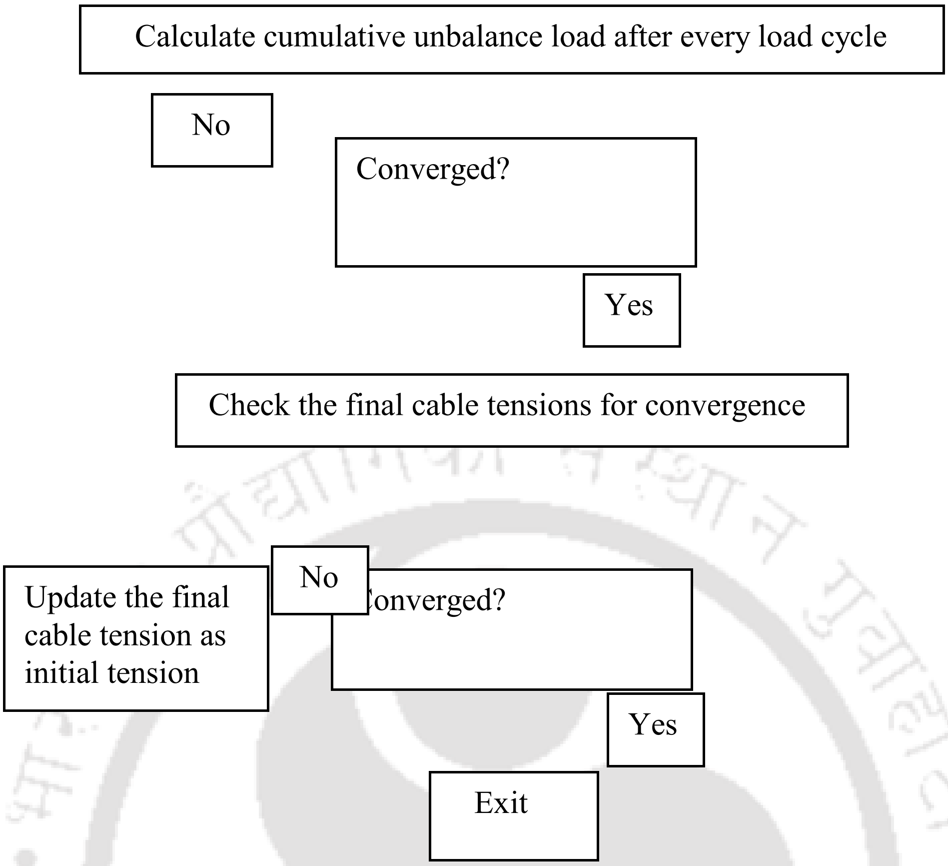

Fig. 2.16 Flow chart for the nonlinear static analysis

2.6 Results and Discussion

The results of nonlinear static analyses and the corresponding modal characteristics of all the four numerical models have been presented in this section.

2.6.1 Nonlinear static analysis: dead load deformed shape

The initial and final cable tensions along with the ultimate cable tension for all the cables for the proposed updated *Model IV* have been shown in Table 2.2. The cable numbers as indicated in Fig. 2.4. The final cable tensions in the individual cables have been found to be in the vicinity of 50% of their ultimate tensions. This would result in an equivalent Young's modulus that is essentially equal to the original modulus, which is in agreement with the observations in Wilson *et. al.* (1991a).

The deflected shapes of the bridge, corresponding to *Model I* and *Model IV,* have been shown in Figs. 2.17 and 2.18. The vertical displacements of the spine and horizontal displacements of the pylons have been exaggerated to appreciate the deflected shape for the scale of the structure. The presented shapes in Figs. 2.17 and 2.18 correspond to the two extreme modeling schemes. The deflected shapes corresponding to the intermediate models have not been shown as the difference between them is not appreciable. The computed deflections of the dead load deformed structure for the four numerical models have been presented for select spine nodes as shown in Table 2.3.

It is evident from the tabulated data that the midspan deflection for the *Model I* is downward, while the same has an upward trend from *Model I* to *Model IV*. The value ranges from -0.02m (downwards) to +0.97m (upwards) indicating that the models are gradually stiffening from *Model I* to *Model IV*. The other spine point deflections are also observed to be compatible with the midspan deflection. The deflections for the select pylon nodes (Table 2.4) are also showing close correspondence with the spine deflections. While a rightward deflection of 0.008 m has been observed at the top of the left pylon node for *Model I*, a leftward deflection of 0.208 m has been observed for the node at the same location for *Model IV*.

Thus, it is observed from results in Table 2.3 and 2.4, that the models with the cables idealized as catenary element are stiffer in comparison to the ones with cables modeled as equivalent truss element. Further, it has been observed that the models taking into account of *P-* effect in beam element formulation are stiffer than their counterparts without the same. Hence, it is concluded that the model involving the *P-* effect as well as the catenary cable element is the stiffest. The modal characteristics of the four models have been presented in the next section. Comparison of these characteristics with those from the numerical model of Wilson *et. al.* (1991a) and experimental observations [Wison *et. al.* (1991b)], would help to establish whether the proposed updated model is the best candidate for model updating.

2.6.2 Modal analysis: frequencies and mode shapes

The modal characteristics of the four models have been evaluated in this section and have been compared with established results.

(a) Comparison by visual inspection: The observations from visual inspection have been presented in Table 2.5. The (*)'s indicate missing modes in the numerical models. It has been observed that the flexural modes (1, 2 and 7) for all the four numerical models correspond well with the respective modes from the numerical model by Wilson *et. al.* (1991a) as well as with those from experimental observations [Wilson *et. al.* (1991b)]. However, a stiffening trend has been exhibited from *Model I* to *Model IV* as indicated by progressively increasing frequencies. This stiffening effect may be attributed to the consideration of *P-* effect in nonlinear analysis as well as due to adoption of catenary element to model the cable in place of truss element. It has been observed that these mode shapes and frequencies from model *IV* resemble the experimental observations very closely.

The most significant observation in terms of mode shapes is that the first two coupled torsional-transverse/transverse-torsional modes of *Models I & II* are strikingly different from the corresponding modes of *Models III & IV.* A more precise understanding of this interesting observation may be attained by studying the numerical difference among the modes through Modal Assurance Criteria (MAC).

(b) Comparison of numerical models: numerical comparison with MAC: The MAC is a measure for examining the numerical similarity or dissimilarity of two modes, which may not be perceptible by visual examination. The MAC number is defined as a matrix of normalized inner product of mode shape vectors [Zhang *et. al.* (2000)] as expressed in,

(2.32)

where, is the modal amplitude at the location l *of the* i*th mode of model* a, *while* is the modal amplitude at the location *l* of the *i*th mode of model *b; p* is the order of mode shape vector. MAC equal to unity indicates a good agreement between the two mode shapes while the same equal to zero indicates no agreement between the same.

The comparative MAC study corresponding to different modes among the numerical models has been presented in Table 2.6. Visual observations have also been tabulated to supplement the MAC values. The MAC is examined for a particular mode between *Models I & III,* i.e. to observe the difference of modal characteristics of model with cable modeled as truss element against that with cable modeled as catenary element. These two classes of models do not consider *P-* effect for deck and pylon in nonlinear static analysis. Similarly, the MAC is examined for *Models II & IV,* which take into account of *P-* effect for deck and pylon in nonlinear static analysis.

It has been observed that the MAC numbers are close to unity corresponding to the numerical mode numbers 1, 2, 5, 6 and 7. The MAC numbers for higher modes are also close to unity and have not been reported. On the other hand, it has been observed in Table 2.6, the MAC numbers corresponding to 3rd and 4th modes are close to zero. It implies that the 3rd and 4th modes of the models with cables modeled as truss elements (*Models I & II*) are entirely different from the respective modes of the models with cables modeled as catenary element (models *II & IV*). By visual inspection, the 3rd mode is transverse-torsional in *Models III & IV* whereas it is torsional-transverse in *Models I & II*. Similarly the 4th mode is torsional-transverse in *Models III* and *IV* whereas it is transverse-torsional in *Models I* and *II*.

2.6.3 Selection of updated model

In this section, the best updated model is selected from the four numerical models. It has already been observed from Table 2.5 that the *Model IV* simulates the experimentally observed modal characteristics to the closest extent. As such, this model is the most suitable update of the numerical model of Wilson *et. al.* (1991a). However, a more comprehensive comparison of this model with the earlier numerical model [Wilson *et. al.* (1991a)] vis. a vis. the experimental result presented by Wilson *et. al.* (1991b) has been attempted here.

The comparison of frequencies of the first few flexural modes has been presented in Fig. 2.19. It has been observed that the proposed numerical model *IV* conclusively updates the earlier numerical model [Wilson *et. al.* (1991a)] as far as capturing of identified flexural frequencies are concerned. Most importantly, the models with catenary element (*Models III & IV)* are successful in simulating the observed transverse-torsional behavior of the structure. Thus, the most significant observation of the present study is the representation of the transverse-torsional mode by the *Model IV* (as well as by *Model III)*. It is worth recalling that this distinctive behaviour of model is due to catenary element being weaker in the plane orthogonal to the plane of the cable (for the present case, the global transverse plane). This conclusively establishes the importance of catenary element in modeling the cable in a cable stayed bridge. It has also been observed that among the *Models III & IV,* the latter represents the transverse behavior better and the frequencies captured by it are the closest to the experimental results.

Comparison of torsional frequencies obtained from the numerical model proposed by Wilson *et. al.* (1991a) and that obtained from the updated model *(Model IV)* against those of the experimental observation have been shown in Fig. 2.20. It is evident from the plot that *Model IV* suitably updates the earlier numerical model with respect to the torsional modes as well. Another noteworthy observation is that there is a softening effect in all the numerical models as the number of torsional modes increases. This is in agreement with Wilson *et. al.* (1991a). It has been explained that as the section become more and more twisted in case of higher torsional modes, the actual structure becomes stiffer due to warping resistance. In contrast, the torsional stiffness of the finite element model does not change as the equivalent torsional constant J_{eq} remains constant. This softening effect is more pronounced in the *Models I & II* as well as in the numerical model proposed by Wilson *et. al.* (1991a). However, it is least conspicuous in *Model IV* with its higher torsional frequencies being fairly close to those of the experimentally determined values. This is another important observation in favour of the *Model IV* to be regarded as the best updated model. Important mode shapes, corresponding to the updated model (*Model IV*) have been shown in Fig. 2.21.

2.7 Conclusion

The study successfully updates the numerical FE model of a cable-stayed bridge to represent the experimentally observed modes to the closest extent. The most significant observation of the study is that the updated model with the cables modeled as catenary elements, reproduces the transverse behavior of the bridge, which the earlier numerical model with cable as truss element fails to represent. Simultaneously, this model also reproduces the flexural modes more closely. The model further succeeds in representation of higher torsional modes with frequencies closer to the experimentally determined values. Thus, the proposed model is an appropriate update of the earlier model. The model is also numerically compact as it uses constraint equations for representation of bearing elements and rigid links. The study employs a mixed-incremental-iterative non linear static analysis scheme accounting for *P*-effect for deck and pylon to arrive at the dead load deformed configuration. This model, by virtue of its compactness, may serve as a base for linear dynamic analysis and also for active control study.

Table 2.2 Initial and final cable tensions for the *Model IV*

Cable No.	Ultimate tension (MN)	Initial tension (MN)	Final tension (MN) (*Model IV*)	Percentage of Ultimate tension (%)

1, 28, 29, 56	14.3	4.29	7.01	49
2, 27, 30, 55	14.3	4.29	7.12	50
3, 26, 31, 54	10.8	3.24	5.23	48
4, 25, 32, 53	10.8	3.24	4.94	46
5, 24, 33, 52	5.6	1.68	2.82	50
6, 23, 34, 51	5.6	1.68	2.54	45
7, 22, 35, 50	5.6	1.68	2.35	42
8, 21, 36, 49	5.6	1.68	2.38	42
9, 20, 37, 48	5.6	1.68	2.42	43
10, 19, 38, 47	5.6	1.68	2.85	50
11, 18, 39, 46	8.6	2.58	4.15	48
12, 17, 40, 45	8.6	2.58	3.96	46
13, 16, 41, 44	10.8	4.29	5.32	49
14, 15, 42, 43	10.8	4.29	5.35	50

Table 2.3 Displacements (m) of representative spine nodes for *Models I-IV*

Node locations	*Model I*	*Model II*	*Model III*	*Model IV*
Left side span, centre	2.25e-03	-8.38e-03	-1.75e-02	-7.04e-02
1/4 centre span	-8.10e-03	3.46e-02	8.46e-02	3.80e-01
Midspan	-2.06e-02	8.82e-02	2.16e-01	9.70e-01
3/4 centre span	-8.09e-03	3.46e-02	8.45e-02	3.80e-01
Right side span, centre	2.55e-03	-8.14e-03	-1.90e-02	-7.05e-02

Table 2.4 Displacements (m) of representative pylon nodes for *Models I-IV*

Node Location	*Model I*		*Model II*		*Model III*		*Model IV*	
	Left	Right	Left	Right	Left	Right	Left	Right
Lower strut joint	7.68e-5	-7.6e-5	-2.38e-4	2.3e-4	-7.05 e-4	7.05 e-4	-2.66e-3	2.65e-3
Deck level Joint	8.83e-5	-8.8e-5	-3.76e-4	3.7e-4	-1.05 e-3	1.05 e-3	-3.97e-3	3.97e-3
Upper strut joint	2.13e-3	-2.1e-3	-9.07e-3	9.1e-3	-2.05 e-3	2.05 e3	-9.58e-2	9.57e-2
Lower cable joint	2.72e-3	-2.7e-3	-1.16e-2	1.2e-2	-2.43 e-2	2.43 e-2	-1.22e-1	1.22e-1
Upper cable joint	8.08e-3	-8.1e-3	-2.02e-2	2.0e-2	-4.83 e-2	4.83 e-2	-2.08e-1	2.08e-1

Table 2.5 Comparison of modal characteristics

Mode No.	Modal frequencies (Hz) and nature of modes					
	Model I	*Model II*	*Model III*	*Model IV*	Numerical model [Wilson *et. al.* (1991a)]	Experimental observation [Wilson *et. al.*(1991b)]
1	0.371 (flexural)	0.373 (flexural)	0.373 (flexural)	0.375 (flexural)	0.371 (flexural)	0.375 (flexural)
2	0.48 (flexural)	0.48 (flexural)	0.49 (flexural)	0.5 (flexural)	0.5 (flexural)	0.5 (flexural)
3	0.57 (tor-trans)	0.58 (tor-trans)	0.57 (trans-tor)	0.58 (trans-tor)	0.577 (tor-trans)	0.56 (trans-tor)
4	*	*	*	*	*	0.63 (transverse)
5	*	*	*	*	*	0.70 (tor-trans)
6	0.63 (trans-tor)	0.68 (trans-tor)	0.70 (tor-trans)	0.73 (tor-trans)	0.633 (tor-trans)	0.74 (tor-trans)
7	0.77 (flexural)	0.78 (flexural)	0.78 (flexural)	0.8 (flexural)	0.77 (flexural)	0.8 (flexural)
8	*	*	*	*	*	0.80 (torsional)
9	0.73 (mixed-tor)	0.78 (mixed-tor)	0.81 (mixed-tor)	0.86 (mixed-tor)	0.733 (mixed-tor)	0.89 (mixed-tor)
10	0.85 (flexural)	0.87 (flexural)	0.88 (flexural)	0.88 (flexural)	0.854 (flexural)	0.89 (flexural)

(* indicates missing mode in numerical models)

Table 2.6 Comparison of MAC Values

Numerical mode number	Nature of mode		MAC values	
	Models I & II	*Models III& IV*	*Models I & III*	*Models II &IV*
1	Flexural	Flexural	0.99	0.98
2	Flexural	Flexural	0.98	0.98
3	Torsional-transverse	Transverse-torsonal	2.3e-08.	3.5e-08.
4	Transverse-torsonal	Torsional-transverse	2.6e-13	2.7e-13
5	Flexural	Flexural	0.99	0.99
6	Mixed-torsional	Mixed-torsional	0.99	0.98
7	Flexural	Flexural	0.98	0.98

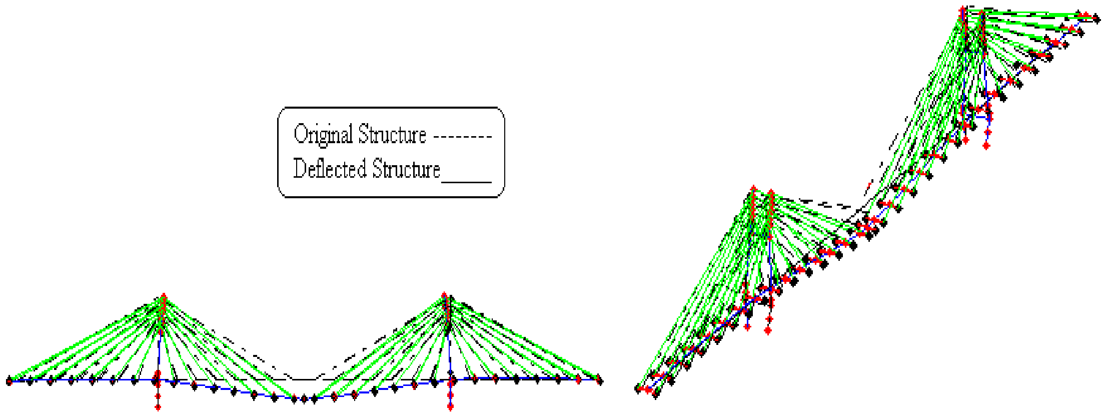

(a) Side view (b) Isometric view

Fig 2.17 Deflected shape for *Model I*

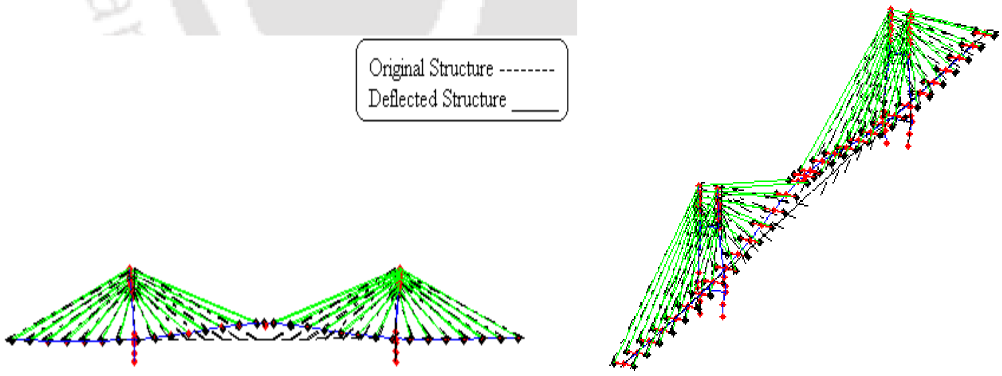

(a) Side view (b) Isometric view

Fig.2.18 Deflected shape for *Model IV*

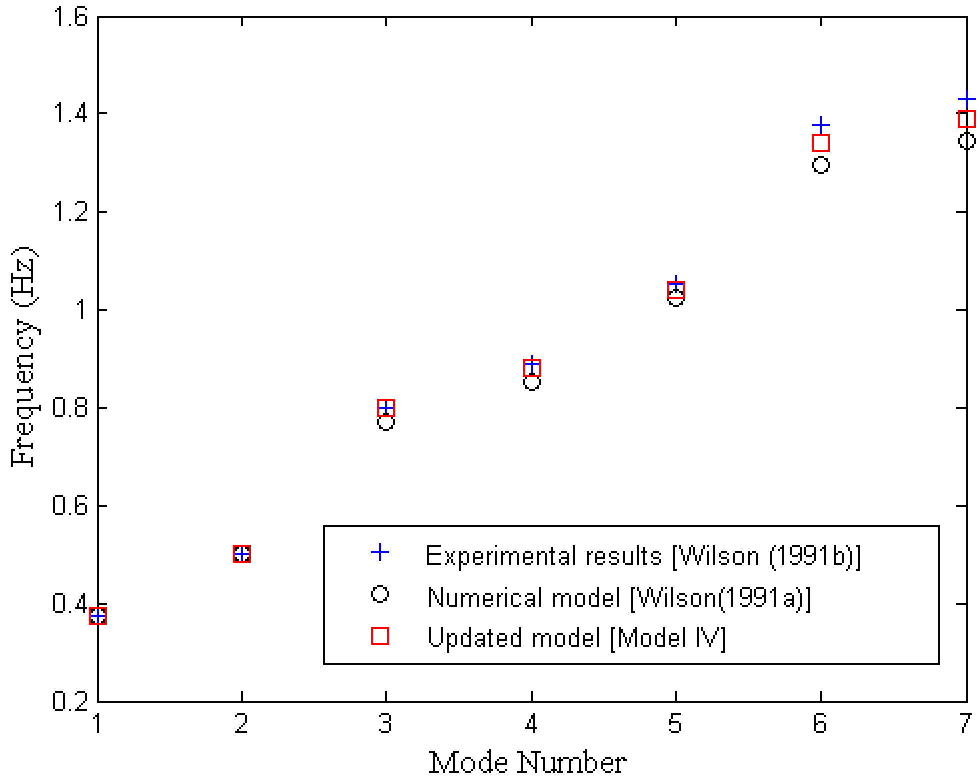

Fig. 2.19 Comparison of flexural modes for different models

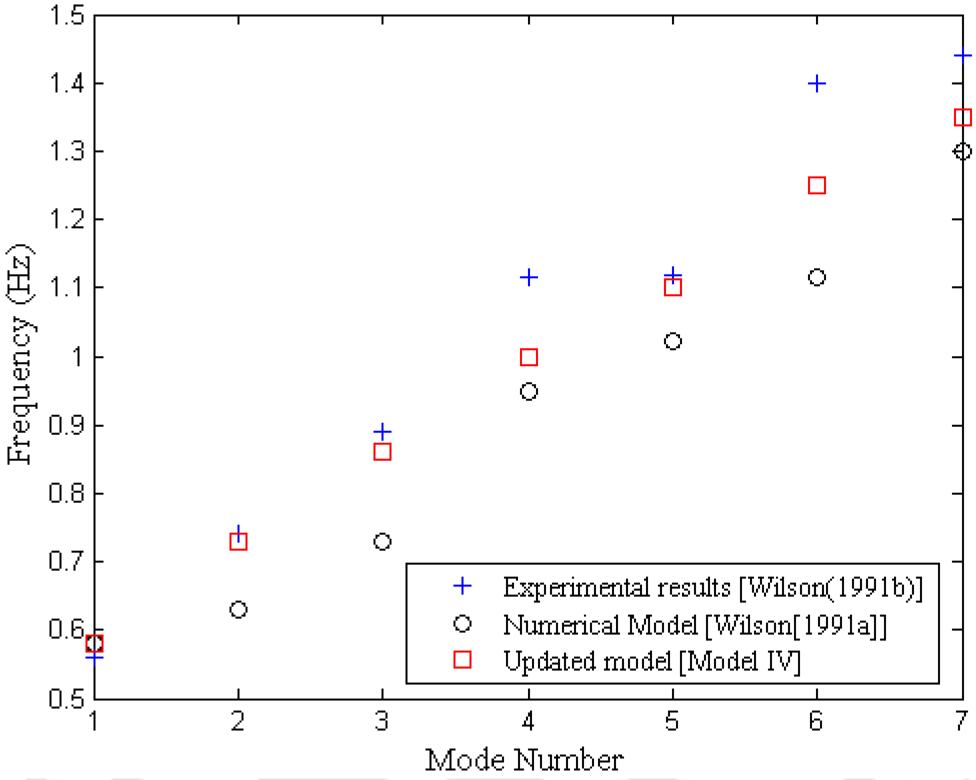

Fig. 2.20 Comparison of torsional modes for different models

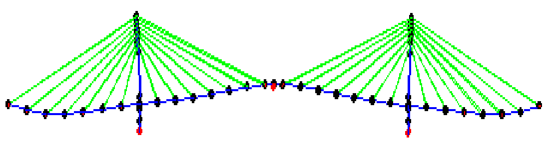

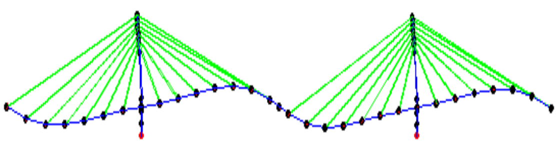

First (flexural, 0.375Hz)

Second (flexural, 0.50Hz)

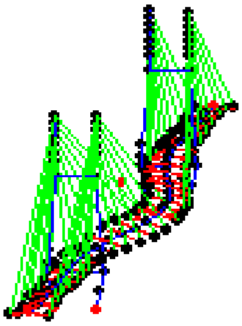

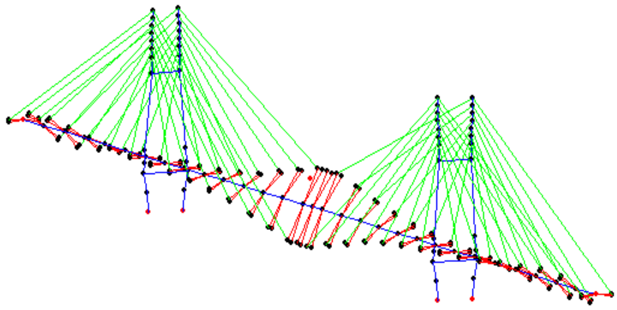

Third (trans- tor, 0.58Hz)

Fourth (tor-trans, 0.73Hz)

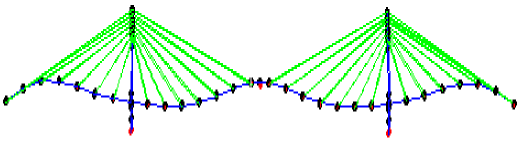

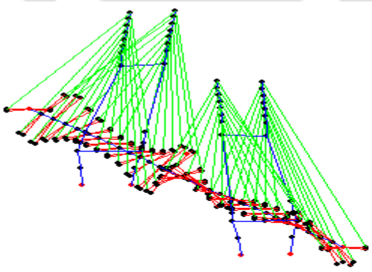

Fifth (flexural, 0.80Hz)

Sixth (mixed-tor, 0.86Hz)

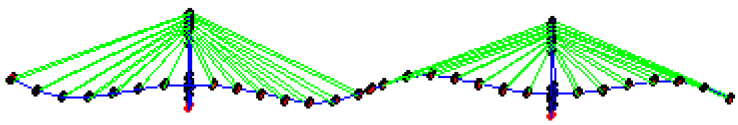

Seventh (flexural, 0.88Hz)

Fig. 2.21 Mode shapes of the updated model

Chapter 3

DESIGN OF ACTIVE CONTROLLERS FOR SEISMIC RESPONSE CONTROL OF THE QUINCY BAYVIEW BRIDGE

3.1 Introduction

In this chapter, design of active controllers for the Quincy Bayview Bridge, Illinois, USA has been undertaken for control of structural responses against seismic excitations. The updated model from the preceding chapter has been used to arrive at mathematical model for design of the controllers. However, the large number of degrees of freedom of the model poses problem in designing a practical controller. Hence, the model is reduced by Guyan reduction scheme to eliminate certain degrees of freedom. The reduced model has been validated by comparing its dynamic response with those obtained from the updated model. The control evaluation model has been formed after removing the constraint equations used to represent the bearings corresponding to the longitudinal dofs, and making provisions for attachment of actuators in those locations. The model has then been represented in state space and is further reduced by using the balance realization technique. The reduction process has again been validated comparing the transfer function of the balance realized model with that for control evaluation model. This reduced model is called the control design model. Three representative earthquakes have been used for the present study of seismic response control. Two active controllers, one against uniform support excitation and the other corresponding to the multiple support excitations, have been designed to control the response of the bridge against these earthquakes. Further, multiple support excitation case has been considered for two different angles of attack of earthquake excitation and time lag of incidence of earthquake wave in different supports. Evaluation criteria of the controller, which are indicative of how the controller reduces the peak pylon forces, are chosen from the existing literature [Dyke *et. al.* (2000)]. It is ensured that the cable tensions are within the permissible limits. It has been observed that the active controllers fulfill the evaluation criteria. The controller has been designed in the Matlab® environment using Simulink® of the Control System Toolbox.

3.2 Broad Framework of Active Control

An active control scheme for any structure against external excitations comprises of feedback from sensors at key locations, a digital controller to decide about the controlling forces and actuators to apply the forces at appropriate locations. The broad framework for an active control strategy has been illustrated in the flowchart in Fig. 3.1.

The numerical model of the system is created for implementation of the active control strategy in the flowchart shown in Fig. 3.1. The external excitations/disturbance and the performance objectives are to be specified. The sensors and actuators are then numerically interfaced with the model. The model is then reduced to a manageable level for achieving computational efficiency. Subsequently, the system is represented in states space to facilitate the implementation of the control strategy. The digital implementation of the controller is performed while maintaining the observability and controllability of the system with respect to the sensor and actuator configuration. The performance objectives for the control strategy are formed. The controller is designed for optimal efficiency by trial and error and is evaluated against the performance objectives.

The core of any active control strategy is the numerical model of the structure. Hence the true representation of the structure in the numerical model is of utmost importance. The numerical model, which is taken up for the current control study, has already been validated in Chapter 2 for accurate representation of dynamic properties of the original structure. However, this model has be modified, reduced and represented appropriately before it could be used for design of the controller. The various intermediate models needed for the evaluation of the controlled and uncontrolled response have been illustrated in Fig 3.2. The models shown in the figure have been discussed in detail in the next sections.

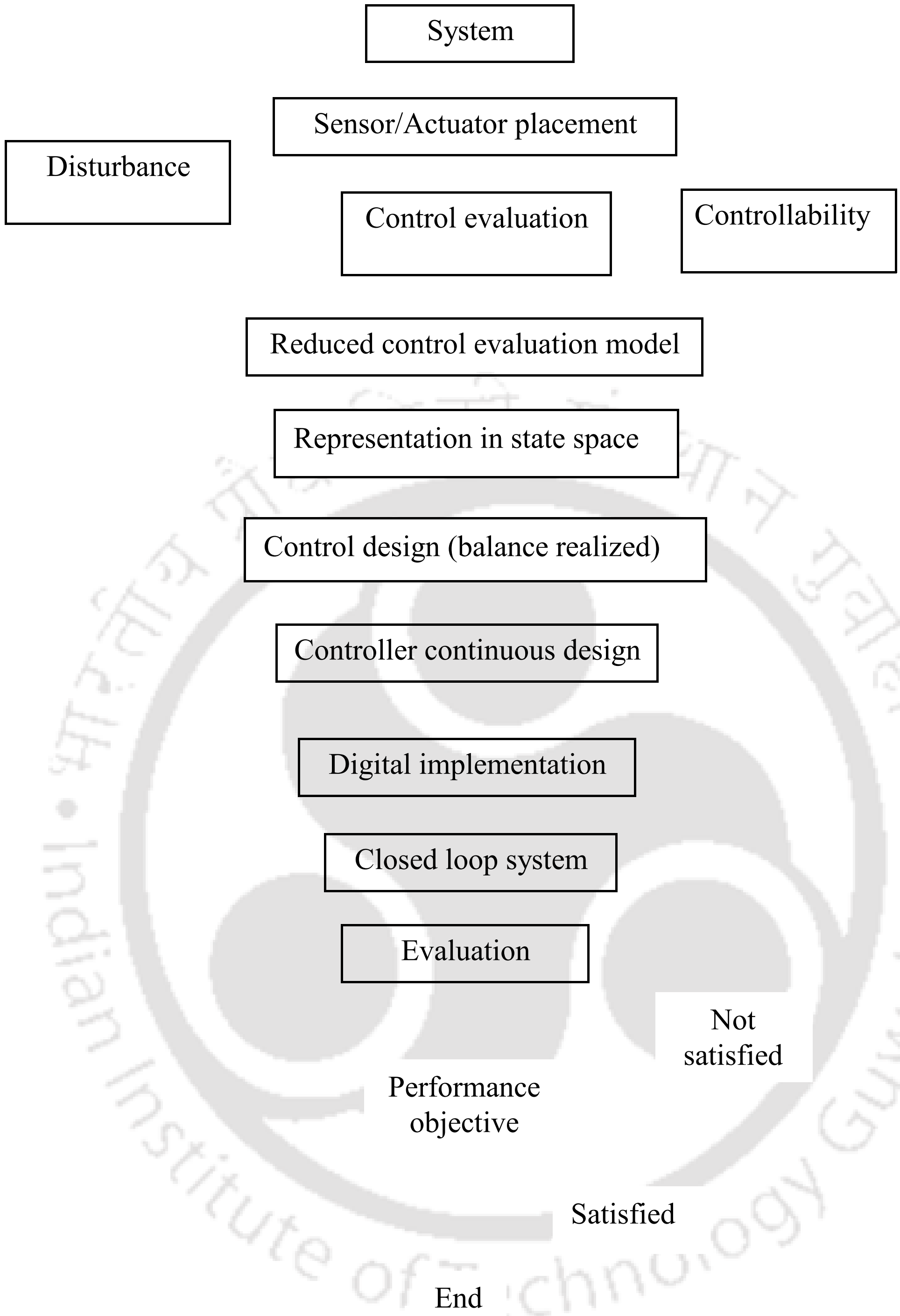

Fig. 3.1 Flowchart for active control strategy

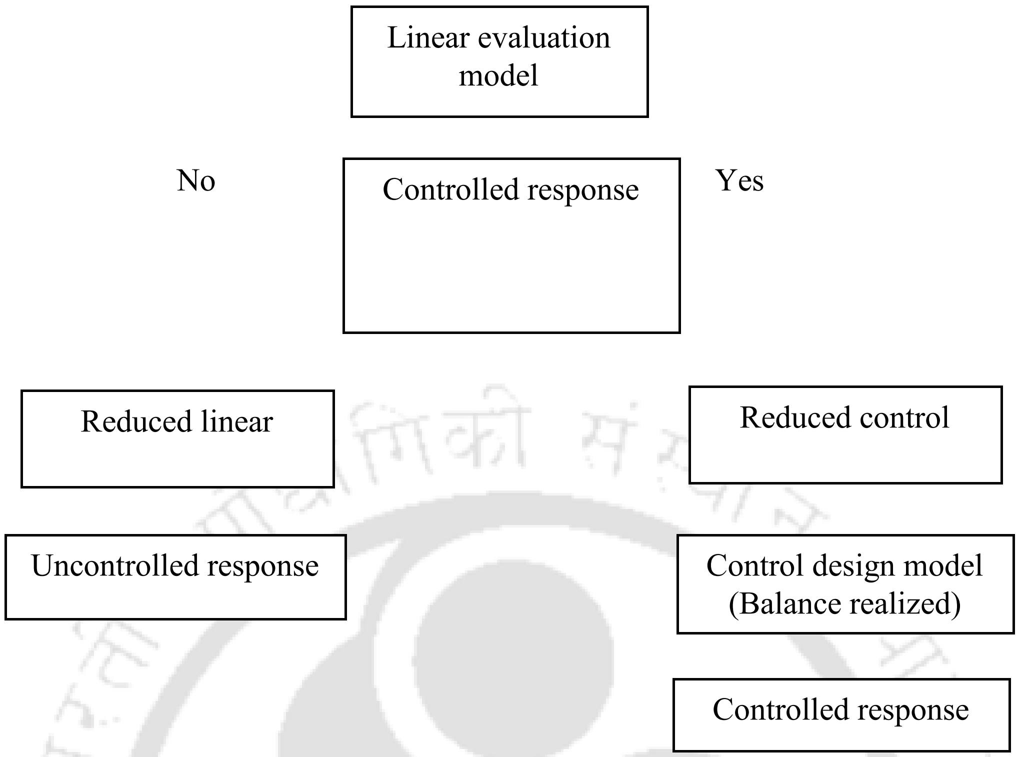

Fig. 3.2 Model reduction strategy

3.3 Linear Evaluation Model

The model for evaluation of dynamic response has been adopted from the updated model from Chapter 2. The rational behind using this model for dynamic analysis has been illustrated in Fig. 3.3.

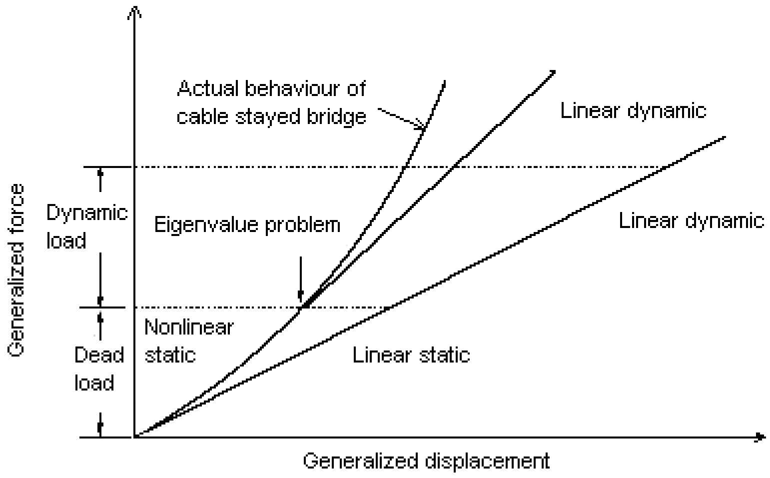

Fig. 3.3 Linear evaluation model

It is appreciated that most of the nonlinearity in flexible structure such as cable stayed bridge is contributed by large dead load. Since the major source of nonlinear behavior has already been incorporated in the model through the dead load-deformed configuration along with the representative tangent stiffness matrix, a linear dynamic analysis is considered to be sufficient for simulation of the dynamic behaviour during earthquake excitations. Ahmed *et. al.* (1991) compared the cases of linear dynamic and nonlinear dynamic analysis based on the dead load deformed configuration of a cable-stayed bridge of 300 m centre span. It was concluded that the difference between the results of both the analyses was very small. Wilson *et. al.* (1991a) adopted the same approach for comparing modal characteristics with identified data for the bridge considered in the current study. More recently Dyke *et. al.* (2003) adopted this approach for the benchmark control problem of cable stayed bridge. The adoption of a linear dynamic model reduces the complication of time variant system matrices in state space approach of modern control. It may be mentioned that that the time variant system matrix arising out of dynamic nonlinearity can involve choosing different weighting matrix in the objective function for optimal control, requiring a lot more computational time. This will pose difficulty in the design of a practical controller. Moreover, formation of system matrix in every time step might create controllability and observability problem in some step which may jeopardize the practical viability of the numerical solution. Hence the updated model has been used as it is for the evaluation of uncontrolled response against a selected few earthquakes. The same model has been further modified for developing the control evaluation model.

3.4 Control Evaluation Model

The model for control evaluation has been formed by incorporating the effect of the controllers in the structure. The controllers are designed to minimize structural response in the longitudinal direction, which is the most important direction in case of seismic behaviour of a long span bridge. The practical locations for actuators are between the deck and the abutment as well as between the deck and the pylons. They are oriented longitudinally below the edge girders and connected to abutment and lower strut of the pylon as shown in the Figs. 3.4 (a) and (b) respectively. This placement of the actuators in the interface of the deck and supports is to be incorporated in the control evaluation model. This has been done by first removing the constraint equations corresponding to the bearing links in the deck abutment and deck-pylon locations in the linear evaluation model. The actuators have been introduced in the model by connecting the dofs released from the constraints. The model is henceforth called the control evaluation model.

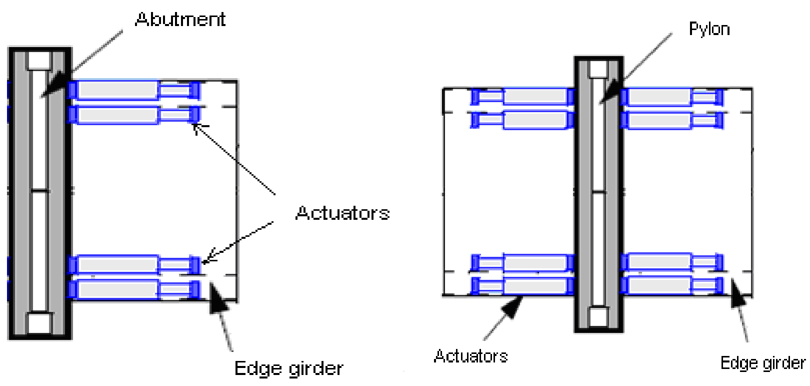

(a) At Abutment **(b) At deck pylon location**

Fig. 3.4 Actuator placement

This placement of the actuators in the interface of the deck and supports is to be incorporated in the control evaluation model. This has been done by first removing the constraint equations corresponding to the bearing links in the deck abutment and deck-pylon locations in the linear evaluation model. The actuators have been introduced in the model by connecting the dofs released from the constraints. The model is henceforth called the control evaluation model.

3.5 Reduced Linear Evaluation Model

The linear evaluation model still has a large number of degrees of freedom rendering it unmanageable for efficient implementation of control strategy. Guyan reduction scheme has been adopted in the study to arrive at a compact model the dynamic characteristics of which will be in good agreement with those of the original model.

3.5.1 Guyan reduction scheme

In Guyan reduction scheme, proposed by Guyan and Irons, the dofs of the FE model have been designated as either *slaves* or *masters.* The *slave* dofs are required to move as dictated by the motion of the *masters*. Only the master dofs appear in the equation of motion corresponding to the reduced order model. The method follows from the equation of motion for undamped free vibration of structures, which is written as,

(3.1)

where, **z** represents the displacement vector and is its second time derivative, M **is** the mass matrix, **K** is the stiffness matrix of the structure.

The eigen value problem corresponding to Eq (3.1) with dofs partitioned according to *master* dofs and slave *dofs* can be written as,

(3.2)

The lower partition in Eq. (3.2) can be solved for and substituted into the upper partition to get a reduced system that contains only as dofs; but matrices of such reduced system will be frequency-dependent. To obtain a frequency-independent system, Guyan and Irons suggested that the relations between *slaves* and *masters* should be dictated *entirely* by *stiffness coefficients* [Cook *et. al.* (2002)]. Following equation has been obtained ignoring the mass coefficients of the lower partition of Eq. (3.2),

(3.3)

Thus, all the dofs may be expressed in terms of *masters* by the following equation,

(3.4)

where,

(3.5)

in which, **I** is the identity matrix. Physically, the *j*th column of **T** represents the static displacement in all the dofs when *j*th *master* has a unit displacement and all other *masters* have zero displacement. This displacement state is also called a constraint mode.

Thus, the reduced eigen value problem can be stated as,

(3.6)

where, and (3.7)

For making proper dynamic analysis, damping property of the structure should ideally be known. In this study, the damping in the system has been evaluated on the on the basis of assumed value of modal damping. This is done by assigning 3% of critical damping to each mode. This value is logical for the material and structural characteristics of the present cable stayed bridge. The damping matrix has been written as,

(3.8)

where, is the reduced modal matrix, and and are the natural frequency in (rad/sec) and modal damping ratio of *r*th mode respectively.

3.5.2 Selection of master dofs

The *master* and *slave* dofs have been carefully selected for implementation of the Guyan reduction scheme so as to arrive at a reduced model that compares well with the dynamic characteristics of the linear evaluation model. The dofs of the following nodes have been retained: (i) the top nodes of each pylon, (ii) the lowest nodes of pylons that connect the cables, (iii) nodes at the joints of the structure; (iv) nodes or dofs where member forces are sought to be controlled; (v) every second node of the deck; and, (vi) the rotational dofs of all spine nodes about the longitudinal and vertical axes. Further, for multiple support excitations the support dofs have also been retained.

3.5.3 Validation of reduction scheme

Applying the Guyan reduction scheme to the structure with the matrices partitioned according to the above *master* and *slave* dofs, the linear evaluation model has been reduced to a system with 296-dofs. The first 100 natural frequencies of this reduced model have been compared and found to be matching well with the linear evaluation model with 458-dofs. Henceforth this model will be referred to as the reduced linear evaluation model. The transfer function tool has been utilized to validate the reduction process so that the dynamic characteristics of the reduced linear evaluation model correspond to the linear evaluation model. The transfer function has been represented by *bode* plot invoking the function *bode.m* from control system toolbox of Matlab®. *Bode* computes the magnitude and phase of the frequency response of Linear Time Invariant (LTI) models [Matlab®]. The magnitude has been plotted in decibels (dB), and the phase in degrees. The decibel calculation for magnitude has been computed as , where is the system's frequency response. A comparison of transfer functions of ground acceleration to displacement at the top of left pylon for the linear evaluation model and that for reduced linear evaluation model has been shown in Fig. 3.5. This plot is representative of dynamic behaviour of the bridge as it shows the response at top of the structure from excitations at the ground. From Fig. 3.5, it has been observed that both magnitude and phase for the two models matches well upto 10 Hz, which is a fairly sufficient range. The contribution of additional modes with frequencies higher than 10Hz is insignificant for calculation of dynamic response for the structure under study as the first 84 frequencies of the linear evaluation model are within this limit.

3.5.4 Modal characteristics of reduced linear evaluation model

The first seven undamped frequencies (Hz) of the reduced linear evaluation model have been found as 0.375, 0.5, 0.58, 0.73, 0.8, 0.86 and 0.88. These agree well with the frequencies of the linear evaluation model. This reduced model is a compact representation of the structure and can be used for linear dynamic analysis and for constructing the state space model for designing an active controller. Representative sample of mode shapes corresponding to the reduced linear evaluation model has been shown in Fig. 3.6.

3.6 Reduced Control Evaluation Model

The reduced control evaluation model has been developed from the control evaluation model from section 3.4. The same reduction procedure has been followed as in case of reduced linear evaluation model in section 3.5.

3.7 Problem Formulation

In this section the basic concepts pertaining to response control of the cable stayed bridge against uniform and multiple support seismic excitations have been presented. The uniform support excitation is rather logical in case of spatially limited structures such as buildings. In this approach, input earthquake is assumed to excite all the supports at the same time. However, for structures such as the cable stayed bridge, with supports well apart, the multiple support excitation approach is more appropriate. In this approach, supports are subjected to different excitations. In the present study, both the types of excitations have been examined.

3.7.1 Uniform support excitation

The governing equation of motion corresponding to the reduced control evaluation model with uniform support seismic excitation and control thereon is written as,

(3.9)

where, is the control force vector, , being a diagonal matrix indicating the locations of control forces to the structure, is the ground acceleration, while is the vector of earthquake influence coefficients and T **is the transformation** matrix for reduction as shown in Eq. (3.5).

3.7.2 Multiple support excitations

In this section, a modified equation of motion has been presented in order to allow for different motions of the supports. The displacement vector has two components, namely which is the absolute displacement vector of the master nodes of superstructure and as the displacement vector of the supports. The equation of motion as shown in Eq. (3.9) with inclusion of effects from support dofs is written in the partitioned form [Chopra (1996)] as,

(3.10)

Here the subscript *g* specifies the support dofs. The mass , stiffness and damping are the respective reduced matrices corresponding to the reduced control evaluation model developed following the procedure presented in section 3.5.1. The support displacements , support velocity , and support acceleration have been specified from earthquake records. The displacements of superstructure *master* dofs and support forces are to be determined through analysis.

The displacements have been separated into two parts as in Eq. (3.11). This is done so that the governing Eq. (3.10) can be written in a form similar to that for uniform support excitation of Eq. (3.9)

(3.11)

In this equation, is the vector of structural displacements due to static application of the prescribed support displacements at each time instant and hence is known as quasi-static displacements of the master dofs. The remainder displacement is the dynamic displacements of the *master* dofs. The displacement vectors and are related through,

(3.12)

where, are support forces necessary to statically impose displacements , which vary with time. It follows from Eq. (3.10),

(3.13)

Substituting Eq. (3.11) into Eq. (3.13) and arranging for an equation of motion in terms of dynamic displacement and simplifying the same in line of Eq. (3.9) by getting rid of superscript *t*,

(3.14)

where,

(3.15)

Here is termed as effective earthquake force. Eq. (3.12) gives,

(3.16)

With Eq. (3.12), quasi-static displacements can be expressed in terms of specified support displacements at any instant t,

(3.17)

Here, the matrix is called the influence matrix ( ) as it represents the influence of the support displacements on the structural displacements. Substituting Eq. (3.17) in Eq. (3.15) and simplifying the expression for in Eq. (3.14):

(3.18)

3.8 Analysis Tool

The reduced control evaluation model of the structure has been analyzed for the combined effect of earthquake excitation and control forces with a tool developed by Ohtori and Spencer (1999). This tool enables the Matlab® user to interface with a complied C code for solving the dynamic equation using Newmark-β method. The compiled code is masked as S-function in Simulink® block. The reduced mass ( ), stiffness and damping ( ) matrices from Eqs. 3.9 and 3.18 have been introduced as the parameters for the S-function.

3.9 State Space Representation of the System

Modern control algorithm uses a particular representation of the structure-control system involving the numerical model of the structure, sensors and actuators. This is called the state space representation. The *state* of a system can be defined as a set of quantities at a given instant of time in order to determine the behaviour of the system completely. These quantities (such as displacements, velocities and accelerations in the present case) constituting the state are called the *state variables*. The hypothetical space, spanned by the state variables, is called the *state space*. In the *state space* representation, a second order governing equation is transformed into two first order differential equations called the *state* equations. In addition to this, an *output* equation is to be formed to define the relation between output and the state variables. In contrast to classical methods (such as transfer function approach), state space method deals directly with the governing differential equation of the system in the time domain. Representing the governing equation in first order state equation makes it possible to directly solve the state equation in time, using standard numerical methods and efficient algorithms. Since the state space equations are always of first order, irrespective of the system's order or the number of inputs and outputs, the greatest advantage of state space method is that there is no distinction between single input-single output systems and multivariate systems. This approach allows efficient design and analysis of multivariable systems with the same ease as that for single variable systems. Dealing with linear systems, state space method results in repetitive *linear algebraic* manipulations (such as matrix inversion, matrix multiplications, solutions of linear matrix equations etc.), which are easily performed in a computer. The linear algebraic manipulation for state space method is easy with the use of high level programming language such as Matlab®. This saves a lot of drudgery that is common when working with inverse Laplace transformation of transfer matrices.

In this section the state space representation of the dynamical equation of the reduced system against seismic excitation has been presented. The input and output matrices have been formulated using the state space forms of the equations governing the motions corresponding to uniform support and multiple support excitations respectively.

3.9.1 State matrices: uniform support excitation

The governing equation of motion for the reduced control evaluation model as in Eq. (3.9) has been rearranged to arrive at the state space representation of the system as,

(3.19)

The displacement ( ) and velocity ( ) have been expressed as the states, and the Eq. (3.19) can be arranged as:

(3.20)

Here, is the system *matrix or* state *matrix determined using the* properties of the structure to be controlled and is the combined external *force* and *control input* mapping matrix.

Outputs of the system can be represented in terms of,

(a) Displacement: (3.22)

(b) Velocity: (3.23)

(c) Acceleration: **(3.24)**

In a general expression, the state space equations take the following form,

(3.25)

Here, **x** represents the state vector. The matrix is called the state *matrix* for the reduced system. It is also called the (dynamical) *system* matrix as it describes the dynamics of the system through the modal characteristics. *is the external excitation and control input mapping* matrix. This matrix represents the linear transformation by which deterministic inputs influence the next state.

is the *sensor output mapping* matrix. This describes how the internal states have been transferred as measurement **y**. is called the direct feed-through *matrix. The* output vector **y** has three vector components: measurement vector and evaluation vector . The measurement outputs are the structural dynamic displacement ( ), velocity ( ) and absolute accelerations ( ), which are fed as input to the sensors. Connection outputs consist of the displacement, velocity and absolute accelerations of the dofs that have been connected to the actuators. Evaluation outputs represents the member force vector, which has been used to evaluate the performances of the active controllers. Thus, the sensor output mapping matrix has been formed as,

(3.26)

Here, and map measurement and evaluation quantities respectively. m atrix is expressed as,

(3.27)

where, matrix and matrix map ground excitation and control input respectively.

3.9.2 State matrices: multiple support excitations

The governing equation of motion for the reduced control evaluation model as in Eq. (3.18) has been rearranged to arrive at the state space representation of the system as:

(3.28)

To arrive at an expression for the states, , Eq. (3.28) has been written as:

(3.29)

Here, is the system *matrix or* state *matrix and,*

is the *combined external force* and

control input mapping matrix. Output of the system can be represented in terms of:

(a) Displacement: (3.30)

(b) Velocity: (3.31)

(c) Acceleration:

(3.32)

In a general expression, the state space equations take the following form:

(3.33)

Here, the state matrices bear the same meaning as in Eqs. (3.25). Similarly, the input-output mapping matrices are also the same as explained in Eqs. (3.26) and (3.27).

3.10 Problem Statement for Design of Controller

In this section, the controller has been defined with respect to measuring devices (sensors), controlling devices (actuators) and control algorithm. The formulation for interfacing of sensors and actuators with the model for control evaluation has also been stated. This interface has been done through measurement output . The evaluation output , corresponding to responses e.g. forces/moments at key locations, has also been defined. All these input and output measurement vectors have been specified in terms of node number and dof corresponding to the control evaluation model. The controller is to be evaluated against selected evaluation criteria.

Linear Quadratic Gaussian (LQG) algorithm has been used for the active control strategy.

3.10.1 Components of control system

The block diagram for the proposed active control system has been shown in Fig. 3.7.

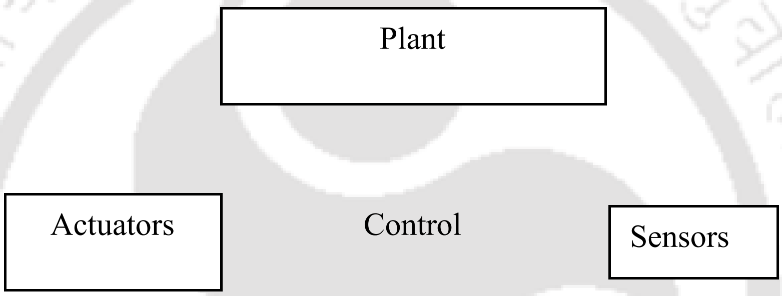

Fig. 3.7 Block diagram representation of active control system

The plant here corresponds to the control evaluation model as developed in section 3.4. This plant has been excited by the earthquake excitation . The evaluation parameters have been calculated using the analysis tool as described in section 3.8. The measurements have been fed to the sensors. The sensor output data has been given as input to the discrete controller as . The controller signal u **has then been** converted to an actuator signal **f**, which acts as input to the plant.

The sensors have been defined to measure the outputs of the control evaluation model as,

(3.34)

(3.35)

where, is the continuous-time state vector of the sensors measured in Volts.

The discrete-time control algorithm takes the form:

(3.36)

(3.37)

where, is the discrete-time state vector at each sampling time , is the discrete time control command and is the discrete-time input vector from the sensors. In may be mentioned that the analog signal from the sensors, have been discretized in time and quantized through analog-to-digital (A/D) converter as . The actuator-structure interaction has been neglected in this study. The interfacing of the actuators with the bridge model has been done through,

(3.38)

(3.39)

where is the continuous-time force output (kN) of the actuators applied to the structure and is the continuous-time output vector from the control device output model, comprising forces produced by individual control devices, device stroke, device acceleration and has been used for evaluation of control strategy.

3.10.2 Evaluation criteria for the controller

It is appreciated that structural integrity is more important than serviceability issues for a cable-stayed bridge subjected to seismic excitation. Thus, the controller has been evaluated on the basis of how it reduces the shear force and bending moment responses in the key locations, such as the base of the pylons and pylon deck connection points. At the same time it has been ensured that the cable tensions do not approach zero as it would destabilize the structure.

Three representative earthquake excitations have been considered for the evaluation of the controllers. The details of these earthquakes excitations are: (i) *El Centro (N-S)*, recorded at Imperial Valley, Valley Irrigation District substation in El Centro, California, during Imperial Valley, California earthquake of 18 May 1940 with PGA of 0.35*g*; (ii) *Mexico City (N-S)*, recorded at Galeta de Campos station with site geology of meta-andesite breccia on 19 September 1985 with PGA of 0.14*g*, and (iii) *Gebze, Turkey (N-S)* recorded at the Gebze Tubitak Marmara Arastirma Merkezi on 17 August 1999 with PGA of 0.27*g*. The Mexico City earthquake has been selected as the site conditions of Mexico City is similar to that of the site of the bridge considered. Other two earthquakes have been selected to represent different excitation characteristics. The adopted excitations have a wide range of characteristics and the robustness of the controller may be validated if it controls the responses of the bridge against these earthquakes.

In case of multiple support excitations, time lag has been considered for incidence of excitations among different supports of the bridge. This is based on the distances among supports and velocity of the earthquake wave. The left abutment has been assumed to experience a specified motion first and the delay at which the left pylon, right pylon and the right abutment would experience the same has been calculated on the basis of the time of travel of the L-wave of the earthquake to the respective supports. The speed of the L-wave has been considered as 3km/sec. Two incidence angles of the earthquake have been considered for multiple support excitations to check the controller. The incidence angle has been defined as the angle between the longitudinal direction of the bridge and the N-S component of the wave of the earthquake. Accordingly two cases have been considered: Case-1, an incidence angle of 15^0 with delay of [0 0.05 0.13 0.17] sec for the supports from left to right, and Case-2, an incidence angle of 45^0 with corresponding delay as [0.0 0.03 0.10 0.13] sec.

The evaluation criteria have been adopted from Phase-I benchmark control problem for seismic response of cable-stayed bridges proposed by Dyke *et. al.* (2000). The first six criteria evaluate controller performance in reducing peak responses, the second five criteria consider the norm of responses over the entire time record and the last seven criteria evaluate the requirement of the control system. The first two evaluation criteria are dimensionless measures of the shear force at pylon base and deck level. These are represented as,

(3.40)

(3.41)

where, is the base shear at the *ith pylon,* is the maximum uncontrolled base shear (at the two pylons), is the shear at the deck level in the *i*th pylon. is the maximum uncontrolled shear at the deck level of the two pylons, and indicates absolute value. The subscript t *stands for the time* duration of the earthquake. The values of , and all other values used in calculations of the evaluation criteria have been provided in the Tables 3.1 and 3.2 for uniform support excitations and multiple support excitations respectively.

The second set of evaluation criterion comprises of dimensionless measures of the moments at the key locations of the both the pylons as given by,

(3.42)

(3.43)

where, is the overturning moment at the base of the *ith pylon,* is the maximum uncontrolled base moments in the two pylons, is the moment at the deck level in the *i*th pylon. is the uncontrolled moment at the deck level in the two pylons.

The fifth evaluation criterion is a dimensionless measure of the deviation in the tension in the stay cables from the respective cable tension from linear evaluation model given by,

(3.44)

where, is the tension in the *ith cable in the linear evaluation model and* is the time varying actual tension in the cable. This criterion is needed to examine the possibility of failure or unseating of cable.

The sixth evaluation criterion is a measure of peak deck displacement at the abutments.

(3.45)

where, is the displacement of the bridge deck at the *i th location and* is the maximum uncontrolled deck response at these locations. This criterion is included to consider the likelihood of impact of the deck at these locations.

The seventh and eight criteria are dimensionless measures of norms of the base shear and the shear at the deck level in each of the pylons respectively and are given by,

(3.46)

(3.47)

where, is the maximum norm of the uncontrolled base shears of the two pylons, and is the maximum norm of the uncontrolled shear at the deck level of the pylons.

The norm of the response denoted by is defined as,

(3.48)

where, is defined as the time required for the response to attenuate.

The ninth and the tenth evaluation criteria are the dimensionless measures of the norms of the overturning moment and the moment at the deck level in each of the pylons respectively and are given by,

(3.49)

(3.50)

where, is the maximum norm of the uncontrolled base moments of the two pylons, and is the maximum norm of the uncontrolled shear at the deck level of the pylons.

The eleventh evaluation criterion is a dimensionless measure of the norm of the deviation in time-varying tension in the stay cables from the cable tension obtained from the linear evaluation model and is given by,

(3.51)

The twelfth evaluation criterion deals with the maximum force generated by the actuator(s) and is described as,

(3.52)

where is the force generated by the *ith actuator over the time history of each* earthquake, and W = 142005 kN is the weight of the superstructure of the bridge.

The thirteenth criterion is based on the stroke of the actuator(s). This performance measure is given as,

(3.53)

where, is the stroke of the *ith actuator over the time history of each earthquake,* and is the maximum uncontrolled displacement at the top of the tower relative to the ground.

The fourteenth evaluation criterion is a dimensionless measure of the maximum instantaneous power required to control the bridge and is defined as,

(3.54)

where, is the instantaneous power required by the *ith control device, and* is the peak uncontrolled velocity at the top of the pylons relative to ground. Values for have been provided in Table 3.1 against uniform support excitations and Table 3.2 against multiple support excitations for each of the three earthquakes. , where is the velocity of the *ith actuator.*

The fifteenth evaluation criterion is a non-dimensional measure of the total power required to control the bridge and is defined as,

(3.55)

The sixteenth evaluation criterion is the total number of actuators required in the control system to control the bridge response,

Number of actuators (3.56)

The seventeenth evaluation criterion is the total number of sensors required for the proposed control strategy.

Number of sensors (3.57)

The final evaluation criterion is a measure of the resources required to implement the control algorithm and is given by the dimension of the state written as,

Dim ( ) (3.58)

where, is the discrete-time state vector of the control algorithm given in Eq. (3.36).

All criteria except for , , and - are dependent on direction. They have been evaluated for longitudinal *(X)* direction for uniform support excitation and for both longitudinal *(X)* and transverse *(Z)* directions in case of multiple support excitations. It may be mentioned that the longitudinal excitation have the worst effects on the structural integrity of a cable stayed bridge. In the present study multiple support excitations have been applied at an inclination to the longitudinal direction. Hence, the control parameters have been evaluated in both *X* and *Z* directions for multiple support excitation case. A summary of evaluation criteria has been provided in Table 3.3.

The uncontrolled key responses of the bridge for uniform support excitation against the three earthquakes that have been shown in Table 3.1. The uncontrolled responses against multiple support excitations corresponding to the two angles of incidence have been presented in Table 3.2.

Table 3.3 Summary of definition of evaluation criteria

Peak responses	Normed responses	Control strategy
Base shear	Base shear	Peak force
Shear at Deck Level	Shear at Deck Level	Device stroke
Overturning Moment	Overturning Moment	Peak Power

Moment at Deck Level Moment at Deck Level Total Power

Cable Tension Cable Tension number of control

devices
number of sensors

dim( )

Deck Disp at Abutment

3.10.3 Constraints/ limitations in the design of the controller

The constraints in designing of active controllers have been listed as per the benchmark problem [Dyke *et. al.* (2000)]:

1. Though theoretically, the absolute acceleration of all the nodes of finite element model can be measured with sensors, it is not practical to place sensor at all the nodes as it would increase the cost of implementation of control strategy tremendously.

2. The time step for controller must be equal to the time step of numerical integration in Newmark-β method for solving the equilibrium equation for dynamic response. The time step for numerical integration has been kept less than to one-fiftieth of the time period of fundamental time period (0.05 sec).

3. The precision of A/D-D/A controller is 16 bit and its range is 10 Volts. Because of this range, the command signal to control device has a constraint of V, where is the ith component of the control signal.

4. The RMS noise content of each measured response is 0.03V. This is 0.3% of the +ve or –ve range of the A/D converters. The noises have been modeled as Gaussian rectangular pulse process with pulse width similar to the time step of integration i.e. 0.02 sec.

5. The proposed hardware requirement for the controller is required to be practical in nature keeping in view of availability. Further, the computational time required by the controller is to be less to enable practical implementation of the scheme.

6. The control algorithm is required to be stable.

7. The tensions in the stay cables should be kept within certain limits. The lower bound for this is necessary so as to prevent unseating of the cables while upper bound ensures that the cable tensions do not approach their limiting stress levels. In the present case the lower limit has been kept at $0.2T_{ui}$ while the upper limit has been fixed at $0.7T_{ui}$ with T_{ui} being the ultimate cable tension in the ith cable. The ultimate cable tensions have already been presented in Table 2.1 of Chapter 2.

3.11 Design of Controller

In this section, the detailed design for an active controller has been discussed. Linear Quadratic Gaussian (LQG) designs have been proposed for the active controller. The physical components of the control system have been considered first.

3.11.1 Sensors

Both acceleration sensors and displacement sensors have been used to measure responses from appropriate locations and to feedback the same into the control algorithm. Bare minimum number of sensors has been employed in view of prohibiting cost of the sensors. The number and locations of the sensors are in line with the benchmark control problem of cable-stayed bridge proposed by Dyke *et. al.* (2003). The sensor arrangement for uniform support excitation and multiple support excitations have been considered separately.

(a) Uniform support excitations: Five accelerometers and four displacement sensors have been employed for this control scheme. Two accelerometers have been located on top of each of the pylons over the legs and one has been located on the deck at mid span. These accelerometers have been oriented to measure the absolute acceleration in the longitudinal *(X)* direction of the bridge. The natural frequency of the accelerometers have been chosen in such a way that it is at least an order of magnitude higher than the highest natural frequency of the structure that has been sought to be controlled. The selected accelerometers have a range of frequency upto 3000 rad/sec. Sensor dynamics has been neglected as an idealization in order to avoid sensor-structure interactions. Out of four displacement sensors, two each have been positioned between each of the pylons and deck.

It has been ensured that the sensor measurements are within the range of the A/D converters (as mentioned in subsection 3.10.3) by choosing appropriate sensor-sensitivities. For the accelerometers, the sensitivity has been fixed at 7 V/g (*i.e.* 7 Volts = 9.81 m/sec^2) allowing for measurement of a highest acceleration of 1.42g with a -10V to +10V range. In case of the displacement sensors, the sensitivity has been kept at 100 V/m (*i.e.*, 10 V = 0.10 m) allowing for a maximum actuator stroke of ±0.1 m for a signal of ±10 V. This range has been found to be sufficient from the control results (Table 3.5).

The sensor system has already been defined as in Eqs. (3.34) and (3.35),

(3.59)

where, represents measurement vector of either absolute accelerations or device displacements in Volts, stands for measurement vector of continuous-time absolute accelerations or device displacements in physical units (*i.e.*, m/sec^2 for accelerations and m for displacements), and is the measurement noise of sensors. stands for sensor gain matrix and is expressed as,

(3.60)

where, = 0.714 V/ (m/sec2) is the sensor gain for acceleration and = 100 V/m is the sensor gain for displacement.

The simulation of the controller has been done using the graphical tool Simulink® from the control system tool box of Matlab®. It may be mentioned that Simulink® is a component based modeling for a large system. This facilitates to arrange a complex model into separate files, where each file is a separate model [Matlab®]. By virtue of this, each design component may be modeled, simulated and tested individually. Simulink® makes it possible to design efficient control system by proper utilization of the computational capability of a computer.

The Simulink® sensor block has been shown in Fig. 3.8. As explained in Eq. (3.59), the gain block converts the continuous time acceleration measurements from physical units to Volts. A measurement noise with an RMS value of 0.03 V has been included as shown in Eq. (3.59).

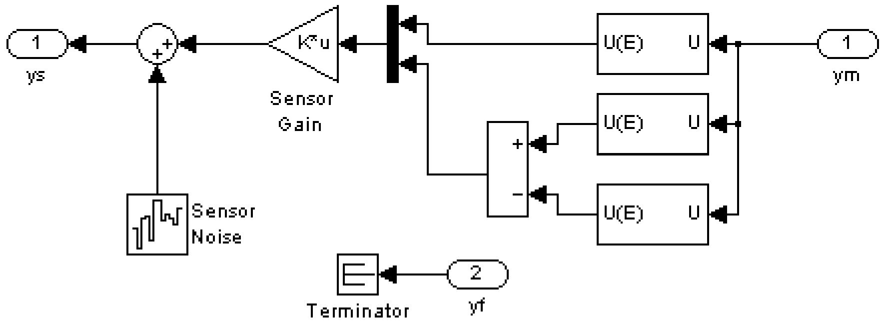

Fig. 3.8 Simulink® sensor block in Matlab®

(b) Multiple support excitations: In this case, fourteen accelerometers and four displacement sensors have been used. Out of these, six accelerometers have been located on top of the four pylon legs. Out of these, four have been oriented to measure the accelerations in the longitudinal *(X)* direction and the remaining two have been oriented to measure accelerations in the transverse *(Z)* direction. Eight accelerometers have been located on the deck, including one at mid-span, oriented to measure longitudinal accelerations. Remaining seven accelerometers have been oriented to measure transverse accelerations. Out of these seven sensors, two have been placed at each of side-spans, two have been located at quarter point of mid-span and the remaining one at mid-span. The accelerometers have the same characteristics as those used in the uniform support excitation case. Two displacement sensors have been placed between the each of the pylon and deck interface. All the displacement measurements have been obtained along the longitudinal direction of the bridge (global *X*-direction). The displacement sensors used also have the same characteristics as in the previous case of the uniform support excitation. The senor system has been defined as in Eqs. (3.34) and (3.35) with the sensor gain matrix written as,

(3.61)

3.11.2 Actuators

The choice of actuator locations is made in line with the benchmark problem by Dyke *et. al.* (2003). Since the primary objective of the control strategy is to minimize the base shear and deck shear of the pylons, the choice of locations for the actuators are limited. Only viable locations have been observed to be the deck-pylon interfaces and deck-abutment joints. Twenty four numbers of hydraulic actuators have been used to control the seismic response in both uniform and multiple support excitation cases. The placements of actuators have already been illustrated in Fig. 3.4. The governing equations for the actuators are as in Eqs. (3.38) and (3.39). These may be written as,

(3.62)

(3.63)

where, is the control force vector, D_d *is the actuator gain (i.e. the relationship* between the input voltage and the desired control force) and accounts for the gain of all the actuators used at each location. In the present study, actuator-sensitivity has been kept at $= 42.5$ kN/V allowing for the constraint of ±10V = 425 kN (as mentioned in subsection 3.10.3). It implies that a maximum capacity of 425 kN has been assumed for the actuators. For the present case takes the form,

(3.64)

The Simulink® actuator block has been shown in Fig. 3.9. As actuator-structure interaction has been neglected (considering the actuators to be ideal), no connection outputs have been provided to the devices in the Simulink® block.

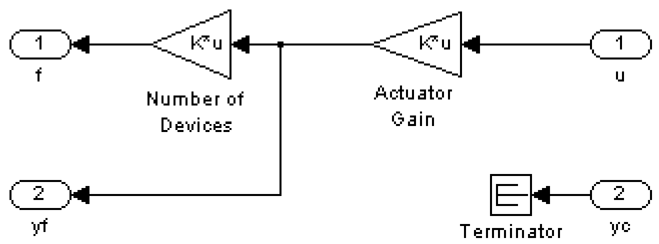

Fig. 3.9 Simulink® actuator block in Matlab®

3.11.3 Control design model

The state space model formed in section 5 is of very large order. Active control strategy based on this model is impractical due to high control response time when implemented in field. Hence it has been attempted to reduce the state space model using the concept of balance realization. The state space system matrices of the model have been converted into canonical form before balancing the model according to the system's controllability and observability grammians [23]. Balance realization reduces the system by removing the states with less controllability and observability grammians. A function *balreal.m*, available in Matlab® has been used in this purpose. The reduced order model, thus formed in Matlab®, is called the control design model. Two reduction schemes, one each for the uniform support excitation and multiple support excitations have been discussed separately here.

(a) Uniform support excitation: This model comprises of 30 states after balance realization. Transfer functions have been used to show that the control design model retains the dynamic characteristics of the control evaluation model with 916 states. Comparative *Bode* plots have been used to show these transfer functions between ground acceleration and displacement of top of left pylon for the cable stayed bridge as shown Fig. 3.10.

It has been observed that the two plots overlap for both magnitude and phase upto 10 Hz, which a sufficient range to portray the dynamics of the cable-stayed bridge. The control design model has the same outputs as in case of the control evaluation model shown in Eq. (3.25). The state space system corresponding to this model has been represented by the equations,

(3.65)

(3.66)

(3.67)

where, is the control design state vector, and are the system state matrices for the reduced system. Further, **is the regulated output vector (regulated outputs** are the displacement of the abutment nodes), which has been mapped through the mapping matrices, , and . Similarly, is the measurement vector which has been obtained through the mapping matrices, , and . is the ground acceleration and **is the control signal vector. It is clear from the above** formulation that the inputs to the control design model are the ground excitation at the base of the structure and the control signals from the devices. On the other hand, the inputs to the control evaluation model include the ground excitation and the applied control forces to the structure as in Eq. (3.9).

(b) Multiple support excitations: As the excitation is applied bi-directionally, in this case 60 states have been retained. The resulting model has the same outputs as the reduced control evaluation model as in Eq. (3.33). The state space system corresponding to this reduced order model is as follows,

(3.68)

(3.69)

(3.70)

where, the notations bear the same meaning as in Eqs. (3.65) to (3.67). The vector notations stands for support accelerations and for velocity at supports due to the multiple support excitations. The inputs to the control evaluation model include the ground excitation and the applied control forces to the structure as in Eq. (3.10).

3.11.4 Control algorithm

The control algorithm for the present work has been discussed in this section. The simplest form of feedback control, namely the Quadratic optimal feedback Regulator (LQR), has not been adopted for the current study as it is not practical to put sensor to measure all the states of the system. LQG controller has been used here as it works on the basis of measurements from limited sensors. The LQG controller is an LQR working in conjunction with an observer to reconstruct the unavailable states. Kalman filter has been used as the observer. A filter is constructed from a deterministic system which yields a random signal with desired statistical properties when excited by random signals. In the present case, the random signal is the earthquake input which comes as process noise into the system.

The Kalman filter has been designed as a linear time-invariant filter to reduce the effects of measurement noise on control system. The construction of the filter is based *minimization* of a statistical measure of the *estimation error*

where, is the estimated state-vector *of the actual unmeasured state vector* .

The state equation of the Kalman Filter is that of a time-varying observer and can be written for the control design model as,

(3.71)

where, is the gain matrix *of the Kalman Filter (also called* optimal observer gain *matrix*). Being an *optimal* observer, the Kalman Filter is a counterpart of the optimal regulator (LQR). However, while the optimal regulator minimizes an objective function based on transient and steady-state response together with control effort, the Kalman Filter minimizes the *covariance of the estimation error*. This *state estimation* carried out by the Kalman filter as an *observer* has been incorporated into the control system in the form of a *compensator*.

Thus, the combination of optimal regulator (LQR) with optimal observer (Kalman Filter) results in an *optimal compensator*. Since the optimal compensator has been based on a linear plant, a quadratic objective function, and an assumption of white noise which has Gaussian probability distribution, the optimal compensator is known as *Linear, Quadratic, Gaussian* (LQG) compensator. Steps followed in designing the LQG controller are [Tewari (2002)]:

(1) Design of an *optimal* regulator for the plant is to be carried out assuming *full-state feedback* (i.e. assuming that all the states are available for measurement) and an objective function. The regulator is designed to generate a control input, , based upon the measured state vector .

(2) Design of a Kalman Filter for the plant assuming a known control input ,
a measured control output , and earthquake excitation as white noises with known power spectral densities. The Kalman Filter has been designed to provide an optimal *estimate* of the state-vector .

(3) Combination of the separately designed optimal regulator and Kalman Filter into an optimal compensator which generates the input vector , based upon the estimated state-vector , rather than the actual state-vector , and the measured output vector .

The solution to the LQR problem is a linear, constant gain feedback given by,

(3.72)

where, is the solution of the LQR problem and is the reconstructed state from the Kalman Filter. The cost function chosen to be minimized in the LQR problem is written as,

(3.73)

The regulated outputs have already been defined in Eqs. (3.66) and (3.69). The controlled cost matrix corresponds to eight control device locations and accordingly **R** is a [8×8] identity matrix. The state weighting matrix for the four weighted outputs of deck displacements at abutment has been chosen as,

(3.74)

where Q is the weight arrived at by trial and error for maximum control. For multiple support excitations the state weighting matrix has been chosen as,

(3.75)

where, is the weighing factors for four deck displacements at deck abutment joints and and is the weighting factor for deck acceleration (X) *at mid-span.*

The duality between the design of the regulator and the Kalman filter has been explained with the relationship of the algebras of the two problems. The LQR gain in Eq. (3.72) has been given by Dyke *et. al.* (2000) as,

(3.76)

where, is the solution of the algebraic Riccati equation given by,

(3.77)

The notations used in this equation are defined as,

(3.78)

(3.79)

(3.80)

(3.81)

The gain has been determined using the Matlab® 7.0 routine lqry.m *within the* control toolbox.

The Kalman Filter optimal estimator is given by,

(3.82)

(3.83)

where, **S** is the solution of the algebraic Riccati equation given by,

(3.84)

The notations used in the above equation are defined as,

(3.85)

(3.86)

(3.87)

(3.88)

System noise (earthquake excitation) has been considered as stationary white noise while measurement noise has been considered to be identically distributed, statistically independent Gaussian white noise process. The ratio of spectral density of the two noises has been assumed as . The Kalman gain L **has been** determined using the Matlab® routine *lqe.m* within the control toolbox.

The controller has been put in the form of Eqs. (3.36) and (3.37) for digital implementation of the control algorithm. The conversion of the continuous state space system to discrete system has been done with bilinear transformation in Matlab® using the *c2dm.m* routine within the control toolbox. The discrete state space system is given as,

(3.89)

(3.90)

The Simulink® block of Matlab® used to represent the control algorithm in simulation has been illustrated in Fig. 3.11.

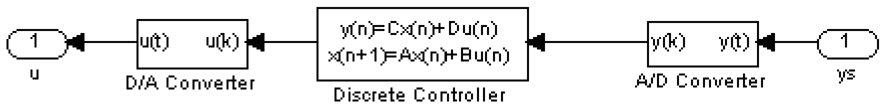

Fig. 3.11 Simulink® block for implementation of digital controller

The analog signal from the sensors y_S is converted to a digital signal by A/D converter. The discrete controller works with the digital information and sends a digital output for the converter. The digital signal is then converted to analog one by the D/A converter. This analog signal **u** is input to the actuator to trigger the actuating force for controlling response of the bridge.

3.12 Numerical Simulation

The Simulink® block in Matlab® used for numerical simulation of control implementation has been illustrated in Fig. 3.12. The Simulink® works as an assemblage of different components of structure-control combination. In the block diagram, the plant of the control system is the control evaluation model. The property matrices of the control evaluation model e.g. mass, damping and stiffness matrices have been masked into block diagram. The plant is acted on by the earthquake excitations and control forces and is analyzed using Newmark-β method. The evaluation and measurement outputs have been used appropriately for evaluation of the controller and for feeding the sensors respectively. The sensor data is used to reconstruct the states and the same is used for development of the controller. It may be mentioned that the controller has been designed based on the control design model from subsection 3.11.3. The controller sends the control signal and completes the loop. The noise to the system are modeled and fed appropriately into the blocks.

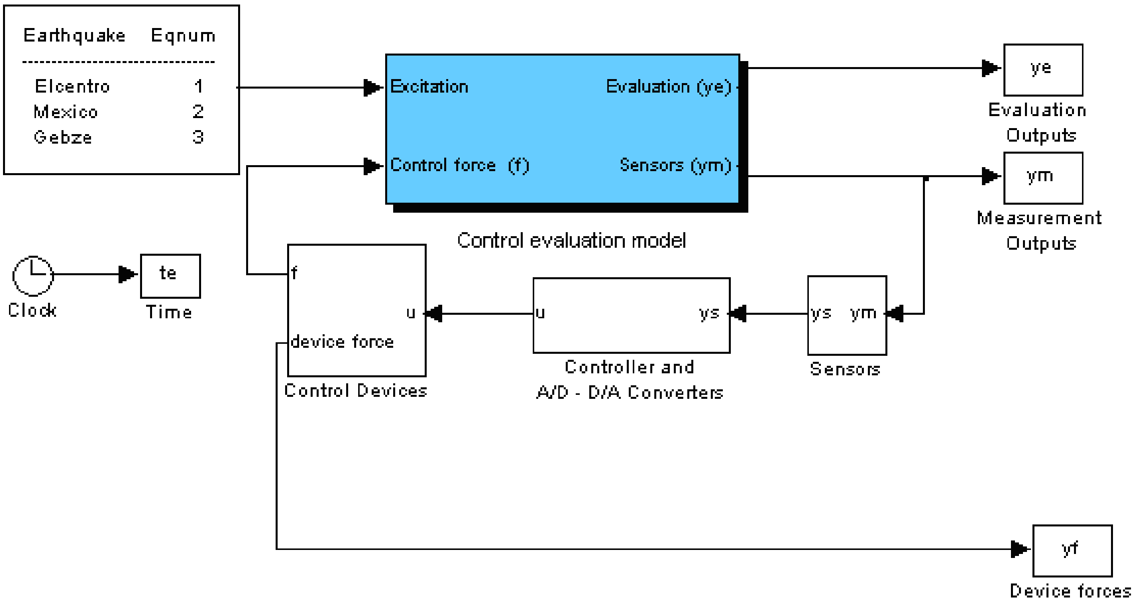

Fig. 3.12 Simulink® model in Matlab®

3.13 Results and Discussion

The performance of the controller has been evaluated and discussed in this section for both uniform support excitations and multiple support excitations. The results have been shown in terms of evaluation criteria as listed in Table 3.3.

3.13.1 Uniform support excitation

The results for uniform support excitation have been presented in Table 3.4. These results correspond to a value of the state weighting matrix multiplication factor in Eq. (3.74). The controller reduces the responses of base shear and overturning moment of the pylon to considerable extent as indicated by evaluation criteria J_1 and J_3 respectively. However, during this process the deck shear and deck moment have increased marginally (evaluation criteria J_2 and J_4 respectively). The reduction of base shear and overturning moment of the pylon is of great practical importance as these are significant criteria for pylon design and can reduce the cost of pylon considerably. In addition to reducing the peak responses at strategic locations, the controller effectively reduces the norm of base shear and overturning moment significantly (criteria J_7 and J_9). It may be recalled that the norm of response is indicator of response averaged over a time (Eq. 3.48) and this index shows how the controller has been effective over the entire excitation period.

The control performances of base shear and overturning moment responses in case of the left pylon corresponding to all the three representative earthquakes have been presented in Figs. 3.13 and 3.14 respectively. It has been observed from the Fig. 3.13 that substantial reduction in base shear has been achieved through the controller with highest reduction of peak response as 46.42% (in the case of the Mexico City earthquake). Similar trend has also been observed in the case of control of peak response of overturning moment, where a maximum of 60.61% reduction in peak overturning moment has been observed against the El Centro earthquake (Fig. 3.14). The controlled and uncontrolled cable tensions corresponding to three earthquake excitations have been shown in Figs. 3.15 to 3.16. The upper and lower acceptable range of cable tensions have been shown with broken lines. The controlled cable tensions have been found to be well within this prescribed limit. It has also been observed that the cable tensions in the uncontrolled cases move towards a narrower band into the prescribed range. It has been observed that the out of range cable tensions in the uncontrolled structure under El Centro excitation have been brought within the limit in the controlled case. The peak demand on the actuators in terms of force, stroke, and velocity in achieving the stated control performance against each of the earthquakes (Table 3.4) have been presented in Table 3.5. It has been observed that the force requirements as well as the velocity requirements are feasible in a device of this size. The design capacity of the actuators against uniform support excitations for the selected earthquakes is thus 300 kN.

3.13.2 Multiple support excitation

The results of multiple support excitations have been presented in this section. The results are obtained using value of and in the state weighting matrix expressions in Eq. (3.75). These results have been presented under two headings corresponding to the two angles of incidences, i.e, Case-1 and Case-2 (subsection 3.10.2).

(a) Case-1: The performance of the controller against different evaluation parameters have been presented in Table 3.5. It has been observed that the controller reduces the response of base shear and overturning moment of the pylons to considerable extent in the direction of its orientation (global *X*). However the shear force and the bending moment experienced by pylons at deck level have been controlled to a lesser extent. It has also been noticed that the respective key responses in the transverse direction (global *Z*) have slightly increased over the uncontrolled responses. It may be recalled that actuators have been oriented in the global *X* direction and it is natural that these are not effective in controlling the forces in the transverse direction. The reduction of pylon forces of great practical importance as these are significant criteria for pylon design and can reduce the cost of pylon considerably.

The control performances of base shear and overturning moment for pylon-I against the representative earthquakes have been presented in Figs. 3.18 and 3.19 respectively. The highest control with respect to the base shear has been observed to be 35.63% and that in case of overturning moment has been found to be 33.77%. The controlled and uncontrolled cable tensions have been illustrated in Figs. 3.20 to 3.22. The controlled responses have brought within a narrower band within the permissible band (indicated by broken lines). It has been observed that the out of range cable tensions in uncontrolled case corresponding to the El Centro excitation has been brought within the permissible limit in the controlled case. The peak demands on force, stroke, and velocity for the actuator for each of the earthquakes are presented in Table 3.7. The peak actuator force has been observed to be within the actuator capacity 425 kN. Other requirements, e.g. device stroke, and device velocity have also been observed to be feasible in a device of this size.

(b) Case-2: The performance of the controller against different evaluation criteria have been presented in Table 3.8. It has been observed that the controller is highly successful in controlling shear force bending moments at key locations in the pylons in the longitudinal direction of the bridge. In a similar observation with Case-1, the transverse components of the pylon forces have increased marginally for the controlled case. This may be explained in the same manner as in Case-1 that the actuator being oriented along the longitudinal direction it is natural not to have any controlling effect in the transverse direction of the bridge.

The control performances of base shear and base moment responses against the three earthquakes have been presented in Figs. 3.23 and 3.24 respectively. The controller shows encouraging results in this excitation case too as evident from the representative figures. The controlled and uncontrolled cable tensions have been illustrated in Figs. 3.25 to 3.26. They have been found to be well within this limit. As in the Case-1, the out of range cable tensions of El Centro excitation case has been corrected in the controlled case. The peak values of the force, stroke, and velocity for the controller for each of the earthquakes have been shown in Table 3.9. It has been observed that these requirements are feasible in a device of this size. It has been observed from Tables 3.7 and 3.9 that the capacity 425 kN is sufficient for actuators against multiple support excitations for the selected earthquakes.

3.14 Conclusion

Two active controllers have been designed to control seismic response of a Quincy Bayview cable-stayed bridge against select earthquakes. An updated finite element model has been used in this study to arrive at the linear evaluation model, reduced model and finally the state space model that has been used to construct the control design model. The active controller shows effective control capability in controlling key pylon responses against the selected earthquake. The present controller has been found to be a realistic one as it has been based on an updated finite element model of the cable-stayed bridge.

Table 3.1 Uncontrolled maximum responses against uniform support excitations

Response	Definition	Earthquakes		
		El Centro	Mexico City	Gebze
(kN)		1.243	0.317	0.411

(kN)	1.296	0.427	0.742
(kNm)	2.780	0.556	1.829
(kNm)	5.91	2.31	2.97
(m)	5.783	2.221	3.391
	1.389	0.398	0.675
	1.195	0.525	0.591
	0.297	0.812	1.613
	0.496	1.896	2.467
(m)	4.371	2.093	3.977
(m/sec)	7.160	3.643	6.066

Response	Direction	Definition	Case-1			Case-2		
			El Centro	Mexico	Gebze	El Centro	Mexico	Gebze

(kN)	*X*	1.64×10^4	0.66×10^4	0.94×10^4	1.19×10^4	0.63×10^4	0.75×10^4
(kN)	*Z*	0.36×10^4	2.76×10^4	0.29×10^4	0.49×10^4	2.38×10^4	0.42×10^4
(kN)	*X*	1.57×10^3	0.79×10^3	0.97×10^3	1.74×10^3	0.76×10^3	0.98×10^3
(kN)	*Z*	1.79×10^3	0.51×10^3	1.39×10^3	2.39×10^3	0.73×10^3	1.57×10^3
(kNm)	*X*	1.73×10^5	0.72×10^5	0.80×10^5	1.07×10^5	0.32×10^5	0.49×10^5
(kNm)	*Z*	1.21×10^5	0.77×10^5	0.89×10^5	1.96×10^5	0.69×10^5	1.41×10^5
(kNm)	*X*	0.62×10^5	0.29×10^5	0.32×10^5	0.57×10^5	0.14×10^5	0.33×10^5
(kNm)	*Z*	0.84×10^5	0.84×10^4	2.19×10^4	0.35×10^4	0.99×10^4	2.59×10^4
(m)	*X*	3.34×10^{-2}	1.27×10^{-2}	2.07×10^{-2}	2.19×10^{-2}	0.98×10^{-2}	1.98×10^{-2}
(kN)	*X*	1.59×10^3	0.89×10^3	0.79×10^3	1.57×10^3	0.81×10^3	0.67×10^3
(kN)	*Z*	0.49×10^3	0.27×10^3	0.26×10^3	0.53×10^3	0.26×10^3	0.30×10^3
(kN)	*X*	1.49×10^2	0.89×10^2	0.88×10^2	1.47×10^2	0.82×10^2	0.76×10^2
(kN)	*Z*	1.99×10^2	0.17×10^2	0.98×10^2	2.39×10^2	0.89×10^2	1.21×10^2
(kNm)	*X*	0.34×10^5	0.19×10^5	0.18×10^5	0.34×10^5	0.17×10^5	0.15×10^5
(kNm)	*Z*	1.63×10^4	0.82×10^4	0.81×10^4	1.79×10^4	0.80×10^4	0.96×10^4
(kNm)	*X*	0.61×10^4	0.36×10^4	0.36×10^4	0.61×10^4	0.35×10^4	0.31×10^4
(kNm)	*Z*	0.32×10^4	0.99×10^3	1.69×10^3	0.37×10^3	1.35×10^3	1.99×10^3
(m)	*X*	9.54×10^{-2}	7.55×10^{-2}	8.37×10^{-2}	9.92×10^{-2}	7.65×10^{-2}	7.99×10^{-2}
(m/sec)	*X*	1.16	0.62	0.83	1.25	0.59	0.79

Table 3.2 Uncontrolled maximum responses against multiple-support excitation

Table 3.4 Evaluation criteria of the active controller against uniform support excitation

Value	El Centro	Mexico	Gebze	Maximum
J_1	0.7488	0.8025	0.9838	0.9838
J_2	0.9375	0.9778	0.9432	0.9778
J_3	0.6061	0.5064	0.5433	0.6061
J_4	0.7488	0.8025	0.9838	0.9838
J_5	0.185	1	0.159	0.185
J_6	1.65	4.21	3.73	3.73
J_7	0.6555	0.5013	0.5463	0.6555
J_8	0.9566	0.9643	0.9366	0.9643
J_9	0.6055	0.4943	0.5104	0.6055
J_{10}	0.8463	0.9291	0.9827	0.9827
J_{11}	0.023	0.009	0.015	0.023
J_{12}	1.895	6.1	1.803	1.895
J_{13}	1.26	1.08	1.98	1.98
J_{14}	3.71	1.6	7.2	7.2
J_{15}	5.6	3.1	7.1	7.1
J_{16}	24	24	24	24
J_{17}	9	9	9	9
J_{18}	30	30	30	30

Table 3.5 Actuator requirements for uniform support excitation

Response	El Centro	Mexico	Gebze	Max

Force(kN)	269.08	86.57	255.99	269.99
Stroke(m)	0.0549	0.0227	0.0786	0.0786
Vel (m/sec)	0.3156	0.1546	0.3012	0.3156

Table 3.6 Evaluation criteria for active controller for multiple support excitation: Case-1

Value	Direction	El Centro	Mexico	Gebze	Maximum
J_1	X	0.6437	0.6832	0.7238	0.7238
	Z	1.0352	1.1134	1.0562	1.1131
J_2	X	0.8952	0.9012	0.9867	0.9867
	Z	0.9565	0.9732	0.9932	0.9932
J_3	X	0.6623	0.7025	0.7536	0.7536
	Z	1.0526	1.0496	1.0231	1.0526
J_4	X	0.8323	0.8529	0.9365	0.9365
	Z	1.1023	1.000	1.0025	1.1023
J_5	X	0.2125	0.0912	0.1863	0.2125
J_6	X	1.0985	1.7365	1.9125	1.9125
J_7	X	0.5237	0.5823	0.6321	0.6321
	Z	1.0123	1.0825	1.1126	1.1126
J_8	X	0.8223	0.8726	0.9236	0.9236
	Z	0.9825	0.9925	0.9912	0.9925
J_9	X	0.6231	0.6423	0.6821	0.6821
	Z	1.0521	1.0921	1.0689	1.0921
J_{10}	X	0.8526	0.8741	0.9124	0.9124
	Z	1.0234	1.0924	1.0125	1.0924
J_{11}		1.825	1.426	1.589	1.825
J_{12}		2.8307	1.687	2.8	2.8307
J_{13}		0.542	0.473	0.781	0.781
J_{14}		2.589	1.239	4.528	4.528
J_{15}		4.989	2.571	5.287	5.287
J_{16}		24	24	24	24
J_{17}		14	14	14	14
J_{18}		60	60	60	60

Table 3.7 Actuator requirements for multiple support excitation: Case-1

Response	Direction	El Centro	Mexico	Gebze	Max

Force(kN)	X	410.11	240.39	403.89	410.11
Stroke(m)	X	0.0421	0.0318	0.0686	0.0686
Vel (m/sec)	X	0.5156	0.1865	0.2912	0.5156

Table 3.8 Evaluation criteria for active controller for multiple support excitation: Case-2

Value	Direction	El Centro	Mexico	Gebze	Maximum
J_1	X	0.6858	0.6687	0.7023	0.7023
	Z	1.0134	1.0468	1.0367	1.046
J_2	X	0.8790	0.9978	0.9896	0.9978
	Z	0.9845	0.9700	0.9932	0.9932
J_3	X	0.6889	0.7287	0.7926	0.7926
	Z	1.0100	0.997	0.987	1.0100
J_4	X	0.8434	0.8636	0.8856	0.8865
	Z	1.0014	1.0010	1.0125	1.0125
J_5	X	0.2376	0.1098	0.1967	0.2376
J_6	X	1.2124	1.9736	2.1581	2.1581
J_7	X	0.5489	0.6047	0.6475	0.6475
	Z	1.0067	1.0431	1.0866	1.0866
J_8	X	0.8014	0.8967	0.9456	0.9456
	Z	0.9923	0.9876	1.0078	1.0078
J_9	X	0.6645	0.6621	0.7069	0.7069
	Z	0.9987	1.0065	1.0459	1.0459
J_{10}	X	0.8723	0.9023	0.9367	0.9367
	Z	1.0348	1.0469	1.0543	1.0543
J_{11}		1.886	1.445	1.690	1.886
J_{12}		2.5301	1.672	2.25	2.5301
J_{13}		0.560	0.606	0.793	0.793
J_{14}		2.652	1.425	4.125	4.125
J_{15}		4.569	2.670	5.124	5.124
J_{16}		24	24	24	24
J_{17}		14	14	14	14
J_{18}		60	60	60	60

Table 3.9 Actuator requirements for multiple support excitation: Case-2

Response	Direction	El Centro	Mexico	Gebze	Max
Force(kN)	*X*	370.25	240.35	345.36	370.25
Stroke(m)	*X*	0.0549	0.0349	0.0586	0.0586
Vel (m/sec)	*X*	0.2945	0.2123	0.2234	0.3156

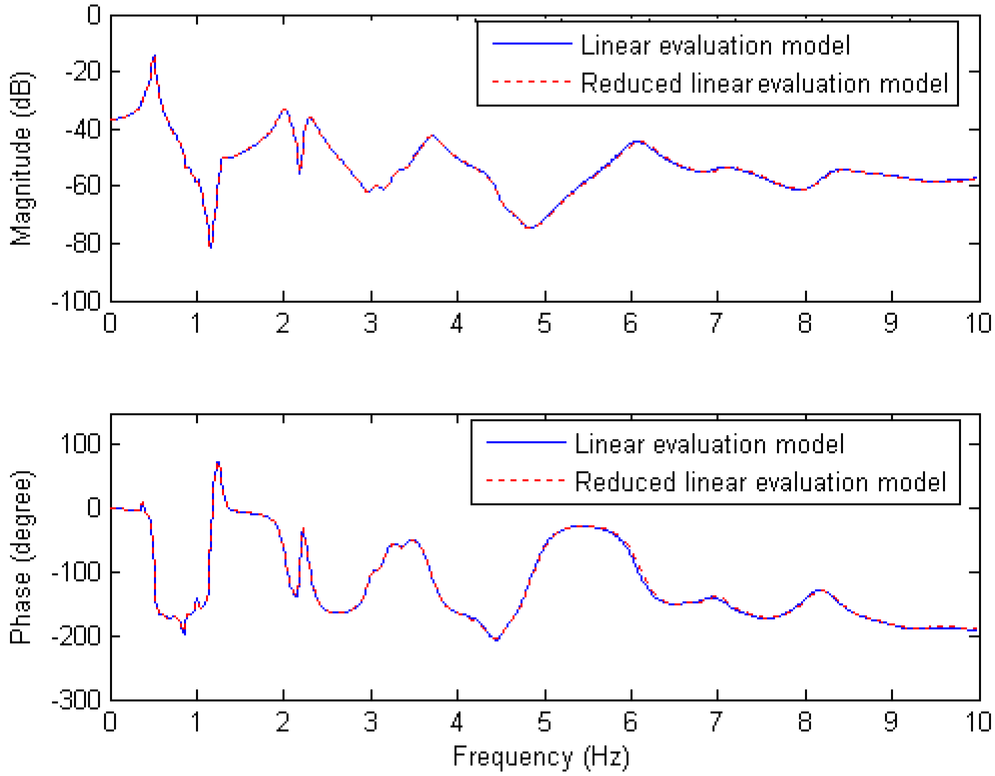

Fig. 3.5 Transfer function of ground acceleration to displacement at top of l eft pylon

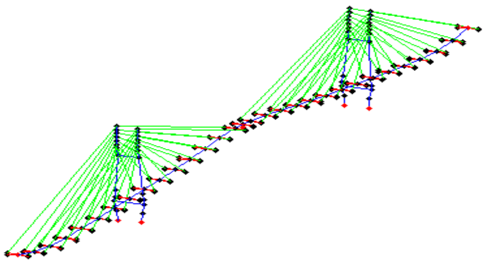

First mode (flexural, 0.375Hz)

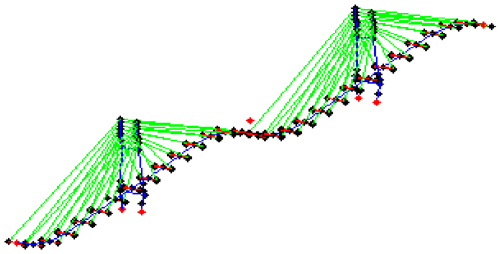

Second mode (flexural, 0.50Hz)

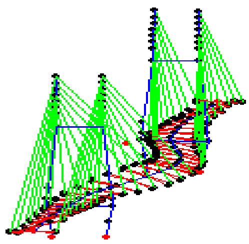

Third mode (trans-torsional, 0.58 Hz)

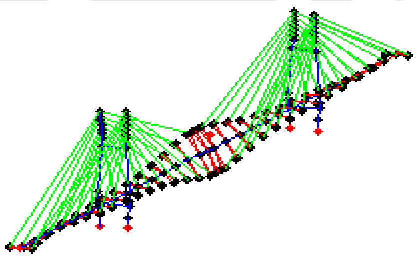

Fourth mode (tor-transverse, 0.73 Hz)

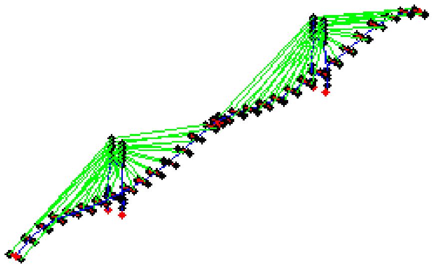

Fifth mode (flexural, 0.80 Hz)

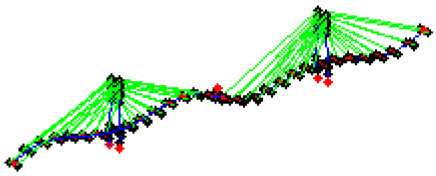

Sixth mode (flexural, 0.86 Hz)

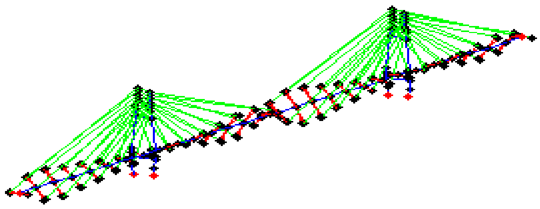

Seventh mode (mixed-torsional, 0.88 Hz.)

Fig. 3.6 Mode shapes of the reduced linear evaluation model

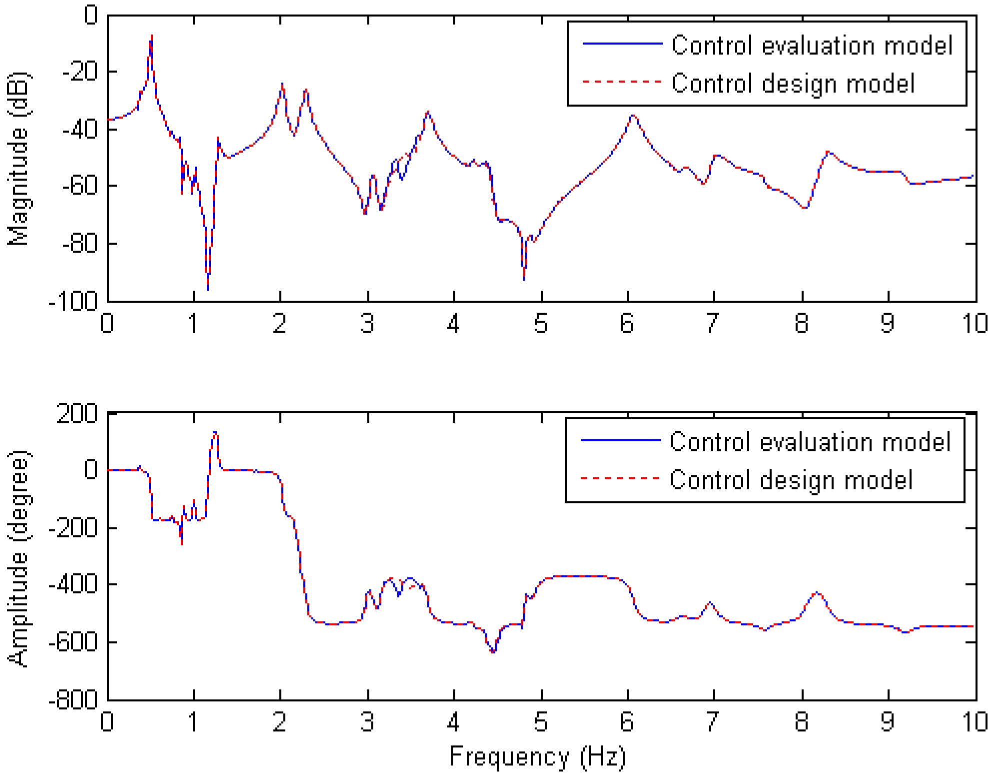

Fig. 3.10 Transfer function of ground acceleration to displacement at top of left pylon

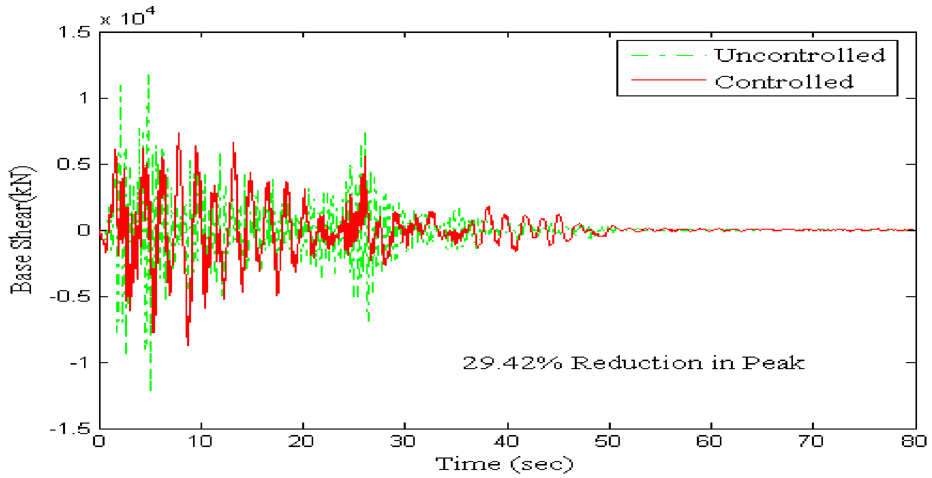
x 10^4
1.5
1
0.5
0
-0.5
-1
-1.5
Base Shear(kN)
Uncontrolled
Controlled
29.42% Reduction in Peak
0
10
20
30
40
50
60
70
80
Time (sec)

(a)

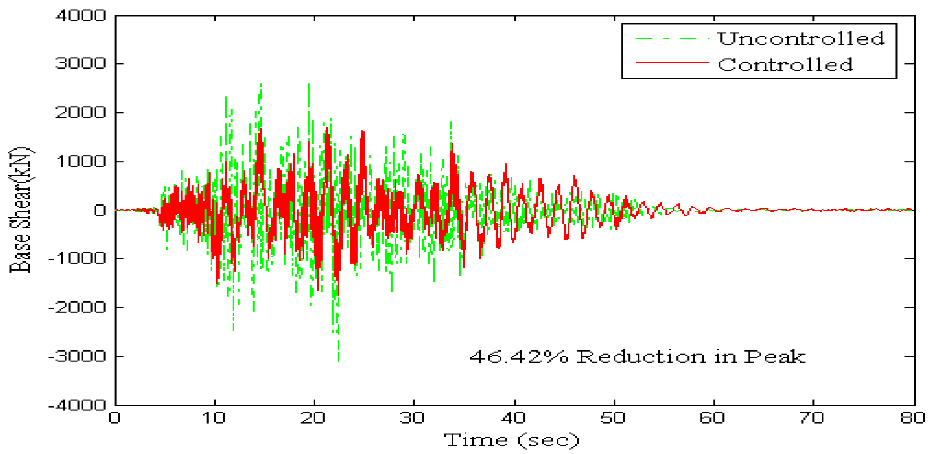
4000
3000
2000
1000
0
-1000
-2000
-3000
-4000
Base Shear(kN)
Uncontrolled
Controlled
46.42% Reduction in Peak
0
10
20
30
40
50
60
70
80
Time (sec)

(b)

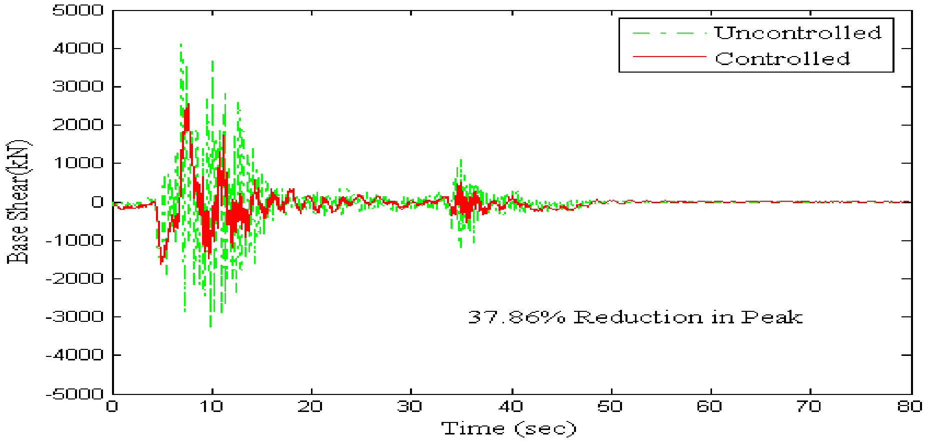

(c)

Fig. 3.13 Time history of base shear in pylon I against uniform support excitation: El Centro earthquake, (b) Mexico City earthquake, (c) Gebze earthquake

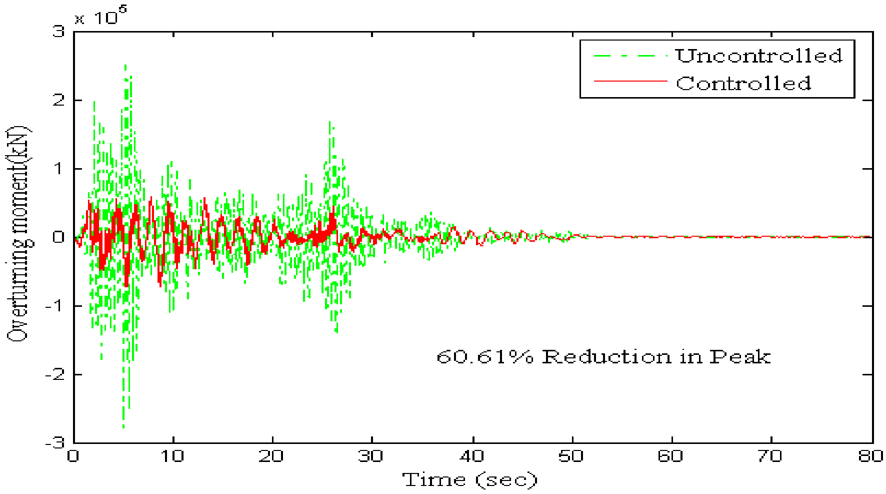

(a)

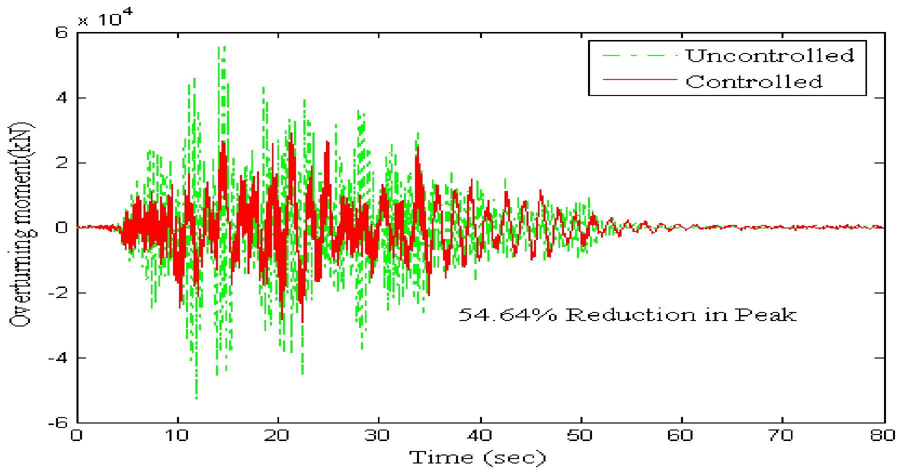

(b)

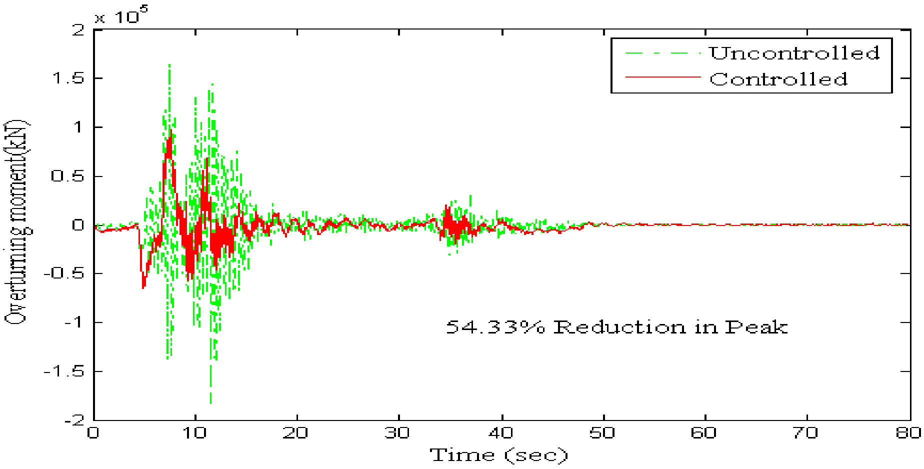

(c)

Fig. 3.14 Time history of overturning moment in pylon I against uniform support excitation: (a) El Centro earthquake, (b) Mexico City earthquake, (c) Gebze earthquake

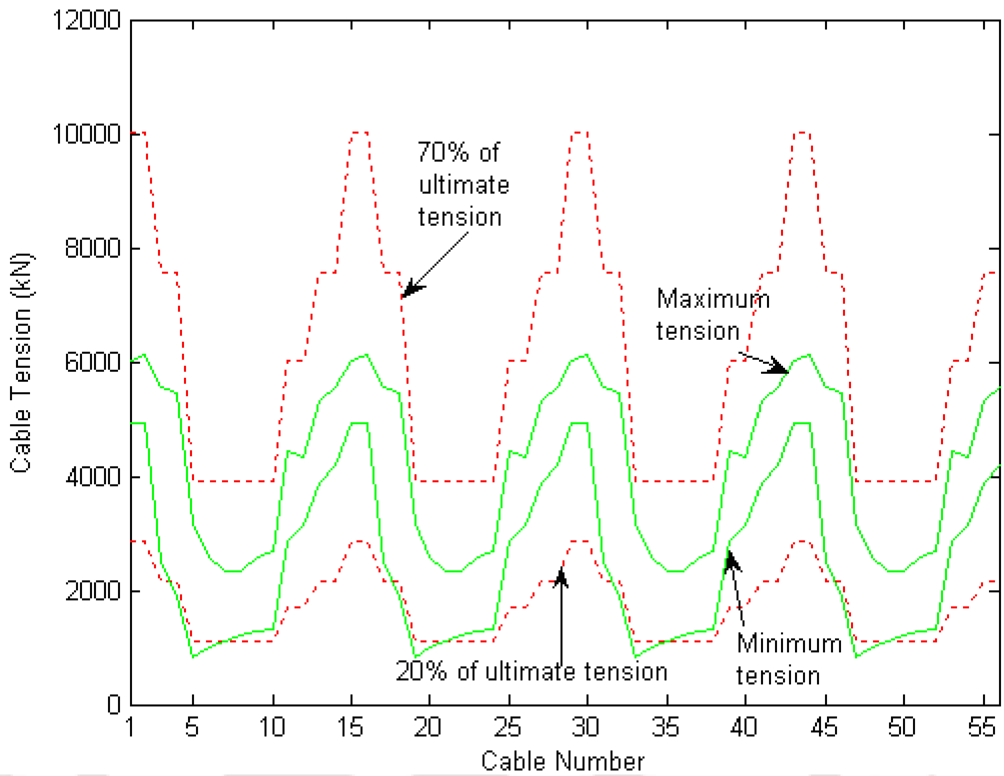

12000
10000
8000
6000
4000
2000
0
Cable Tension (kN)
1
5
10
15
20
25
30
35
40
45
50
55
Cable Number
70% of ultimate tension
Maximum tension
20% of ultimate tension
Minimum tension

(a)

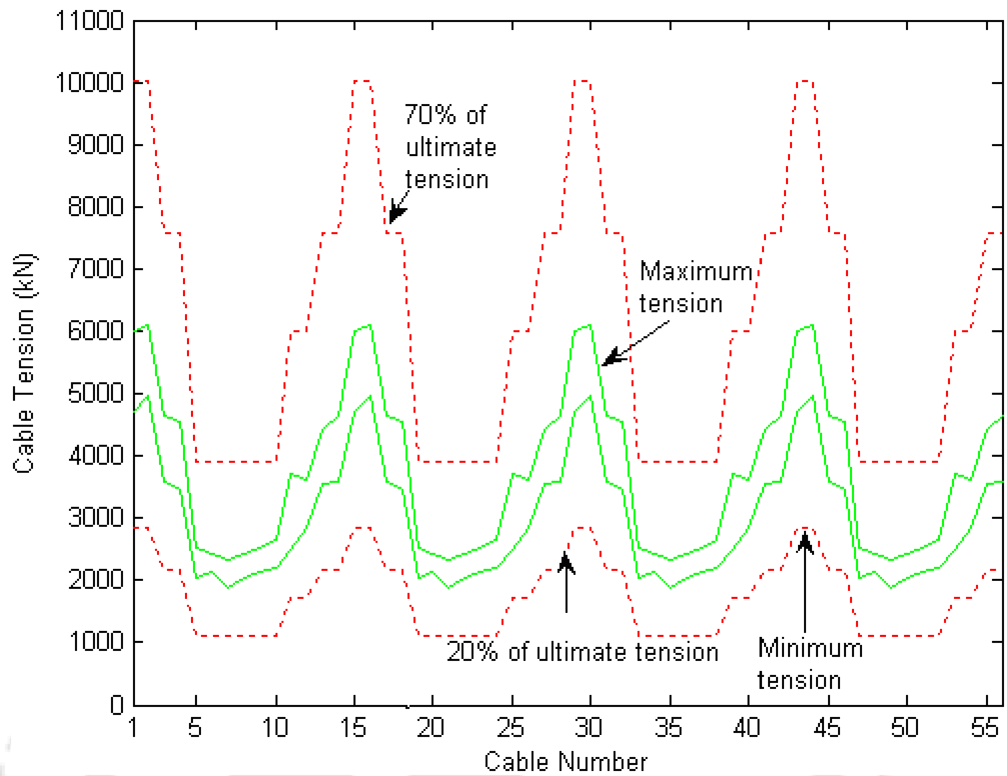

(b)

Fig. 3.15 Cable tension against uniform support excitation of El Centro earthquake: (a) Uncontrolled response, (b) Controlled response

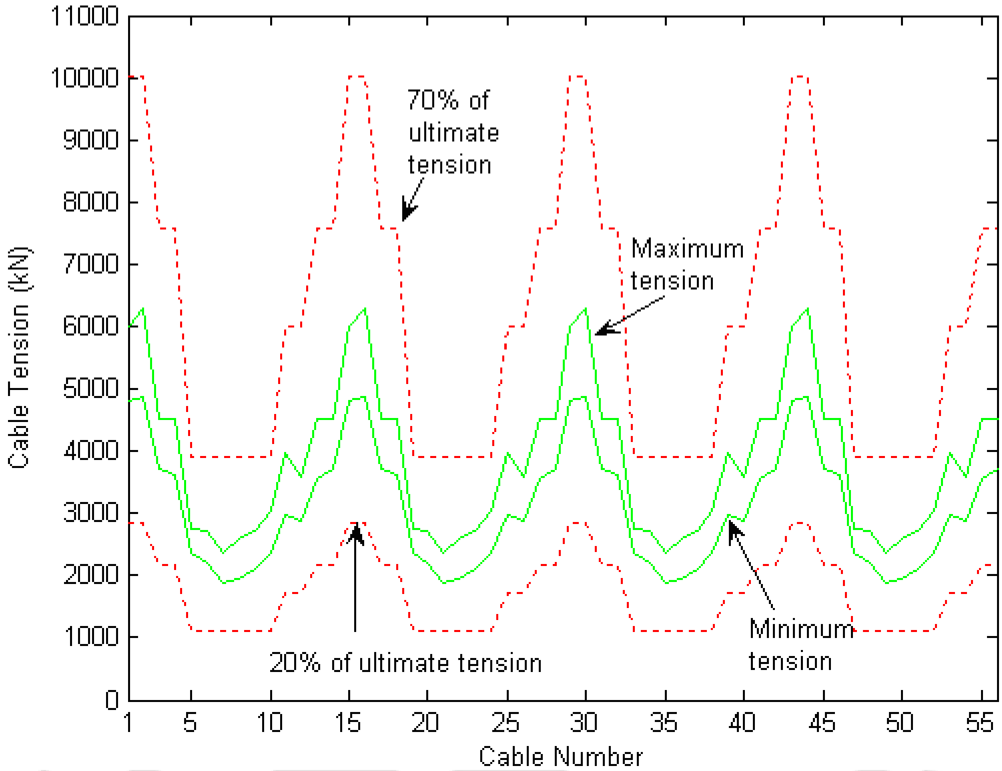

Cable Tension (kN)
Cable Number
70% of ultimate tension
Maximum tension
Minimum tension
20% of ultimate tension
0
1000
2000
3000
4000
5000
6000
7000
8000
9000
10000
11000
1
5
10
15
20
25
30
35
40
45
50
55

(a)

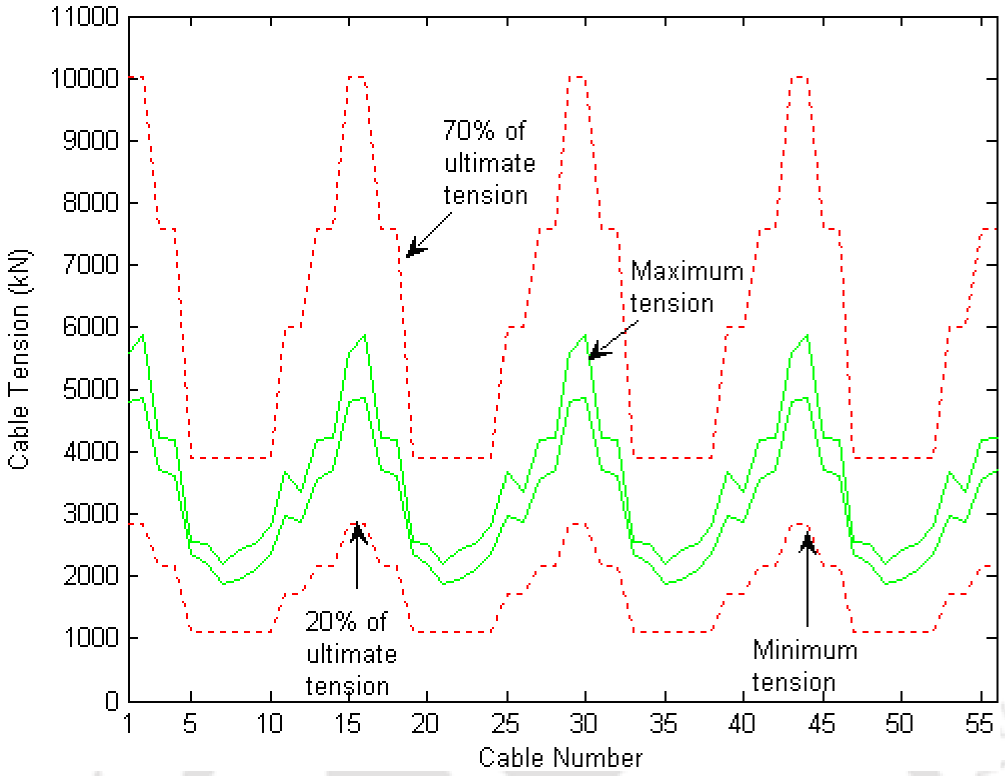

(b)

Fig. 3.16 Cable tension against uniform support excitation of Mexico City earthquake: (a) Uncontrolled response, (b) Controlled response

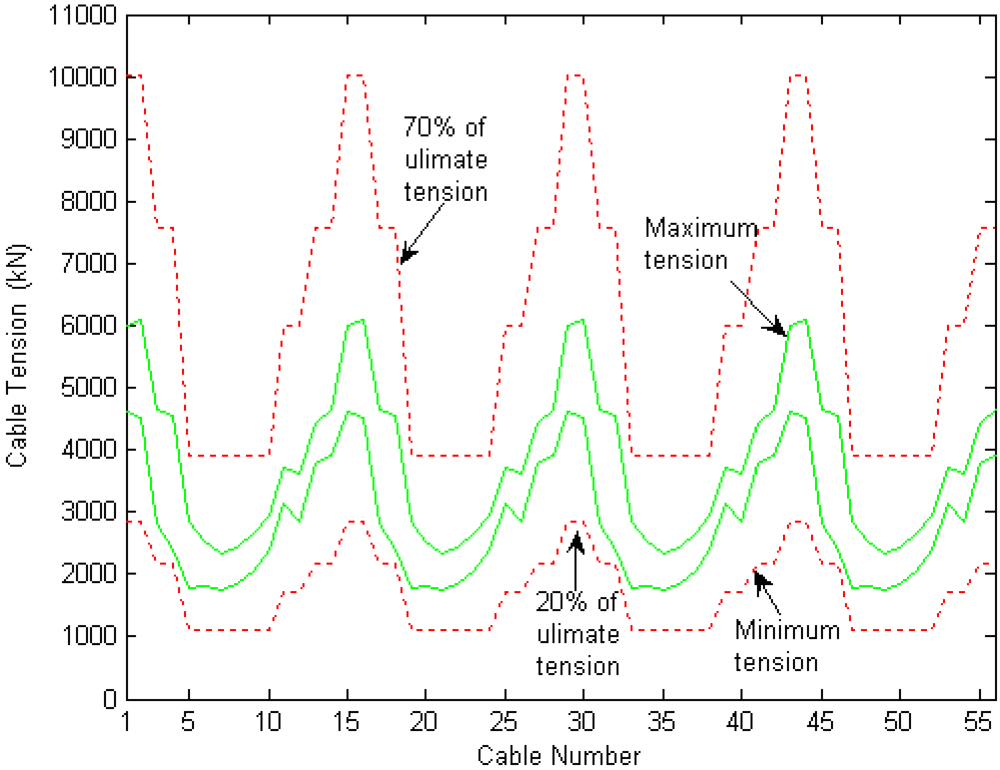
Cable Tension (kN)
Cable Number
70% of
ulimate
tension
Maximum
tension
20% of
ulimate
tension
Minimum
tension

(a)

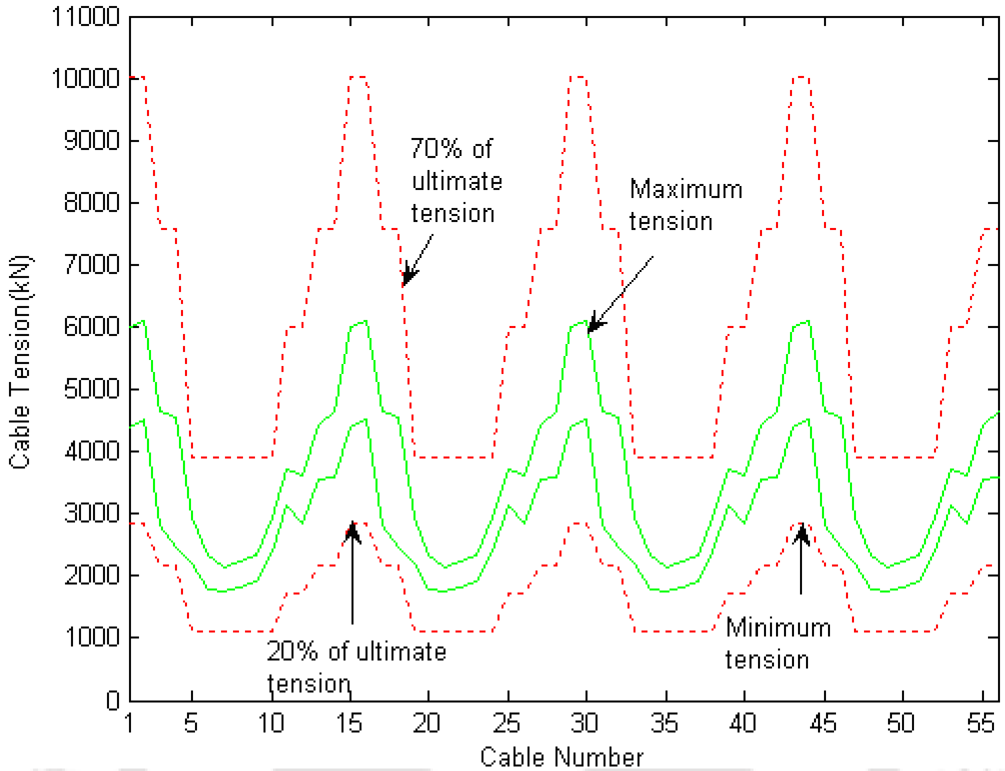

(b)

Fig. 3.17 Cable tension against uniform support excitation of Gebze earthquake: (a) Uncontrolled response, (b) Controlled response

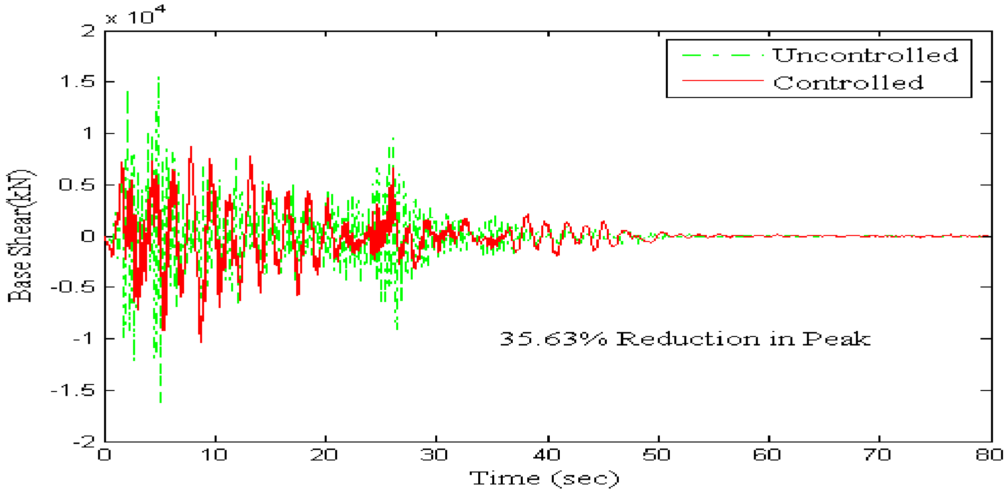

x 10^4
Uncontrolled
Controlled
35.63% Reduction in Peak
Base Shear(kN)
Time (sec)

(a)

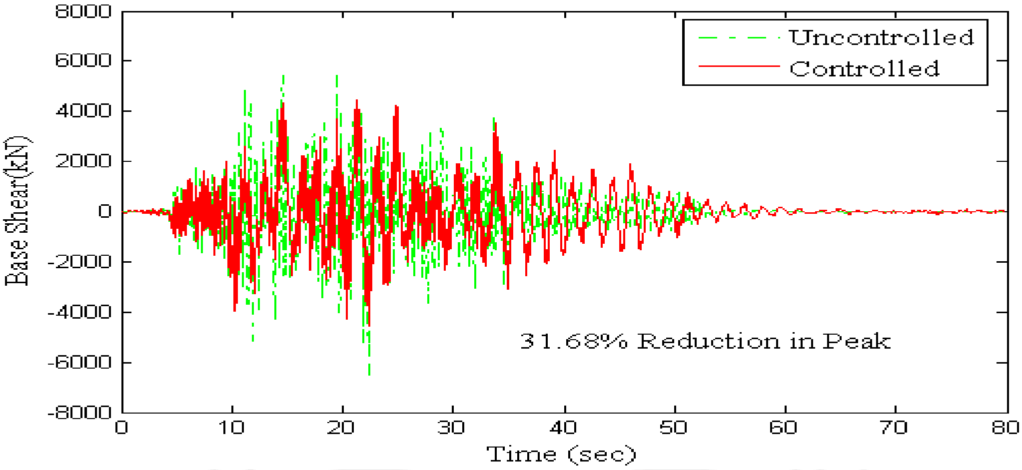

Uncontrolled
Controlled
31.68% Reduction in Peak
Base Shear(kN)
Time (sec)

(b)

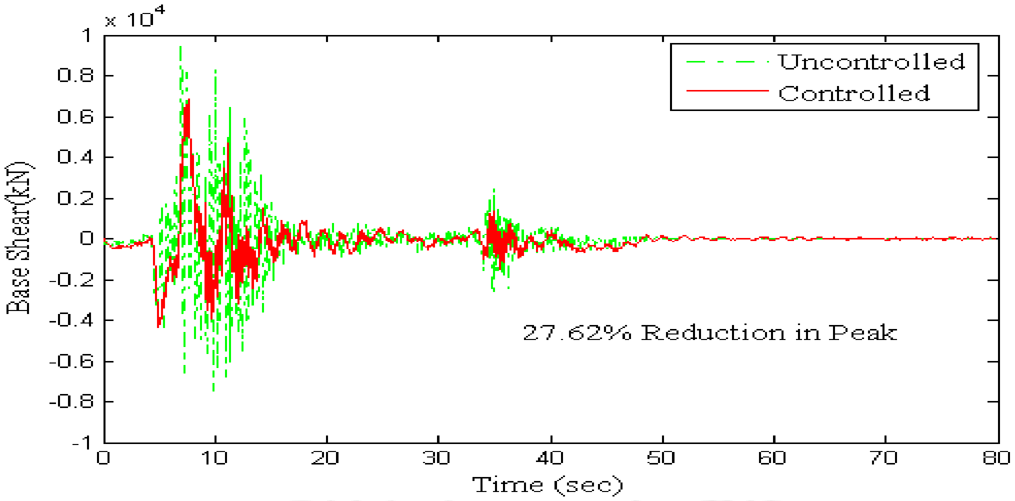

(c)

Fig. 3.18 Time history of base shear in pylon I against multiple support excitation (Case-1): (a) El Centro earthquake, (b) Mexico City earthquake, (c) Gebze earthquake

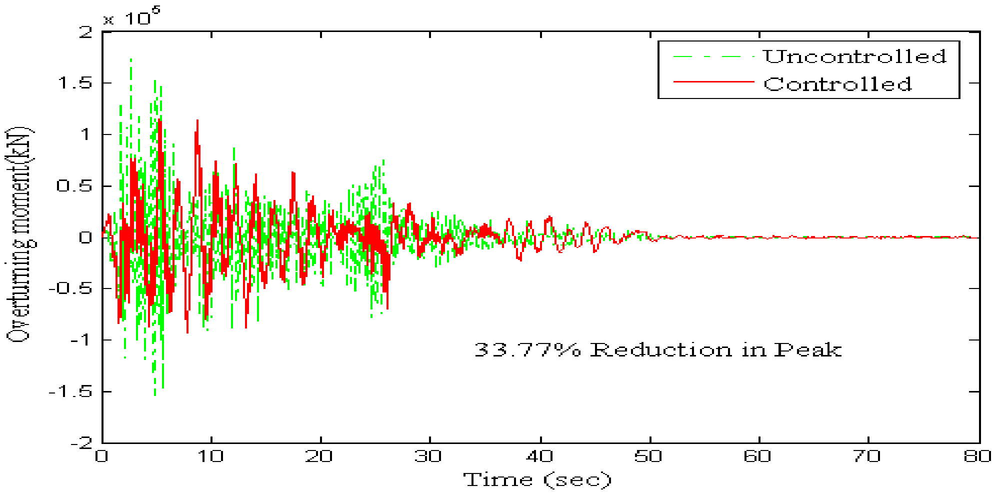

(a)

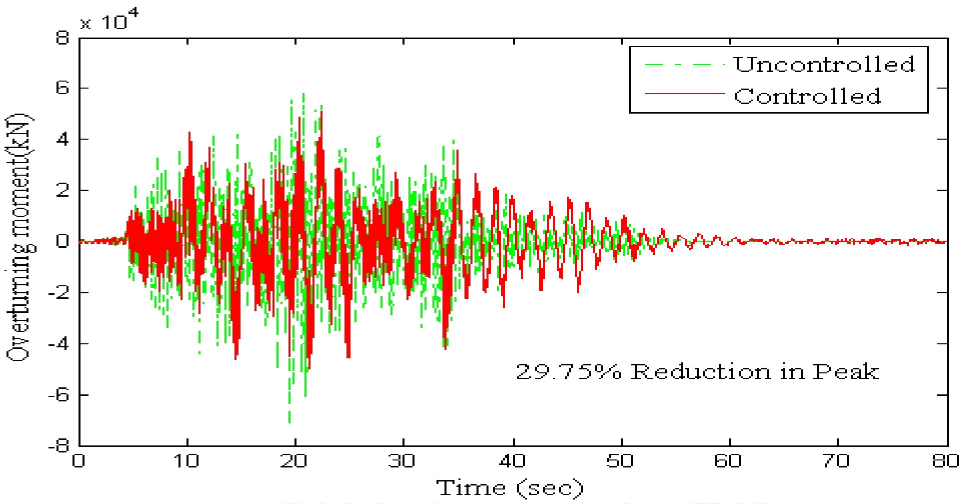

(b)

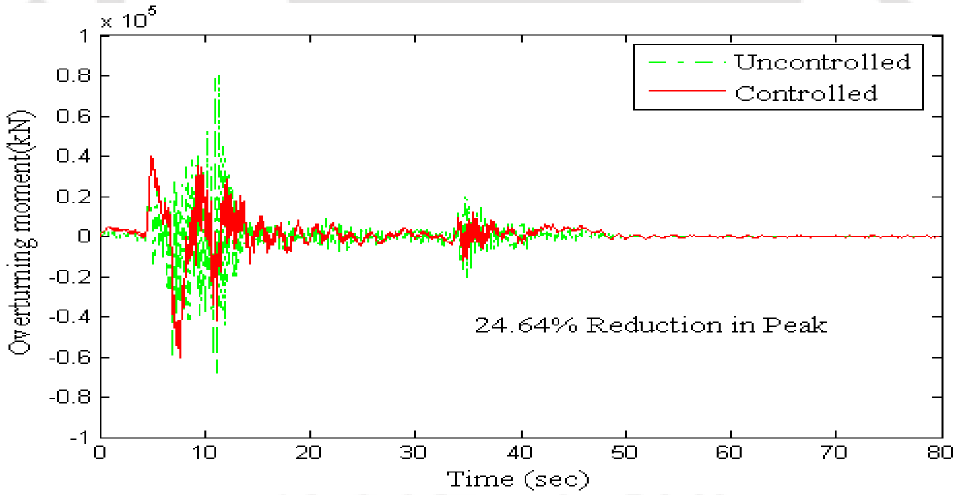

(c)

Fig. 3.19 Time history of overturning moment in pylon I against multiple support excitation (Case-1): (a) El Centro earthquake, (b) Mexico City earthquake, (c) Gebze earthquake

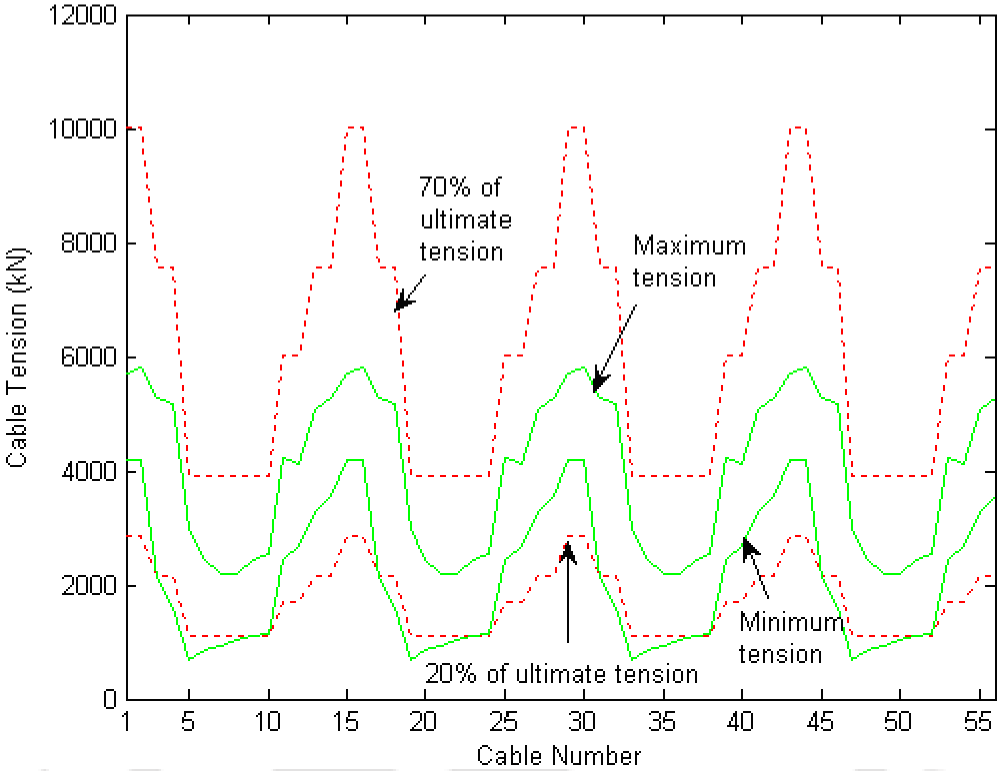

12000
10000
8000
6000
4000
2000
0
Cable Tension (kN)
1
5
10
15
20
25
30
35
40
45
50
55
Cable Number
70% of ultimate tension
Maximum tension
Minimum tension
20% of ultimate tension

(a)

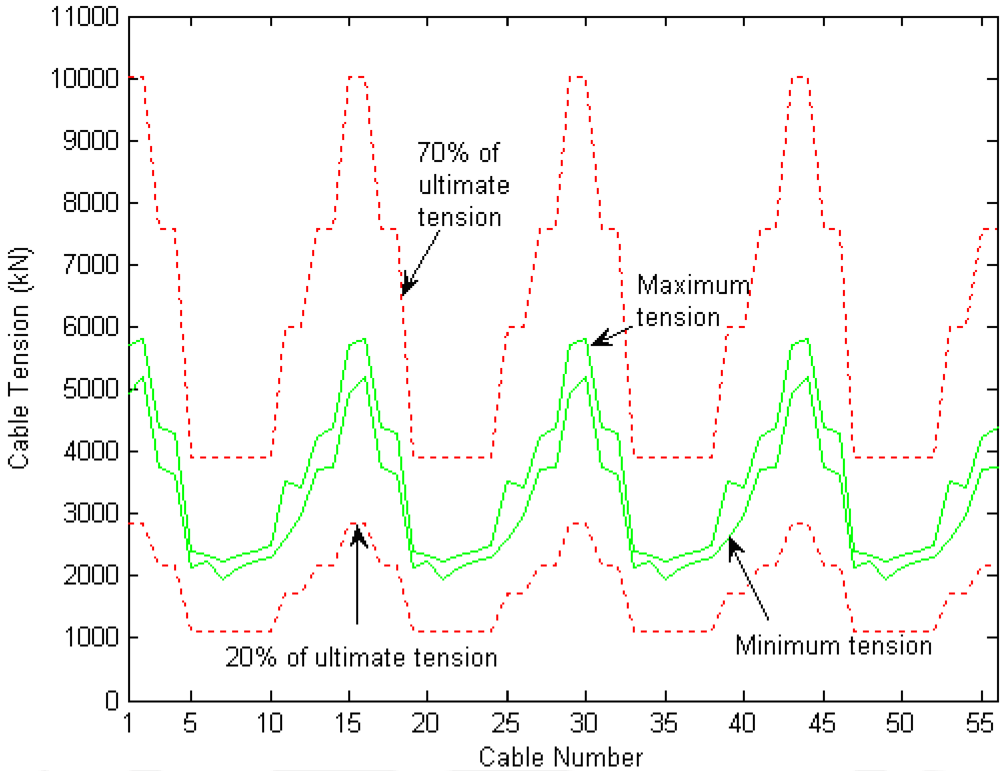

(b)

Fig. 3.20 Cable tension against multiple support excitation (Case-1) of El Centro earthquake: (a) Uncontrolled response, (b) Controlled response

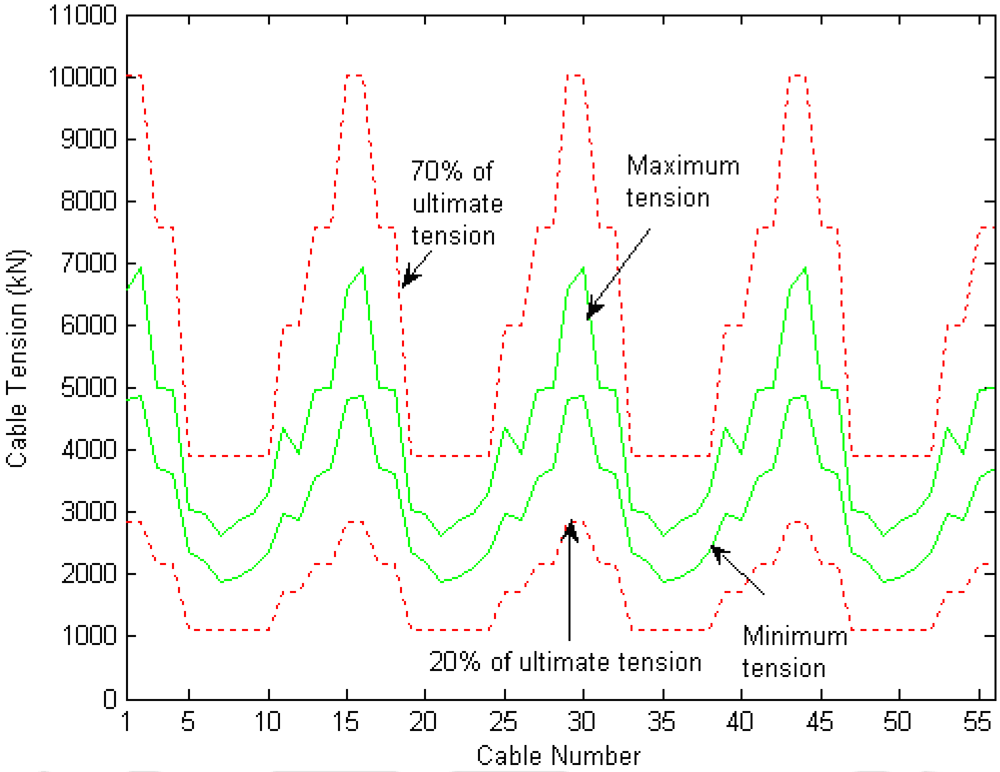
Cable Tension (kN)
Cable Number
70% of ultimate tension
Maximum tension
Minimum tension
20% of ultimate tension

(a)

(b)

Fig. 3.21 Cable tension against multiple support excitation (Case-1) of Mexico City earthquake: (a) Uncontrolled response, (b) Controlled response

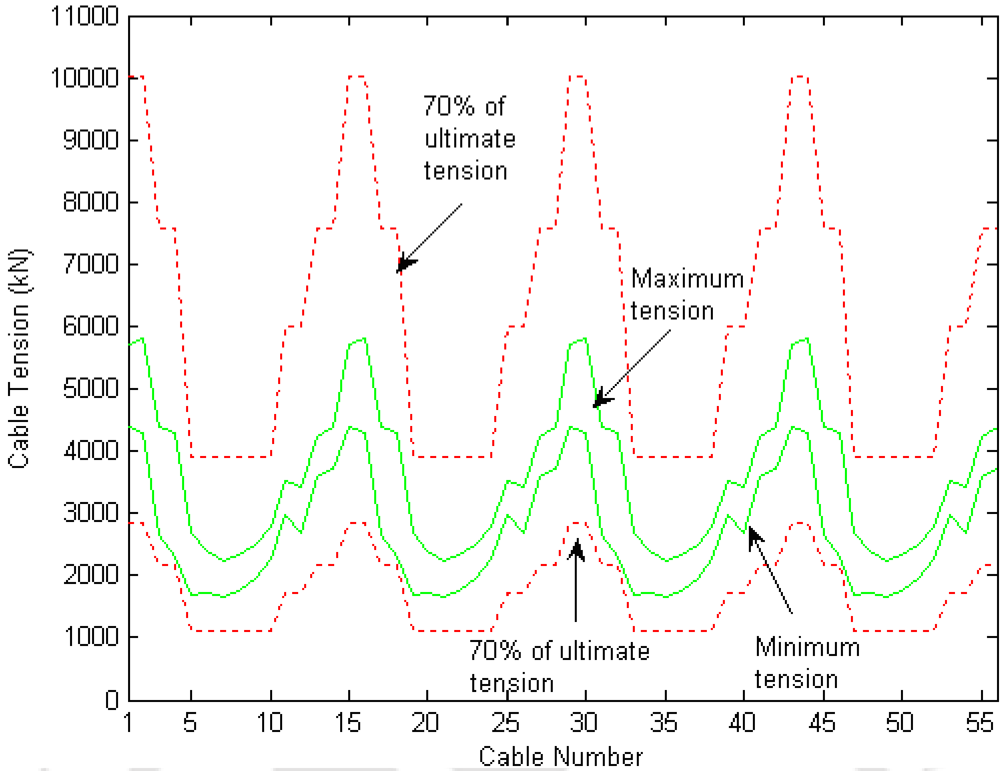

11000
10000
9000
8000
7000
6000
5000
4000
3000
2000
1000
0
Cable Tension (kN)
1
5
10
15
20
25
30
35
40
45
50
55
Cable Number
70% of ultimate tension
Maximum tension
70% of ultimate tension
Minimum tension

(a)

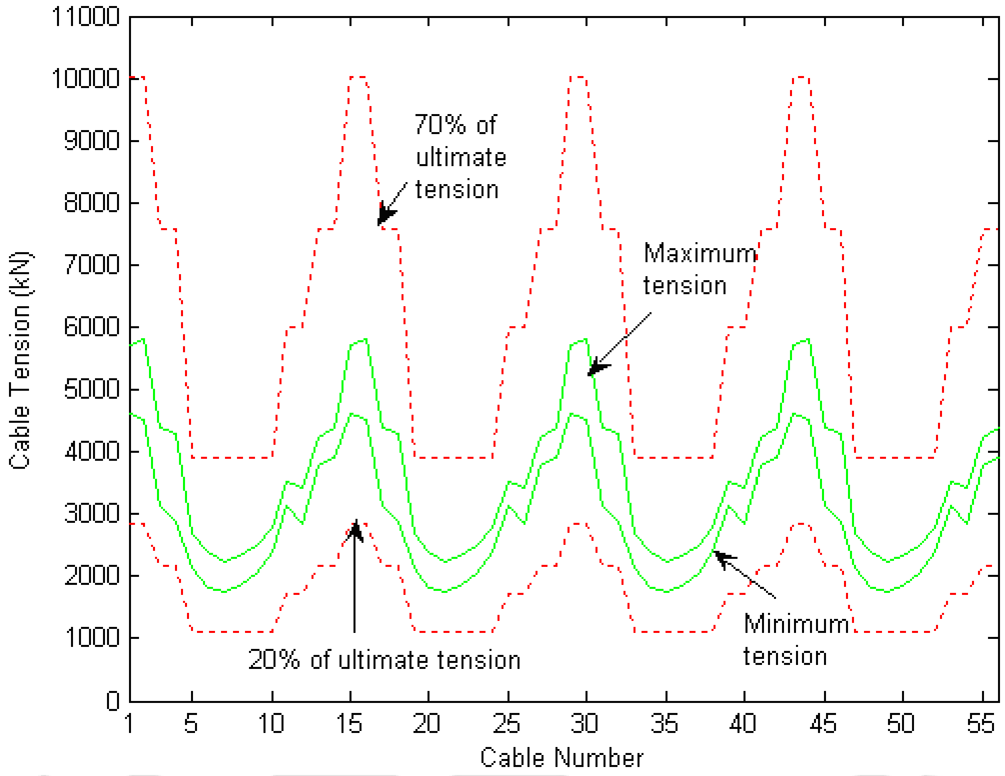

(b)

Fig. 3.22 Cable tension against multiple support excitation (Case-1) of Gebze earthquake: (a) Uncontrolled response, (b) Controlled response

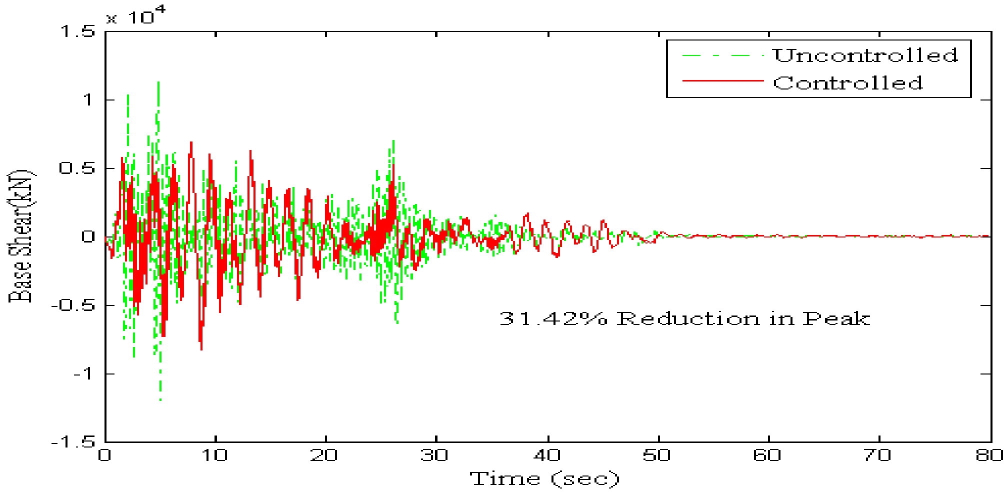

x 10^4
Uncontrolled
Controlled
31.42% Reduction in Peak
Base Shear(kN)
Time (sec)

(a)

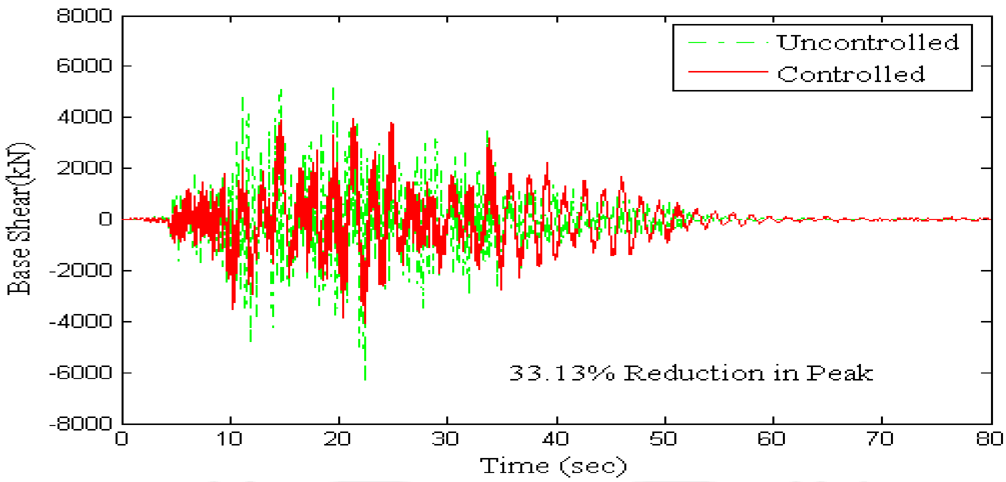

Uncontrolled
Controlled
33.13% Reduction in Peak
Base Shear(kN)
Time (sec)

(b)

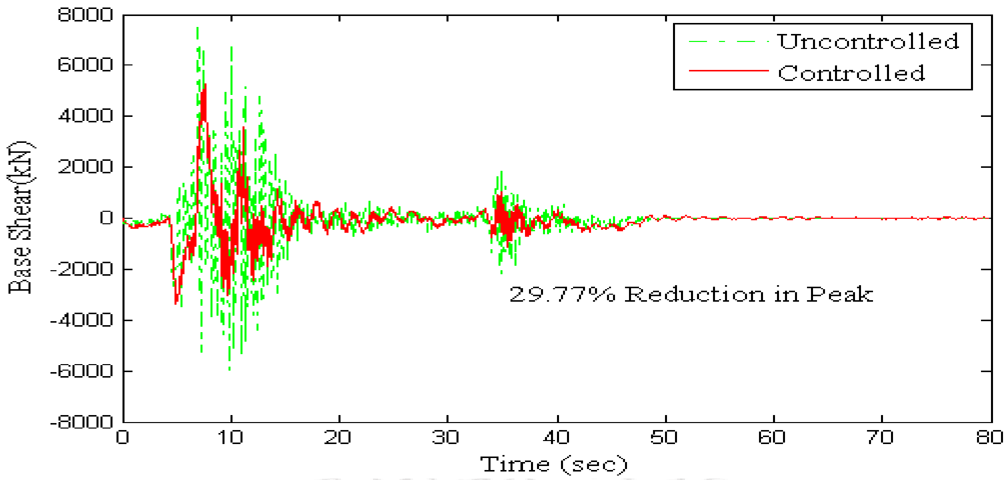

(c)

Fig. 3.23 Time history of base shear in pylon I against multiple support excitation (Case- 2): (a) El Centro earthquake, (b) Mexico City earthquake, (c) Gebze earthquake

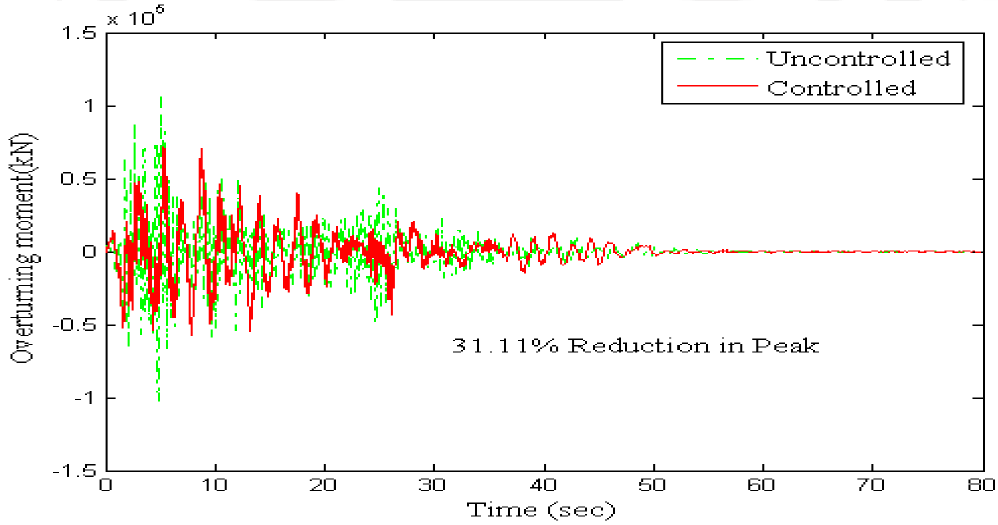

(a)

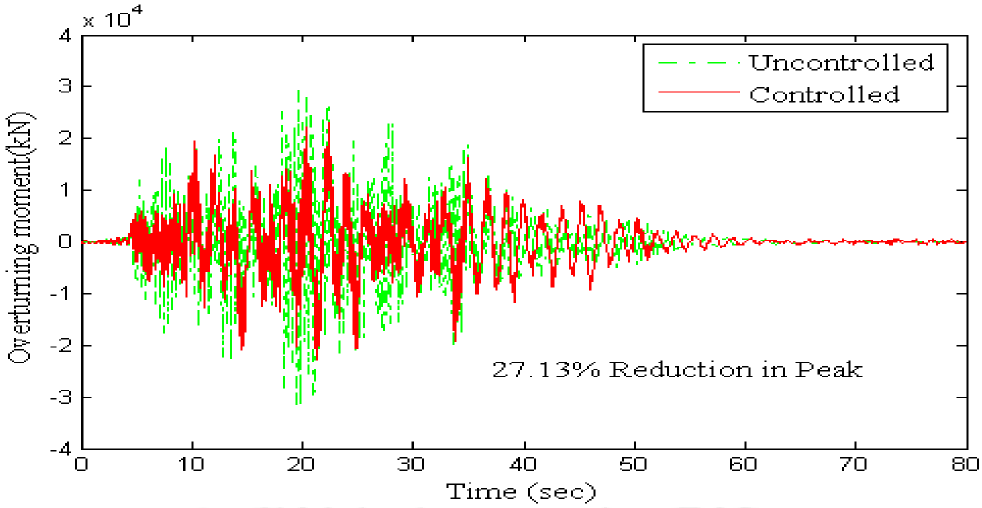

(b)

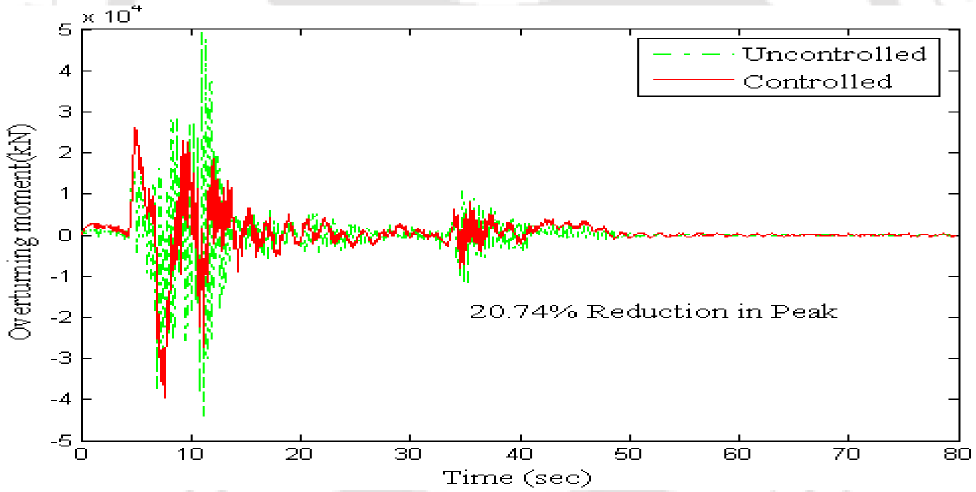

(c)

Fig. 3.24 Time history of overturning moment in pylon I against multiple support excitation (Case-2): (a) El Centro earthquake, (b) Mexico City earthquake, (c) Gebze earthquake

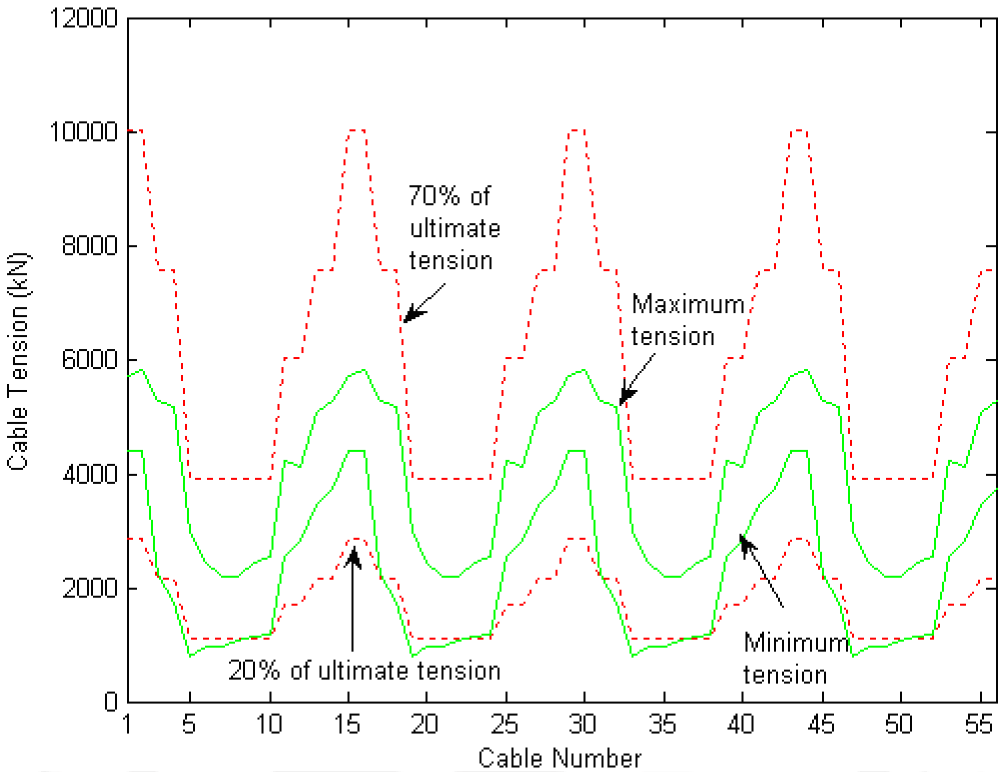

12000
10000
8000
6000
4000
2000
0
Cable Tension (kN)
1
5
10
15
20
25
30
35
40
45
50
55
Cable Number
70% of
ultimate
tension
Maximum
tension
Minimum
tension
20% of ultimate tension

(a)

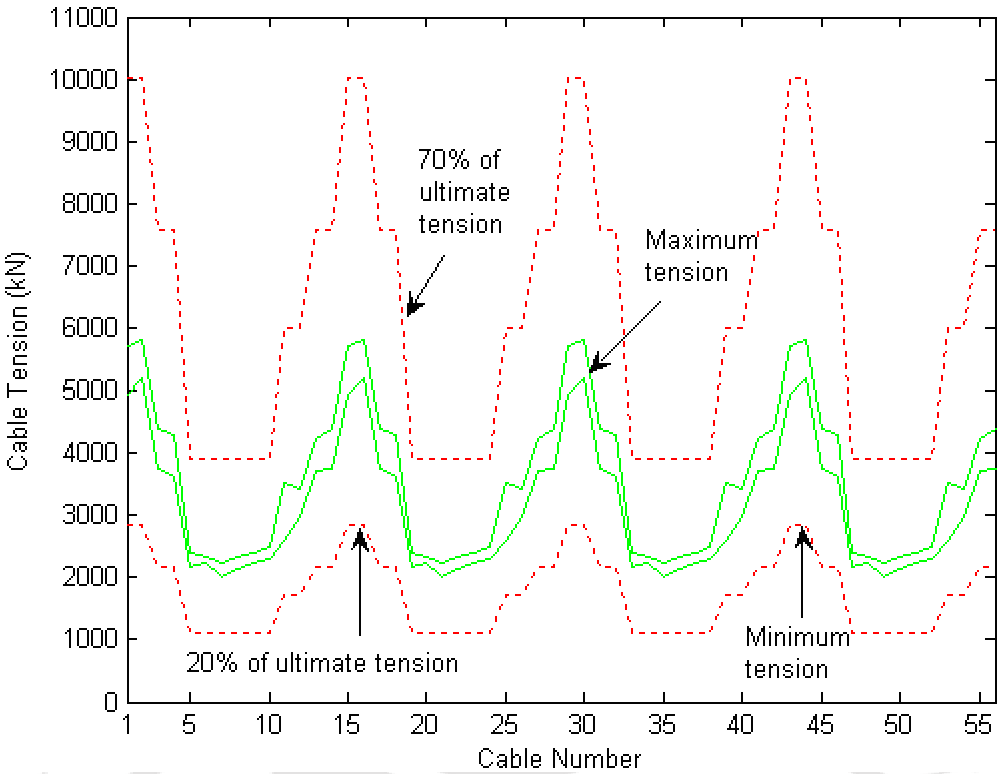

(b)

Fig. 3.25 Cable tension against multiple support excitation (Case-2) of El Centro earthquake: (a) Uncontrolled response, (b) Controlled response

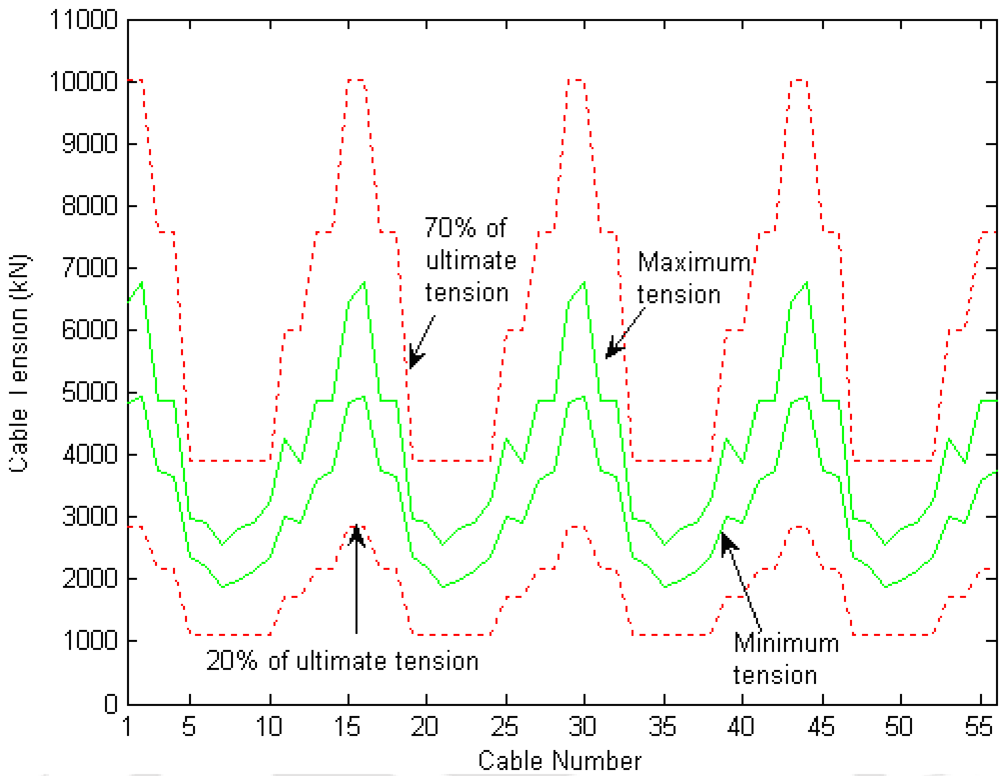
11000
10000
9000
8000
7000
6000
5000
4000
3000
2000
1000
0
Cable Tension (kN)
1
5
10
15
20
25
30
35
40
45
50
55
Cable Number
70% of ultimate tension
Maximum tension
20% of ultimate tension
Minimum tension

(a)

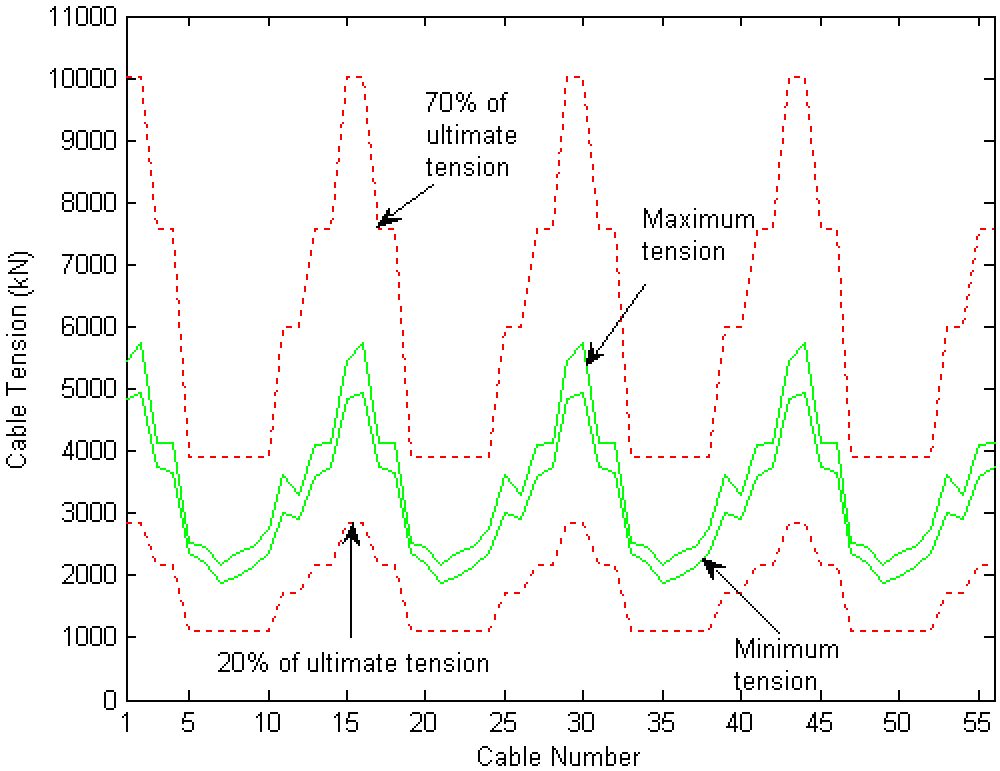

(b)

Fig. 3.26 Cable tension against multiple support excitation (Case-2) of Mexico City earthquake: (a) Uncontrolled response, (b) Controlled response

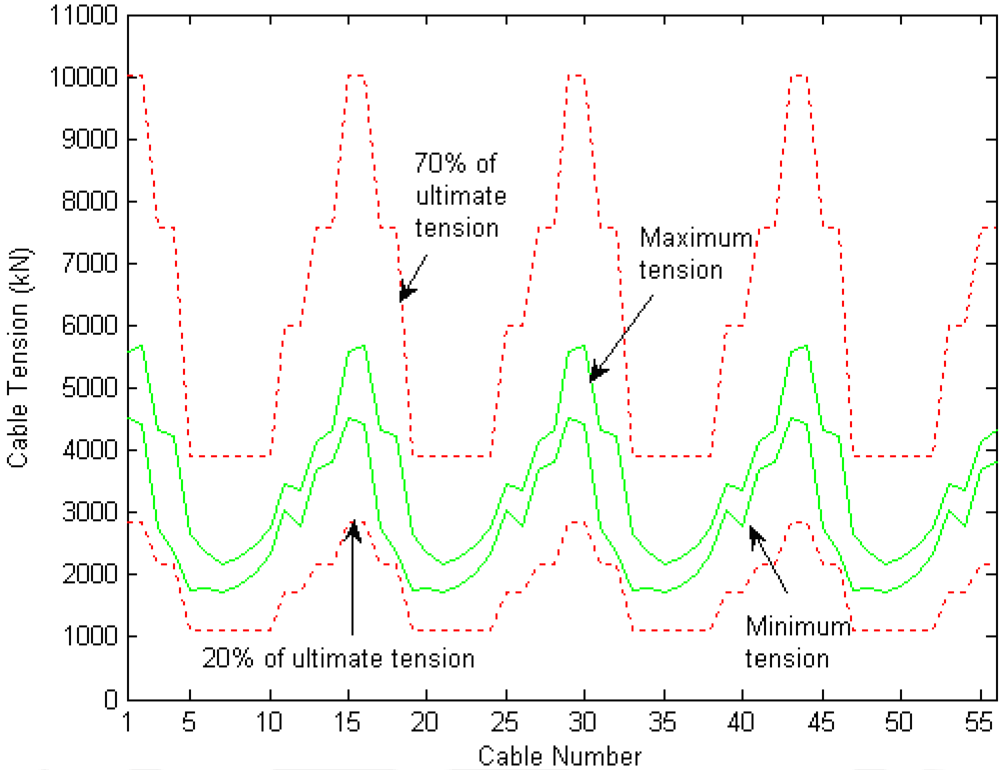

Cable Tension (kN)
Cable Number
70% of ultimate tension
Maximum tension
Minimum tension
20% of ultimate tension

(a)

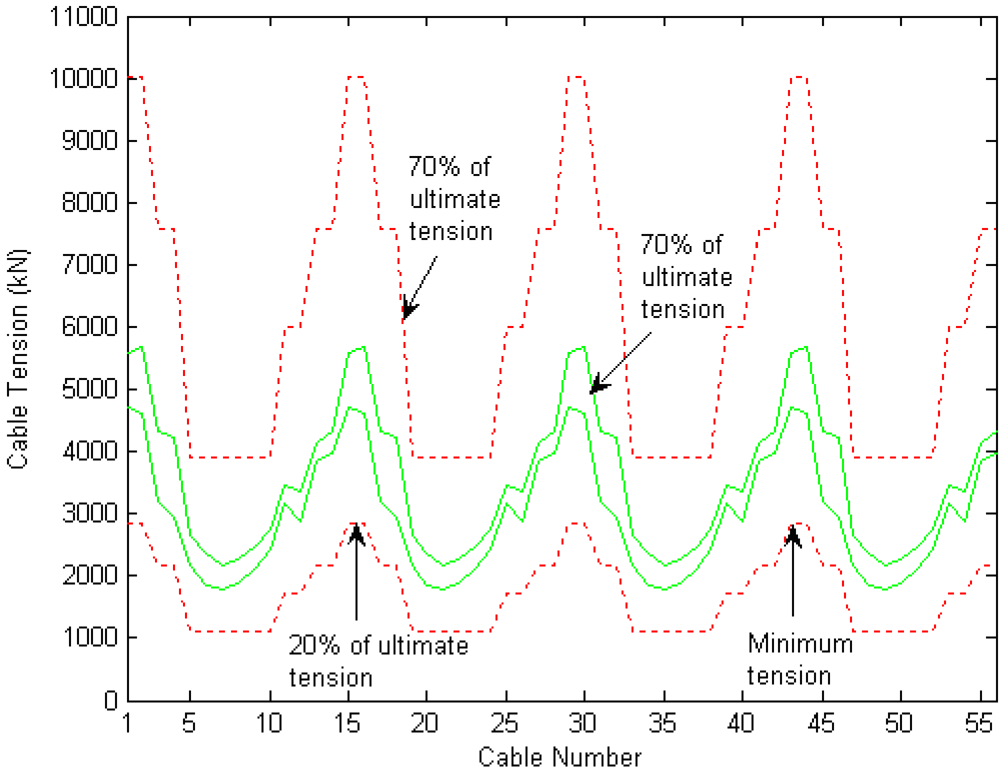

(b)

Fig. 3.27 Cable tension against multiple support excitation (Case-2) of Gebze earthquake: (a) Uncontrolled response, (b) Controlled response

Chapter 4

MODEL UPDATING OF BILL EMERSON MEMORIAL BRIDGE, MISSOURI, USA

4.1 Introduction

This chapter focuses on the model updating of the Bill Emerson Memorial Bridge, Missouri, USA. Unlike the model updating as described in Chapter 2, where update has been carried out based on already available modal frequencies and mode shapes from ambient vibration data, identification of modal parameter is a part of the present study. The model selected for updating was originally adopted for benchmark control problem for seismic response studies [Dyke *et. al.* (2000), Turan (2001)]. The model was subsequently modified and transferred to Matlab® and was used for structural health-monitoring study by Caicedo (2003). The bridge has been instrumented with a total of 66 accelerometers distributed in the structure and the surrounding soil [Celebi (2006)]. System identification using ambient vibration data [Song *et. al.* (2006)] established limitations of the analytical model in simulating the experimentally observed modal data. In the present study, modal identification has been carried out using SSI method. Out of the available 66 accelerometer data, 25 channels time histories, collected from relevant locations have been used for identification of the modal characteristics. This method showed similar results to that obtained by ARMAV (Auto-Regressive and Moving Average Vector) as reported by Song *et. al.* (2006). Further, it has used less number of parameters resulting in faster and easier implementation. SSI has also shown improvement over NExT-ERA (Natural Excitation Technique and Eigenvalue Realization Algorithm) with slightly higher average MAC (Modal Assurance Criteria) values and lower MAC standard deviations [Caicedo *et. al.* (2006)]. The updating of finite element model [Caicedo (2003)] has been attempted using the identified modal characteristics. Updating parameters have been identified and an optimization strategy has been adopted to arrive at an analytical model of a structure that represents modal identification results to the closest extent. A three step optimization methodology has been adopted for this purpose. First, an initial local minimum has been obtained using a trust-region algorithm. The goal of the optimization procedure is to minimize an objective function that measures the difference between both the natural frequencies and mode shapes of the numerical model with the corresponding identified modal parameters. Secondly, MGA is used to obtain other solutions, which are significantly different in nature from the first solution but all have similar values of the objective function. The solutions, which are obtained with MGA may not be local or global minima but can be used as starting point to calculate a new local minimum. Finally, another minimization of the objective function is performed using the solutions of the MGA as initial conditions for the optimization. It has been observed that the identified modal parameters have been represented well by the updated model [Caicedo *et. al.* (2006)].

4.2 Description of Original Model

The cable-stayed bridge used for this study is the Bill Emerson Memorial Bridge in Missouri, USA shown in Fig. 4.1. The bridge crosses the Mississippi River in Cape Girardeau, Missouri, and was designed by the HNTB Corporation [Hague (1997)]. The bridge was opened to traffic on Dec 13, 2003.

Fig. 4.1 Bill Emerson Memorial Bridge, Missouri, USA

Dyke *et. al.* (2000) formulated the benchmark control problem on this bridge with the design of an active controller against seismic excitation. Many researchers used the model for the benchmark control studies [He *et. al.* (2001), Caicedo *et. al.* (2003), Yang *et. al.* (2003), Park *et. al.* (2003a,b,c) , Bontempi *et. al.* (2003), Iemura *et. al.* (2003), Dai *et. al.* (2004), Kim *et. al.* (2005), Park *et. al.* (2005)] structural health monitoring [Caicedo (2003)] and structural identification [Song *et. al.* (2006)]. The structural details of the bridge have been given in detail by Dyke *et. al.* (2000) and Caicedo (2003).

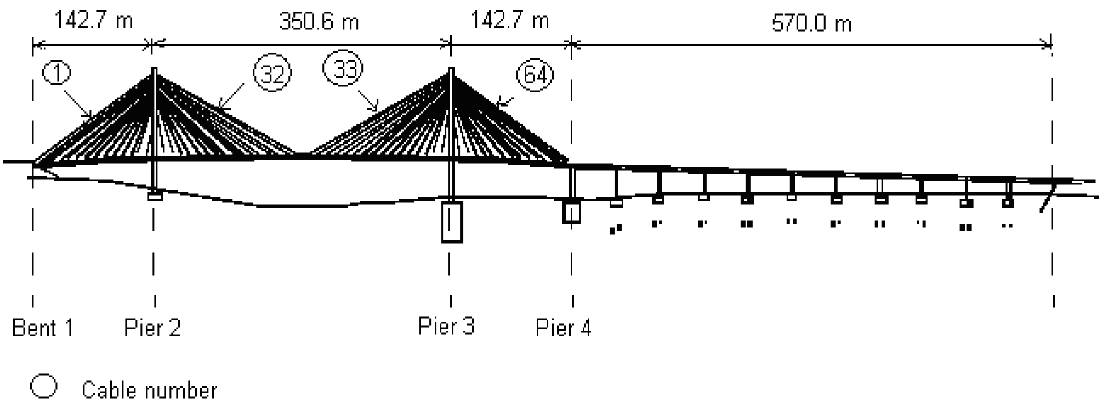

Fig. 4.2 Line diagram of the bridge [Dyke *et. al.* (2003)]

4.2.1 Structural data

A line diagram of the bridge has been shown in Fig. 4.2. The main bridge has two H-shaped pylons. Twelve additional piers are used in the approach from the right. The total length of the bridge is 1205.8 m. The main span of the cable-stayed bridge is 350.6 m and each of the side spans is 142.7 m. The bridge has four vehicle lanes and two bicycle lanes with a total width of 29.3 m. Sixteen numbers of shock transmission devices of capacity 6.67 MN each are employed in the interface between the pylon and the deck. They are oriented in the longitudinal direction of the bridge to allow for expansion of the deck due to temperature rise. These devices are found to be extremely stiff under dynamic condition and were considered as rigid links [Dyke *et. al.* (2000)]. The bridge deck is restrained in the transverse direction in the deck pylon support with earthquake restrainers. Further, the deck is restrained in the vertical direction at both the pylons. The bearings at Bent 1 and Pier 4 are designed to allow longitudinal displacement and rotation about the transverse and vertical axes.

The heights of H shaped pylons are 102.4 m at Pier 2 and 108.5 m at Pier 3. The pylons are made of reinforced concrete with a characteristic strength (f_c') of 37.92 MPa. Each pylon supports 64 cables, totaling 128 numbers of cables in the bridge. The elevation and cross sectional details of the pylons have been illustrated in Fig. 4.3.

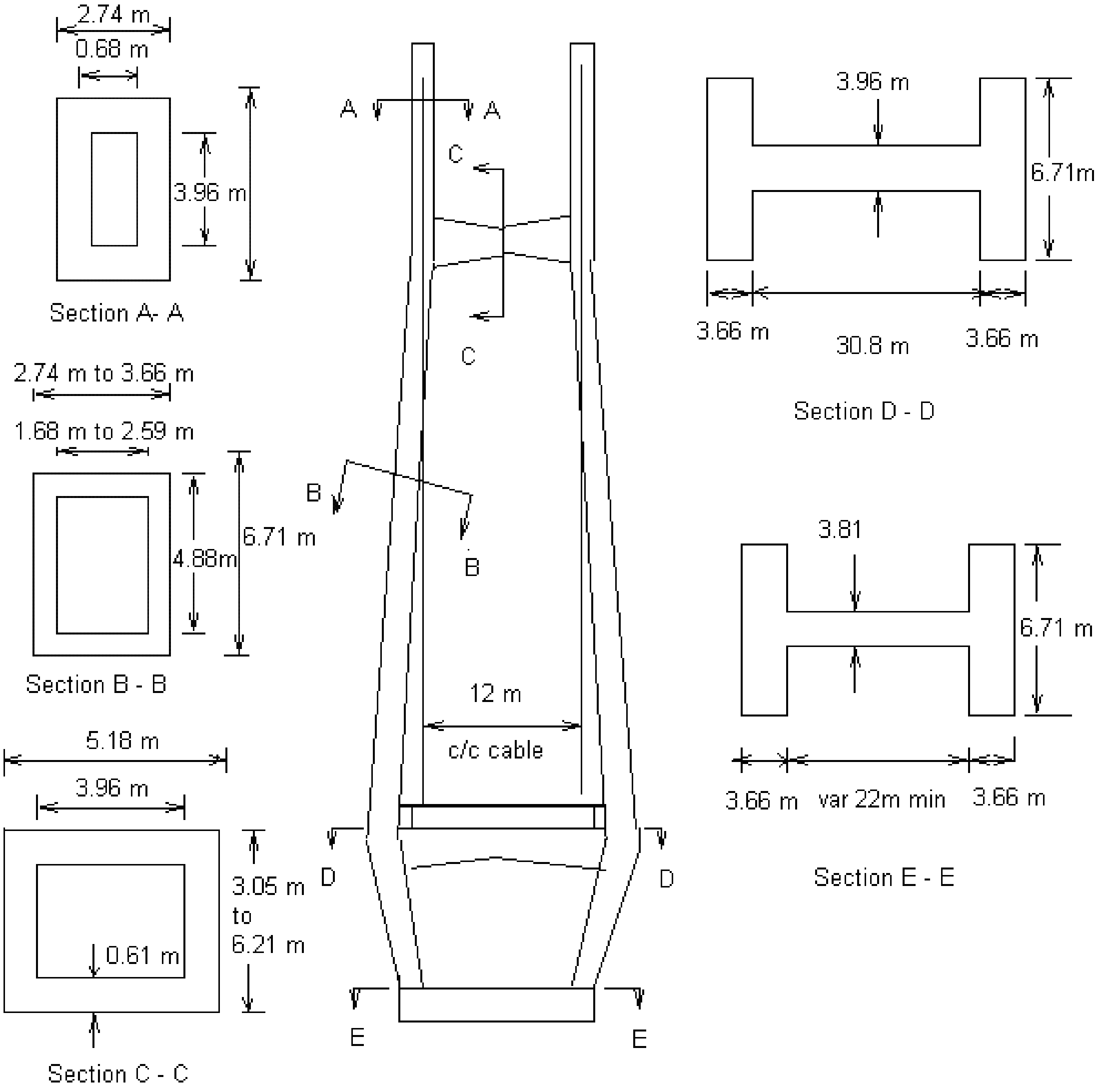

Fig. 4.3 Pylon details [Dyke *et. al.* (2003)]

The cables are made of high-strength, low-relaxation steel (ASTM A882 grade 270). The smallest cable area is 28.5 cm^2 and the largest cable area is 76.3 cm^2. The cables are covered with polyethelyne piping to resist corrosion.

The deck consists of a concrete slab supported by two steel girders located along each side of the deck and connected to the stay-cables. The steel grade used is ASTM A709 with yield strength (f_y) of 344 MPa. The concrete slabs are made of prestresssed concrete with a characteristic strength ($f_c{}'$) of 41.36 MPa. Additionally a concrete barrier is located in the centre of the bridge, and a railing is placed along the edge of the deck. The cross section of the deck is as shown in Fig. 4.4.

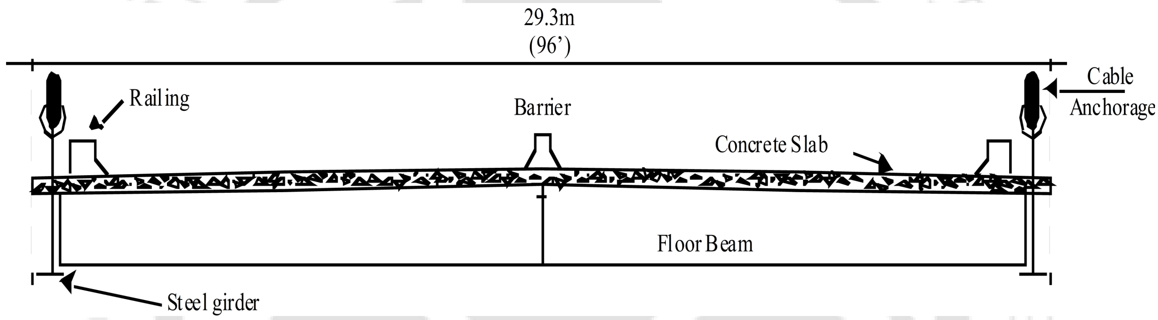

Fig. 4.4 Cross section of the deck [Dyke *et. al.* (2003)]

The material properties of the bridge and mass details for different bridge elements have been presented in Tables 4.1 and 4.2 [Dyke *et. al.* (2003)].

Table 4.1 Material density

Material	Density(kg/m^2)
Reinforced concrete	2402.77
Prestressed Concrete	2482.86
Seal concrete	2366.06
Stay cable grout	2322.68
Structural steel	7849.08
Cables	7849.08

Table 4.2 Mass details of deck components

Item	Mass per unit length(kg/m)
Silica fume concrete layer	34.15
Precast concrete deck	125.21
Steel girder	11.67
Floor beam	0.87
Railing	8.61
Barrier	7.73
Total	188.41

4.2.2 Finite Element Model

A finite element model of the Emerson Bridge was previously developed for the benchmark problem for seismic response control of cable-stayed bridges by Dyke *et. al.* (2000). This model was developed in Abaqus® as enumerated by Turan (2001) and the system matrices were transferred to Matlab® for control and simulation. The model was subsequently modified and transferred to the Matlab® environment for structural health monitoring study [Caicedo (2003)]. The present model has been adopted from the study of Caicedo (2003). The finite element model has 573 nodes, 418 rigid links, 156 beam elements, 198 nodal mass elements and 128 cable elements. This has been illustrated in Fig. 4.5. The rigid links were modeled using constrain equations as in Eqs. (2.30). The pylon bases were considered as fixed. This was justified on the basis of the fact that the foundations are attached to bedrock.

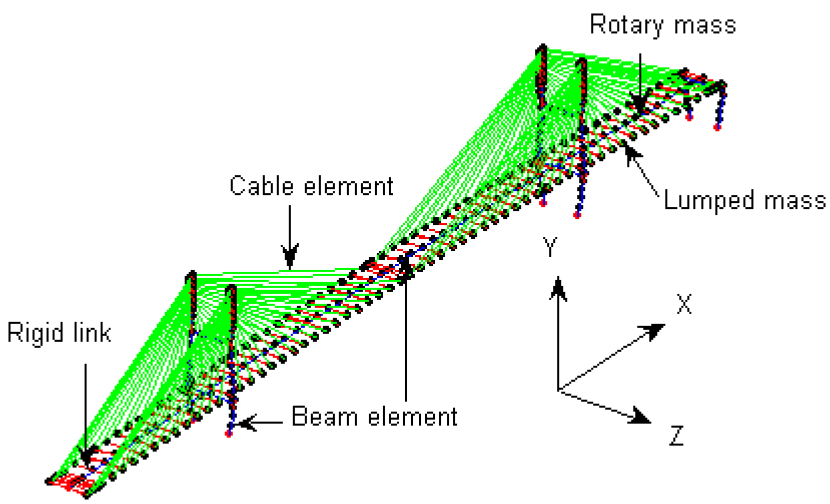

Fig. 4.5 Finite element model

As the cables are attached to the deck above its neutral axis, and to the pylon outside the pylon's neutral axis, connectivity of the cables to the deck and pylons were made with the help of rigid links. These connections are illustrated in Figs. 4.6 and 4.7. This arrangement ensures that the length and inclinations of the cables agree with those in the drawings. Further, by this arrangement the moment induced to the tower due to the cable forces have appropriately been taken care of. The cables were modeled as truss element with equivalent elastic modulus shown in Eq. (2.26). The design tension obtained from construction drawings were assigned to each cable as initial tension.

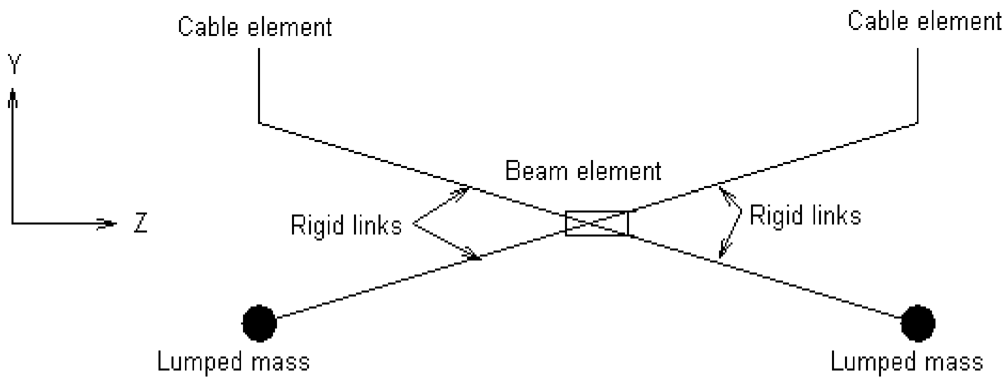

Fig 4.6 Finite element model of deck cross-section [Dyke *et. al.* (2003)]

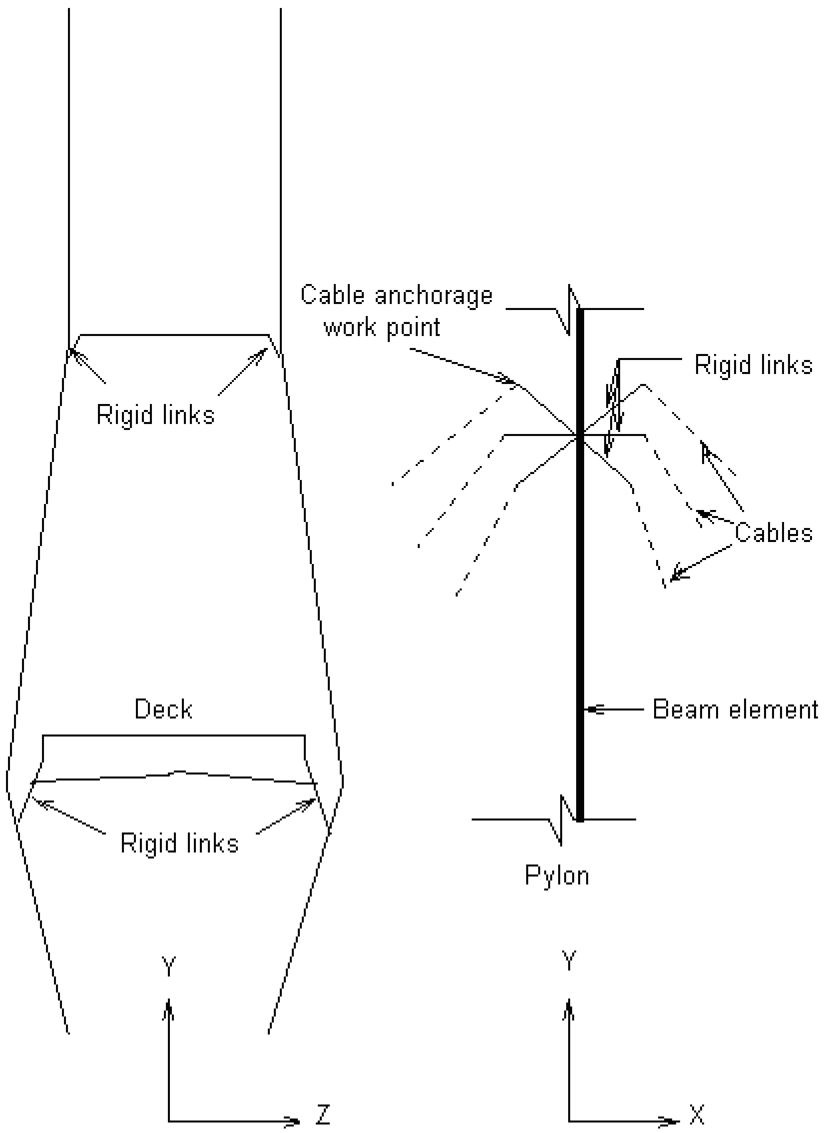

(a) Model of pylon **(b) Connection between pylon and cable**

Fig. 4.7 Finite element model of pylon [Dyke *et. al.* (2003)]

The deck was treated as an equivalent steel open section (C-shaped), as proposed by Wilson *et. al.* (1991a). The web of the C-section represented the steel beams and flanges represented the concrete slab. The axial stiffness of the deck was calculated by converting the area of the concrete slab into an equivalent steel area of 1.844 m^2 using the moduli of elasticity of steel and concrete. The values of moment of inertia for a typical deck section were obtained as: I_y = 160.67 m^4, I_z = 0.6077 m^4 and J_{eq} = 0.0677 m^4. The location of the neutral axis was found to be 1.77 m above the bottom of the steel beam. The torsional stiffness of the deck was obtained as per the method enumerated in Wilson *et. al.* (1991a) and has already been explained in Chapter 2, in Eqs. (2.2) through (2.4).

The deck was idealized as a spine with half the deck masses lumped at both sides of the spine. Cables were connected to the spine with rigid links as shown in Fig. 4.5. The material and sectional properties of the C-section was ascribed to the spine. The spine was modeled using beam elements incorporating stability functions to take account of P- effect. Total deck mass comprising the masses of steel beams, concrete slab, railings, and barriers was calculated as 2645.7 kg/m. The vertical distance of lumped mass and the spine was considered as the distance between mass centre and shear centre.

Corrections for mass moment of inertia were applied to the spine node as the distributed masses are lumped and placed at the end of the rigid links. The calculation for these corrections was carried out in a manner similar to that explained in Chapter 2, using Eqs. (2.5) and (2.6). The corrections for a typical section of the deck were calculated as, Δ_x 4.43×10^6 kgm^2, Δ_ψ 4.45×10^6 kgm^2, Δ_z 18.3×10^3 kgm^2. The deck and pylons were modeled using beam elements incorporating stability function to account for P- effect.

4.2.3 Modal characteristics

A mixed incremental-iterative method [Caicedo (2003)] was used to perform the nonlinear static analysis in order to arrive at the dead load deformed equilibrium position. Here, the unbalanced load was applied in an incremental manner and iterations were performed for each increment. The procedure has already been explained in section 2.4. The model from the dead load deformed configuration has been used to determine the dynamic characteristics of the structure through eigenvalue analysis. The first four flexural frequencies (Hz) as obtained from this study were: 0.291, 0.392, 0.608, 0.674.

4.3 System Identification

Ambient vibration results have been used for modal identification of this bridge. The cable stayed bridge exhibits a complex range of mode shapes such as flexural, transverse, torsional, coupled transverse torsional modes etc. For such a flexible structure, it is a costly proposition to capture all the mode shapes with sensors. However, first few flexural modes may be easily captured by sensing the vertical and transverse acceleration data at salient locations of the bridge.

4.3.1 Location of sensors

In the present study sensor data has been used to reconstruct first few flexural modes. Out of the total of 66 accelerometers, evenly distributed in the superstructure, substructure and surrounding soil, 23 are vertical sensors, 11 are sensors in the longitudinal direction of the bridge and remaining 22 are oriented in the transverse direction. However, for the present study data from only 25 sensors, located at key locations of the superstructure as illustrated in Fig. 4.8, have been utilized.

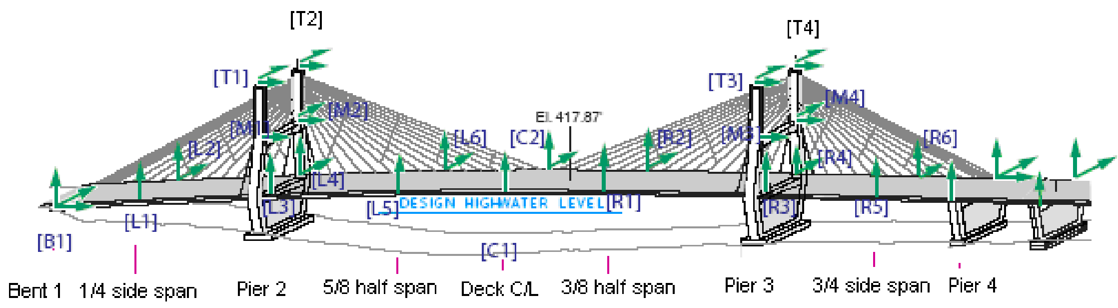

Fig. 4.8 Locations of sensors

4.3.2 Characteristics of signals

In the present study, six hours of twenty five channels of acceleration data corresponding to sensors located in the deck and pylons have been used for modal identification. The sensor information of 17 accelerometers on the deck located in the vertical direction and 8 accelerometers located in the pylon oriented in the longitudinal direction have been used for the modal identification. The characteristics of the signals have been presented here.

(a) Signals: Three acceleration time histories collected at strategic sensor locations have been presented here. These sensor signals from mid-span, left pylon top and right pylon top have been shown in Figs. 4.9 to 4.11. The duration of these data collected was 2.5 hours and sampling rate was at 0.005 sec (200 Hz). Accordingly, a total of 18 10^4 measurements were taken.

(b) PSD of the signals: The plots of Power Spectral Density (PSD) for the signals at critical locations have been presented here. A PSD is indicative of how the energy content of a signal is distributed over a frequency range. Accordingly the peaks of the PSD indicate the resonating frequencies which are the natural frequencies of vibration of the structure. Thus, PSD of signal collected at strategic locations would give the idea of the distribution of predominant modal frequencies. The PSDs for two of the representative signals namely signal from midspan and signal from left pylon top have been illustrated in Figs. 4.12 and 4.13. The PSD of the signal from the right pylon top sensor has not been shown as it has been observed to be similar to that of left pylon by virtue of near symmetry of the structure.

It is worth noting that certain flexural modal frequencies are missing from the PSD of the mid-span signal, which is due to the particular positioning of the sensors. For example, the second flexural modal frequency is absent from the PSD of the signal from mid-span as the sensor location has coincided with the node in the mode shape corresponding to the second flexural frequency.

4.3.3 Modal Identification

The data were originally collected at 200 Hz and have been resampled to 5 Hz for the identification of the fundamental modes of vibration only. This re-sampling is done to avoid handling of enormous data while keeping the minimum necessary information. It is appreciated that for appropriate modal identification the minimum sampling rate should be twice the highest frequency of interest. The present resampling rate of 5 Hz can identify modes of frequency upto 2.5 Hz, which is sufficient range for the present problem.

The classical modal parameter identification techniques that involve frequency or time-domain analysis of dynamic responses corresponding to forced vibration cannot directly be applied to the output-only vibration data. This is due the fact that the input excitations are not measured in the test. In a previous study, ARMAV was used by Song *et. al.* (2006) to detect the natural frequencies and mode shapes of the Bill Emerson Memorial Bridge using sixteen channels of acceleration data from the sensors on the deck. The SSI method has been used in the present study, where the acceleration records are used to identify the modal parameters of the structure. Here a general background of subspace identification is presented.

(a) Subspace identification: The term 'Subspace' arises from the fact that linear models can be obtained from row and column 'spaces' of certain matrices, calculated from input output data from dynamic testing. Typically the columns of these matrices contain information about the model. The rows of these matrices may be used to obtain a Kalman state sequence directly form the input output data without any knowledge of the system. Subspace identification is divided into three types: (1) Deterministic, (2) Stochastic, (3) Combined deterministic-stochastic. Deterministic subspace identification is used, where external input is measurable. Stochastic subspace identification technique deals with the case where no measured input data is available. Combined deterministic stochastic method unites the two preceding methods.

Subspace identification algorithms are based on system theory, linear algebra and statistics as illustrated in Table 4.3.

Table 4.3 Components of subspace identification

System	Geometry	Algorithm
High order state sequence	Projection (Orthogonal or oblique)	QR-decomposition
Low order state sequence	Determine finite dimension subspace	(Generalized) singular value decomposition
System matrices	Linear relations	Least squares

The main conceptual advantages of subspace method over the classical methods are [Van *et. al.* (1996)]:

- The state of a dynamical system is emphasized in the context of system-identification, whereas the ‘classical’ approaches are based on input-output framework. This difference in approaches has been illustrated in Fig. 4.14. Kalman filter states can be obtained from the identification data using tools from linear algebra such as QR and singular value decomposition. Thus, in contrast to highly nonlinear optimization approach of the classical methods, this method *conditionally linearizes* the problem.

- Whereas the classical identification methods uses the least squares approach, subspace method uses modern algorithms like QR decompositions, singular valued decomposition and its generalizations and angle between subspaces.

- Seemingly different methods like deterministic, stochastic and combined stochastic deterministic system identification methods can be treated by the same geometric concepts and algorithms in this method by virtue of its conceptual and algorithmic simplicity.

- The conceptual simplicity of subspace algorithms makes it possible to have user-friendly software implementation.

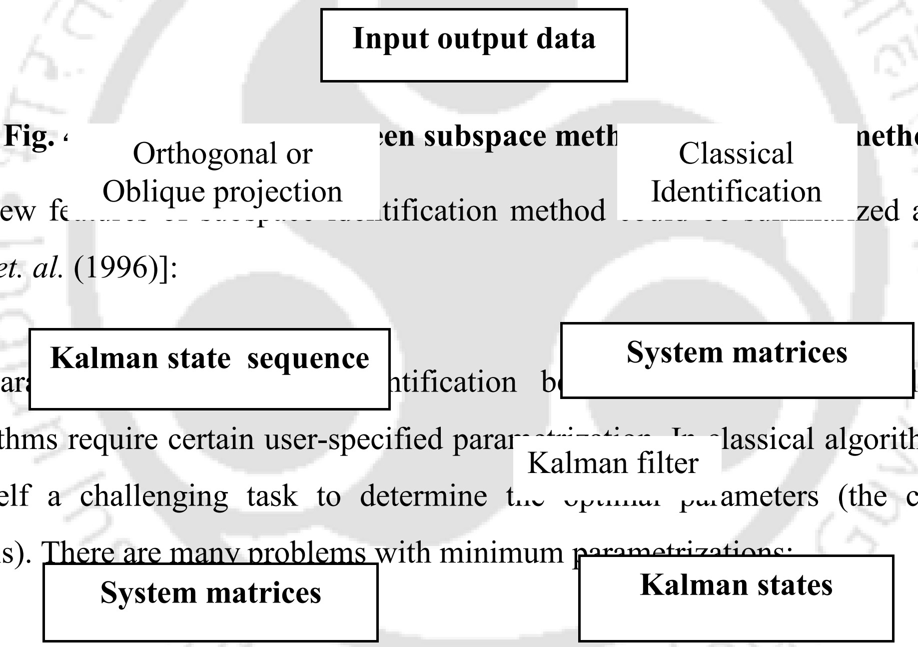

Fig. [illegible] en subspace meth[illegible] nethod

The new fe[illegible] tification method [illegible] zed as below [Van *et. al.* (1996)]:

(1) Par[illegible] ntification b[illegible] em, the algorithms require certain user-specified param[illegible] lassical algorithms, it is in itself a challenging task to determine t[illegible] ameters (the canonical models). There are many problems with minimum parametrizations:

- Can lead to numerically ill-conditioned problem, with the results being extremely sensitive to small perturbations.

- There is a need of *overlapping* parametrizations, as none of the limited parametric model can cover all the possible systems.
- Only minimal state space models are feasible in practice. If there are uncontrollable but observable (deterministic) modes, this requires special parametrizations.

The subspace method does not suffer from any of these problems. The only parameter to be user-specified in this model is the order of the model, which can be determined by inspection of certain singular values.

(2) Convergence: Subspace identification algorithms are fast. There are no convergence problems as these algorithms are not iterative. They never get stuck in local minima or suffer from any convergence problems. In short, they always produce a (sub-optimal) result, which is often surprisingly good for practical data. Its numerical robustness, by virtue of its elegant algorithms from linear algebra, is also a special feature. The user is not confronted with instability problems.

(3) Model Reduction: A major interest of researchers is to design control system based on identified model. It is well appreciated that in using a linear control theory the complexity of controller is directly proportional to the order of the system. Hence model reduction is an important issue. In subspace identification, the reduced model can be obtained *directly* without having to compute first the high order model. This feature has been highlighted in contrast to that of classical methods in Fig. 4.15.

Several subspace identification algorithms are available in the literature [Abdelghani *et. al.* (1998)] such as the eigensystem realization algorithm [Juang *et. al.* (1985), Juang *et. al.* (1986)]. A common mathematical background for subspace algorithms for linear systems is presented by Van *et. al.* (1996).

The SSI technique is a time-domain method that directly works with time data, without converting them to correlations or spectra. The algorithm identifies the state space matrices based on the measurements by using robust numerical techniques. Once the mathematical description of the structure (the state space model) is found, it is straightforward to determine the modal parameters. Recently Giraldo *et. al.* (2006) compared the SSI technique with other output only identification methodologies such as eigensystem realization scheme (ERA), Eigensystem realization scheme with data correlations (ERA/DC), the prediction error method through least squares (PEM/LS). It was concluded that the SSI technique requires less parameters to setup, resulting in a faster and easier implementation than other algorithms for a successful implementation.

Input output data

Subspace Identification

Classical Identification

Fig 4.1: ... reduction processes of subspa... ...nd classical identification

(b) Theoretical background of SSI: The subspace identification algorithms deliver a

Reduced state sequence

High order model

d... ...variant state space model of ... is expressed by the following difference equations [Van *et. al.* (1996)]:

Least Squares

Model reduction

Reduced model

Reduced model

(4.1)

(4.2)

with, **(4.3)**

Here the vectors *and* are the measurements of m inputs and l outputs of the process at time instant k. The vector *is the state vector of the process at* discrete time instant k and contains the numerical values of n states at instant k. and *are unmeasurable vector signals, which are considered as zero* mean, white vector sequences and is the kronekar delta.

The matrix is called the system matrix (dynamical). It describes the dynamics of the system completely characterized by its eigenvalues. *is the* input matrix, which represents the linear transformation by which deterministic inputs influence the next state. *is the output matrix. This describes how the internal* states translate into measurement . *is called the direct feed-through* matrix which locates the external input to the system. The matrices ,

, *are the covariance matrices of the noise sequences* w_k *and* v_k. ***The*** matrix pair is assumed to be observable, which implies that all the modes *can* be observed in the output and can thus be identified. The matrix pair

is assumed to be controllable, which in turn implies that all the *modes* of the system are excited by either the deterministic input *and/or the* stochastic input . The graphical representation of the system is presented in Fig. 4.16. In this figure, a linear time invariant system with inputs *, outputs* and states is described by the four matrices A, B, C **and** D**. The symbol** Δ represents a delay. Subspace identification calculates the system matrices from which modal parameters can be identified.

The stochastic subspace identification problem has been presented next [Van *et. al.* (1996)]. It is called the stochastic subspace identification (SSI) technique, when the input is stochastic. This system is represented in Fig. 4.17. In contrast with the general representation of the subspace identification system as in Fig. 4.16, here the external input vector *is absent.*

B Fig. 4.16 Sub Δ identification sy C

Δ Fig. 4.17 SSI syst C

A

With reference to Fig. 4.17, outp *generated by the unknown stochastic*

D

system of order *n*

A

(4.4)

(4.5)

with, **(4.6)**

The objectives of SSI are to determine:

- The order *n* of the unknown system,
- The system matrices **A**, **C** upto within a similarity transformation (similarity transformation converts the states, which do not necessarily have physical meaning, into a physically meaningful states) and **Q**, **S**, **R** so that the second order statistics of the output of the model and of the given output are equal.

Here Kalman filter states of a realization are obtained from row space projection of Hankel matrices. With the knowledge of these states, the identification problem simplifies to a solution of a linear set of equations, and the solution of the same provides easy estimate of matrices of the realizations. The algorithm implemented in this study is described in detail by Van *et. al.* (1996).

The Hankel matrix is of the form:

(4.7)

where, is the random response of the system at time k, *and the two subscripts on* *Y* denote the time index of the upper left and bottom left elements respectively. It is assumed herein that the number of columns of the Hankel matrix approaches infinity ( ). *Considering* as the orthogonal projection of the row space of (known at the future) onto the row space of (known at the past),

(4.8)

with, (4.9)

It can be shown that the observability matrix can be calculated from the matrix $\mathbf{L}_i$ using a singular value decomposition as described by Van *et. al.* (1996) and Arici *et. al.* (2005),

(4.10)

where, is the Kalman state sequence and is the observability matrix. The system matrices **A** and **C** can then be calculated using the equation,

(4.11)

The algorithm is called subspace algorithm as it retrieves system related matrices as subspaces of projected data matrices.

The natural frequencies and damping ratios of the structure can be calculated from the eigenvalues of **A** and the output shapes can be calculated as, , where is the eigenvectors of **A** and is the matrix of identified mode shapes. The matrix will have as many rows as sensors are in the structure and as many columns as modes are identified. The coordinates of the mode shapes can be identified at the location of the sensors.

4.3.4 Identification of modal properties

The modal characteristics have been identified with the SSI following the procedure explained in the previous subsection. After the modal parameters are identified with subspace identification, an automated recognition scheme [Giraldo *et al*. (2006) and

Giraldo (2006)] has been used to detect the true modes from those created by noise and numerical errors. The data available is divided into 36 windows of 10 minutes of data. A set of natural frequencies, mode shapes and damping ratios has been obtained for each window. The true modes of vibration have been recognized by identifying parameters within some specific predefined values. The parameters used to identify real modes are the natural frequency, MAC and damping values. For a specific mode, the acceptable identified natural frequency should be within 30% of the mean of identified frequency, the damping value should be lower than 5%, and the MAC values of the identified mode shapes should be higher than 0.98. Only modes with more than 5 hits (the same frequency identified more than five times) have been assumed to be real modes and the others have been discarded as noise. The standard deviation of each natural frequencies and the mean MAC value of the corresponding mode shapes have been calculated following the equations,

(4.12)

(4.13)

where, is the standard deviation of the *ith natural frequency,* is the j^{th} frequency identified corresponding to the *i*th natural frequency (i.e. hits in Fig. 4.18 in different windows corresponding to the same natural frequency), and is the mean of all the *j* frequencies identified. is the mean value of the MAC calculated between the identified *j*th mode shape corresponding to the *i*th natural frequency , and the mean mode shape . 1 *is the dimension of total mode shapes identified.*

Lower standard deviation on the natural frequencies and mean MAC values closer to one are assumed to be identified with higher confidence and are given higher weightage on the objective function used for model updating as described in the next section.

4.3.5 Identified parameters

The details of identification by SSI have been presented in Fig. 4.18. Here Fig. 4.18 (a) describes the distribution of hits corresponding different frequencies whereas Fig. 4.18 (b) shows the histograms of hits corresponding to frequencies. The hits around 0.2 Hz are scattered and considered to be from noise rather than from structural frequencies.

The first four modal parameters identified with the SSI have been presented in Table 4.4. The number of hits corresponds to the number of times the same mode has been identified when the identification process has been repeated along all the windows. The natural frequencies and damping ratios shown have been calculated as the average of all the identified parameters for each mode.

Overall, the natural frequencies are very similar with those identified with ARMAV by Song *et al.* (2006). SSI is also observed to be better than NExT-ERA in terms of performance [Caicedo *et. al.* (2006)] as represented in Table 4.5. Comparing Table 4.4 with Table 4.5 is has been observed that SSI shows high average MAC values and low MAC standard deviation.

However, the damping property of real large cable-stayed bridges is not fully understood yet due to the complicated damping mechanism of the bridges [Ren *et. al.* (2005)]. It is known that bridge damping in general varies with the amplitude of vibration. Therefore, the applicability of an identified damping ratio through ambient vibration tests is still an issue that needs to be evaluated further by using other identification techniques or other dynamic tests with large vibration amplitudes.

4.4 Model Updating

The modal updating is done here by introducing optimal parametric improvisations on the original finite element model by minimizing a cost function involving the identified modal characteristics. An optimization technique called MGA has been adopted. MGA creates several possible good solutions for a problem by eliminating bad alternatives. These solutions are different in nature of updating parameters but provide similar modal characteristics with similar value of cost function. A variation of the Hop, Skip and Jump method (HSJ) proposed by Brill *et. al.* (1992) is used in this study. The properties of the numerical model have been updated such that its modal parameters would match the identified natural frequencies and mode shapes to the closest extent.

4.4.1 Updating parameters

Three different types of parameters have been considered for updating the finite element model: (i) mass of the deck, (ii) moment of inertia of the spine beam, and (iii) the rotational stiffness of the connection between the deck and the pylons. A total of 66 translational lumped masses have been used to model the deck. Assuming that the mass distribution is symmetric due to the symmetry of the bridge, this can be reduced to 33 parameters to optimize, which is still a large number. As it is unlikely to have a sudden change in the mass along the deck, the numbers of parameters has been reduced to 3 master masses at 3 locations along the deck. The other 30 masses have been calculated by fitting a spline between the 3 master masses. The support of the bridge at Bent 1, the support at Pier 2, and centre of the main span have been selected as the locations for the 3 master masses as shown in Fig. 4.19.

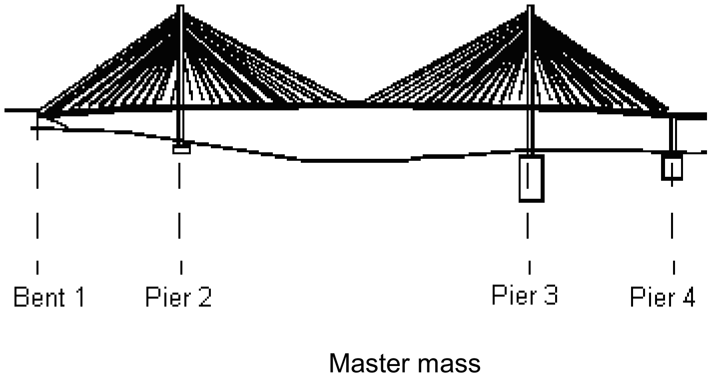

Fig. 4.19 Locations of master masses

Two parameters have been used to update the connection between the deck and the supports. Using the symmetry of the bridge one parameter has been used for Bent 1 and Pier 4 and a second parameter has been used for the connection at the Pier 2 and Pier 3. The introduction of rotary stiffness to the connections has been done through spring element as illustrated in the Figs. 4.20 to 4.23. Only one parameter has been used to update the moment of inertia of the spine beam. Therefore, a total of six parameters to be updated have been utilized in this study.

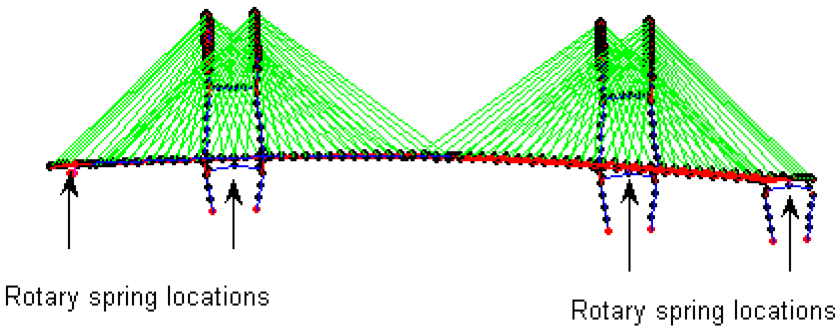

Fig. 4.20 Finite element model with rotary springs

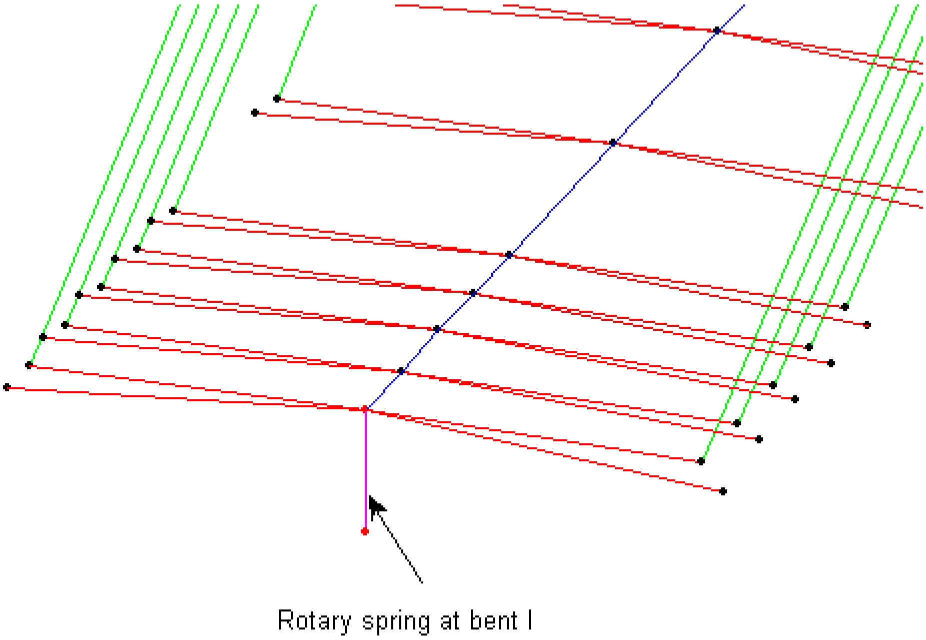

Fig. 4.21 Spring connection details at Bent 1

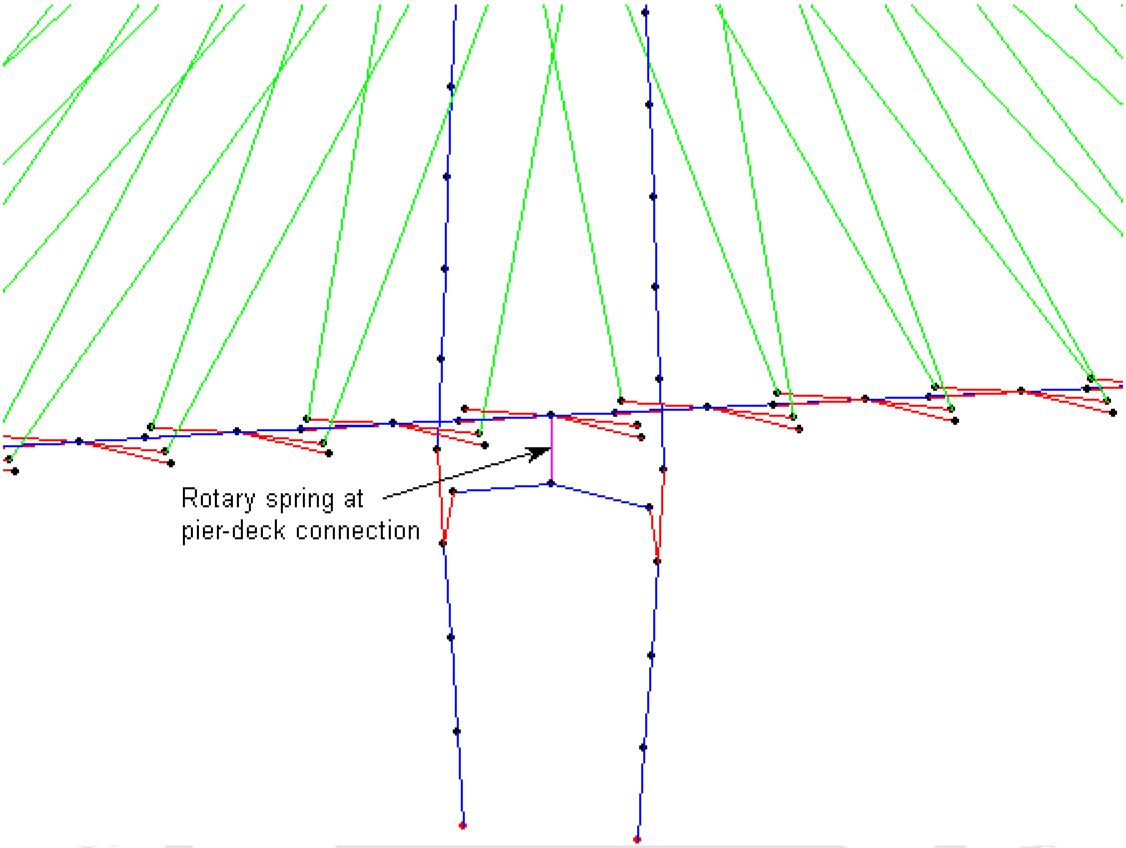

Fig. 4.22 Spring connection details at pylon-deck connection

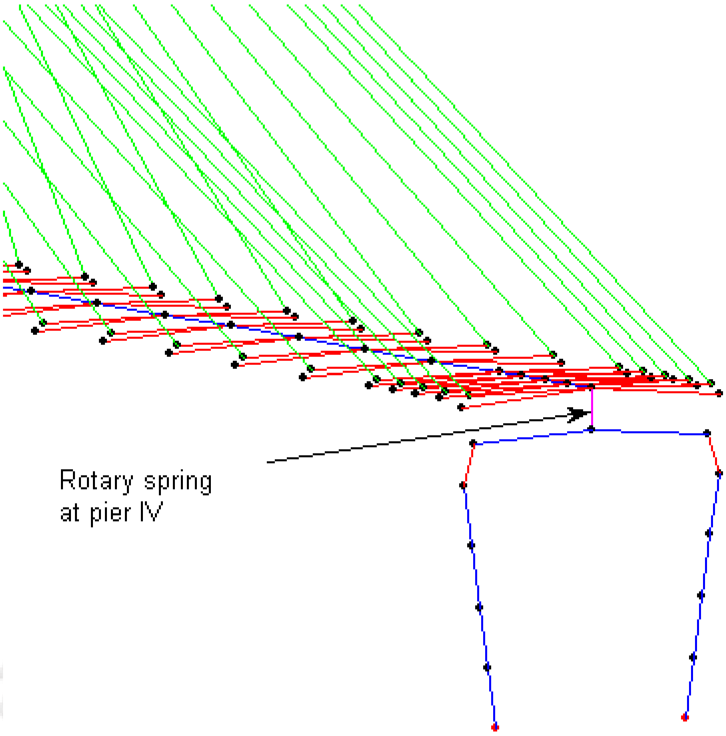

Fig 4.23 Spring connection at Pier 4 and deck

The method used for model updating has three main parts: (i) find a local minima based on the base finite element model; (ii) obtain other solutions using HSJ; (iii) obtain a local minima close to the solutions obtained in the previous step. For all steps a trust-region for non-linear minimization algorithm available in the Matlab® optimization toolbox has been used to minimize an objective function. In the first step, the function to minimize is described by the equation,

(4.14)

where n is the number of identified modes, MAC(,) is the modal assurance criteria between the ith identified mode shape ( ) and the *ith mode shape of the* finite element model , is the ith identified natural frequency, *is* the ith natural frequency of the finite element model, **p** is the vector of parameters to be minimized, and b*ι are the weighting factors for the* i*th natural frequency and* mode shape. The values of and b*ι have been determined form Eqs. (4.12) and* (4.13) using the identified modal parameters. These weights account for the deviations modal characteristics of a particular mode of the updated model from that of the corresponding identified mode. Constraints have been applied to the procedure to assure that the variation of the parameters is not higher than reasonable limits. Constraints have been used to allow a maximum variation of 5% in the masses and the moment of inertia. The stiffness of the connection between the deck and the pylon can change from 0 to 100% of the highest value of stiffness matrix. The FE model by Caicedo (2003) has been used as the initial point for the optimization.

The hypothesis in this study is that the results obtained from the first optimization will provide a solution of the problem; but this solution may not be unique and could be a local minimum. A process similar to HSJ is used to provide other solutions, which are different from the original solution. Here, a new objective function is then defined to obtain the (l+1) th solution as,

(4.15)

where $\mathbf{p}_j$ is the jth solution, denotes dot product and denotes the norm. The value of this function is high if the dot product between the current solution and previous solutions is close to one, while the value of the function is low if the new solution is perpendicular to any other solution found before. Given that orthogonal vectors do not always provide a good fit for the finite element model, constraints have been used to assure that the new solution has a similar performance to the first solution. The constraint used for this optimization is described by the equation,

(4.16)

where, is the value of the objective function shown in Eq. 4.14 for the first solution found, is the value of Eq. 4.14 for the current solution and a ισα constant. In this study α has been selected as 1.06 so as to discard the solutions that vary more than 6% in value of the cost function from that of the first minimum. The result from this second step provides solutions to the problem that are significantly different in the values for updating parameters but have similar values for cost function. The updated model has been selected from these solutions is the one that has the most realistic update for the selected parameters.

4.4.2 Results

The results of the optimization problem have been enumerated in this section.

(a) <u>Optimization solutions</u>: The solutions of optimization (the second step of the procedure) have been presented in Table 4.6. A total of three optimization solutions with comparative values of cost functions have been listed in the table. Different optimized parameters have been listed in the table corresponding to each of these alternative solutions. The optimized variations for mass as a percentage of original mass has been shown for the master locations as in Fig. 4.19. Similarly optimized variation of moment of inertia of spine has been listed for different solutions. Thirdly, the optimum value of rotary stiffness at the bent and piers have been listed as a percentage of maximum stiffness of the FE model by Caicedo (2003). Out of these alternative solutions, the most logical one has been selected for updating the finite element model.

The first solution is obtained using the model by Caicedo (2003) as the starting point. The differences in the three solutions have been appreciated from the tabular representation (Table 4.6). The first solution is based on decreasing the mass of the bridge, specially at the Pier 2 (Loc 2) and at the mid-span. The moment of inertia has also shown to be decreased marginally in this solution. In contrast, the second solution has suggested considerable increase in the rotational stiffness of the connection at the Bent 1 and Pier 4. The mass at the Pier 2 (Loc 2) is shown to be slightly lower than in the first solution while it suggests for only a marginal decrease in the inertia. On the other hand, the third solution lowers the moment of inertia of the spine beam significantly. In this solution the masses at the Bent 1 (Loc 1), Pier 2 (Loc 2) decreases uniformly while that in centre of the span decreases by the same amount as in the first solution. The solution further suggests for an increase in the rotary stiffness at the Bent 1. The values for the objective function $f(\mathbf{p})$ are also shown in the table and these are very similar for all the three solutions. These values are about 44% lower than the value of $f(\mathbf{p})$ for the original model by Caicedo (2003) which has been obtained as 1194.3. The second, third solutions have been observed to be within 6% of the first solution as specified by the parameter α in Eq. (4.16).

(b) <u>Modal characteristics of different solutions</u>: Table 4.7 shows the first four natural frequencies of the model by Caicedo (2003) and those from the optimized models. The MAC values between the identified mode shapes and the numerical modes have also been represented in the table. It is clear that the optimization procedure has resulted in models which have greatly improved natural frequencies as compared to those of the FEM model by Caicedo (2003). The MAC values between identified and numerical modes were high in case of FEM model by Caicedo (2003). These get slightly reduced in case of the optimized models.

(c) <u>Selection of updated model</u>: The first solution from Table 4.6 has been selected for updating the model by Caicedo (2003). As indicated in the table, this solution is the most realistic solution with no unreasonable demand on parametric changes. The second solution has not has not been adopted in spite of having the lowest value for objective function as this solution puts an unreasonably high demand on the increase in rotary stiffness to the degree of 50.34%. The mode shapes from this updated model together with the identified modal ordinates at the sensor locations have been presented in Figs. 4.24 to 4.27. The black dots in the figure indicated the identified modal amplitudes corresponding to the sensor locations.

4.5 Conclusion

This chapter has presented the model updating of the Bill Emerson Memorial Bridge using Model to Generate Alternative (MGA) optimization approach. Records of acceleration from the bridge have been used to identify the modal parameters of the structure using the subspace identification technique. The lowest four flexural modes with frequencies (Hz) of 0.324, 0.413, 0.635 and 0.703 and corresponding mode shapes have been clearly identified. The parameters of a finite element model of the bridge corresponding to the mass and moment of inertia of the deck and rotary stiffness of the connection between deck-abutment and deck-pylon supports have been updated. A trust-region algorithm for non-linear optimization have been used first to minimize the objective function that measures the differences between the modal parameters of the finite element model and the identified mode shapes and natural frequencies. Further, the MGA has been used to obtain other solutions which are significantly different but have similar values of the objective function. The final solution has been selected from these alternatives and has appropriately updated the FE model.

Table 4.4 Identified parameters: SSI

Mode	Hits	Frequency (Hz)	Standard deviation of frequency (Hz)	Damping (%)	Standard deviation of damping (%)	MAC	Standard deviation of MAC
1	31	0.324	0.0036	1.05	0.37	0.9977	0.0019
2	16	0.413	0.0026	0.64	0.09	0.9967	0.0023
3	25	0.635	0.0041	0.67	0.20	0.9983	0.0009
4	21	0.706	0.0032	0.73	0.51	0.9962	0.0046

Table 4.5 Identified parameters: NExT-ERA

Mode	Hits	Frequency (Hz)	Standard deviation of frequency (Hz)	Damping (%)	Standard deviation of damping (%)	MAC	Standard deviation of MAC
1	39	0.324	0.0055	1.41	0.71	0.9963	0.0044
2	37	0.414	0.0045	1.09	0.55	0.9976	0.0029
3	28	0.636	0.0037	1.16	0.70	0.9952	0.0033
4	16	0.708	0.0048	0.96	0.31	0.9904	0.0048

Table 4.6 Alternative solutions from optimization

Solution	Mass (%)			Moment of Inertia (%)	Rotary Stiffness (%)		f(p) (Eq. 4.14)
	Loc1	Loc2	Mid-span		Bent 1 & Pier 4	Piers 2 &3	
1	-0.87	-5.00	-5.00	-2.05	0.02	0.00	494.8
2	-1.17	-4.70	-5.00	-0.18	50.34	0.00	493.8
3	-2.24	-2.03	-5.00	-4.95	8.68	0.00	498.4

Table 4.7 Modal characteristics for alternative solutions

Solution					MAC			
Original FE model	0.291	0.392	0.608	0.674	0.955	0.947	0.968	0.973
1	0.307	0.413	0.635	0.703	0.956	0.944	0.960	0.967
2	0.308	0.413	0.635	0.703	0.956	0.943	0.957	0.966
3	0.307	0.413	0.635	0.702	0.955	0.942	0.957	0.965

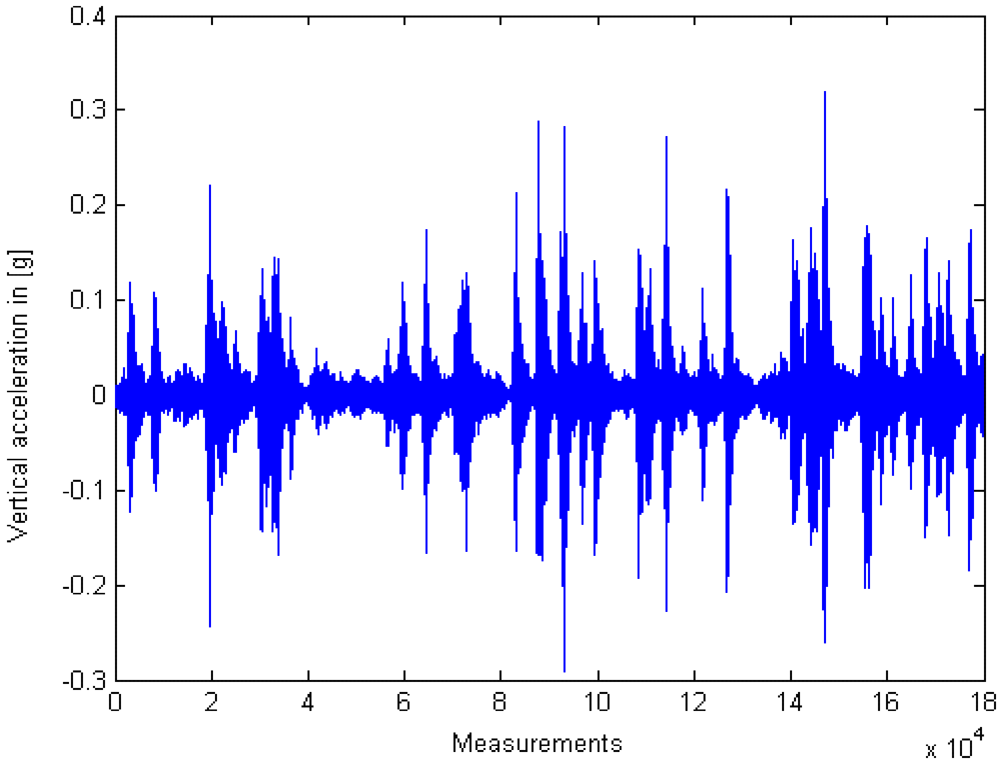

Fig. 4.9 Sensor signal from mid-span (station C1)

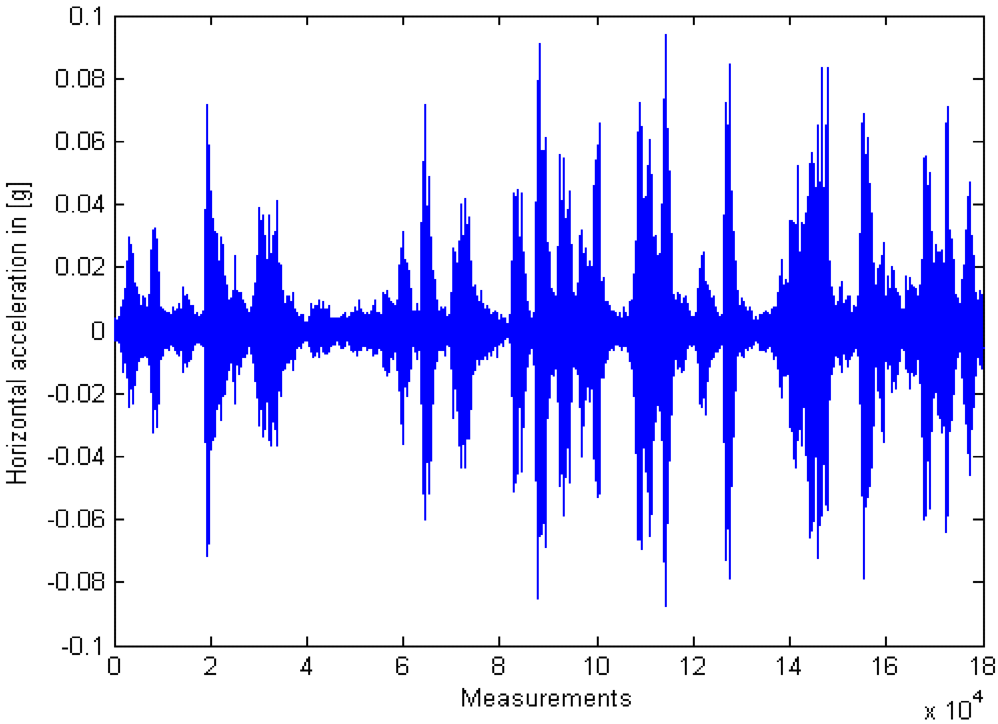

Fig. 4.10 Sensor signal from top of left pylon (station T1)

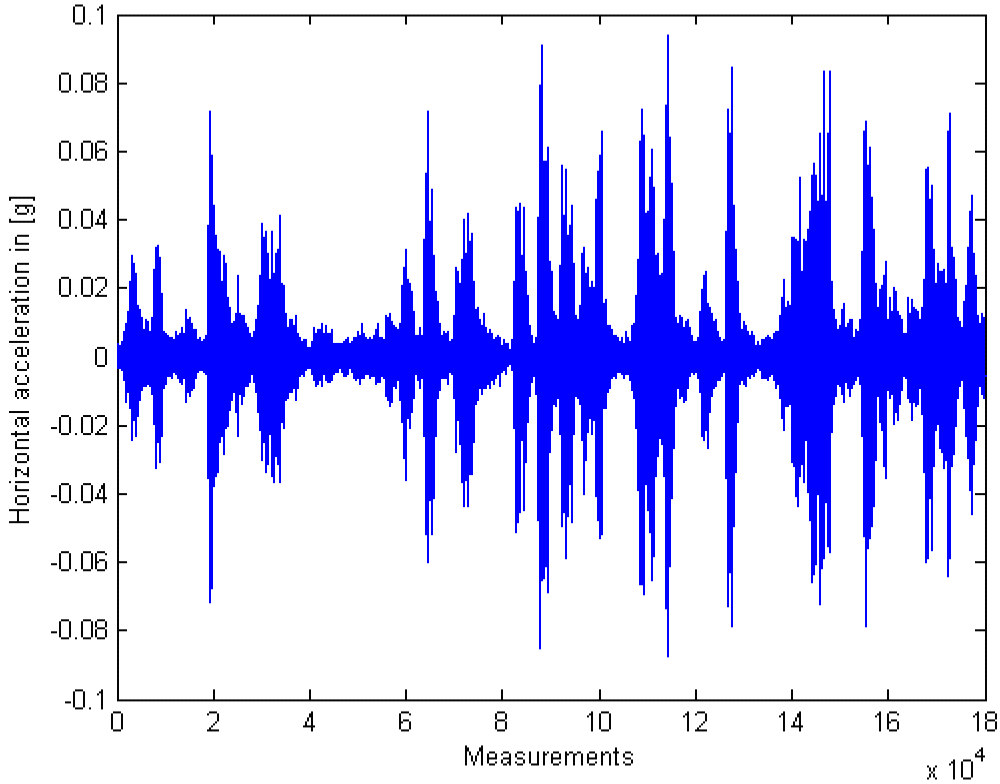

Fig. 4.11 Sensor signal from top of right pylon (station T3)

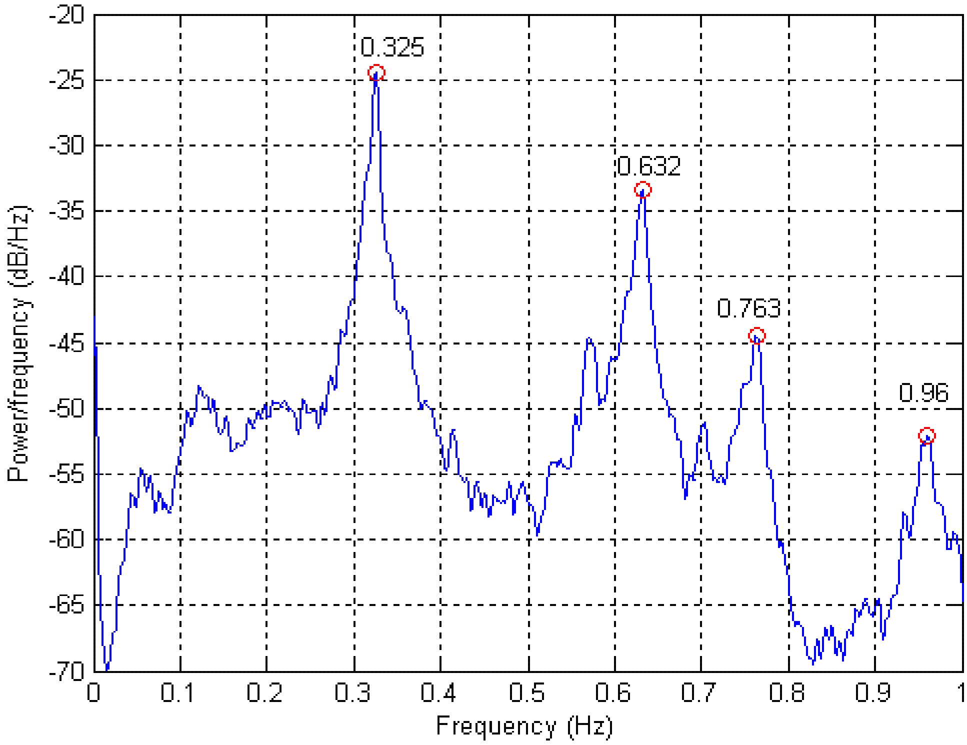

Fig. 4.12 PSD of signal from mid-span

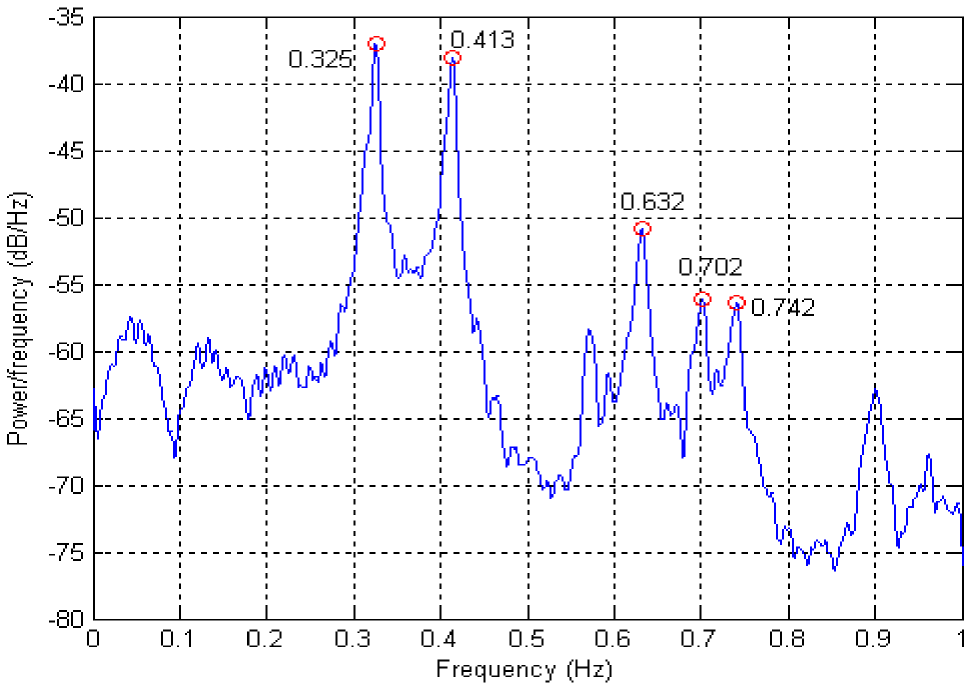

Fig. 4.13 PSD of signal from top of left pylon

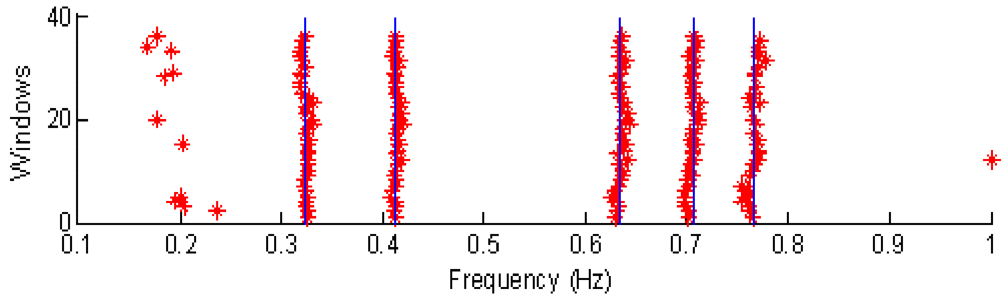

(a)

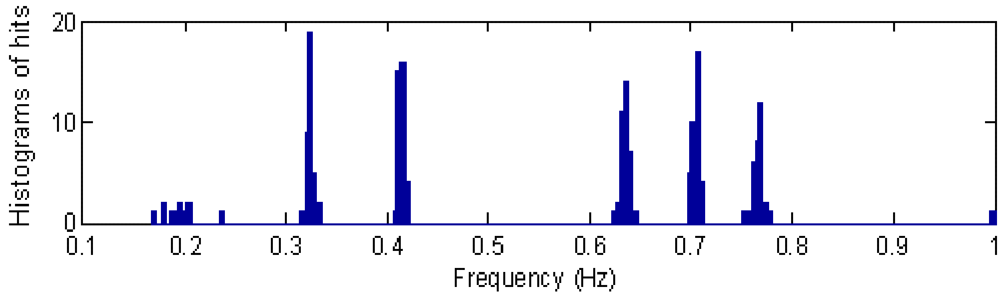

(b)

Fig. 4.18 Details of modal identification by SSI

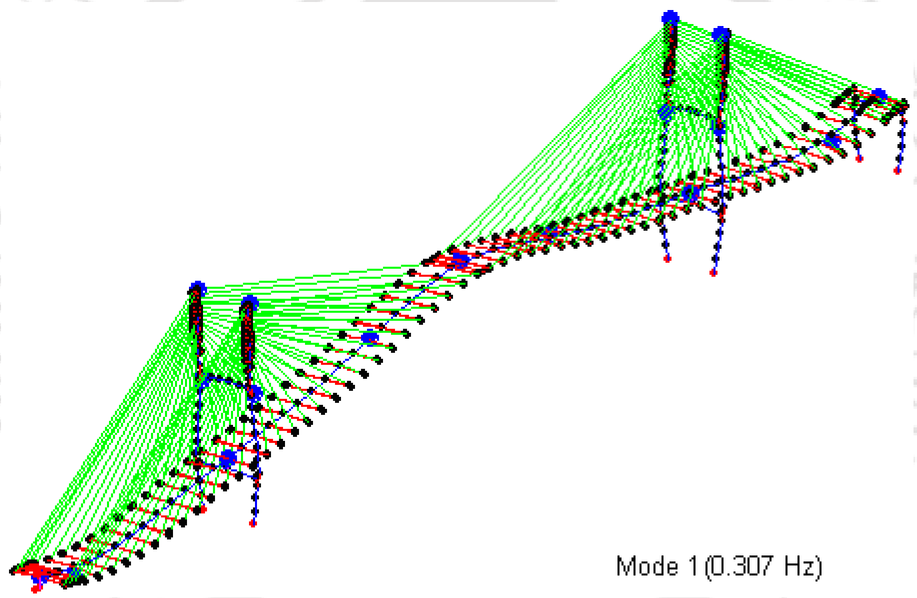

Fig. 4.24 First identified mode

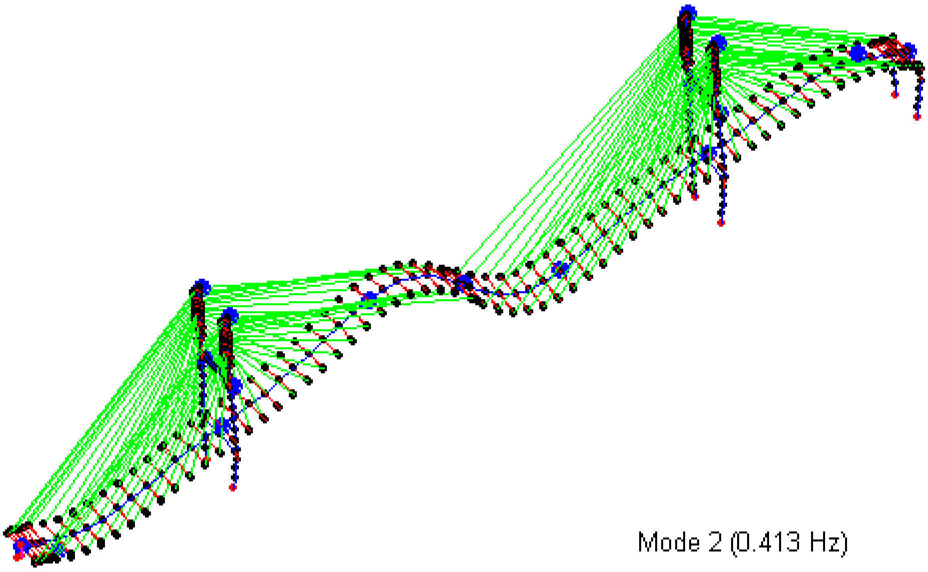

Fig. 4.25 Second identified mode

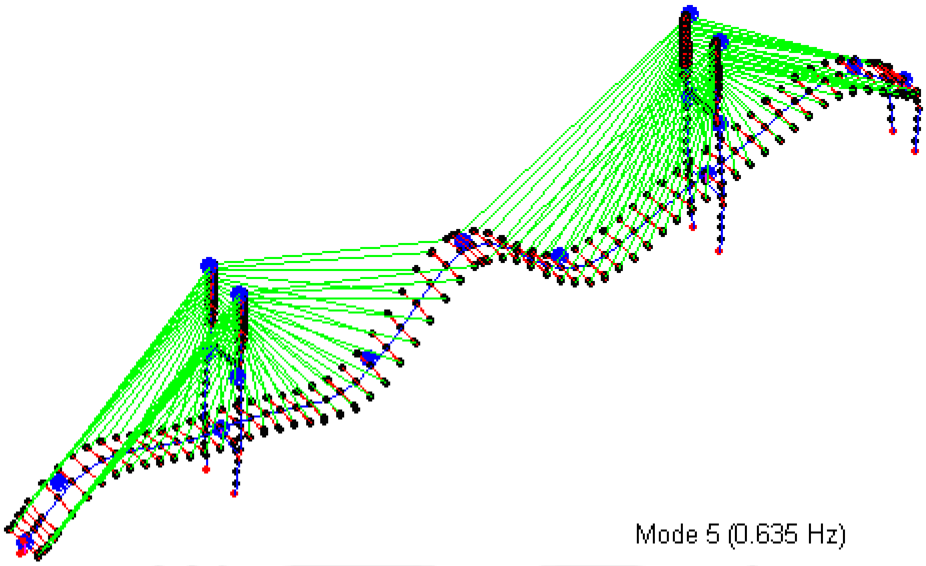

Fig. 4.26 Third identified mode

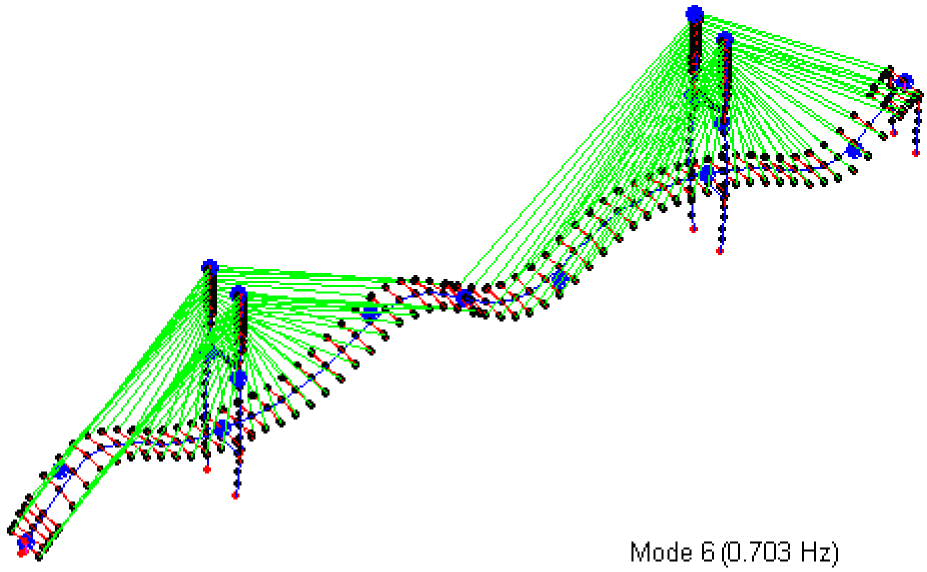

Fig. 4.27 Fourth identified mode

Chapter 5

DESIGN OF ACTIVE CONTROLLERS FOR SEISMIC RESPONSE CONTROL OF BILL EMERSON MEMORIAL BRIDGE

5.1 Introduction

The Bill Emerson Memorial Bridge has already been a subject of phase-I and phase-II benchmark control studies introduced by Dyke *et. al.* (2000) and Caicedo *et. al.* (2003) respectively. Many researchers have contributed to the alternative control studies on this bridge. He *et. al.* (2001), Yang *et. al.* (2003), Park *et. al.* (2003a), Park *et. al.* (2003b), Park *et. al.* (2003c), Bontempi *et. al.* (2003), Iemura *et. al.*

(2003), Dai *et. al.* (2004), Kim *et. al.* (2005), Park *et. al.* (2005) studied various control strategies on this bridge. This bridge has also been a subject of structural health monitoring [Caicedo (2003)] and structural identification [Song *et. al.* (2006)]. However, the FE model that was used for the aforesaid studies was found to be inadequate to simulate the dynamic characteristics of the bridge structure as studied previously by Giraldo *et. al.* (2006) and in Chapter 4. An updated model of the bridge has been developed in Chapter 4 to simulate the experimentally observed flexural modes more precisely. In this chapter, active controllers have been designed based on the updated FE model and the efficacy of these has been tested against select seismic excitations. The procedure adopted for the design of the active controllers is the same as the one followed in Chapter 3. Two active controllers, one against uniform support excitation and the other corresponding to multiple support excitations, have been designed to control the responses at key locations of the bridge against three representative earthquakes. Multiple support excitation case has been considered for two different angles of attack of earthquake excitation and corresponding time lags of incidence of earthquake wave in different supports. The evaluation criteria adopted from the benchmark problem defined by Dyke *et. al.* (2000) have validated the effectiveness of the controller in reducing the peak pylon forces.

5.2 Linear Evaluation Model

The updated model from Chapter 4 has been adopted for carrying out linear dynamic analysis and is termed as the linear evaluation model for the present study. As explained in the previous chapter, this model corresponds to the dead load deformed configuration of the bridge, and the modal characteristics obtained from this model match well with the identified modal characteristics of the bridge from ambient vibration results. The first seven modal frequencies of this updated model are: 0.307 (flexural), 0.413 (flexural), 0.462 (torsional), 0.496 (mixed-torsional), 0.635 (flexural), 0.703 (flexural), 0.712 (lateral-torsional-flexural). This model has been used for response determination of the uncontrolled structure.

5.3 Control Evaluation Model

The control evaluation model has been formed by replacing the constraint equations corresponding to the deck-abutment/pylon joints from the numerical model and replacing them with actuator connections. The procedure has already been described in section 3.4. The first seven frequencies (Hz) of this released structure are: 0.174, 0.303, 0.418, 0.437, 0.490, 0.636 and 0.643.

5.4 Model Reduction

The Guyan reduction scheme has been implemented for reduction of the degrees of freedom to a manageable level for control studies. The procedure for reduction has already been dealt in detail in section 3.5. The retained dofs have also been selected in the line of subsection 3.5.2. The reduction process has been validated by the use of transfer function. The *Bode* plot in Fig. 5.1 shows comparison of transfer functions corresponding to the linear evaluation model and the reduced linear evaluation model in transferring ground acceleration from ground to pylon top. The procedure for arriving at the plot has already been dealt with in detail in subsection 3.5.3. It has been observed from Fig. 5.1 that the plots for the two models matches well in both magnitude and phase upto 10 Hz, which is a fairly sufficient range. In the case of multiple supports excitations the support dofs have been retained in the reduced linear evaluation model. The first seven mode shapes of the reduced model have been illustrated in Fig. 5.2 and these agree well with those from linear dynamic model. A reduction strategy, similar to that in section 3.6, has been followed to arrive at the reduced control evaluation model which will be used for design of the controller.

5.5 State Space Representation of the System

State space representation of the system is a prerequisite for designing an active controller for the structure. This procedure has already been discussed in detail in section 3.9 of this work.

5.6 Problem Statement for Design of Controller

The problem statement for control design is the same as followed in section 3.10. The components of the control system have also been discussed in the same section. The Simulink® block as illustrated in Fig. 3.12 has been adopted for simulation of control. The representative earthquakes considered in the benchmark case [Dyke *et. al.* (2000)] have been adopted for this study to evaluate of the controller. The selection criteria for the earthquake excitations and the details of the earthquakes have already been discussed in detail in subsection 3.10.2 of this dissertation. However, in comparison to the Quincy Bayview Bridge discussed in Chapter 3, there is a difference in the time lags of incidence of earthquake excitations for multiple support case for this bridge. This is due to differences in distances between the supports of the present bridge from that of Quincy Bayview Bridge. The time lag has accordingly been revised as: [0 0.05 0.16 0.20] sec for incidence angle of 15^0 and [0 0.03 0.12 0.15] sec for incidence angle of 45^0. It may be recalled that the incidence angle has been selected as the angle between the longitudinal direction of the bridge(X) and the *N-S* wave of the earthquake. Accordingly two cases have been considered: Case-1, an incidence angle of 15^0 with delay of [0 0.05 0.16 0.20] sec for the supports from left to right, and Case-2, an incidence angle of 45^0 with corresponding delay as [0 0.03 0.12 0.15] sec.

The evaluation criteria have been kept as the same as in the benchmark case [Dyke *et. al.* 2000)]. These criteria have already been explained in Chapter 3 (subsection 3.10.2, Table 3.3). However, for the present cable-stayed bridge the value of total weight (W) of the superstructure in Eqs. (3.52), (3.54) and (3.55) is 5,10,000 kN [Dyke *et. al.* (2000)].

The uncontrolled maximum responses for uniform support case for the updated model have been presented in Table 5.1. The uncontrolled responses corresponding to multiple support excitation has been shown in Table 5.2. These have been used for determination of the evaluation criteria. The notations used here are the same as explained in Eqs. (3.40) to (3.58).

The constraints and limitations in the control design for the problem have been retained as in the benchmark case [Dyke *et. al.* (2000)] and as explained in subsection 3.10.3. The safe range (between 20% and 70% of ultimate tension) for cable tensions during excitation, prescribed by Dyke *et. al.* (2000) for the benchmark problem, has been adopted for the present study too. The ultimate cable tensions for the cables have been adopted from the tabulated values by Dyke *et. al.* (2000).

5.7 Design of Controller

In this section the design detail for an active controller based on a LQG algorithm has been presented. The theoretical background and formulation used for the design of the controller has already been explained in the section 3.11. As explained, accelerometers and displacement sensors have been used as measurement devices while hydraulic actuators act as controlling devices. The configurations of the sensor and actuator have been kept same as the benchmark problem by Dyke *et. al.* (2000).

5.7.1 Sensors

Separate arrangements of sensors have been used for the control design against uniform support and multiple support excitations respectively as explained in this subsection.

(a) <u>Uniform support excitations</u>: Four displacement sensors and five accelerometers have been employed for measuring the responses. The arrangement of the sensors has been kept the same as in the benchmark problem which is described in subsection 3.11.1 (a). The accelerometers have a sensitivity of 7 V/*g* (*i.e.* 7 Volts = 9.81 m/sec^2) and thus are able to measure upto 1.42*g* within a range from -10 V to +10 V. This has been considered sufficient for measurement of the acceleration for the present case. In case of the displacement sensors, the sensitivity has been kept at 30 V/m (*i.e.*, 10 V = 0.33 m) allowing for a maximum actuator stroke of ±0.1 m for a signal of ±10 V.

(b) <u>Multiple support excitations</u>: Fourteen accelerometers and four displacement sensors have been used in this case. The arrangements of the sensors have been kept the same as the benchmark files by Dyke *et. al.* (2000) and have been discussed in detail in subsection 3.11.1 (b). The sensitivities of the sensors have been kept the same as in the uniform support case as in subsection 5.7.1 (a). The Simulink® sensor block used here has already been illustrated in Fig. 3.9.

5.7.2 Actuators

Twenty four numbers of hydraulic actuators have been employed for seismic response control in this study. These have been placed on the deck pylon interface and deck abutment/pier interface. The actuators have been oriented in the longitudinal direction of the bridge (global *X*) as in the benchmark files by Dyke *et. al.* (2000). The arrangement of the actuators has been illustrated in Fig. 1.2. The governing equations for interfacing these to the model have already been documented in detail in the benchmark files [Dyke *et. al.* (2000)] and have been discussed in section 3.10.1. However, the actuator-sensitivity for actuators have been selected as 155 kN/V allowing for the constraint of ±10 V = 1550 kN. This is sensitivity has been used assuming a maximum capacity for the actuators as 1550 kN.

5.7.3 Control design model

The states space representation of the system has been made more compact to facilitate a practically implementable controller. This is done by removing the states with less controllability and observability grammians following the procedure as enumerated in section 3.11.3. The resulting system has been termed as the control design model. Thirty numbers of states have been retained for uniform support excitation. Transfer functions have been used to show that the control design model retains the dynamic characteristics of the control evaluation model. Comparative *Bode* plots represent these transfer functions between ground acceleration and displacement of top of left pylon for the cable stayed bridge as shown Fig. 5.3.

It has been observed that the two plots match sufficiently in magnitude and phase upto 4 Hz. It may be mentioned that this frequency range covers the modal representation upto the 98th mode, which a sufficient range to portray the dynamics of the cable-stayed bridge. Sixty numbers of states have been retained for multiple support excitation. The state space representation of the system for both uniform support and multiple support excitations have been carried out following the same procedure as in subsection 3.10.3 of this dissertation.

The LQG control algorithm adopted for the design of the controller has already been explained in subsection 3.11.4 and has not been repeated here.

The Simulink® block used for numerical simulation of the controller has been adopted as the same as described in section 3.12 of this thesis.

5.8 Results and Discussion

The performance of the controller against different evaluation criteria have been presented in this section. The control efficacy of the controllers has been discussed separately for uniform support and multiple support excitations.

5.8.1 Uniform support excitation

In this case, the control performance has been obtained using the state weigthing matrix .The performance of the controller against different evaluation criteria have been presented in Table 5.3. It has been observed from the values of J_1 and J_3 that the controller reduces the responses of base shear and overturning moment of the pylons to considerable extents. This reduction of base shear and overturning moment is significant from the point of view of structural safety. The peak deck shear and deck moment have decreased significantly (J_2 and J_4). The controller further reduces the normed responses of base shear and overturning moment significantly as indicated by the evaluation criteria J_7 and J_9. This validates the effectiveness of the controller over the entire excitation period.

The control performances in case of base shear and overturning moment for pylon I against the representative earthquakes have been presented in Figs. 5.4 and 5.5

respectively. A maximum control in the order of 68.86% has been observed in case of base shear. The highest control of 70.70% has been obtained for overturning moment. However, the controlled responses of overturning moment have shown an increase over the uncontrolled response towards the end of the excitation period. This may be attributed to the spillover effect [Preumont (2002)], where the removed states during balance realizations excite the retained states. The controlled and uncontrolled cable tensions have been illustrated from Figs. 5.6 to 5.8. The controlled response of the cables are strictly within the upper and lower acceptable range of cable tensions. It may be observed that the out of range cable tensions of El Centro excitation case has been brought within the limit. The peak values of the force, stroke, and velocity for the actuator for each of the earthquakes have been presented in Table 5.4. It has been observed that an actuator-capacity of 1550 kN is sufficient in for implementation of the control strategy. Other requirements such as stroke and velocity are feasible in a device of this size.

5.8.2 Multiple support excitation

The performance of the controller has been evaluated against the two cases of multiple support excitations enumerated in section 5.6. The performance in terms of the evaluation criteria have been obtained with a state weighting matrix

.

(a) Case-1: The performance of the controller as per different evaluation criteria have been presented in Table 5.5. It has been observed that the controller is effective in reducing the base shear and overturning moment in the pylons to considerable extent in the direction of its orientation (global *X*) as indicated by the values of J_1 and J_3. The deck shear and deck moment have also decreased significantly (J_2 and J_4.). It has also been noticed that the shear and moments at the bases and deck level of the pylons have increased marginally in the transverse direction (global *Z*). It is natural that the controller is not effective in controlling responses in the direction (*Z*) perpendicular to its orientation (*X*). However, these increases may be considered insignificant in comparison to reduction in base shear and overturning moment of the pylons.

The control performances in case of base shear and base moment responses against the representative earthquakes have been presented in Figs. 5.9 and 5.10 respectively. The highest control observed in case of base shear is 68.94% and that for overturning moment is 66.13%. The controlled and uncontrolled cable tensions have been illustrated in Figs 5.11 to 5.13. The controlled responses, indicated by thick lines, are well within the acceptable range shown by broken lines. In a similar observation, as in case of the uniform support excitation, the out of range cable tensions during El Centro excitation has been controlled adequately by the controller.

The peak demand on the actuators in terms of force, stroke, and velocity during multiple support excitations (Case-1) have been listed in Table 5.6. The force requirement is well within the capacity of the actuator (1550 kN). The force requirements as well as the velocity requirements are feasible in a device of this size.

(b) Case-2: The performance of the controller as per different evaluation criteria has been presented in Table 5.7. It has been observed that the controller is effective reducing the peak response of base shear and overturning moment for the pylon to considerable extent in the direction of its orientation (global *X*) .The peak deck shear and deck moments have also been reduced significantly. It has also been noticed the controller responses for shear and moments at base and deck level of pylons have increased marginally in the transverse direction (global *Z*). However, these increases may be considered insignificant in comparison to the degree of control achieved in base shear and overturning moment for the pylons.

The performance of the controller in reducing base shear and overturning moment of the pylons against the earthquakes has been presented in Fig. 5.14 and 5.15 respectively. The maximum control observed in case of base shear is 66.99% and corresponding highest controlled performance in case of overturning moment is 68.18%. The performance of the controller in controlling the cable tensions have been shown in Figs. 5.16 to 5.18. The cable tensions in the uncontrolled cases move towards a narrower band into the range of acceptable maximum and minimum cable tensions (broken lines). In this case too, the out of range cable tensions of El Centro excitation case has been brought into control.

The peak values of the force, stroke, and velocity for the controller for each of the earthquakes have been listed in Table 5.8. The demand of actuation force is well within the capacity (1550 kN) of the actuator. The force requirements as well as the velocity requirements are feasible in a device of this size.

5.9 Conclusion

Two active controllers have been designed to control seismic response of the Bill Emerson Memorial Bridge, USA against select earthquakes. An updated finite element model has been used in this study to arrive at the linear evaluation model, reduced control design model and finally the state space model that has been used to construct the active controller. The active controllers show effective control capability in controlling key pylon responses against sample earthquake excitations. It has been ensured that the cable tensions are within safe limits while controlling the responses at those key locations.

Table 5.1 Uncontrolled maximum responses against uniform support excitation

Response	Definition	Earthquakes		
		El Centro	Mexico	Gebze
(kN)		4.937	1.289	3.097
(kN)		4.913	1.641	3.257
(kNm)		1.157	2.015	7.037
(kNm)		2.348	8.987	1.148
(m)		9.987	2.523	7.231
		5.391	1.529	2.719
		4.698	1.974	2.730
		1.349	3.321	5.964
		2.327	7.095	9.742
(m)		2.371	4.393	2.977
(m/sec)		1.231	3.543	6.279

Table 5.2 Uncontrolled maximum responses against multiple-support excitation

Response	Direction	Definition	Case-1			Case-2		
			El Centro	Mexico	Gebze	El Centro	Mexico	Gebze
(kN)	X		6.46×10^{4}	2.73×10^{4}	3.49×10^{4}	4.93×10^{4}	2.58×10^{4}	2.73×10^{4}
(kN)	Z		1.48×10^{4}	1.95×10^{4}	1.15×10^{4}	6.36×10^{4}	8.93×10^{3}	1.76×10^{4}
(kN)	X		6.16×10^{3}	3.01×10^{3}	4.02×10^{3}	6.34×10^{3}	2.92×10^{3}	3.36×10^{3}
(kN)	Z		6.72×10^{3}	2.31×10^{3}	5.15×10^{3}	8.93×10^{3}	2.77×10^{3}	5.93×10^{3}
(kNm)	X		1.33×10^{6}	5.23×10^{5}	7.18×10^{5}	9.64×10^{5}	4.71×10^{5}	5.73×10^{5}
(kNm)	Z		4.67×10^{5}	2.93×10^{5}	3.32×10^{5}	7.31×10^{5}	2.64×10^{5}	5.23×10^{5}
(kNm)	X		2.31×10^{5}	1.23×10^{5}	1.33×10^{5}	2.24×10^{5}	1.35×10^{5}	1.23×10^{5}
(kNm)	Z		1.21×10^{5}	3.18×10^{4}	8.34×10^{4}	1.41×10^{4}	4.01×10^{4}	9.65×10^{4}
(m)	X		9.93×10^{-2}	4.56×10^{-2}	5.32×10^{-2}	8.42×10^{-2}	3.36×10^{-2}	5.32×10^{-2}
(kN)	X		6.17×10^{3}	3.41×10^{3}	3.01×10^{3}	5.96×10^{3}	3.17×10^{3}	2.52×10^{3}
(kN)	Z		1.92×10^{3}	1.13×10^{3}	9.42×10^{3}	2.12×10^{3}	9.72×10^{3}	1.17×10^{3}
(kN)	X		5.48×10^{2}	3.27×10^{2}	3.29×10^{2}	5.49×10^{2}	3.17×10^{2}	2.93×10^{2}
(kN)	Z		7.69×10^{2}	2.68×10^{2}	3.96×10^{2}	8.85×10^{2}	3.38×10^{2}	4.53×10^{2}
(kNm)	X		1.34×10^{5}	7.62×10^{5}	6.61×10^{5}	1.31×10^{5}	6.47×10^{4}	5.52×10^{4}
(kNm)	Z		6.17×10^{4}	3.11×10^{4}	3.21×10^{4}	6.71×10^{4}	3.01×10^{4}	3.62×10^{4}
(kNm)	X		2.41×10^{4}	1.43×10^{4}	1.49×10^{4}	2.31×10^{4}	1.39×10^{4}	1.21×10^{4}
(kNm)	Z		1.25×10^{4}	4.01×10^{3}	6.24×10^{3}	1.41×10^{3}	5.01×10^{3}	7.32×10^{3}
(m)	X		9.78×10^{-2}	7.43×10^{-2}	9.42×10^{-2}	9.97×10^{-2}	7.67×10^{-2}	9.89×10^{-2}
(m/sec)	X		1.15	0.59	0.77	1.16	0.59	0.68

Table 5.3 Evaluation criteria of the active controller against uniform support excitation

Value	El Centro	Mexico	Gebze	Maximum
J_1	0.4139	0.5260	0.4384	0.5260
J_2	0.9967	1.0867	1.3467	1.3567
J_3	0.3595	0.8867	0.8736	0.8867
J_4	0.6147	0.6078	0.9945	0.9945
J_5	0.1605	0.0067	0.1345	0.1605
J_6	1.6578	1.9867	3.4789	3.4789
J_7	0.2784	0.4097	0.3853	0.4097
J_8	1.0076	0.9974	1.4498	1.4498
J_9	0.2789	0.4075	0.4578	0.4578
J_{10}	0.8324	0.9878	1.5698	1.5698
J_{11}	0.0291	0.014	0.017	0.0291
J_{12}	1.439	5.1	1.63	1.63
J_{13}	0.7745	0.9854	1.6790	1.6790

J_{14}	2.589	1.74	6.9	7.2
J_{15}	4.17	2.95	6.65	6.65
J_{16}	24	24	24	24
J_{17}	9	9	9	9
J_{18}	30	30	30	30

Table 5.4 Actuator requirements against uniform support excitation

Response	El Centro	Mexico	Gebze	Max
Force (kN)	889.78	330.78	901.03	901.03
Stroke (m)	0.1367	0.0756	0.2998	0.2998
Vel (m/sec)	0.7543	0.4529	0.6324	0.7543

Table 5.5 Evaluation criteria for active controller against multiple support excitation: Case-1

Value	Direction	El Centro	Mexico	Gebze	Maximum
J_1	X	0.3723	0.4423	0.3237	0.4423
	Z	1.0287	1.1176	1.0432	1.1176
J_2	X	0.6934	0.8546	0.9547	0.9547
	Z	0.9436	0.9653	0.9863	0.9863
J_3	X	0.3223	0.4025	0.4136	0.4136
	Z	1.0893	1.0579	1.0389	1.0893
J_4	X	0.5592	0.7498	0.8942	0.8942
	Z	0.9976	1.0021	0.9954	1.1021
J_5	X	0.2323	0.1156	0.1573	0.2323
J_6	X	1.0056	1.5765	1.2225	1.5765
J_7	X	0.2398	0.2954	0.2993	0.2993
	Z	1.0113	1.0435	1.0456	1.0456
J_8	X	0.8234	0.8907	0.9432	0.9432
	Z	0.9685	0.9874	0.9901	0.9901
J_9	X	0.2354	0.2986	0.3875	0.3875
	Z	0.9956	1.0321	1.0335	1.0335
J_{10}	X	0.6124	0.7853	0.8124	0.8124
	Z	0.9901	0.9981	0.9993	0.9993

J_{11}	2.351	1.398	1.587	2.351
J_{12}	2.796	1.798	2.786	2.796
J_{13}	0.6432	0.9543	1.0023	1.0023
J_{14}	3.347	2.452	6.73	6.73
J_{15}	4.997	3.873	6.699	6.699
J_{16}	24	24	24	24
J_{17}	14	14	14	14
J_{18}	60	60	60	60

Table 5.6 Actuator requirements against multiple support excitation: Case-1

Response	Direction	El Centro	Mexico	Gebze	Max
Force (kN)	X	1503.98	865.36	1490.75	1503.98
Stroke (m)	X	0.1156	0.0935	0.2638	0.2638
Vel (m/sec)	X	0.7878	0.5439	0.5870	0.7878

Table 5.7 Evaluation criteria for active controller for multiple support excitation:Case-2

Value	Direction	El Centro	Mexico	Gebze	Maximum
J_1	X	0.3635	0.4479	0.3484	0.4479
	Z	1.0304	1.1157	1.0278	1.1157
J_2	X	0.6797	0.8435	0.9398	0.9398
	Z	0.9675	0.9789	0.9945	0.9945
J_3	X	0.3223	0.4258	0.4158	0.4258
	Z	1.0985	1.0342	1.0376	1.0985
J_4	X	0.6012	0.7232	0.8765	0.8765
	Z	0.9956	1.0042	1.0054	1.0054
J_5	X	0.2598	0.1158	0.1745	0.2598
J_6	X	1.2556	1.8673	1.6784	1.8673
J_7	X	0.2664	0.3187	0.3287	0.3287
	Z	0.9864	1.0054	1.0089	1.0089
J_8	X	0.8198	0.9005	0.9973	0.9973
	Z	0.9843	0.9939	1.0067	1.0067

J_9	X	0.2591	0.3106	0.4075	0.4075
	Z	0.9894	1.0032	1.0109	1.0335
J_{10}	X	0.6731	0.8472	0.8329	0.8472
	Z	0.9914	0.9992	1.0051	1.0051
J_{11}		2.472	1.412	1.612	2.472
J_{12}		2.572	1.812	2.541	2.572
J_{13}		0.7321	0.9875	1.0014	1.0014
J_{14}		3.546	2.679	6.43	6.73
J_{15}		3.893	2.678	7.963	6.699
J_{16}		24	24	24	24
J_{17}		14	14	14	14
J_{18}		60	60	60	60

Table 5.8 Actuator requirements for multiple support excitation: Case-2

Response	Direction	El Centro	Mexico	Gebze	Max
Force (kN)	X	1389.06	895.05	1178.46	1389.06
Stroke (m)	X	0.1384	0.0945	0.2432	0.2432
Vel (m/sec)	X	0.5693	0.5926	0.4893	0.5926

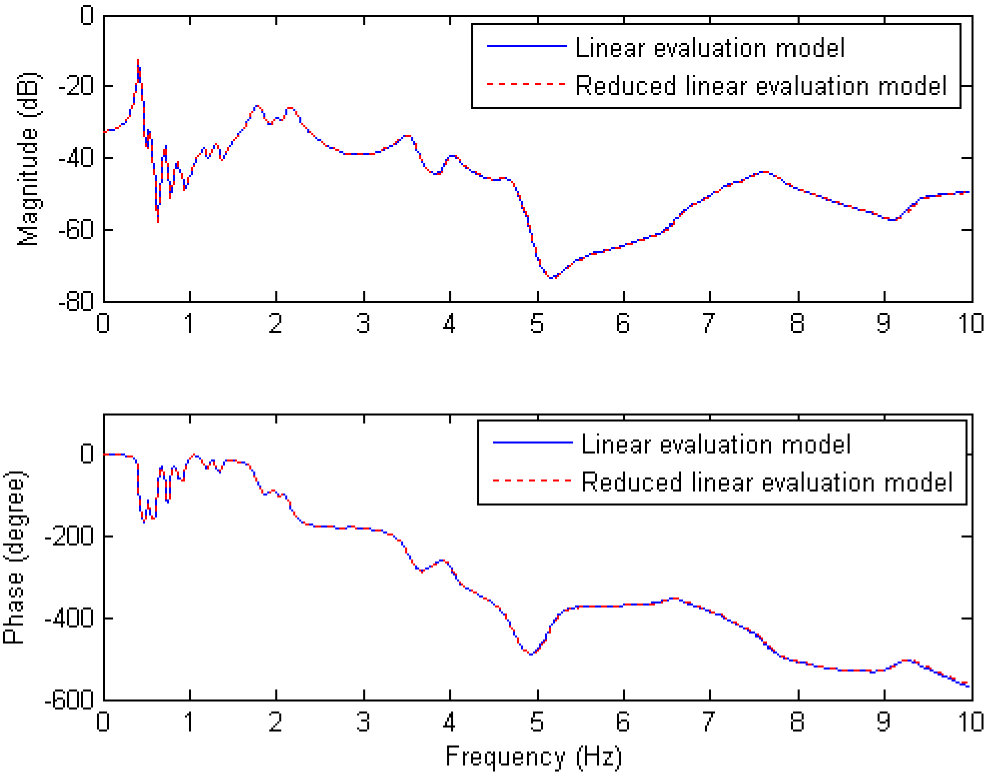

Fig. 5.1 Transfer function of ground acceleration to displacement at top of left pylon

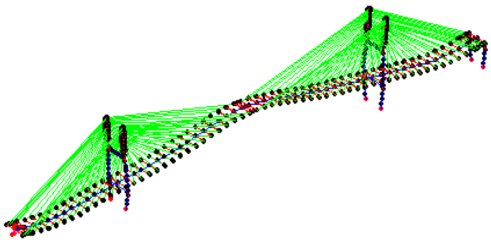

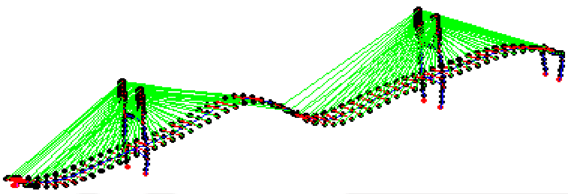

First mode (flexural, 0.307 Hz)

Second mode (flexural, 0.413 Hz)

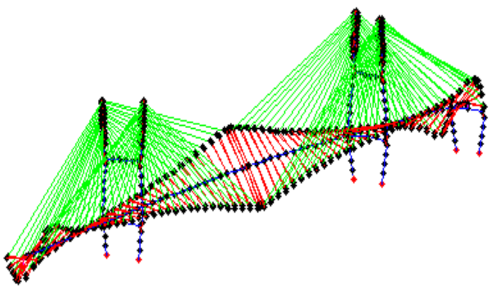

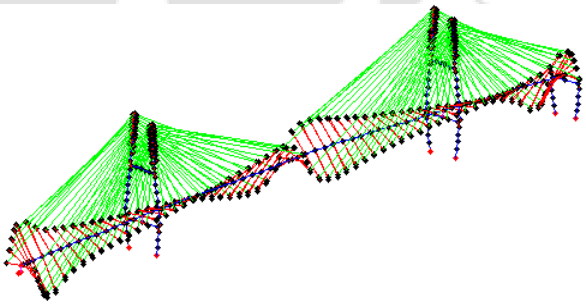

Third mode (torsional, 0.462 Hz)

Fourth mode (mixed-torsional, 0.496 Hz)

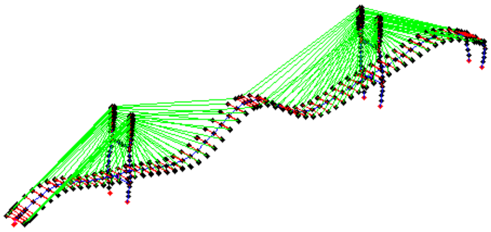

Fifth mode (flexural, 0.635 Hz)

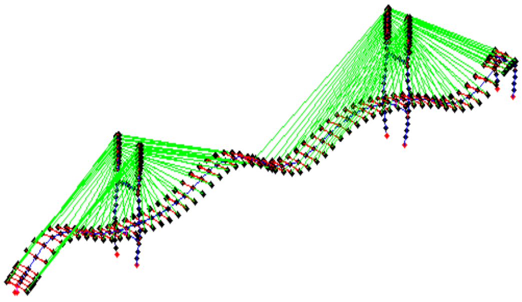

Sixth mode (flexural, 0.703 Hz)

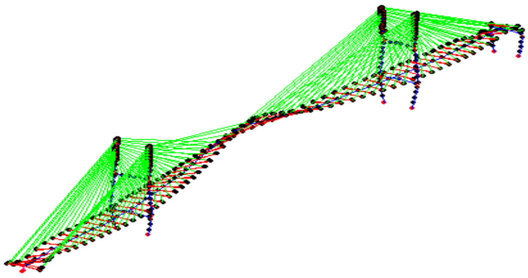

Seventh mode (lateral-torsional-flexural, 0.712 Hz)

Fig. 5.2 Mode shapes of the reduced linear evaluation model

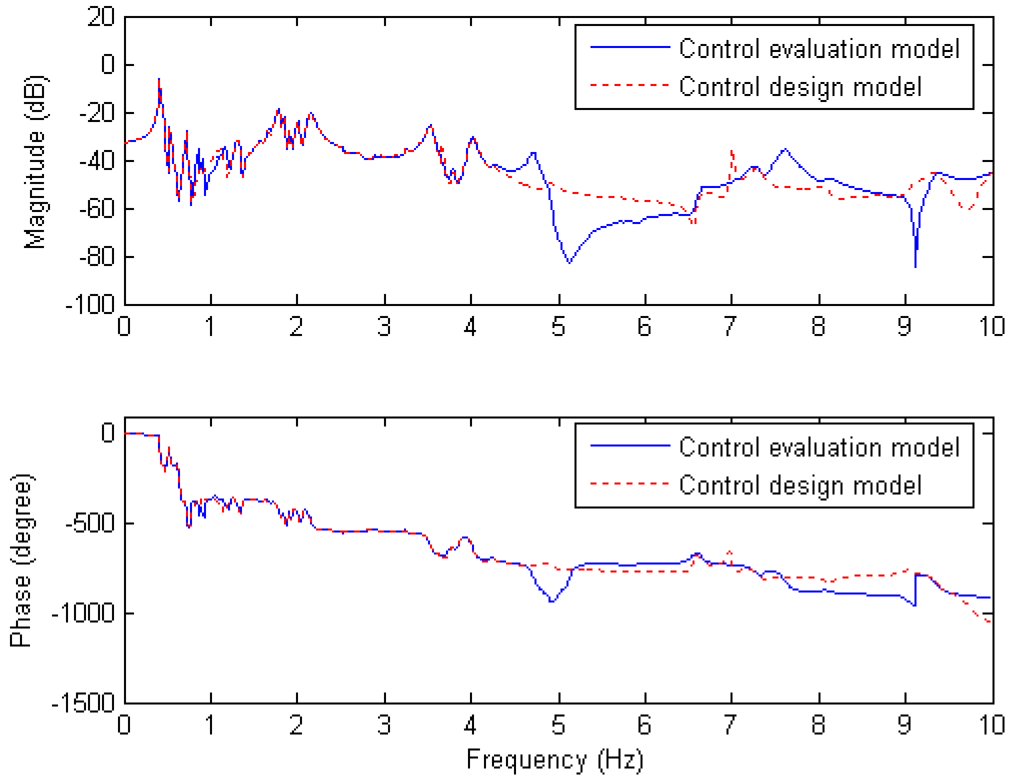

Fig. 5.3 Transfer function of ground acceleration to displacement at top of left pylon

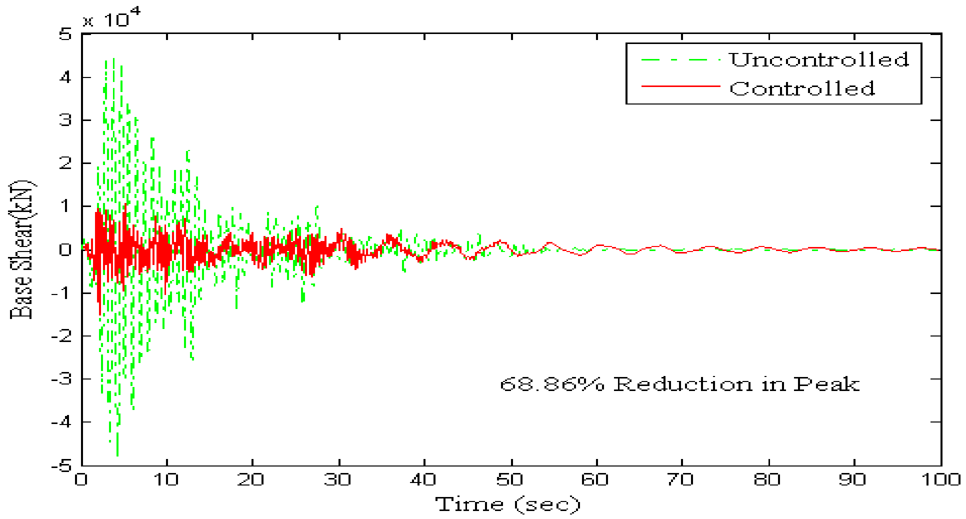
x 10^4
Uncontrolled
Controlled
Base Shear(kN)
68.86% Reduction in Peak
Time (sec)
5
4
3
2
1
0
-1
-2
-3
-4
-5
0
10
20
30
40
50
60
70
80
90
100

(a)

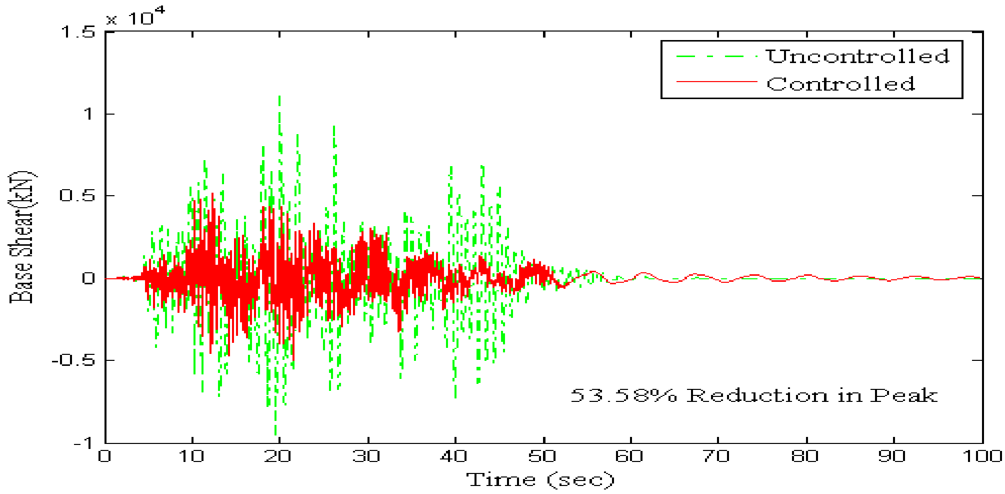
x 10^4
Uncontrolled
Controlled
Base Shear(kN)
53.58% Reduction in Peak
Time (sec)
1.5
1
0.5
0
-0.5
-1
0
10
20
30
40
50
60
70
80
90
100

(b)

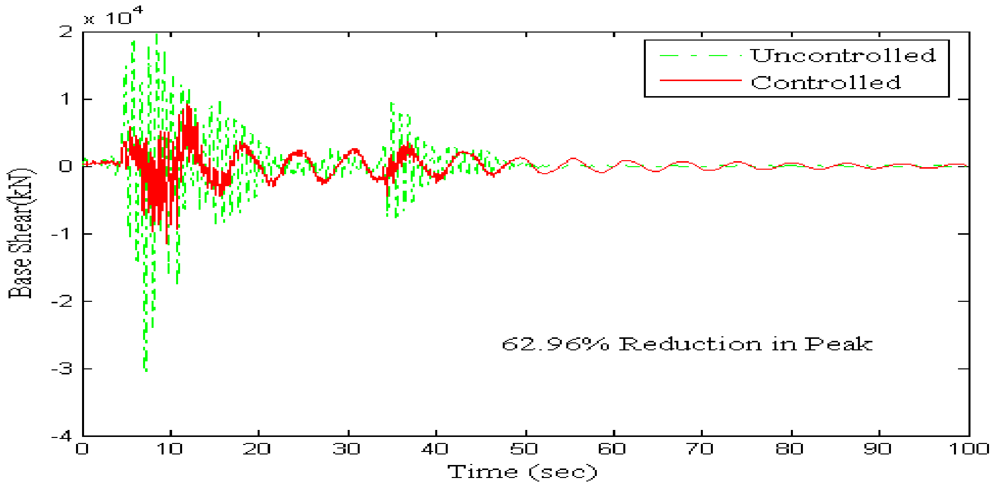

(c)

Fig. 5.4 Time history of base shear in pylon I against uniform support excitation: (a) El Centro Earthquake, (b) Mexico City Earthquake, (c) Gebze Earthquake

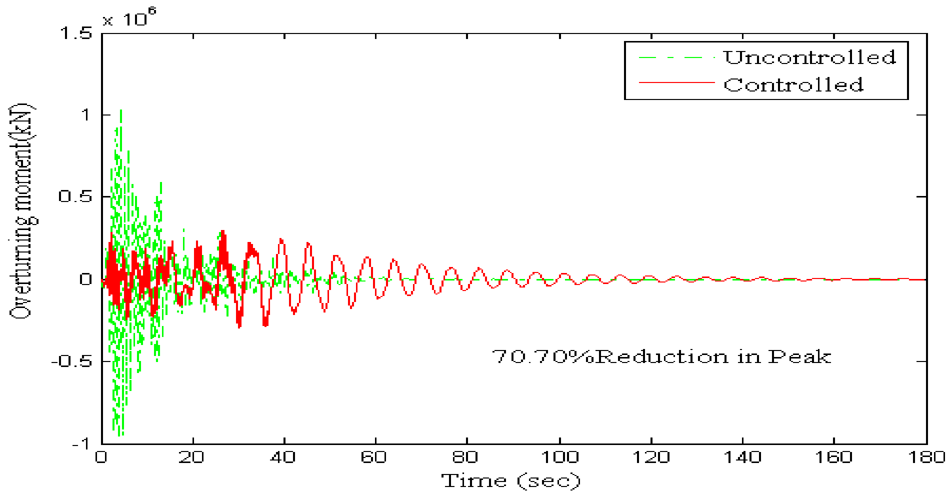

(a)

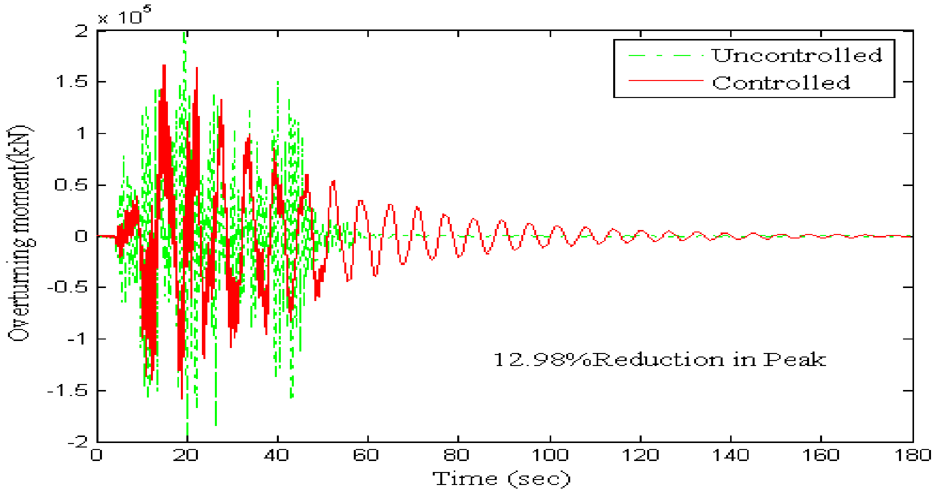

(b)

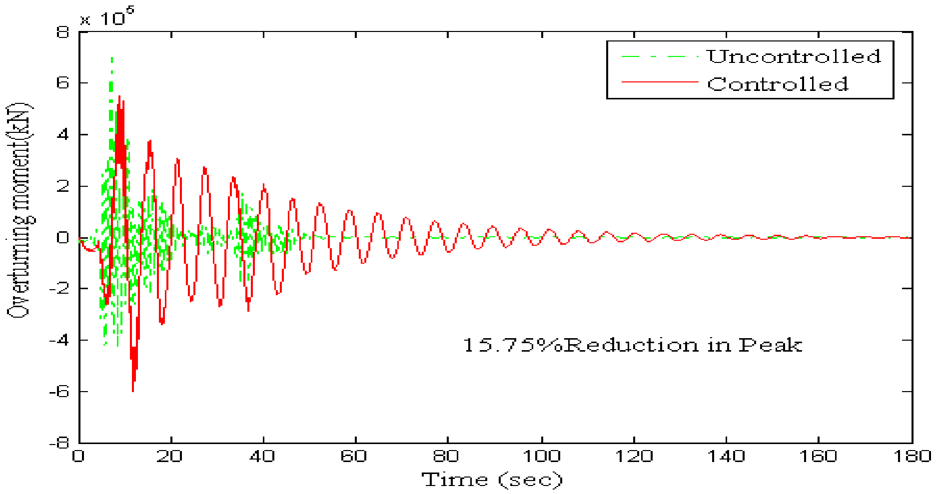

(c)

Fig. 5.5 Time history of overturning moment in pylon I against uniform support excitation: (a) El Centro earthquake, (b) Mexico City earthquake, (c) Gebze earthquake

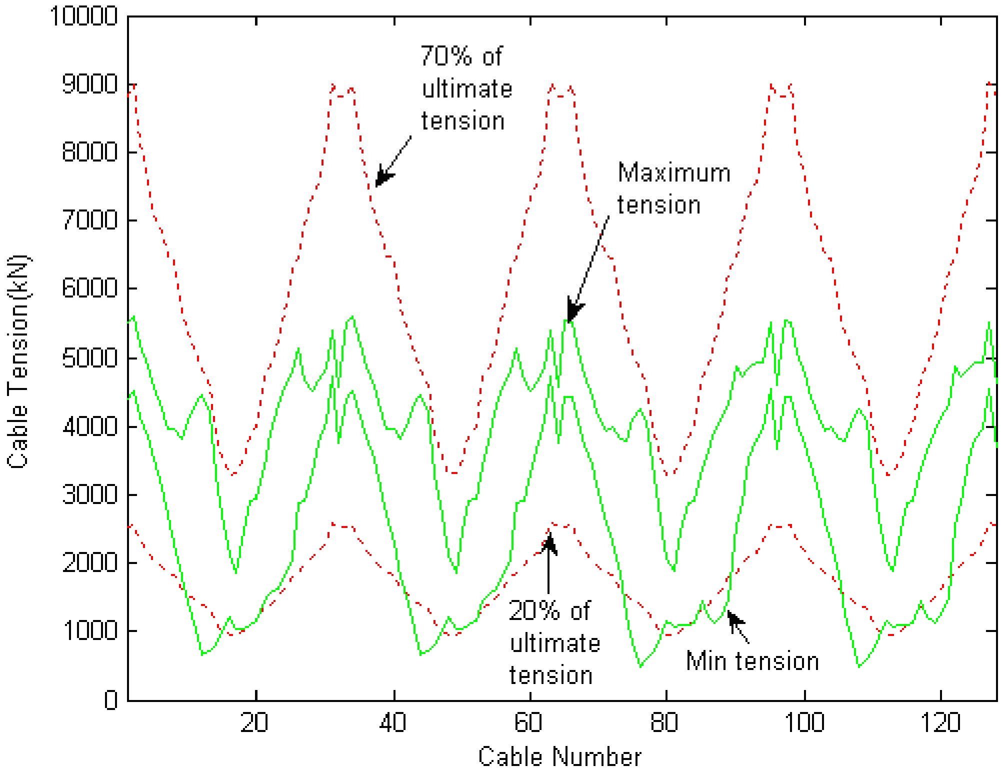

70% of
ultimate
tension
Maximum
tension
20% of
ultimate
tension
Min tension
Cable Tension(kN)
Cable Number
10000
9000
8000
7000
6000
5000
4000
3000
2000
1000
0
20
40
60
80
100
120

(a)

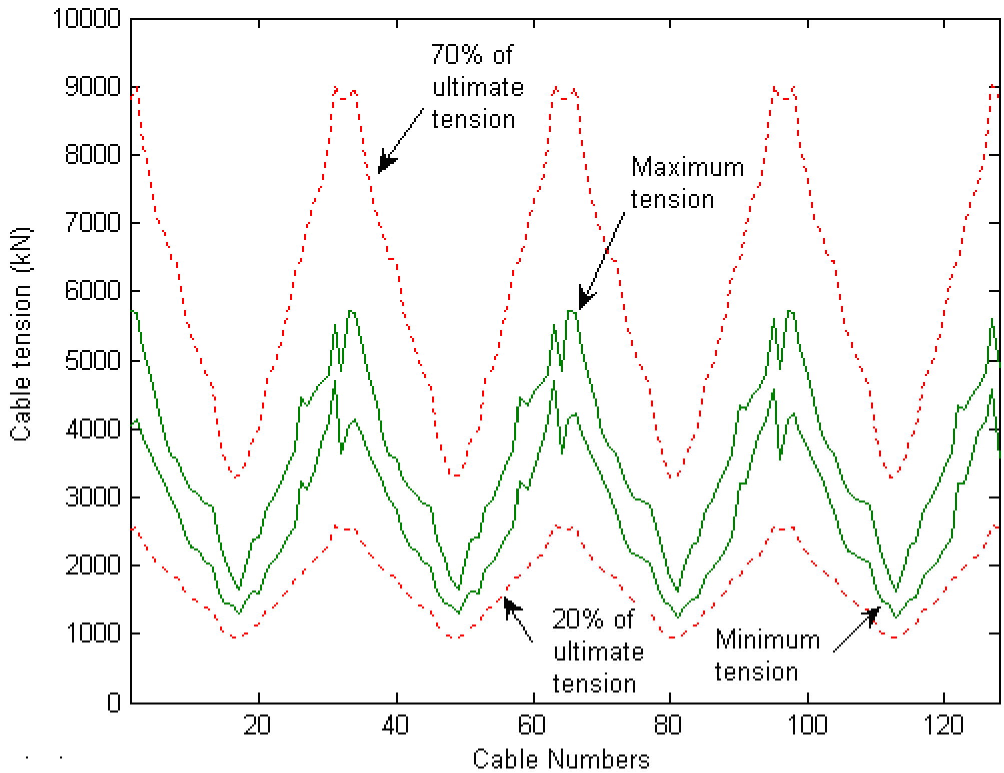

(b)

Fig. 5.6 Cable tension against uniform support excitation of El Centro earthquake: (a) Uncontrolled response, (b) Controlled response

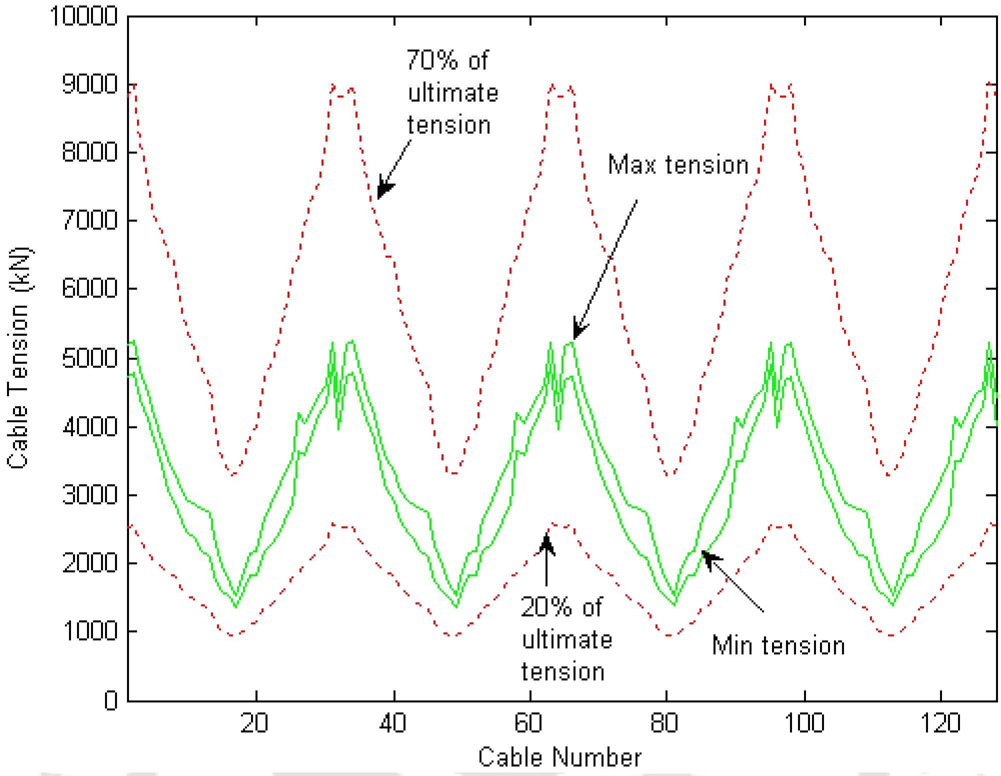

10000
9000
8000
7000
6000
5000
4000
3000
2000
1000
0
Cable Tension (kN)
70% of
ultimate
tension
Max tension
20% of
ultimate
tension
Min tension
20
40
60
80
100
120
Cable Number

(a)

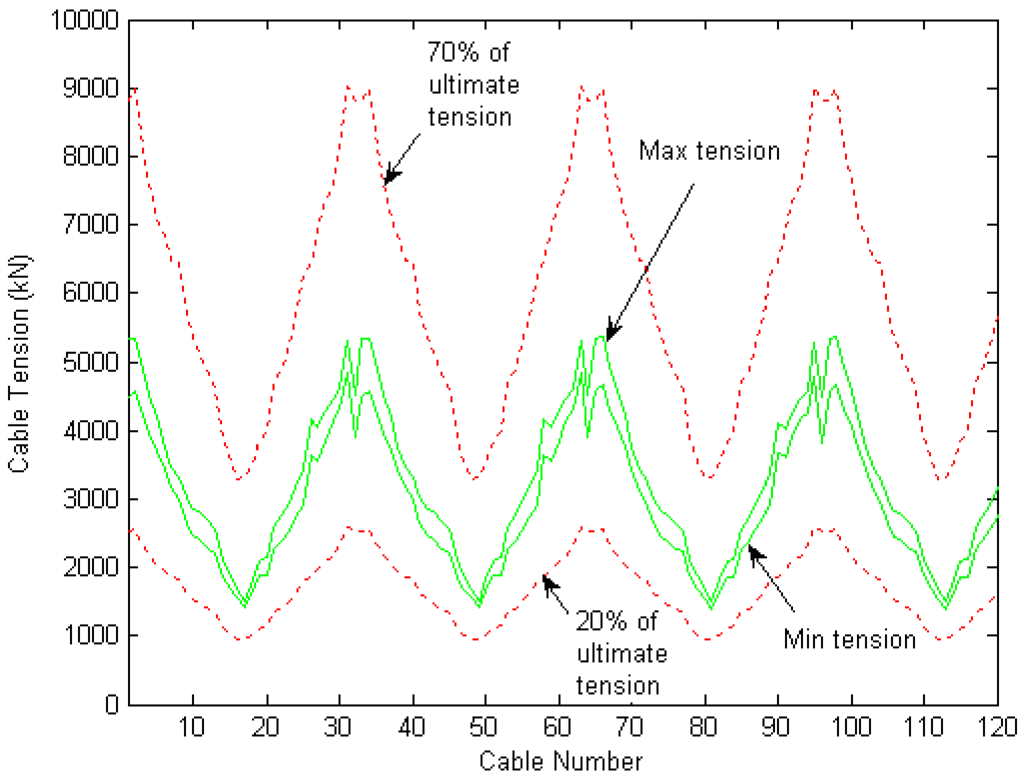

(b)

Fig. 5.7 Cable tension against uniform support excitation of Mexico earthquake: (a) Uncontrolled response, (b) Controlled response

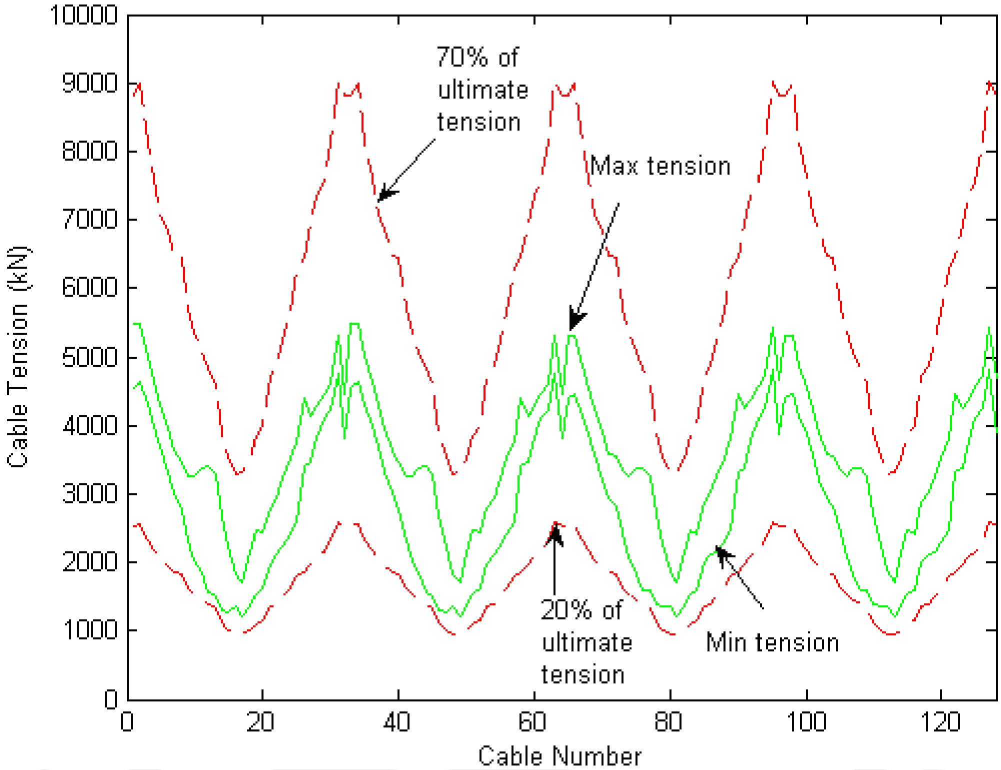

10000
9000
8000
7000
6000
5000
4000
3000
2000
1000
0
Cable Tension (kN)
0
20
40
60
80
100
120
Cable Number
70% of
ultimate
tension
Max tension
20% of
ultimate
tension
Min tension

(a)

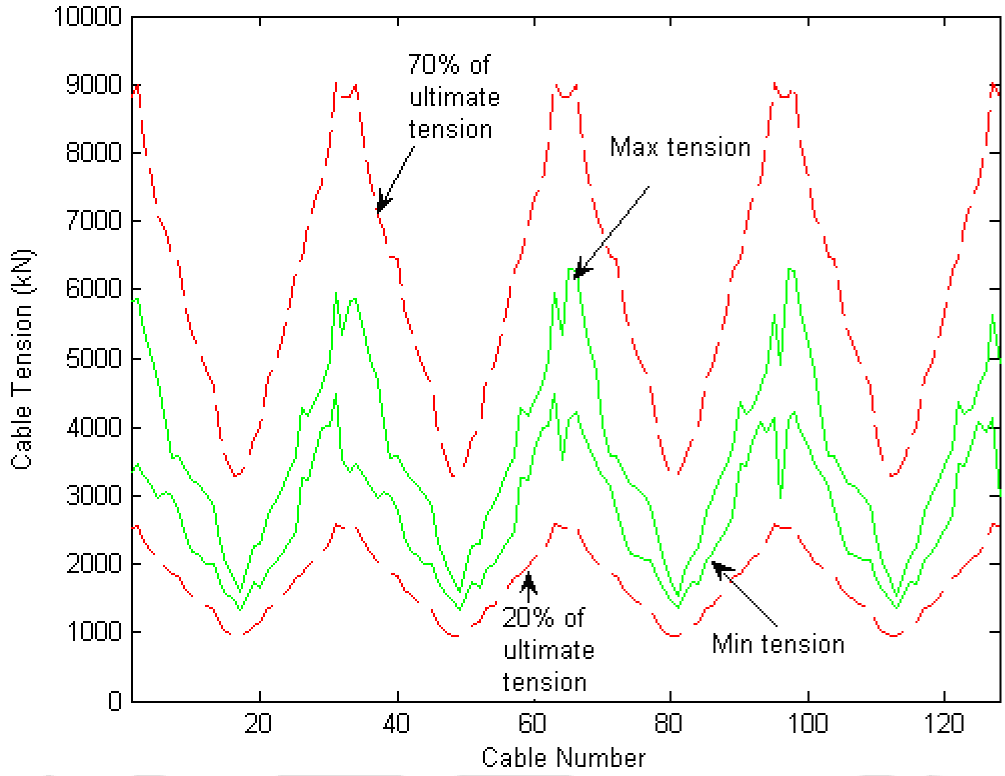

(b)

Fig. 5.8 Cable tension against uniform support excitation of Gebze earthquake: (a) Uncontrolled response, (b) Controlled response

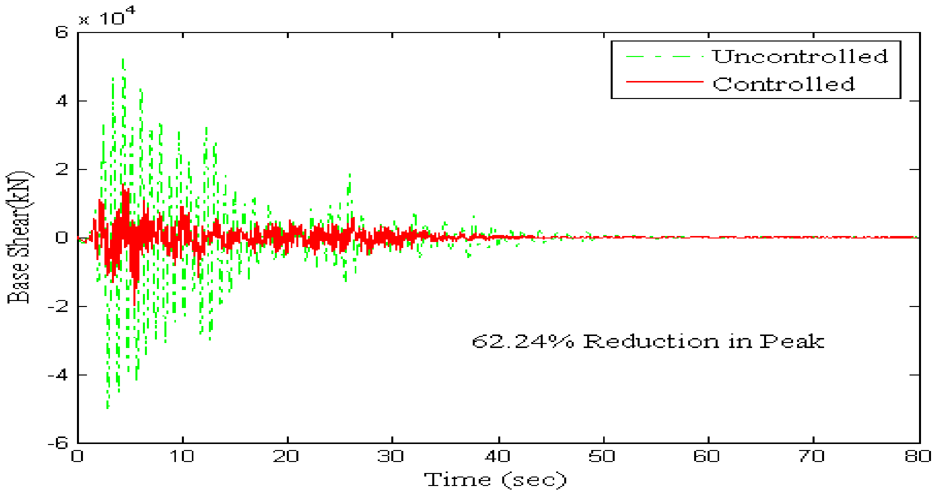
x 10^4
Uncontrolled
Controlled
Base Shear(kN)
62.24% Reduction in Peak
Time (sec)

(a)

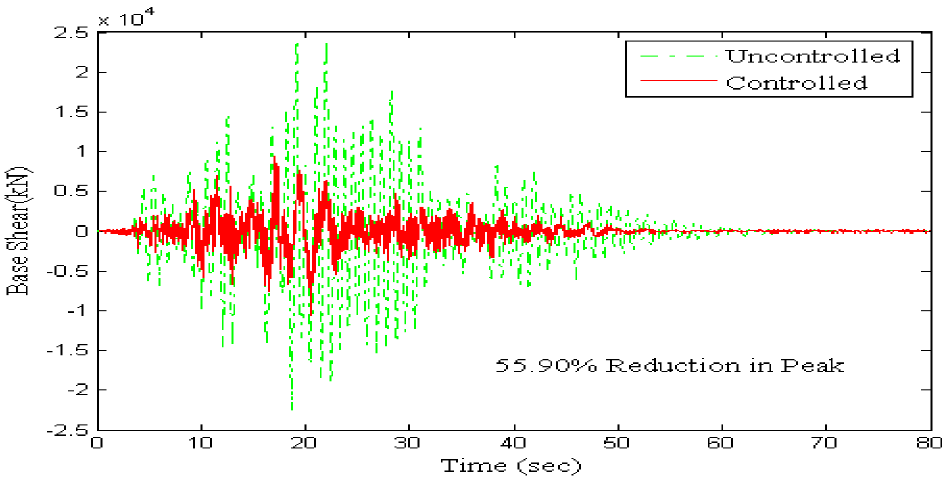
x 10^4
Uncontrolled
Controlled
Base Shear(kN)
55.90% Reduction in Peak
Time (sec)

(b)

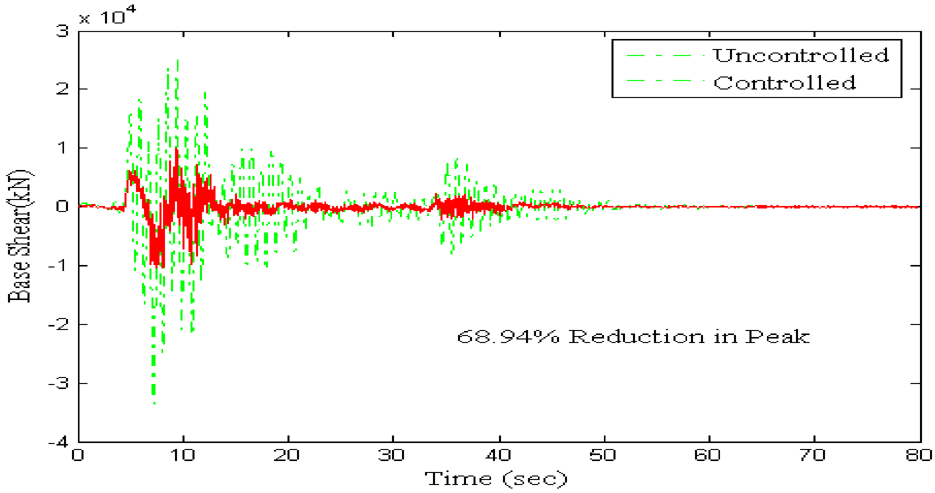

(c)

Fig. 5.9 Time history of base shear in pylon I against multiple support excitation (Case-1): (a) El Centro earthquake, (b) Mexico City earthquake, (c) Gebze earthquake

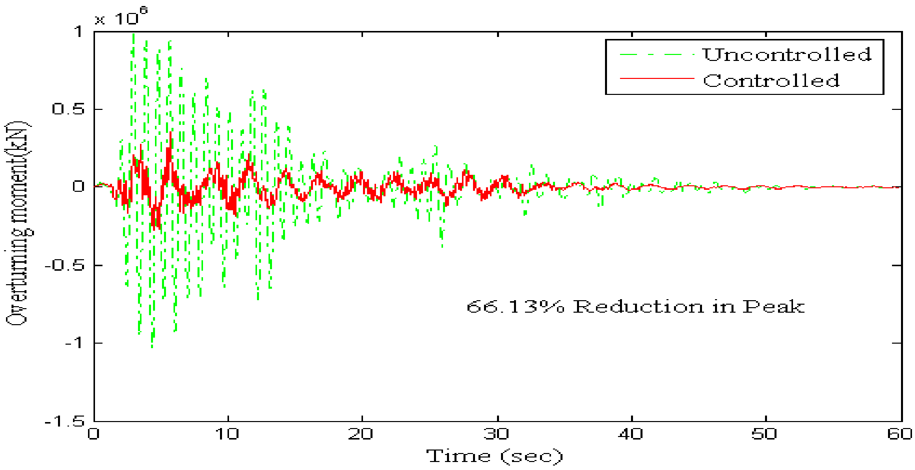

(a)

(b)

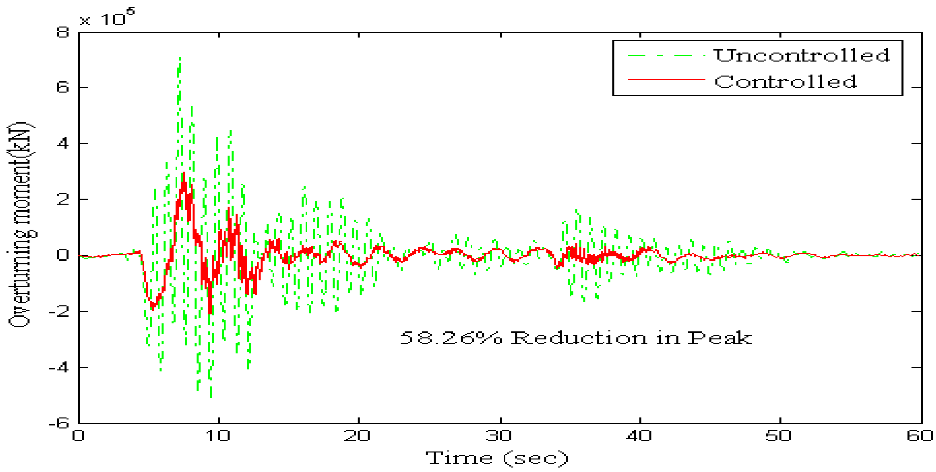

(c)

Fig. 5.10 Time history of overturning moment in pylon I against multiple support excitation (Case-1): (a) El Centro earthquake, (b) Mexico City earthquake, (c) Gebze earthquake

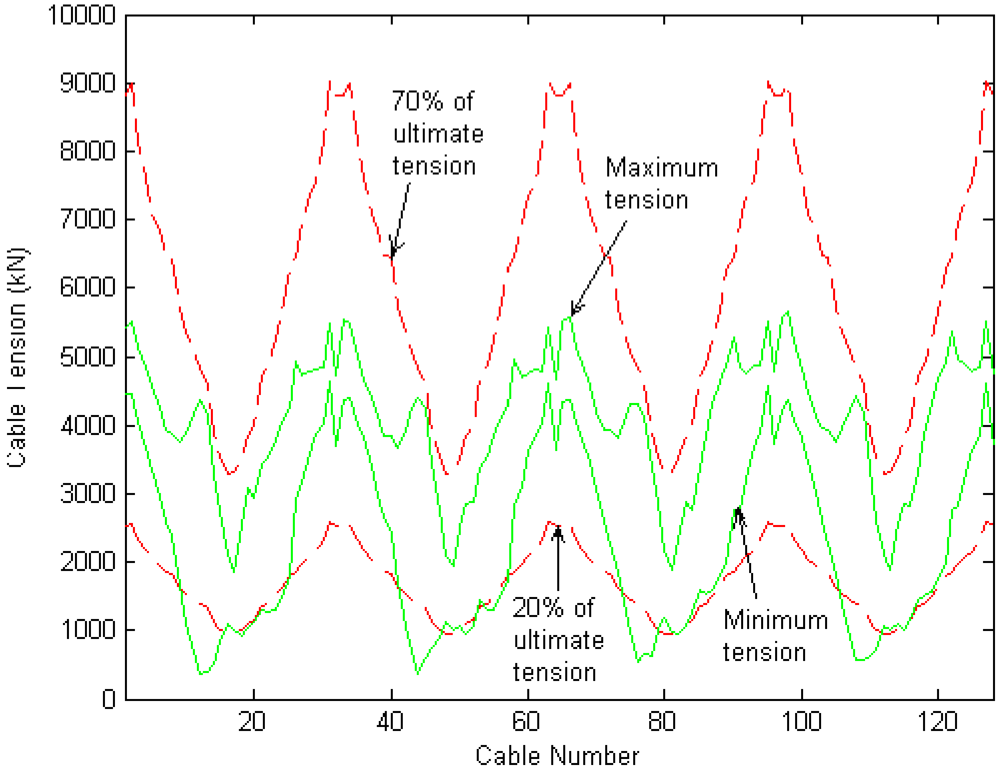
10000
9000
8000
7000
6000
5000
4000
3000
2000
1000
0
Cable Tension (kN)
20
40
60
80
100
120
Cable Number
70% of
ultimate
tension
Maximum
tension
20% of
ultimate
tension
Minimum
tension

(a)

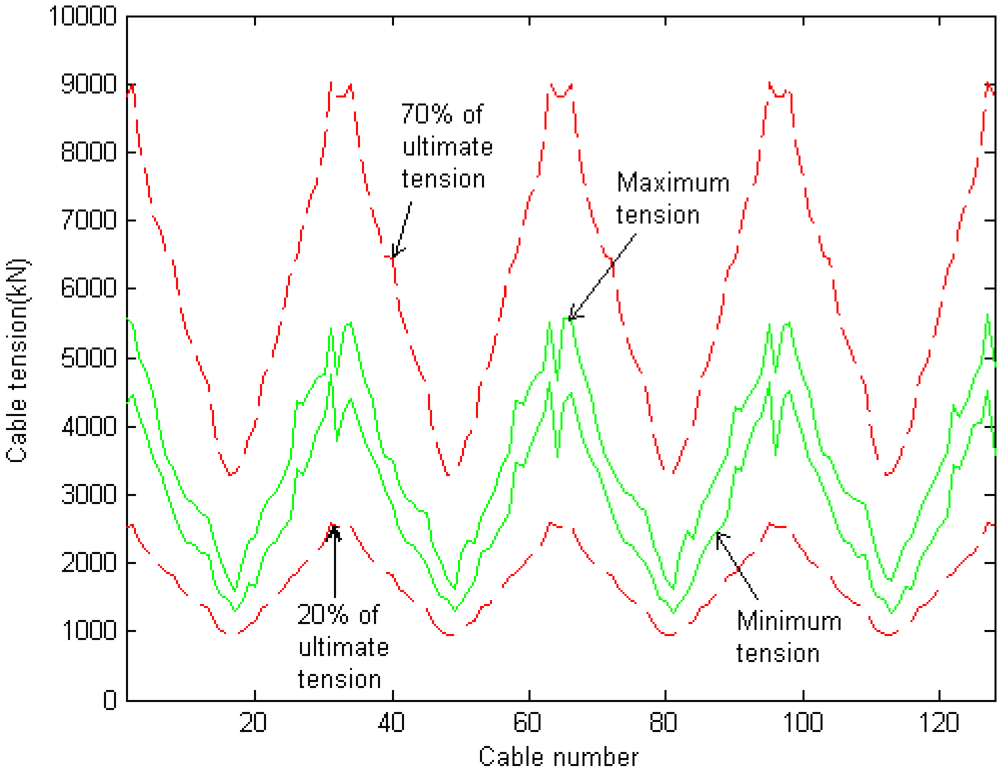

(b)

Fig. 5.11 Cable tension against multiple support excitation (Case-1) of El Centro earthquake: (a) Uncontrolled response, (b) Controlled response

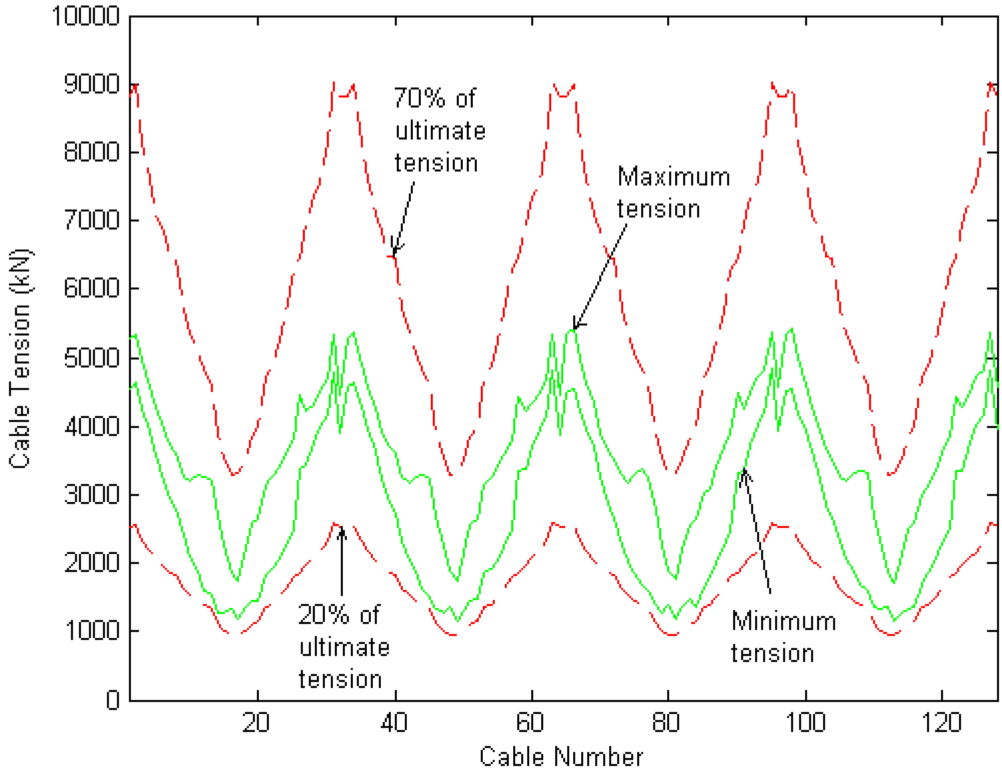
10000
9000
8000
7000
6000
5000
4000
3000
2000
1000
0
Cable Tension (kN)
20
40
60
80
100
120
Cable Number
70% of
ultimate
tension
Maximum
tension
20% of
ultimate
tension
Minimum
tension

(a)

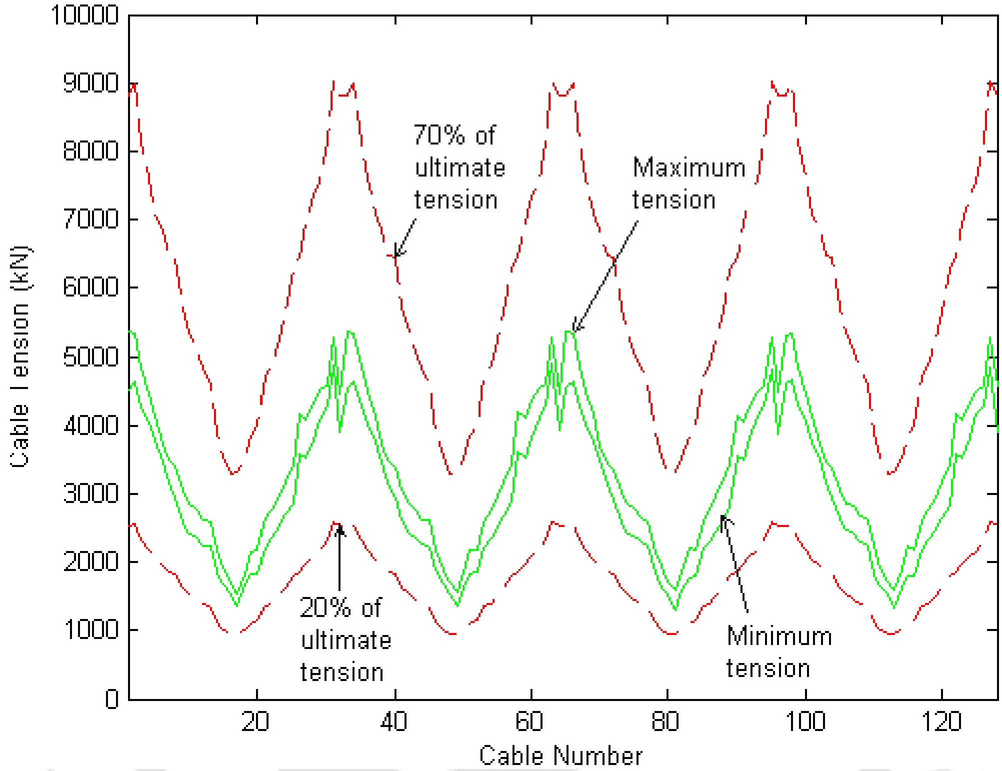

(b)

Fig. 5.12 Cable tension against multiple support excitation (Case-1) of Mexico City earthquake: (a) Uncontrolled response, (b) Controlled response

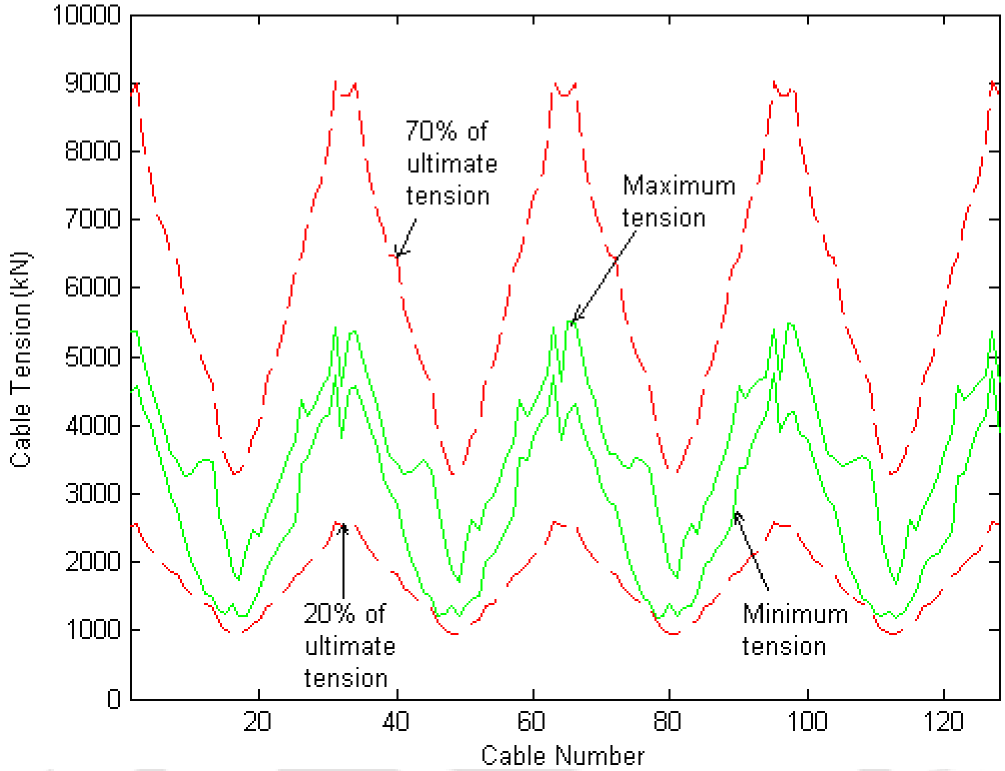

10000
9000
8000
7000
6000
5000
4000
3000
2000
1000
0
Cable Tension (kN)
20
40
60
80
100
120
Cable Number
70% of ultimate tension
Maximum tension
20% of ultimate tension
Minimum tension

(a)

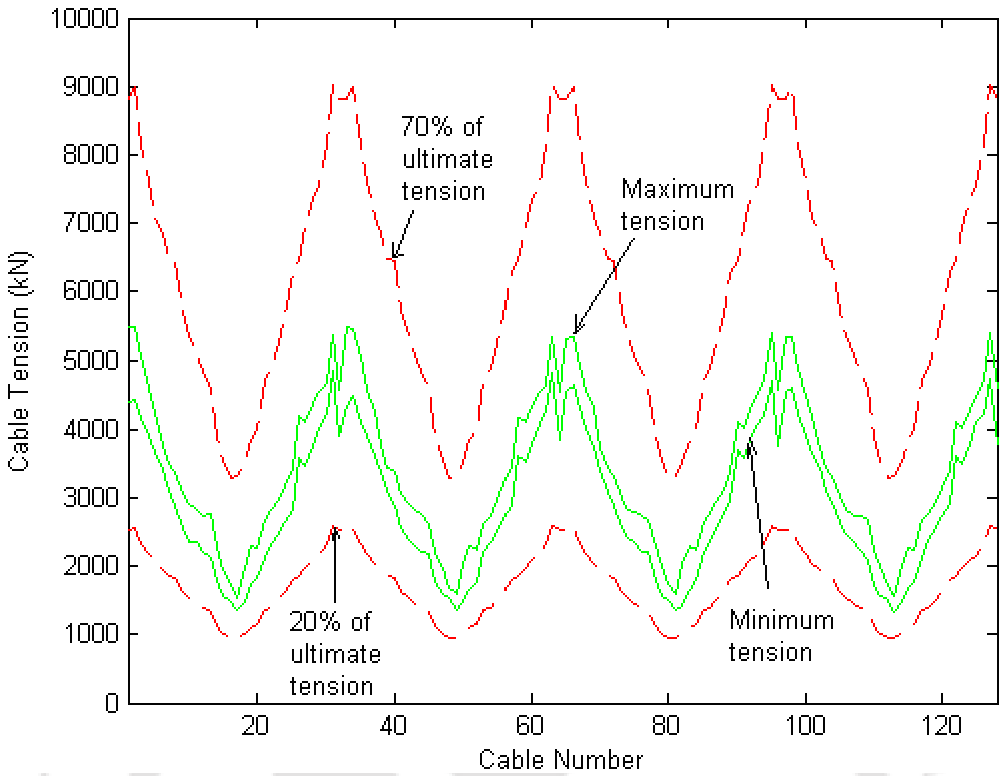

(b)

Fig. 5.13 Cable tension against multiple support excitation (Case-1) of Gebze earthquake: (a) Uncontrolled response, (b) Controlled response

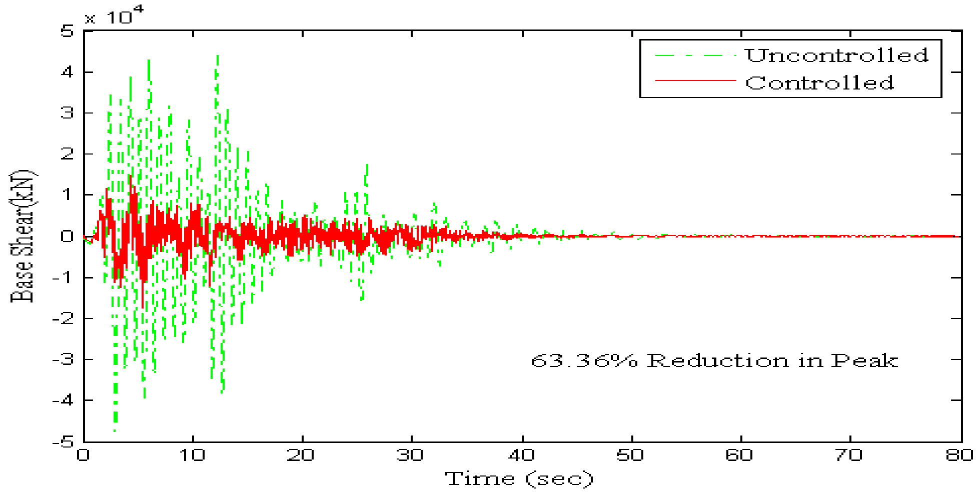
x 10^4
Uncontrolled
Controlled
63.36% Reduction in Peak
Base Shear(kN)
Time (sec)

(a)

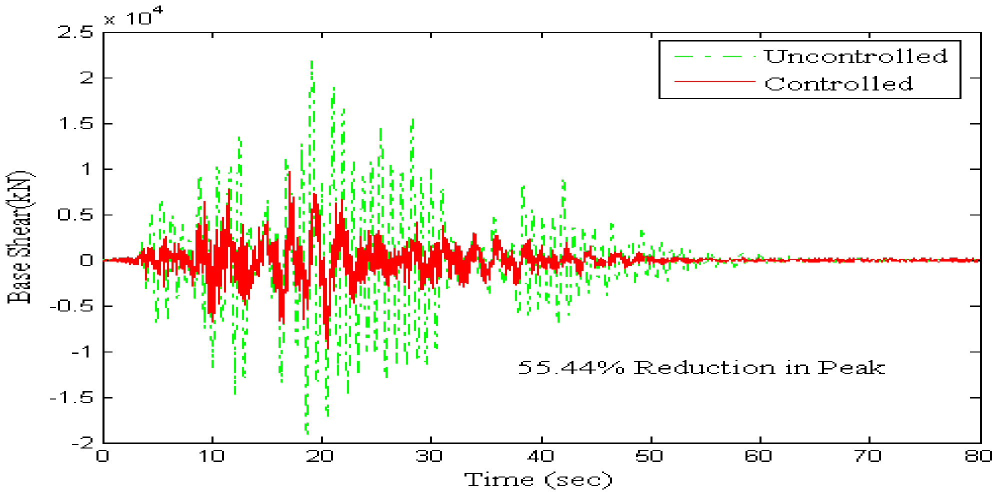
x 10^4
Uncontrolled
Controlled
55.44% Reduction in Peak
Base Shear(kN)
Time (sec)

(b)

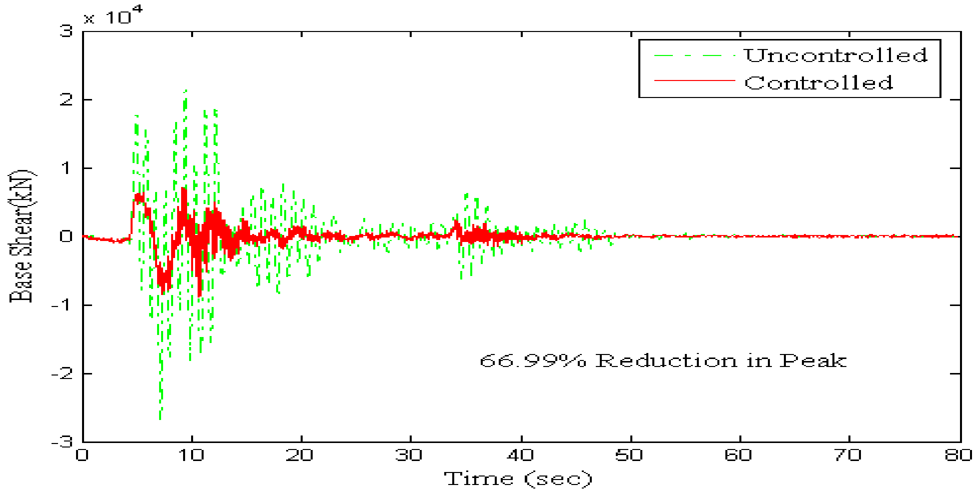

(c)

Fig. 5.14 Time history of base shear in pylon I against multiple support excitation (Case -2): (a) El Centro earthquake, (b) Mexico City earthquake, (c) Gebze earthquake

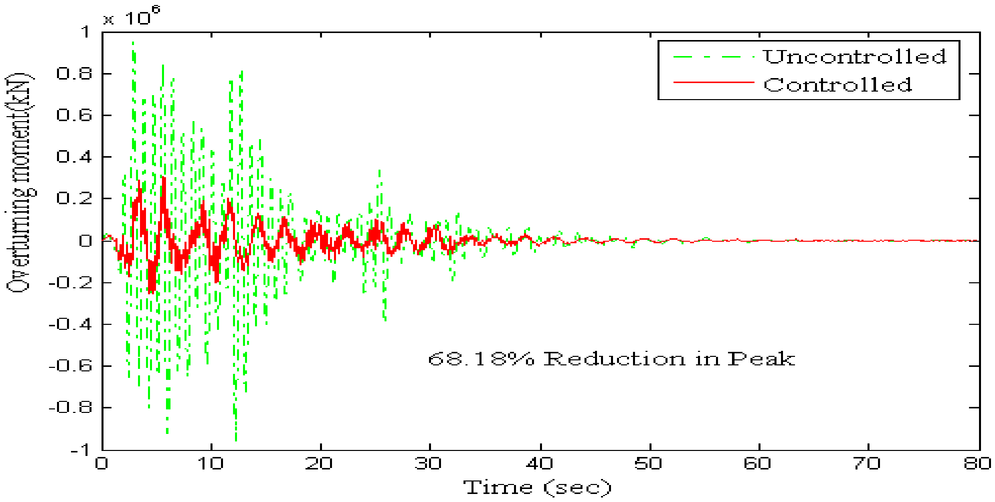

(a)

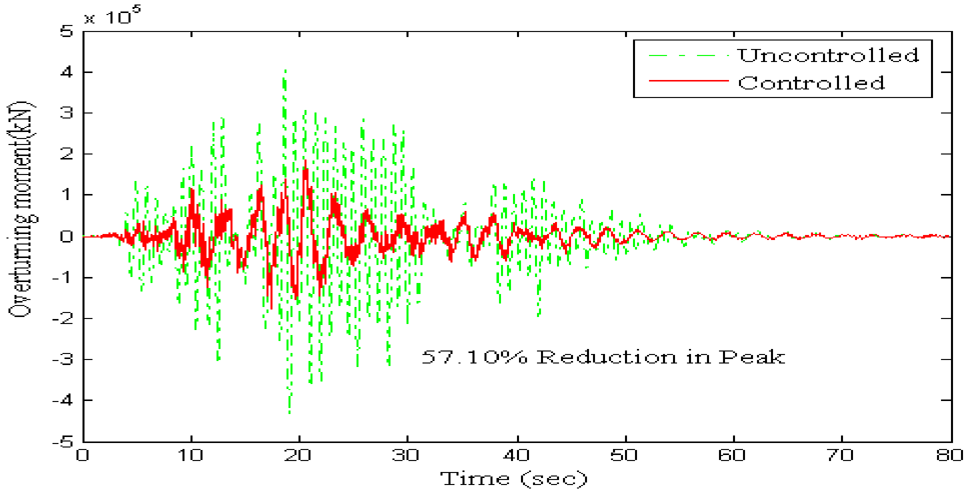

(b)

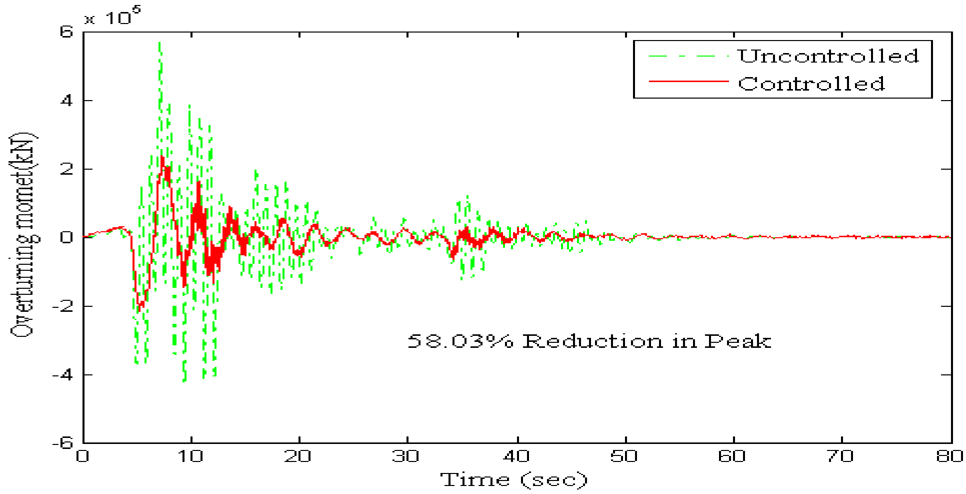

(c)

Fig. 5.15 Time history of overturning moment in pylon I against multiple support excitations (Case-2): (a) El Centro earthquake, (b) Mexico City earthquake, (c)Gebze earthquake

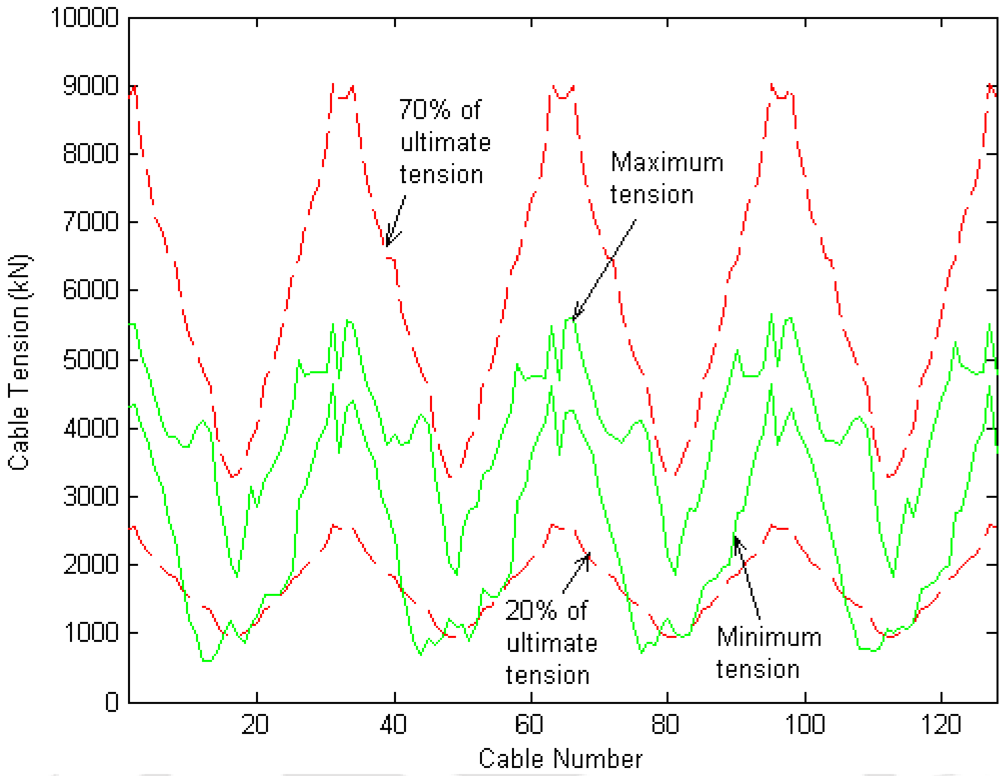

10000
9000
8000
7000
6000
5000
4000
3000
2000
1000
0
20
40
60
80
100
120
Cable Tension (kN)
Cable Number
70% of ultimate tension
Maximum tension
20% of ultimate tension
Minimum tension

(a)

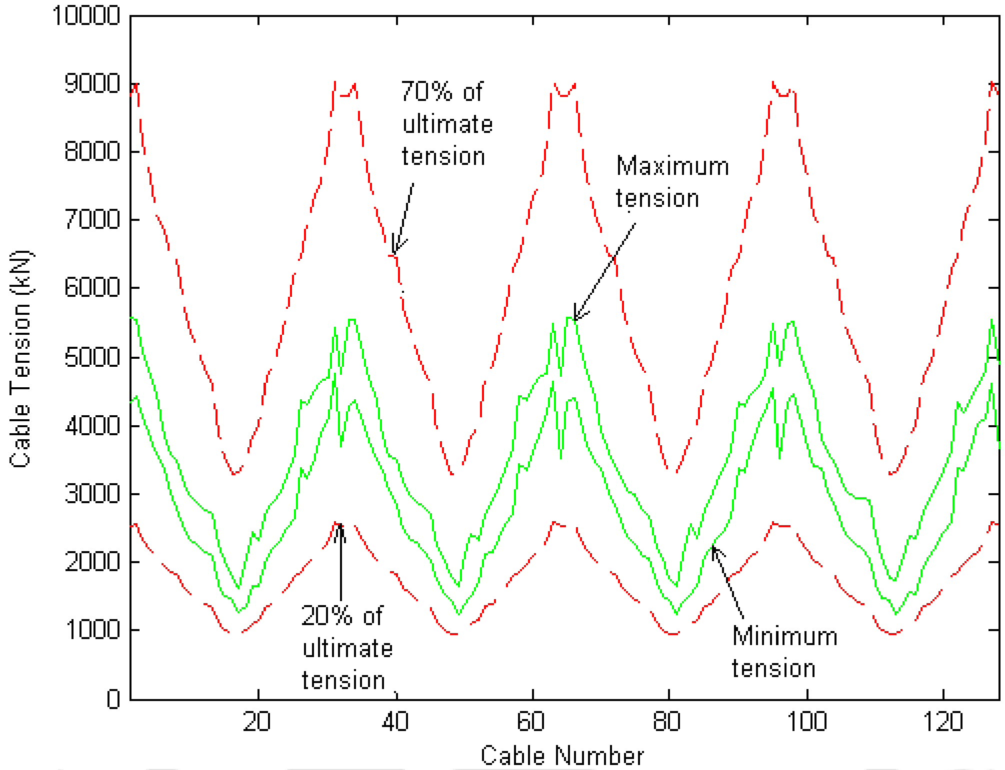

(b)

Fig. 5.16 Cable tension against multiple support excitation (Case-2) of El Centro earthquake: (a) Uncontrolled response, (b) Controlled response

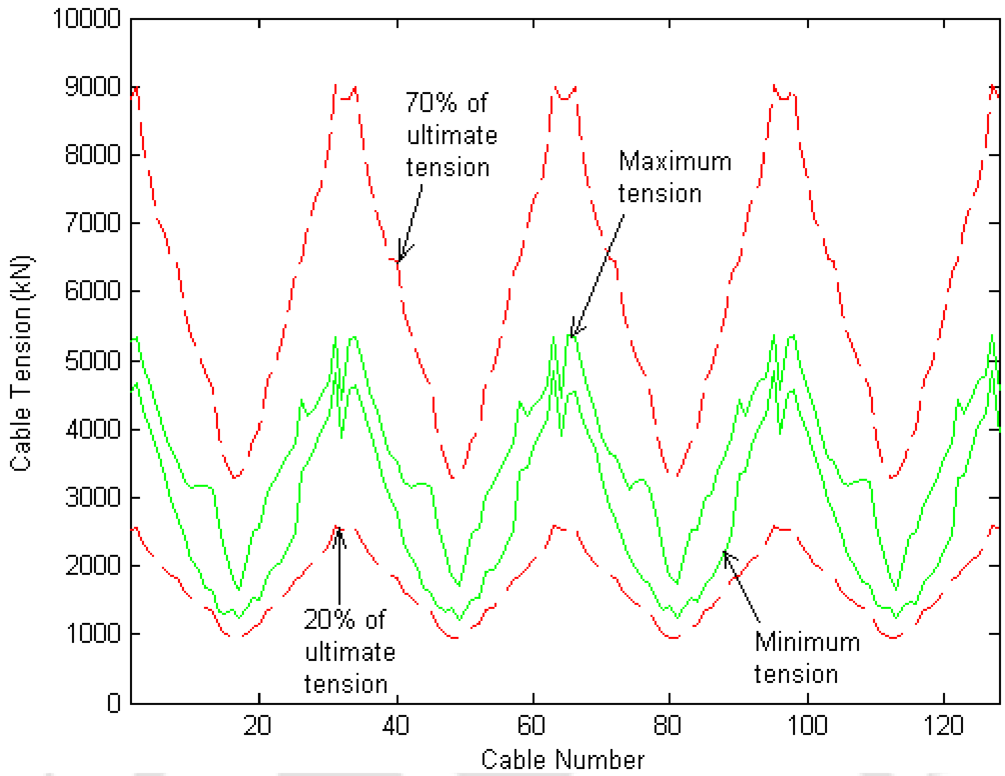
10000
9000
8000
7000
6000
5000
4000
3000
2000
1000
0
Cable Tension (kN)
20
40
60
80
100
120
Cable Number
70% of
ultimate
tension
Maximum
tension
20% of
ultimate
tension
Minimum
tension

(a)

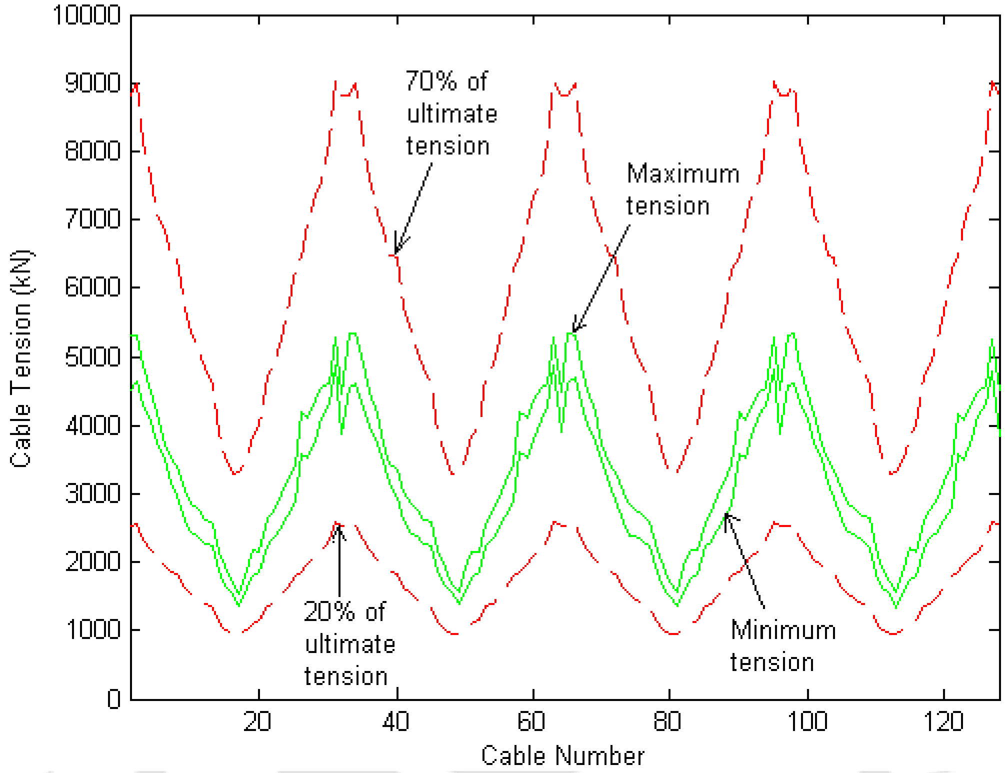

(b)

Fig. 5.17 Cable tension against multiple support excitation (Case-2) of Mexico City earthquake: (a) Uncontrolled response, (b) Controlled response

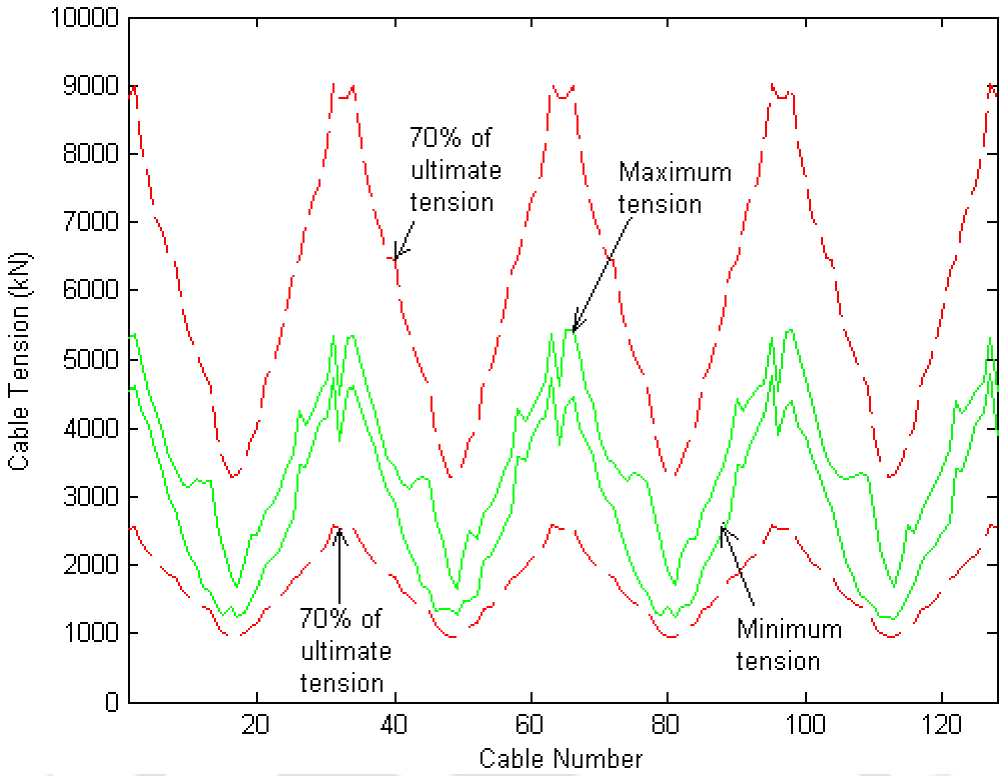

10000
9000
8000
7000
6000
5000
4000
3000
2000
1000
0
Cable Tension (kN)
20
40
60
80
100
120
Cable Number
70% of
ultimate
tension
Maximum
tension
70% of
ultimate
tension
Minimum
tension

(a)

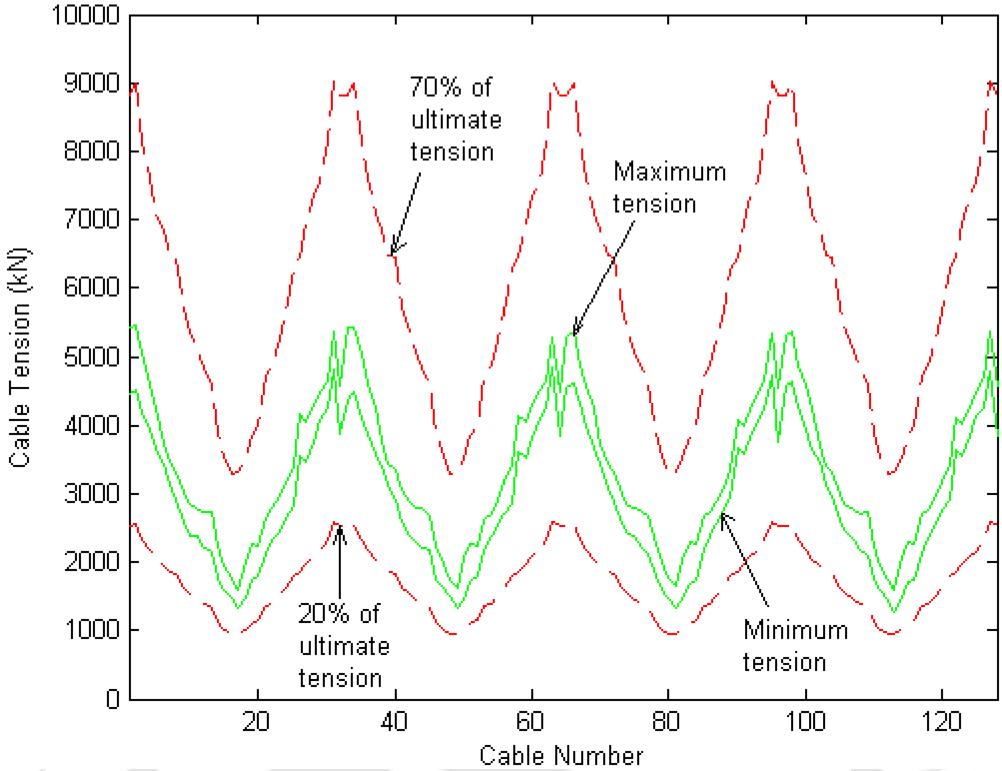

(b)

Fig. 5.18 Cable tension against multiple support excitation (Case-2) of Gebze earthquake: (a) Uncontrolled response, (b) Controlled response

Chapter 6

Summary and Conclusion

6.1 Introduction

In this concluding chapter, the analysis of results and summary of conclusions from the current study work have been presented. Significant contributions of the present research have also been listed. The suggestions for further research have been presented at the end.

6.2 Analysis of Results and Summary of Conclusions

The finite element (FE) model of a cable-stayed bridge, Quincy Bayview Bridge of Illinois, USA [Wilson *et. al.* (1991a)] could not simulate satisfactorily certain experimentally observed modes [Wilson *et. al.* (1991b)]. Accordingly, an update of the model has been carried out with an objective of arriving at a model that represents the experimentally observed modal parameters to the closest extent. One of the major steps in updating has been in the form of appropriate modeling of cables. The elastic catenary element [Jayaramn (1981), Karoumi (1999)] has been used to model the cables as an alternative to the truss element with equivalent Young's modulus. To study the effect of these alternative cable models on overall behaviour of the sample cable stayed bridge, two numerical models have been developed using above mentioned modeling approaches of cable. In this study stability functions have been used to account for nonlinearity arising out of beam-column effect in deck and pylon for analysis of bridge subjected to dead load. The effect of stability function has been evaluated for both the models. Thus, four numerical models have been formed for comparative study of the behaviour of the bridge to arrive at the updated model. Further, dofs of all the models have been reduced to make them compact and numerically stable. Constraint equations have been used to model the rigid links and bearing elements. The non linear static analysis of the bridge against dead load has been undertaken using a mixed-incremental iterative scheme for all the four alternative models. The modal characteristics of these models have been evaluated based on the dead load deformed configuration of the bridge and compared with those obtained from experimental observations. These characteristics have also been compared with the modal characteristics of the FE model by Wilson *et. al.* (1991a). The model with catenary element and stability functions for beam element formulation has been successful in simulation of experimental modal characteristics to the closest extent, and hence the same has been chosen as the updated model. It has been observed that the model could represent the experimentally observed flexural and torsional/mixed-torsional modes appropriately. However, the most significant result obtained is the simulation of the transverse behaviour of the bridge. The updated model reproduces the experimentally observed transverse mode of the bridge, which the numerical model proposed by Wilson *et. al.* (1991a) had failed to reproduce. It has been concluded that the weaker out-of-plane stiffness of the catenary element is responsible for this significant improvement in modal characteristics of the updated model. This model has also been observed to capture the higher torisonal modes better than the model by Wilson *et. al.* (1991a). It has also been concluded that the use of catenary element has significantly contributed to closer representation of the flexural modes by accounting for geometric nonlinear behaviour of the bridge. Moreover, the use of stability functions in beam element formulation has demonstrated a stiffening effect on the numerical models. This updated model has been used for linear dynamic analysis and for subsequent active control study.

The updated finite element model of Quincy Bayview Bridge, Illinois, USA has been used to design active controllers to control the response of the bridge against three representative earthquakes. The controller has been designed to control pylon responses at key locations. Both uniform support excitation and multiple supports excitations have been considered for the seismic response analysis. For multiple supports excitations different angles of incidence and corresponding time lags have been considered. Incidence angle of 15^0 and 45^0 has been considered for this study. The updated numerical model has been further reduced by Guyan method. This reduction has been validated by comparing transfer functions of the updated and reduced models for representations of appropriate dynamic response. The reduced model has been numerically interfaced with control devices, and has been represented in the states space. The model has again been reduced by balance realization to form a practical controller with 30 states for uniform support excitations and 60 states for multiple supports excitations. The controllers have been tested adopting similar performance indices as used in the benchmark problem [Dyke *et. al.* (2000)]. The evaluation process has been numerically simulated using Simulink® from control system toolbox of Matlab®. The controllers have been found to be effective in controlling key pylon responses such as the base shear and overturning moment against selected earthquakes. In the uniform support excitation case, a maximum of

46.42% control has been observed for base shear and 60.61% control have been realized against overturning moment. During this exercise, the cable tensions have been observed to be within safe range of 20% to 70% of ultimate tensions of the cables. Most importantly, the cable tensions exceeding this range during uncontrolled excitations have also been brought within the safe limits. As a result of this, possible unseating of the cables in the real structure can be avoided and the structure remains stable throughout the excitation. The requirements for sensors and actuators have been observed to be within available hardware specifications. The number of sensors employed for uniform support excitations is nine and that for multiple support excitations is fourteen. The number of actuators engaged in each case is twenty four. The frequency range of the sensors is upto 3000 rad/sec, which is within available hardware range. The sensitivities of acceleration sensors (7V/g) and displacement sensors (100V/m) are also practically feasible from hardware point of view. The demands for acceleration measurements and displacement measurements are fulfilled with the sensor sensitivities within a range of ±10V signal. Similarly, the demand on the actuators has also been found to be realistic in nature. For the uniform support case, maximum demand for actuation force is 269.99 kN. Highest demand for maximum actuator stroke is only 0.0786 m and that for actuator velocity is 0.3156 m/sec. A similar trend has also been observed in case of multiple support excitations. A maximum of 35.63% control has been observed in case of base shear and a 33.77% of control has been observed in case of overturning moments for both the angles of incidence of the earthquakes. The controlled cable responses have also been observed to be within safe limits. Similar actuator requirements for the multiple support excitations case have been observed. The required specifications are: capacity of 410 kN, stroke of 0.0686 m and device velocity of 0.52 m/sec. All these hardware demands are practically feasible. The numbers of sensors and actuators have also been observed to be optimum and economically feasible.

The FE model of Bill Emerson Memorial Bridge, Missouri, USA adopted by Dyke *et. al.* (2000) and Caicedo (2003) does not represent the initial flexural modes identified by Song *et. al.* (2006). Records of ambient vibration acceleration data from the bridge [Celebi (2006)] have been used to identify the modal parameters of the structure using the Subspace Identification (SSI) technique [Van *et. al.* (1996)]. The lowest four flexural mode shapes have been clearly identified using this technique. The updating of the FE model has been attempted using optimization the selected structural parameters are: (1) Mass of the deck, (2) Transverse moment of inertia of the deck and (3) Rotary stiffness of the connections between deck-abutment and deck-pylon supports. The objective function for optimization has been formed with appropriate weights for differences between the identified modal parameters with those from the FE model. A trust-region algorithm for non-linear minimization has been used first to minimize the objective function and to arrive at the initial solution. Further, an optimization technique namely, *Model to Generate Alternative* (MGA) [Brill *et. al.* (1992)] has been used to obtain alternative solutions that have similar values of objective function but have different values for the optimization parameters. Three alternative solutions have been chosen within 6% variation of objective function of the first solution. Out of these three alternative solutions, two have put unreasonably high values of stiffnesses for the rotary springs. Only one solution provides optimized parameters that would result in the most realistic updated model. This solution has been selected for updating the FE model.

The updated FE model of Bill Emerson Memorial Bridge, Missouri, USA has been used to design active controllers to control the response of the bridge against three representative earthquakes. Both uniform support excitations and multiple supports excitations have been considered. The multiple support excitations have been defined with different angles (15^0 and 45^0) of incidence of earthquake excitations and for corresponding time lags. The procedure adopted for designing the active controllers for Quincy Bayview Bridge has also been followed here. The sensor and actuator sensitivities have been selected as per the requirements. The controllers have also been tested against the same performance indices. In this bridge also, the controllers have been observed to be very effective in controlling key pylon responses, such as the base shear and overturning moments of the pylon against the selected earthquakes, while maintaining the cable tensions within limit. In the case of uniform support excitations, the maximum control achieved for base shear is 68.86% and the same is 70.70% in case of overturning moment. The maximum demand on the actuator devices has been observed as: actuator force: 901.93 kN, device stroke: 0.2998 m and device velocity: 0.7543 m/sec. In case of multiple supports excitations, the highest control against base shear at pylon has been observed as 68.94% and that for overturning moment as 68.18%. The highest demand on the actuators in this case are: actuator force: 1503.98 kN, device stroke: 0.2638 m and device velocity: 0.7878 m/sec. The controllers designed in this study have been found to be practical from hardware point of view. The numbers of sensors are nine and fourteen for uniform support and multiple support excitations respectively. The number of actuators employed in each of the cases is twenty four. These resources have observed to be within economically viable limit. Another noteworthy observation is that the cable tensions of the bridge are well within the acceptable range during the numerical simulation of the controller.

6.3 Contribution of the Present Research

The contribution of the present work lies in the implementation of the elastic catenary element in a 3-D FE model of a cable-stayed bridge for simulation of the experimentally observed behaviour closely. In updating FE model of the second cable-stayed bridge, SSI method has been used to identification of modal characteristics and these has been used for optimization of updating parameters. Both the updating approaches have been successfully implemented.

The contribution of the present study is also significant in terms of design of controllers. It has been established that control of a flexible structure of the magnitude of a cable-stayed bridge is complex. Thus, the design of the active controller based on the updated model is a contribution towards evolving more realistic control strategy.

6.4 Suggestion of Future Research

Scope for future research of the present work lies in using more sophisticated system identification technique for both the bridges as ambient vibration does not excite the higher modes. There is further scope for using more detailed identification data to update the finite element models. Moreover, the damping property of real large cable-stayed bridges is not fully understood yet due to the complicated damping mechanism of the bridges [Zhang *et. al.* (2000)]. It is known that bridge damping in general varies with the amplitude of vibration. Therefore, the applicability of an identified damping ratio through ambient vibration tests is still an issue that needs to be evaluated further by using other identification techniques or other dynamic tests with large vibration amplitudes. Most importantly, an identification-based control strategy can be evolved, where control will be based on the identified state space model instead of the commonly used FE model. In view of these observations the following future scopes of research may be identified:

- More detailed identification with larger number of sensors at appropriate locations.
- Extensive identification strategy to identify first few torsional and coupled modes.
- Use of other methods of collection of system identification data of higher amplitude that cannot be obtained through ambient vibration.
- Extraction of damping ratios by more appropriate identification technique.
- More involved update for the bridges using above mentioned strategies.
- Alternative control strategy on both the bridges using updated models arrived at by more elaborate identification.
- Forming a system-identification based control strategy for more accurate and more effective control strategy.

REFERENCES

Abdelghani M, Verhaegen M, Van Overschee P, De Moor B, Comparison study of subspace identification methods applied to flexible structures, *Mechanical Systems and Signal Processing*, **12**, 679 (1998)

Ahmed M. Abdel-Ghaffar, Aly S. Nazmy, 3-D Nonlinear Seismic Behavior of Cable-Stayed Bridges, *Journal of Structural Engineering, ASCE, Vol. 117, No. 11, November, 1991*

Aktan E, Catbas Turer N A, Zhang Zongfen, Structural Identification: Analytical Aspects, *Journal of Structural Engineering, ASCE*, **124(7)**, 817 (1998)

Ali H M and Abdel-Ghaffar A M, Modeling the nonlinear seismic behavior of cable-stayed bridges with passive control bearings, *Computer and Structures*, **54(3)**, 461 (1995)

Arici Y, Mosalam, K M, Modal identification of bridge systems using state-space models, *Structural Control and Health Monitoring*, **12**, 381 (2005)

Baugh J W, Caldwell S C, Brill E D, A Mathematical Programming Approach for Generating Alternatives in Discrete Structural Optimization, *Engineering Optimization*, **28**, 1(1997)

Bontempi Franco, Casciati Fabio and Giudici Massimo, Seismic response of a cable-stayed bridge: active and passive control system (Benchmark Problem), *Journal of Structural Control*, **10**, 169 (2003)

Boonyapinyo Virote, Yamada Hitoshi and Miyata Toshio, Wind Induced Nonlinear Lateral-Torsional Buckling of cable-Stayed Bridges, *Journal of Structural Engineering, ASCE*, **120(2)**, 486 (1994)

Brill E D, Chang S Y, and Hopkins L D, Modeling to generate alternatives: The HSJ approach and an illustration using a problem in land use planning, *Management Science*, **28(3)**, 221 (1982)

Brill E D, Flach J M, Hopkins L D, and Ranjithan S, MGA: A decision support system for complex, incompletely defined problems*, IEEE Transactions on systems, man and cybernetics*, **20(4)**, 745 (1990)

Brownjohn J M W, Xia Pin Qi, Dynamic Assessment of Curved Cable-Stayed Bridge by Model Updating, *Journal of Structural Engineering*, **126(2)**, 252 (2000)

Caicedo J M, Dutta Atanu K, Zarate Boris A, System identification and model updating of the Bill Emerson Memorial Bridge, *4th World Conference on Structural Control and Monitoring*, San Diego, California, USA, 11-13 July (2006)

Caicedo J M, Dyke S J, Moon S J, Bergman, Turan A G and Hague S, Phase II benchmark control problem for seismic response of cable-stayed bridges, *Journal of Structural Control*, **10**, 137 (2003)

Caicedo, J M, *Structural Health Monitoring of Flexible Civil Structures*, D Sc thesis, Washington University in Saint Louis, Saint Louis, Missouri, USA (2003)

Celebi M, Real-Time Seismic monitoring of the New Cape Girardeau Bridge and Priliminary Analyses of Recorded Data: An Overview, *Earthquake Spectra*, **22**, 609 (2006)

Chang C C, Chang T Y P and Zhang Q W, Ambient vibration for long span cable stayed bridges, *Journal of Bridge Engineering*, **6(1)**, 46 (2001)

Chopra A K, *Dynamics of Structures: Theory and Applications to Earthquake Engineering*, Prentice Hall; Upper Saddle River, New Jersey, 351 (1996)

Cook Robert D, Malkus David S, Plesha, Micahael E, Witt Robert J, *Concepts and applications of Finite Element Analysis*, 4th Edition, John Wiley & Sons Inc, New York (2002)

Dai Ze-bing, Hunag Jin-zhi, Wang Hong-xia, Semiactive control of a cable-stayed bridge under multiple support excitations, *Journal of Zhejang university of Science*, **5(3)**, 317 (2004)

Dyke S J, Caicedo J M, Turan G, Bergman L, Hague A and Hague S, Benchmark control problem for seismic response of cable-stayed bridges, *Proceedings of 2nd European Conference on Structural Control,* Paris, 3-6 July (2000)

Dyke S J, Caicedo J M, Turan G, Bergman L, Hague A and Hague S, Phase I benchmark control problem for seismic response of cable-stayed bridges, Journal *of Structural Engineering, ASCE*, **129(7)**, 857 (2003)

Franklin Y, Cheng, *Matrix analysis of structural dynamics-Application and Earthquake analysis*, Marcel Dekker, Inc: New York (2000)

Giraldo, D, A *structural health monitoring framework for civil structures*, Phd thesis, University in St. Louis, USA (2006)

Giraldo, D, Caicedo, J M, Song, W, Mogan, B, and Dyke, S J, Modal identification through ambient vibration: a comparative study, *24th International Modal Analysis Conference, Saint Louis, Missouri* (2006)

Gupta A, Kripakaran P, Mahinthakumar G K, Jr. J W B, Genetic Algorithm-Based Decision Support for Optimizing Seismic Response of Piping Systems, *Journal of Structural Engineering*, **131**, 389 (2005)

Hague S, Composite design for long span bridge, *XV Structures Congress, American Society of Civil Engineers*, Portland, Oregon, USA (1997)

He W L, Agrawal A K and Mahmoud K, Control of seismically excited cable-stayed bridge using semiactive stiffness dampers, *Journal of Bridge Engineering*, **6 (6)**, 376 (2001)

Hirokazu Iemura and Mulyo Harris Pradono, Application of pseudo-negative stiffness control to the benchmark cable-stayed bridge, *Journal of Structural Control*, **10**,187 (2003)

Hongjin Kim and Hojjat Adeli, Wavelet-Hybrid Feedback Linear Mean Squared Algorithm for Robust Control of Cable-Stayed Bridges, *Journal of Bridge Engineering*, **10(2)**, 116 (2005)

Housner G W, Bergman L A, Chaughey T K, Chassiakos A G, Claus R O, Masri S F, Skelton R E, Soong T T, Spencer B F, Yao J T P, Structural control: past, present, and future, *Journal of Engineering Mechanics*, **123(9)**, 897 (1997)

James G H, Carne T G and Lauffer J P, The Natural Excitation Technique (NExT) for Modal Parameter Extraction from Operating Wind Turbines, *SAND92-1666*, Sandia National Laboratories, Albuquerque, NM and Livermore, CA (1993)

James G H, Carne T G, Lauffer J P and Nord A R, Modal testing using natural excitation, *10th International Modal Analysis Conference,* San Diego, CA, 120 (1992)

Jann N Yang, Silian Lin and Faryar Jabbari, H2-based control strategies for civil engineering structures, *Journal of Structural Control*, **10**, 205 (2003)

Jayaraman H B, Knudson W C, A curved element for analysis of cable structures, *Computers and Structures*, **14**, 325 (1981)

Juang Jer Nan, *Applied System Identification*, PTR Prentice Hall Englewood Cliffs, New Jeresey, (1994)

Juang J N and Pappa R S, An Eigensystem Realization Algorithm for Modal Parameter Identification and Model Reduction, *Journal of Guidance*, **8(5)**, 620 (1985)

Juang J N and Pappa R S, Effects of noise on modal parameters identified by the Eigensystem Realization Algorithm, *Journal of Guidance*, **9(3)**, 294 (1986)

Karoumi Raid, Some modeling aspects in the nonlinear finite element analysis of cable supported bridge, *Computers and Structures*, **71**, 397 (1999)

Kwan-Soon Park, Hyun-Moo Koh, Seung-Yong Ok, Chung-Won Seo, Fuzzy supervisory control of earthquake-excited cable-stayed bridges, *Engineering Structures*, **27**, 1086 (2005)

Matlab® version 7.0.0 (R14), The Math Works, Inc. Natick, Massachusetts (2004)

Nazmy A S and Ahmed M Abdel-Ghaffar, Three dimensional nonlinear static analysis of cable-stayed bridges, *Computers and Structures*, **34(2)**, 257 (1990)

Ohtori Y, Spencer B F, A MATLAB-based tool for nonlinear structural analysis, *Proceedings of 13th Engineering Mechanics Conference,* Baltimore, USA (1999)

Park Kwan-Soon, Koh Hyun-Moo, Ok Seung-Yong, Seo Chung-Won, Fuzzy supervisory control of earthquake-excited cable-stayed bridges, *Engineering Structures*, **27**, 1086 (2005)

Park Kyo-Sik and Lee Wong, Jung and Park, Passive-active system for seismic protection of a cable-stayed bridge, *Journal of Earthquake Engineering,* **7(4)**, 615 (2003a)

Park Kyo-Sik, Jung Ghyung-Jo, Spencer B F and Lee In-Won, Hybrid control strategy for seismic protection of a benchmark cable-stayed bridge, *Engineering Structures*, **25**, 405 (2003b)

Park Kyo-Sik, Jung Ghyung Jo, Spencer B F. and Lee In-Won, Hybrid control systems for seismic protection of a phase II benchmark cable- stayed bridge, *J. Struct. Control*, **10**, 231 (2003c)

Preumont Andre, *Vibration Control of Active Structures- An Introduction*, 2nd Edition, Kluwer Academic Publishers, Dordrecht/Boston/London (2002)

Ren W X, Harik I E, Blandford G E, Lenett, M, Basehearh T, Roebling suspension bridge: II. Ambient testing and live load response, *J Bridge Engrg ASCE*, **9(2)**, 119 (2004a)

Ren Wei-Xin, Peng Xue-Lin, Baseline finite element modeling of a large span cable-stayed bridge through field ambient vibration tests, *Computers and Structures*, **83**, 536 (2005b)

Ren Wei-Xin, Peng Xue-Lin, Lin You Qin, Experimental and analytical studies on dynamic characteristics of a large span cable-stayed bridge: *Engineering Structures*, **27**, 535 (2005c)

SAP2000, *Analysis reference manual*, Computers and Structures, Inc: Berkley, California (2002)

Song W, Giraldo, D, Clayton, E H, Dyke, S J and Caicedo, J M, Application of ARMAV for Modal Identification of the Emerson Bridge, *Third International Conference on Bridge Maintenance, Safety and Management*, Porto, Portugal (2006)

Tewari, Asish, *Modern Control Design with Matlab and Simulink*, John Wiley and sons (2002)

Turan, G, *Active control of cable-stayed bridge against earthquake excitations*, Phd thesis, University of Illinois at Urbana-Champaign (2001)

Van, Voerschee P, De Moor B, *Subspace Identification for Linear Systems: Theory - Implementation – Applications*, Kluwer Academic Publishers (1996)

Wang Pao-Hsii, Yang Chiung Guei, Parametric studies on cable-stayed bridges, *Computers & Structures*, **60(2)**, 243 (1996)

Wilson John C, Gravelle Wayne, Modelling of a cable-stayed bridge for dynamic analysis, *Earthquake Engineering and Structural Dynamics*, **20**, 707 (1991a)

Wilson John C, Liu Tao, Ambient vibration measurement on a cable-stayed Bridge, *Earthquake Engineering and Structural Dynamics*, **20**, 723 (1991b)

Xu Y L, Ko J M, Vibration studies of Tsing Ma suspension bridge, *J Bridge Engrg ASCE*, **4(2)**, 149 (1997)

Zhang Q W, Chang C C, Chang, T Y P, Finite element model updating for structures with parametric constraints, *Earthquake Engineering Structural Dynamics*, **29**, 927 (2000)

Zhang, Q W, Chang, T Y P, Chang, C C, Finite-Element model updating for the Kap Shui Mun Cable-Stayed Bridge, *Journal of Bridge Engineering*, **6 (4),** 285 (2001)

BRIEF BIODATA OF THE AUTHOR

The Mr. Atanu Kumar Dutta was born in 1967 at Sivasagar in Assam. He graduated in Civil Engineering with distinction from Regional Engineering College, Surathkal in 1989. He had a brief stint with L&T (ECC) as a graduated trainee. He completed his M Tech degree in Applied Mechanics from IIT Delhi in 1992. Subsequently he joined Irrigation Department, Govt of Assam as an assistant engineer and served the state for five years. In 1997 he joined Jorhat Engineering College, Assam and is working till date in the capacity of a Sr. Lecturer. He enrolled as a research scholar in IIT Guwahati in December, 2002 after securing sponsorship from the Govt of Assam.

PUBLICATIONS BASED ON PRESENT INVESTIGATION

1. Atanu Kumar Dutta, Anjan Dutta, Sajal Kanti Deb, Design of Active controller for Quincy Bayview Bridge, Illinois, USA against seismic excitation: Part I: Model updating, Part II - Control implementation (Communicated to the *Journal of Structural Control and health monitoring*, Dtd, 22nd July, 2007)

2. A. K. Dutta, S. K. Deb, A. Dutta (2006), Active Control of Cable Stayed Bridge against Seismic Excitation: A case study, *International Congress on Computational Mechanics and Simulation (ICCMS - 06)*, Indian Institute of Technology, Guwahati, India, Decemeber 8-10

3. Caicedo Juan M, Dutta Atanu K, Zarate Boris (2006), System identification and model updating of the Bill Emerson Memorial Bridge, *4th World Conference on Structural Control and Monitoring*, San Diego, California, USA, 11-13 July

4. Zarate Boris A, Caicedo Juan M, Dutta Atanu (2006), Model updating of a cable-stayed bridge using MGA, *IMAC-XXV: A Conference & Exposition on Structural Dynamics*, Florida, USA, February 19-22

5. Dutta Atanu K, Deb S K, Dutta A (2006), Active control of a cable stayed bridge against multiple support seismic excitation, *13th Symposium on Earthquake Engineering*, Roorkee, India, Dec 18-20

6. Dutta A K, Deb S K, Dutta A, Active Control of Cable Stayed Bridge against Seismic Excitation: A case study (To be communicated to *Journal of Structural Control*)